Université de Strasbourg
Ecole Doctorale Science de la Vie et Santé (ED 414)

THESE DE DOCTORAT

présentée pour obtenir le grade de
Docteur de l'Université de Strasbourg

Discipline : Science du vivant
Aspects moléculaires et cellulaires de la biologie

Impact de la molécule de la matrice extracellulaire ténascine-C sur la progression et l'angiogenèse tumorale

Falk Saupe
né le 25 Août 1980 à Radebeul (Allemagne)

Composition du jury :

Examinateur :	Prof. Dr. Jan De Mey (Université de Strasbourg)
Rapporteur externe I :	Prof. Dr. Christel Herold-Mende (Université Heidelberg)
Rapporteur externe II :	Dr. Catherine Monnot (Collège de France, Paris)
Directeur de thèse :	Dr. Gertraud Orend (Inserm U682, Strasbourg)
Unité de Recherche :	De l'homéostasie tissulaire au cancer et à l'inflammation Inserm U682 Equipe Gertraud Orend: Implication du microenvironnement sur l'angiogenèse et l'invasion tumorale
Soutenue publiquement :	le 29 Septembre 2011

Für meine Familie

Impact of the extracellular matrix molecule ténascine-C in the microenvironment on tumor progression and angiogenesis

Background: The tumor microenvironment plays an instrumental role in cancer progression. The extracellular matrix molecule tenascin-C is a major component of the cancer specific matrix, is prominently expressed in the tumor microenvironment of several human cancer types and plays a promoting role in malignant tumor progression. Tenascin-C is amongst the genes with a predictive value in human breast cancer metastasis to the lung. High tenascin-C expression levels are linked to tamoxifen resistance in breast cancer and correlate with a bad survival prognosis for patients with glioma or lung cancer. Although tenascin-C is a well established inducer of cancer progression, it is still not well understood how tenascin-C is organized in cancer tissue and by which molecular mechanisms tenascin-C promotes tumor angiogenesis and metastasis.

Aims: The objective of this thesis was to investigate the role of tenascin-C during tumor progression in the immune-competent Rip1-Tag2 (RT2) mouse model of pancreatic neuroendocrine tumorigenesis. A gain-of-function strategy was used to generate the double-transgenic RT2/hTNC mouse model mimicking high expression of tenascin-C in human cancer. The loss-of-function RT2/TNC-/- model was newly established as a complementary mouse model to study the invalidation of tenascin-C in RT2 tumorigenesis. The impact of tenascin-C on tumor angiogenesis was analyzed in more detail at microscopic level using electron microscopy and three-dimensional immunofluorescence reconstruction microscopy. Gene expression profiling was performed to uncover molecular mechanisms of action downstream of tenascin-C.

Results: For the first time it is demonstrated in an immune-competent model of spontaneous tumor formation that tenascin-C expression levels determine the extent of cell proliferation, tumor invasion, tumor angiogenesis and metastasis. The data obtained in these models showed that tenascin-C had a signaling function and plays an important role in tumor onset and during the angiogenic switch. The implication of the Wnt inhibitor DKK1 provides a mechanistic basis for the described tenascin-C actions. Tenascin-C also had a structural function determining tumor vessel architecture and formation of matrix conduits as an additional program to drive tumor malignancy.

Conclusion: Based on the observations, tenascin-C presents an attractive target for blocking tumor angiogenesis and tumor cell dissemination. Therefore, the presented well characterized stochastic tumorigenesis model with different tenascin-C expression could serve as an excellent preclinical model for evaluating the efficacy of drugs targeting human tenascin-C and downstream signaling pathways for repressing tumor angiogenesis and metastasis.

Keywords: tumor microenvironment, extracellular matrix, tenascin-C, angiogenesis, pancreatic neuroendocrine tumor, gene expression profiling

Impact de la molécule de la matrice extracellulaire ténascine-C sur la progression et l'angiogénèse tumorale

Contexte :

Le microenvironnement tumoral joue un rôle déterminant dans le développement des cancers. Il est composé du stroma tumoral qui contient plusieurs protéines secrétées tels que des facteurs de croissance, des cytokines ou des enzymes. Il contient également des cellules stromales recrutées au sein de la tumeur, comme les fibroblastes associés au cancer (CAF), les cellules dérivées de la moelle osseuse (BMDC), les cellules endothéliales (CE) ou les cellules inflammatoires, qui peuvent participer activement à la progression tumorale en favorisant la prolifération cellulaire, l'angiogenèse, l'invasion tumorale et la formation de métastases (Egeblad *et al.*, 2010). La matrice extracellulaire (MEC) est une autre composante majeure du stroma tumoral qui forme un réseau de macromolécules dans lequel les cellules cancéreuses et les autres facteurs sécrétés sont organisés dans une structure tridimensionnelle. La MEC fournit principalement un soutien structurel aux tissus mais peut également interagir directement avec les cellules et modifier leur comportement en terme de survie, de migration, de prolifération ou de morphologie. Les principaux composants de la MEC sont les protéoglycanes, l'acide hyaluronique et les glycoprotéines fibreuses telles que les collagènes, fibronectines, laminines et ténascines (Erickson and Bourdon, 1989; Hay, 1981). L'ensemble de ces composants constitue le microenvironnement de la tumeur dont les modifications exercent un rôle crucial au cours de la progression des cancers (Kalluri and Zeisberg, 2006).

Durant la progression tumorale, la composition de la MEC est activement remodelée non seulement par dégradation, sous l'action d'enzymes lytiques, mais aussi par synthèse et sécrétion de nouveaux composants de la MEC, générant ainsi un microenvironnement pro-tumorigène. La ténascine-C (TNC) constitue une des glycoprotéines de la MEC dont la forte expression a été spécifiquement décrite dans de nombreux cancers humains (Orend and Chiquet-Ehrismann, 2006). Son interaction avec d'autres molécules de la MEC et avec des récepteurs transmembranaires exprimés à la surface des différents types cellulaires présents dans le microenvironnement tumoral affecte l'architecture tissulaire et initie la transduction de signaux impliquées dans la prolifération, l'angiogénèse, l'invasion et la dissémination métastatique.

La TNC a été détectée dans des cancers d'origines variées où elle semble pouvoir jouer un rôle en faveur de la progression tumorale, sa forte expression ayant pu être corrélée avec la formation des métastases ganglionnaires et avec un mauvais pronostic (Midwood and Orend, 2009; Orend and Chiquet-Ehrismann, 2006). Dans des modèles murins *in vivo*

de cancer du sein, l'expression de la TNC est corrélée à la formation de métastases pulmonaires (Calvo *et al.*, 2008; Oskarsson *et al.*, 2011; Tavazoie *et al.*, 2008) et figure au sein d'une signature de gènes à la valeur pronostique dans la formation de métastases pulmonaires du cancer du sein humain (Minn *et al.*, 2005). Des taux élevés de TNC sont associés à la résistance au traitement par le tamoxifène de patientes atteintes de cancers du sein (Helleman *et al.*, 2008) et sont corrèlés à un mauvais pronostic de survie de patients atteints de gliomes ou de cancers du poumon (Orend and Chiquet-Ehrismann, 2006). Si ces données illustrent que la TNC peut promouvoir la progression tumorale, sa distribution et son impact sur le microenvironnement tumoral ainsi que les mécanismes moléculaires impliqués dans son action en faveur de l'angiogénèse et de la dissémination de métastases restent à ce jour largement inexploré.

Objectifs:

L'objectif global de cette thèse a été d'étudier l'impact de la TNC dans la progression des tumeurs neuroendocrines pancréatiques du modèle murin Rip1-Tag2 (RT2), afin de préciser les mécanismes moléculaires contrôlés par la TNC au cours des différentes étapes de la tumorigénèse. Pour cela, une stratégie de gain de fonction a été mise en place en générant un modèle de souris double-transgénique RT2/hTNC mimant l'expression élevée de la TNC dans les cancers humains. En parallèle, un modèle de perte de fonction a été généré dans le but d'analyser la tumorigenèse RT2 en absence de la TNC. En outre, un criblage transcriptionnel a été réalisé pour identifier les gènes cibles modulés par la TNC. Le rôle de la TNC dans le contrôle de l'anatomie des vaisseaux sanguins et de l'architecture tumorale a été analysé en détail par microscopie électronique et par reconstruction tridimensionnelle d'immunomarquages fluorescent.

Approches expérimentales:

Le modèle de souris immunocompétentes RT2 a été utilisé pour étudier les différentes étapes aboutissant au développement d'insulinomes (Hanahan, 1985). Dans ce modèle, l'antigène T du virus simien 40 (SV40 Tag) agit comme un oncogène exprimé sous la dépendance du promoteur de l'insuline et déclenche ainsi la transformation spontanée d'îlots de Langerhans en îlots hyperplasiques (« switch hyperplasiques »). Ceux-ci subissent ensuite le « switch angiogénique », entraînant le développement d'adénomes non-invasifs, puis de carcinomes invasifs de façon reproductible. Des souris transgéniques présentant une expression forcée de la TNC dans les cellules des îlots de Langerhans (Rip-hTNC), précédemment établies dans le laboratoire, ont été croisées avec des souris RT2 pour générer le modèle de souris RT2/hTNC qui mime l'expression élevée de la TNC observée dans les cancers humains. Par ailleurs, les souris dépourvues d'expression de la TNC

(Forsberg *et al.*, 1996) ont été croisées avec des souris RT2 pour générer le modèle de tumorigénèse RT2 en l'absence d'expression de la TNC (RT2/TNC-/-). Les tissus tumoraux ont été analysés par coloration histologique et par quantifications d'immunomarquages. Les ARN issus de tumeurs isolées à différents stades de la tumorigenèse ont été utilisé pour effectuer un criblage transcriptionnel à l'aide de puces à ADN ou par transcription inverse et réaction de polymérisation en chaîne en temps réel (RT-qPCR). Des expériences de perfusion de dextran et de lectine couplés à des fluorophores ont été réalisées pour étudier le rôle de la TNC dans l'angiogenèse tumorale.

Résultats et discussion:

Impact de la TNC sur la croissance et la prolifération tumorale:

Les souris RT2 développent plusieurs tumeurs macroscopiques à l'âge de 12 semaines. Le nombre et le volume des tumeurs macroscopiquement observable, déterminés dans les modèles de gain et de perte de fonction de la TNC, n'ont révélé aucune différence en fonction du niveau d'expression de la TNC (Figure 1A, 1B). Néanmoins, en isolant chaque tumeur de plus d'un millimètre de diamètre des souris de 14 semaines, une réduction significative du volume total tumorale a été observée chez les souris RT2/hTNC suggérant une diminution de la croissance des tumeurs établies dans les souris RT2 surexprimant la TNC (Figure 1C). Dans ces souris RT2/hTNC la diminution du volume tumoral peut être expliquée par la diminution du nombre de tumeurs d'un diamètre supérieur à 3 mm. Ces mêmes souris présentent une augmentation du nombre de tumeurs d'une taille inférieure à 3 mm par rapport aux contrôles (Figure 1D). Ceci suggère que la TNC pourrait agir en faveur de l'initiation tumorale et des étapes précoces de croissance de tumeurs qui n'ont pas pu s'élargir en raison d'un défaut d'alimentation en oxygène et en nutriments. Une étude histologique des tumeurs de souris RT2/hTNC âgées de 10 semaines a été réalisée pour les classer selon leur taille. Cette analyse a révélé que l'expression accrue de la TNC favorise le développement de tumeurs d'une taille supérieure à 0,5 mm chez les souris RT2/hTNC en comparant avec les souris RT2 (Figure 1E).

Ces observations suggèrent que la surexpression de la TNC entraîne une augmentation de la prolifération des tumeurs développées par les souris RT2. Afin de tester cette hypothèse, une analyse de la prolifération cellulaire au sein des tumeurs a été réalisée par quantification des marqueurs phospho-histone 3 (PH3) et KI67. Nous avons ainsi pu mettre en évidence une prolifération accrue des tumeurs présentant une expression forcée de la TNC (Figure 2). Les résultats préliminaires, obtenus sur une petite cohorte de tumeurs, de la quantification du signal KI67 de tumeurs classées en fonction de leur taille, a révélé un taux de prolifération accru dans les petits îlots normaux et hyperplasiques des souris double transgéniques (Figure 2B). Cette observation pourrait expliquer, du moins en partie,

l'augmentation du nombre de tumeurs observées chez les souris RT2/hTNC. Parmi les mécanismes qui pourraient participer à cet effet, il semble plausible que la TNC déclenche le « *switch* hyperplasiques » dans les îlots normaux pendant l'initiation de la tumorigenèse dans les souris RT2. Dans le modèle RT2, une partie seulement des îlots normaux (~50%) est engagée dans un processus de prolifération et d'hyperplasie. Pour déterminer si la proportion d'îlots hyperplasiques est augmentée par la surexpression de la TNC, leur nombre doit être estimé dans des souris RT2 à un plus jeune âge (~5 semaines), lorsque le « *switch* hyperplasique » se met en place et avant que les lésions des îlots effectuent le « *switch* angiogénique » (Parangi *et al.*, 1995).

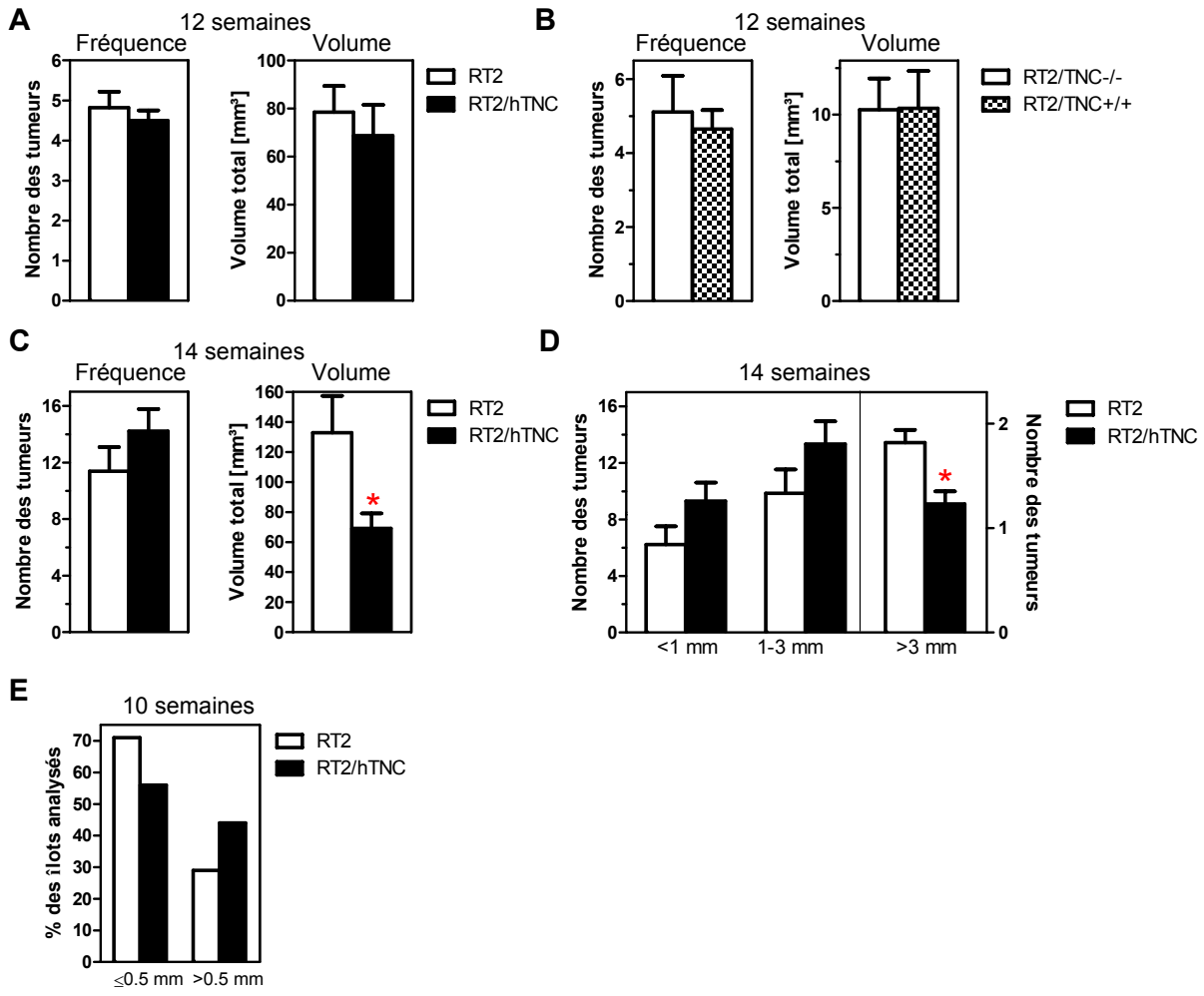

Figure 1 : Impact de la TNC sur la croissance tumorale

(A, B) Quantification macroscopique du nombre et du volume total des tumeurs d'un diamètre supérieur à 1 mm dans les pancréas des souris âgées de 12 semaines du modèle gain de fonction RT2/hTNC (A) et perte de fonction RT2/TNC-/- (B).

(C, D) Quantification du nombre et du volume total des tumeurs après dissection de toutes les tumeurs d'un diamètre supérieur à 1 mm des souris âgées de 14 semaines du modèle RT2/hTNC. (D) montre le nombre des différentes sous-classes de tumeurs en fonction de leur taille. (* $p \leq 0,05$)

(E) Fréquence des tumeurs ≤ 0,5 mm ou > 0,5 mm après classification en fonction de la taille. La quantification a été faite au niveau histologique dans des souris RT2 et RT2/hTNC âgées de 10 semaines. La distribution tend vers une différence significative ($p = 0,0629$; test de Fisher).

A la lumière de ces nouvelles observations, la TNC semble pouvoir constituer une cible thérapeutique potentielle pour le blocage de l'angiogénèse tumorale et de la dissémination métastatique. Dans cette perspective, les modèles de tumorigénèse en présence ou en l'absence de TNC, utilisés et développé au cours de cette étude représenterons d'excellents modèles pré-cliniques pour évaluer l'efficacité de nouveaux agents thérapeutiques ciblant la TNC humaine et les voies de signalisation sous-jacentes dans le but de limiter l'angiogénèse tumorale et la formation des métastases.

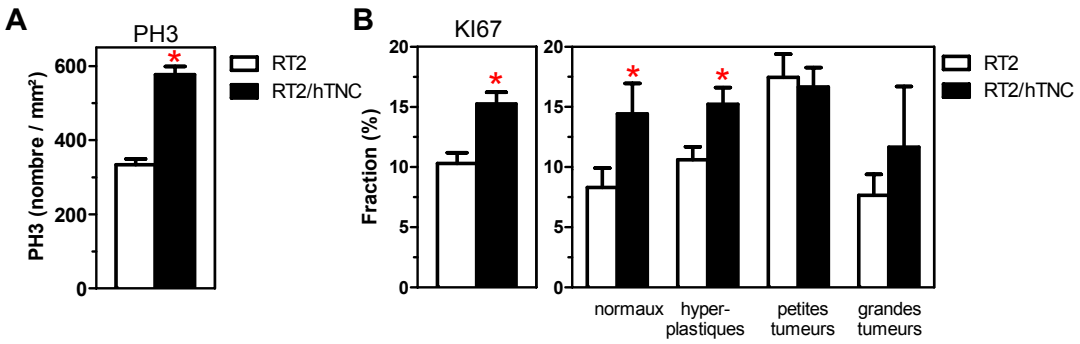

Figure 2 : Impact de la TNC sur la prolifération

(A, B) Quantification des marqueurs de prolifération PH3 (A) et KI67 (B) après immunomarquage des tissus tumoraux des souris RT2 et RT2/hTNC. (B) Pourcentage de cellules positives pour Ki-67 au sein des tumeurs classées selon leur taille (îlots normaux <0.2 mm, hyperplasiques 0.2-0.5 mm, petites tumeurs >0.5 – 1 mm, grandes tumeurs >1 mm). (* $p \leq 0,05$)

Bien que la TNC ne semblent pas avoir un impact significatif sur la croissance de cancer du sein (Oskarsson *et al.*, 2011; Talts *et al.*, 1999; Tavazoie *et al.*, 2008), les données obtenues ici dans le modèle RT2 indiquent que l'expression ectopique de la TNC stimule précocement la croissance tumorale, probablement en accélérant le « *switch* hyperplasique » et en favorisant la prolifération des tumeurs chez les souris RT2/hTNC.

Impact de la TNC sur l'angiogénèse tumorale:

L'angiogénèse est indispensable à la nutrition et l'oxygénation des cellules tumorales ainsi qu'à l'élimination des déchets métaboliques et joue donc un rôle crucial dans la croissance tumorale. La formation de nouveaux vaisseaux sanguins favorise également la formation de métastases et constitue une voie d'échappement permettant la dissémination des cellules cancéreuses et la colonisation d'organes secondaires. L'étude de la distribution de CD31, un marqueur spécifique des cellules endothéliales, nous a permis de mettre en évidence une augmentation de ce marquage dans les tumeurs RT2/hTNC par rapport aux tumeurs contrôles (Figure 3A). La même analyse a été réalisée dans le modèle RT2/TNC-/- (Figure 3B). Ces résultats suggèrent que la vascularisation des tumeurs est corrélée avec le nombre de copies de la TNC et que l'expression de la TNC favorise l'angiogénèse tumorale. En

outre, une analyse préliminaire par sous-classe de tumeurs dans le modèle RT2/TNC-/- a révélé que les îlots normaux et hyperplasiques sont plus angiogéniques dans les tumeurs des souris contrôles comparés avec des tumeurs qui n'expriment pas la TNC (Figure 3B). Ceci suggère que la TNC favorise l'angiogénèse à des stades précoces du développement tumoral.

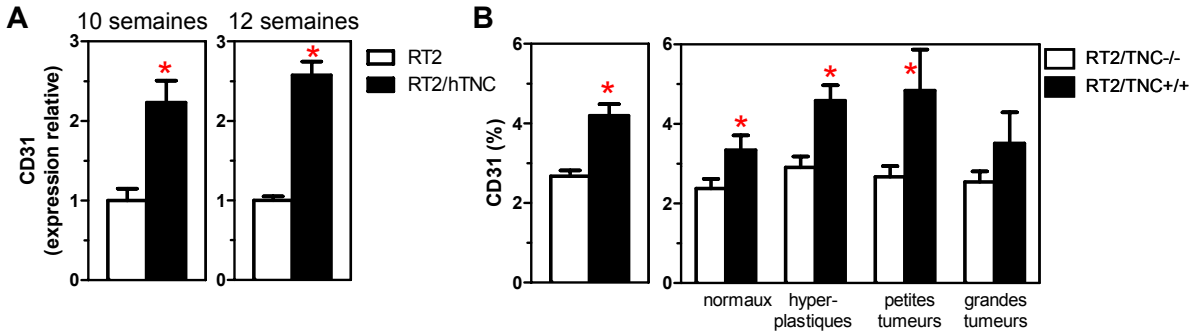

Figure 3 : Impact de la TNC sur l'angiogénèse tumorale

(A, B) Analyse de la vascularisation tumorale par quantification du marqueur endothélial CD31 après immunomarquage dans des tumeurs des souris du modèle RT2/hTNC âgées de 10 et 12 semaines (A) et des souris du modèle RT2/TNC-/- âgées de 12 semaines (B). (* $p \leq 0,05$)

L'analyse des empreintes vasculaires des tumeurs des souris RT2 et RT2/hTNC par microscopie électronique à balayage (MEB) a montré que l'expression forcée de la TNC perturbe l'organisation du réseau vasculaire tumoral. En outre, les vaisseaux sont plus perméables et les vaisseaux présents une densité de branchements accrue en comparaison à une tumeur contrôle (Figure 24, page 53). Ces observations soulèvent la question de la fonctionnalité du réseau vasculaire des tumeurs surexprimant la TNC. Les résultats préliminaires de la quantification du marqueur NG2, spécifique de la couverture péricytaire des vaisseaux tumoraux RT2 semble indiquer une diminution du nombre de péricytes dans les tumeurs surexprimant la TNC (Gasser I., communication personnelle). La couverture des vaisseaux sanguins par des cellules murales, telles que les péricytes, permet la maturation et la stabilisation des vaisseaux sanguins en régulant la prolifération de quelles CE et la circulation sanguine (Crocker *et al.*, 1970; Darland and D'Amore, 1999; Kutcher and Herman, 2009). Une diminution de la couverture péricytaire des vaisseaux tumoraux des tumeurs RT2/hTNC pourrait expliquer la vascularisation tumorale aberrante observée dans l'analyse des empreintes vasculaires par MEB. Finalement, il est possible que, dans les souris RT2/hTNC, une altération de la morphologie et la fonctionnalité du réseau vasculaire, et par conséquent la diminution de la perfusion tumorale, limite la croissance des tumeurs de forte taille.

Impact de la TNC sur l'invasion tumorale et la formation de métastases:

Dans le modèle RT2 une partie des lésions des îlots effectue un « *switch* angiogénique » qui permet le développement de tumeurs solides non-invasives ou de carcinomes invasifs, ces derniers étant à l'origine de la dissémination de cellules tumorales dans des organes distants. Chez les patients atteints d'un glioblastome multiforme (GBM), un fort taux d'expression de la TNC dans les tumeurs est associé au caractère invasif de la tumeur et l'expression stromale de la TNC est corrélée à une survie plus courte (Leins *et al.*, 2003; Sivasankaran *et al.*, 2009). Un effet de la TNC sur la migration de cellules de GBM avait précédemment été décrit. En effet, la culture de cellule de GBM sur une matrice enrichie en TNC stimule la migration induite par LPA/PDGF en provoquant un état d'attachement modéré. (Lange *et al.*, 2008). Ces résultats illustrent le potentiel pro-migratoire de la TNC vis-à-vis des cellules cancéreuses (Chiquet-Ehrismann and Tucker, 2011).

Une évaluation du pourcentage d'adénomes et de carcinomes invasifs nous a permis de mettre en évidence que les souris RT2/hTNC présentant une expression ectopique de la TNC développent une proportion accrue de tumeurs invasives par rapport aux souris contrôles RT2 (Manuscrit 1 Fig. 1E, page 116 et suivants), suggérant une plus forte propension à former des métastases. L'impact potentiel de la TNC sur la formation de micrométastases hépatiques et pulmonaires a été évalué par quantification des taux d'ARN de l'insuline, utilisée comme marqueur spécifique des cellules tumorales. Ces expériences ont révélé qu'une partie des souris analysées développent des micrométastases au niveau du foie et des poumons, un résultat confirmé par immunomarquage de l'insuline. Pour autant, aucune différence significative en terme de développement métastases hépatiques n'a pu été observée en fonction du niveau d'expression de la TNC. Néanmoins, les taux d'expression de l'insuline étaient beaucoup plus élevés dans les poumons des souris présentant une forte expression de la TNC (Figure 4A, B).

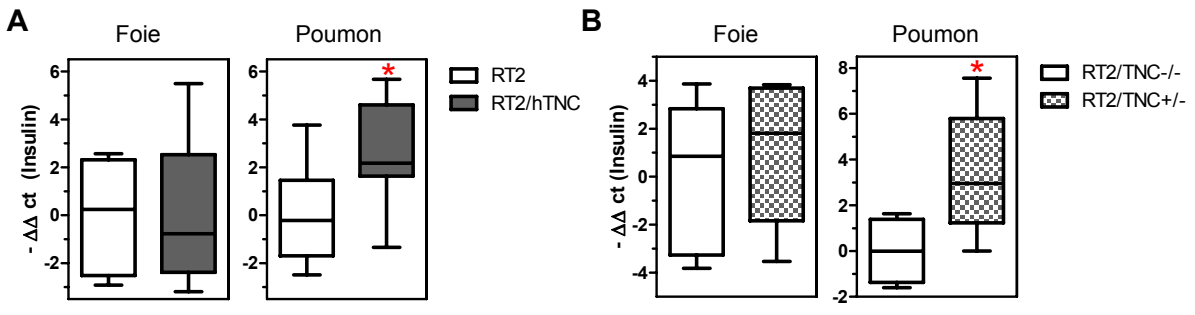

Figure 4 : Impact de la TNC sur la formation des métastases

(A, B) Quantification des micrométastases au niveau du foie et poumon par RT-qPCR pour insuline, utilisée comme marqueur spécifique des cellules tumorales dans des échantillons isolés à partir de souris RT2/hTNC (A) et RT2/TNC-/- (B). (* p ≤ 0,05)

Ces résultats sont en accord avec des études ayant précédemment décrit un lien direct entre l'expression de la TNC et la formation de métastases pulmonaires suite à l'injection en intraveineuse de cellules de cancer du sein en modèles murins (Calvo *et al.*, 2008; Minn *et al.*, 2005; Tavazoie *et al.*, 2008) ou encore dans des modèles de mélanome (Fukunaga-Kalabis *et al.*, 2010). Chez les patients atteints d'un cancer du sein, une forte expression de la TNC dans les tumeurs primaires est corrélée à une réduction de la survie, et une forte expression basale de la TNC confère un avantage sélectif aux cellules cancéreuses dans le microenvironnement pulmonaire par rapport aux cellules dont l'expression de la TNC est réprimée (Oskarsson *et al.*, 2011).

Mécanismes moléculaires d'action de la TNC dans le modèle RT2:

Un autre objectif important de ce travail de thèse à consisté à déterminer au niveau moléculaire les mécanismes d'action de la TNC dans le modèle RT2. La voie de signalisation Wnt/β-caténine jouant un rôle important dans la tumorigénèse (Barker and Clevers, 2006) et dans l'angiogénèse (Franco *et al.*, 2009), nous avons étudié son état d'activation dans les tumeurs des souris RT2 et RT2/hTNC en réalisant un immunomarquage de la β-caténine (Manuscrit 1 Fig. 4C, pages 116 et suivants).

Certaines tumeurs développées par les souris RT2/hTNC présentaient un marquage nucléaire de la β-caténine, un évènement qui n'a pas pu être observé dans les souris contrôles RT2. Aucune différence d'expression de la β-caténine n'a été détectée au niveau transcriptionnel entre les tumeurs RT2 et RT2/hTNC (Tableau 5, page 78). Dickkopf-1 (DKK1), une protéines sécrétée décrite comme un antagoniste de la voie canonique Wnt/β-caténine, est fortement réprimé dans des cellules de glioblastome cultivées *in vitro* sur un substrat de la TNC (Ruiz *et al.*, 2004). Par conséquent, nous avons également évalué l'expression de DKK1 par RT-qPCR dans des tumeurs isolées. Nous montrons ainsi que le nombre de copies de la TNC est inversement proportionnel au niveau d'expression de DKK1, suggérant un lien fonctionnel et une potentielle activation de la voie Wnt/β-caténine suite à la répression de DKK1 par la TNC (Figure 5). Dans le modèle RT2/hTNC, l'expression de plusieurs gènes cibles de la voie Wnt/β-caténine (cyclinD1, cyclinD2, CD44, Slug) est induite dans les adénomes (Figure 5A). En outre, des expériences de culture de lignées cellulaires cancéreuses sur un substrat matriciel enrichi en TNC ont confirmé sa fonction dans l'inhibition de l'expression de DKK1 et dans l'induction de plusieurs gènes cibles de la voie Wnt/β-caténine, notamment dans des cellules de GBM et d'ostéosarcome (Manuscrit 1 Fig. 6C, D, Suppl. Tableau 4, pages 116 et suivants). En résumé, ces résultats préliminaires suggèrent une activation potentielle de la voie Wnt/β-caténine suite à l'inhibition de DKK1 par la TNC.

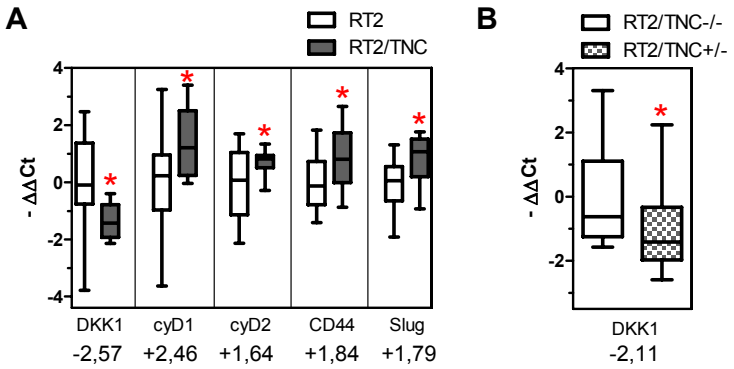

Figure 5 : Activation potentielle de la voie de signalisation Wnt/β-caténine dans le modèle RT2

(A) Quantification de l'expression de l'inhibiteur de la voie Wnt DKK1 et des gènes cibles potentielles de la voie Wnt/β-caténine par RT-qPCR dans des adénomes (> 1 mm) des souris RT2 et RT2/hTNC. (* $p \leq 0,05$)

(B) Quantification *d'*expression de l'inhibiteur de la voie Wnt DKK1 par RT-qPCR dans des tumeurs (> 1 mm) des souris du modèle RT2/TNC-/- avec perte d'expression de la TNC. (* $p \leq 0,05$)

Par ailleurs, il est possible que les faibles taux d'expression de DKK1 influencent également des cellules présentes dans le stroma tumoral. Cette hypothèse est confortée par des expériences de xénogreffes sous-cutanées de cellules d'ostéosarcome KRIB surexprimant DKK1 (KRIB:DKK1). Alors que la surexpression de DKK1 n'affecte pas la prolifération des cellules en culture, les xénogreffes de cellules KRIB:DKK1 aboutissent à la formation de petites tumeurs faiblement vascularisées, par opposition aux xénogreffes de cellules KRIB parentale qui forment de grandes tumeurs richement vascularisées (Manuscrit 1 Fig 7, page 116 et suivants). Ces observations suggèrent que la répression de DKK1, induite par la TNC dans les cellules tumorales, pourrait exercer un effet paracrine sur des cellules présentes au sein du microenvironnement de la tumeur, telles que les CE, les CAF ou encore d'autres cellules stromale exerçant une activité pro-angiogéniques. Des expériences *in vitro* de co-culture sont actuellement menées pour déterminer si une diminution de l'expression de DKK1 dans les cellules tumorales, dépendante de la TNC, peut activer la voie Wnt/β-caténine dans les cellules non-tumorales (A. Heinke, doctorante).

Dans la littérature, des expériences *in vitro* ont permit d'établir que la TNC pouvait exercer un chimiotactisme vis à vis des CE, jouer un rôle dans la différentiation de cellules tumorales en CE (Pezzolo *et al.*, 2011) ou encore favoriser la formation de tubes à partir de CE (Martina *et al.*, 2010; Schenk *et al.*, 1999). De plus, des travaux ont mis en évidence un défaut de revascularisation dans des expériences d'allogreffes cardiaques dans des souris KO pour la TNC, illustrant sa fonction dans la migration des CE (Ballard *et al.*, 2006). La greffe de cellules de mélanomes dans des souris n'exprimant pas la TNC génère des tumeurs faiblement vascularisées et s'accompagne d'une expression réduite du VEGF-A (Tanaka *et al.*, 2004). Enfin, des expériences *in vitro* ont révélé que la TNC peut induire

l'expression et la signalisation de facteurs pro-angiogéniques, tels que EDNRA et PDGFRα dans une lignée cellulaire de GBM (Ruiz *et al.*, 2004). Pour déterminer quels facteurs angiogéniques sont modulés par la TNC dans les tumeurs RT2, les taux de transcrits de plusieurs facteurs pro-angiogéniques (VEGFA, VEGF-R1/2/3, EDNRA, PDGFRα, EphA2, Hey1, Dll4) ont été évalués dans les tumeurs bien développés avaient déjà effectué le « *switch* angiogénique » empêchant de fait l'analyse d'effets précoces de la TNC sur l'angiogénèse tumorale. Néanmoins, aucun des marqueurs analysé ne semble significativement modulé dans nos conditions expérimentales (Tableau 5, page 78). Une limitation potentielle des expériences menées pourrait résider dans une action localisée au sein de la tumeur, rendant discrète une modulation transcriptionnelle sur des insulinomes entiers.

La répression de DKK1 pourrait constituer une base moléculaire alternative expliquant l'augmentation de l'angiogénèse par la TNC. L'impact de DKK1 sur l'angiogénèse tumorale demeure un sujet de controverse. En effet, si un traitement *in vivo* des tissus mésentériques par DKK1 semble exercer un effet pro-angiogénique en favorisant le recrutement de CE progénitrices (Aicher *et al.*, 2008; Smadja *et al.*, 2010) (Glaw *et al.*, 2010), d'autres auteurs ont montré que DKK1 supprime l'angiogénèse induite par le VEGFA dans un modèle *in vitro* de tubulogénèse sur Matrigel (Min *et al.*, 2011).

Des expériences de xénogreffe menées semblent indiquer que la surexpression de DKK1 dans les cellules d'ostéosarcome KRIB bloque la croissance tumorale, vraisemblablement suite à l'inhibition de l'angiogénèse. Ces résultats soutiennent le concept, suggéré par Min *et al,* d'une corrélation inverse entre l'expression de DKK1 et l'angiogénèse tumorale. De façon comparable, le faible niveau d'expression de DKK1 dans les tumeurs développées par les souris RT2/hTNC pourrait expliquer l'augmentation de l'angiogénèse tumorale. *In vitro,* le niveau d'expression DKK1 est fortement inhibé dans des cellules de GBM, d'ostéosarcome, ainsi que dans d'autres lignées cellulaire tumorales cultivées sur un substrat riche en TNC (A. Heinke, communication personnelle). L'ensemble de ces expériences suggère que la répression de DKK1 par la TNC favorise l'angiogénèse tumorale.

Pour découvrir les mécanismes d'action de la TNC dans les étapes précoces de la tumorigenèse, une analyse transcriptionnelle a été réalisée sur des îlots tumoraux non-angiogéniques et angiogéniques purifiés à partir de souris RT2 et RT2/hTNC de 8 semaines, stade auquel s'effectue le « *switch* angiogénique », puis analysés en utilisant le système Affymetrix. Le comptage des îlots isolés a révélé que les souris transgéniques surexprimant la TNC présentent deux fois plus d'îlots angiogéniques que les souris contrôles RT2 (Figure

6A). Cela confirme l'effet pro-angiogénique de la TNC mis en évidence par quantification de l'immunomarquage de CD31 (Figure 3).

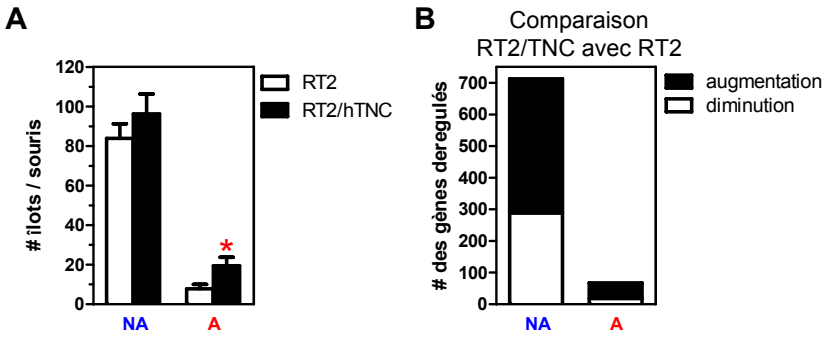

Figure 6 : Mécanismes moléculaires d'action de la TNC dans le modèle RT2

(A) Quantification du nombre d'îlots non-angiogéniques (NA) et angiogéniques (A) dans les pancréas isolés à partir des souris RT2 et RT2/hTNC âgées de 8 semaines. Des souris RT2/hTNC contenaient 2,5 fois plus des îlots angiogéniques que des souris RT2 (* p = 0,023).

(B) Nombre de gènes dérégulés par la TNC dans les îlots non-angiogéniques (NA) et angiogéniques (A).

Si une analyse plus détaillée des gènes cibles doit être complétée, l'hypothèse selon laquelle la TNC joue un rôle important dans la tumorigénèse précoce est soutenue par le fait que près de 10 fois plus de gènes sont dérégulés par la TNC dans les îlots non-angiogéniques par rapport aux îlots angiogéniques (Figure 6B). Néanmoins, ces résultats préliminaires ne semblent pas indiquer une dérégulation des marqueurs « classiques » (par exemple VEGF-A, VEGF-R1/2/3, EDNRA, PDGFRα) de l'angiogénèse suite à la surexpression de la TNC (Tableau 7, page 95). Il est possible que des processus pro-angiogéniques soient déjà activés dans les îlots non-angiogéniques des souris de 8 semaines. Ces données nous amène toutefois à envisager que le programme pro-angiogénique soit mis en place très précocement pendant l'initiation de la tumorigénèse. Afin de tester cette hypothèse, une autre analyse transcriptionnelle a été réalisée sur des îlots pancréatiques normaux de souris non-tumorigéniques Rip-hTNC et de souris sauvage. L'expression forcée de la TNC dans les îlots normaux induit l'expression de nombreuses cytokines et chimiokines régulant le système immunitaire, suggérant une implication potentielle de la TNC dans une signature inflammatoire (Tableau 9, page 107). Des BMDC, telles que les neutrophiles et les macrophages pourraient contribuer à l'angiogénèse induite par la TNC. Dans le modèle RT2, il a été montré que les neutrophiles sont capables de provoquer le « *switch* angiogénique » (Nozawa *et al.*, 2006). Bien qu'une telle signature ne soit pas présente dans les îlots non-angiogéniques des souris RT2/hTNC de 8 semaines, les résultats obtenus sur les îlots normaux Rip-hTNC pourraient être reproduits dans le modèle RT2 dans des stades précoces de la tumorigénèse. Pour affiner ces résultats et tester cette hypothèse, nous envisageons d'étudier dans quelle mesure l'angiogénèse induite par la TNC dans les îlots

normaux et hyperplasiques est corrélable à une augmentation de l'infiltrat de cellules immunitaires dans les tissus tumoraux présentant différents niveaux d'expression de la TNC dans des souris RT2 de 5 semaines, qui n'ont pas encore effectué le « *switch* angiogénique ».

En conclusion, l'utilisation de modèles RT2 présentant différents niveaux d'expression de la TNC nous a permis de montrer que le nombre de copies de la TNC est inversement lié au niveau d'expression de DKK1, l'antagoniste de la voie Wnt/β-caténine. Cependant une activation de la voie Wnt/β-caténine spécifique des cellules tumorales n'a pas pu être démontrée. Des expériences préliminaires réalisées au laboratoire suggèrent un lien entre DKK1 et la vascularisation des tumeurs. En effet, son expression accrue dans les tumeurs formées par les cellules d'ostéosarcome induit une inhibition de la croissance tumorale qui semble reposer sur un défaut de l'angiogénèse. En outre, les premiers résultats d'un criblage transcriptionnel semblent indiquer que la tumorigénèse précoce induite par la TNC pourrait reposer sur la mise en place d'une réponse inflammatoire en faveur de la progression des insulinomes.

<u>L'organisation de la TNC dans le tissu cancéreux et son rôle dans l'angiogenèse tumorale:</u>
Pour préciser la distribution et l'organisation de la TNC dans les tumeurs RT2 nous avons réalisé des immunomarquages à l'aide d'anticorps spécifiquement dirigés contre la TNC. Nous avons remarqué que la TNC n'est pas exprimée de façon homogène au sein des tumeurs, mais présente une distribution privilégiée au sein de structures matricielles tubulaires ou conduits, répartis dans l'ensemble de la tumeur. Nous avons également constaté que la nature de ces structures est complexe et hétérogène : le diamètre de ces conduits varie entre 5 et 30 µm, ils peuvent présenter des formes cylindriques ou irrégulières, et présentent dans certains cas une lumière centrale. Parfois, d'autres molécules de la MEC (laminine, fibronectine, collagène) sont co-exprimées avec la TNC. De plus, certains constituants des vaisseaux sanguins, telles que les CE et la membrane basale, sont absents de ces conduits matriciels. D'autres types cellulaires du stroma comme des fibroblastes ou des macrophages associés aux tumeurs peuvent être étroitement associés à ces structures (Tableau 4, page 74). Des expériences de perfusion de dextran couplé au FITC suggèrent une connexion de certains de ces conduits riches en TNC avec la circulation sanguine (Figure 27, page 58), ce semble être confirmé par microscopie électronique à transmission (Figure 25D, page 55).

En résumé, la TNC participe à la formation de conduits matriciels intra-tumoraux qui pourraient constituer des supports au cours de l'angiogénèse, offrir des voies d'accès privilégiées pour le trafic de cellules immunitaire ou encore favoriser la dissémination et la

formation des métastases. L'étude du modèle RT2 en absence d'expression de la TNC, récemment développé au laboratoire, permettra de déterminer si la présence de la TNC est essentielle pour la formation de ces conduits intra-tumoraux, et d'en préciser la structure, la composition et la fonction.

Conclusions et perspectives:

Dans cette étude, nous montrons pour la première fois dans le modèle RT2 immunocompétent de formation de tumeurs spontanées, que le niveau d'expression de la TNC est déterminant pour la prolifération cellulaire, l'angiogénèse tumorale, l'invasion et la formation de métastases. Les données rassemblées dans les modèles RT2/hTNC et RT2/TNC-/- illustrent que la signalisation dépendante de la TNC joue un rôle prépondérant dans l'initiation de la tumorigénèse, notamment au cours du « *switch* angiogénique ». La répression de DKK1, l'inhibiteur de la voie Wnt/β-caténine, constitue une base moléculaire pour expliquer les mécanismes d'action de la TNC en faveur de la progression des tumeurs. Enfin, l'étude de la vascularisation tumorale et de la distribution de la TNC au sein des tumeurs neuroendocrines nous permet de montrer sa fonction dans le contrôle de l'architecture des vaisseaux tumoraux et a révélé un profil d'expression spécifique au sein de conduits matriciels potentiellement reliés à la circulation sanguine (Figure 7).

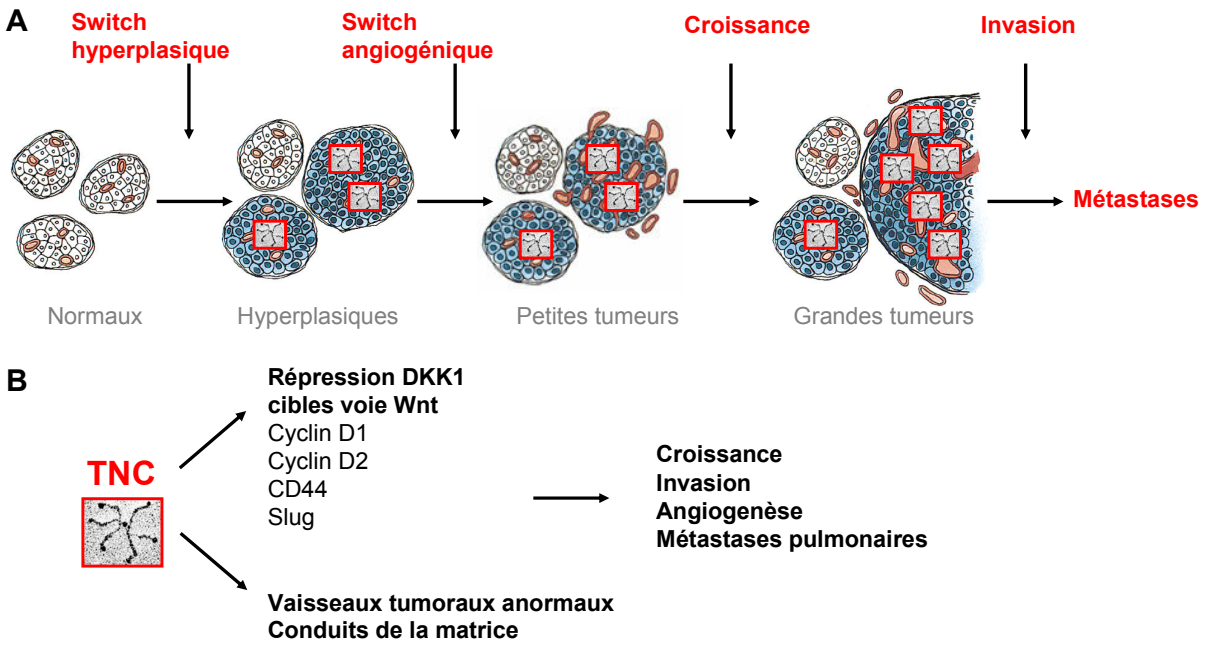

Figure 7 : Impact de la TNC sur la progression tumorale dans le modèle RT2

Schéma illustrant le rôle promoteur de la TNC dans différentes étapes de la progression tumorale dans le modèle RT2 (A). Schéma adapté à partir de Hanahan et Folkman, 1996. La TNC exerce une fonction de signalisation en réprimant DKK1, favorisant ainsi la progression tumorale. La TNC contrôle également l'architecture des vaisseaux tumoraux et participe à la formation de conduits matriciels qui pourraient favoriser la formation des métastases (B). Insert : Micrographe électronique d'un hexamère de TNC visualisé par ombrage rotatoire (Chiquest-Ehrisman and Chiquet 2003).

A la lumière de ces nouvelles observations, la TNC semble pouvoir constituer une cible thérapeutique potentielle pour le blocage de l'angiogénèse tumorale et de la dissémination métastatique. Dans cette perspective, les modèles de tumorigénèse en présence ou en l'absence de TNC, utilisés et développé au cours de cette étude représenterons d'excellents modèles pré-cliniques pour évaluer l'efficacité de nouveaux agents thérapeutiques ciblant la TNC humaine et les voies de signalisation sous-jacentes dans le but de limiter l'angiogénèse tumorale et la formation des métastases.

Manuscript and other scientific contributions

Manuscript 1

This thesis is in part based on the following manuscript (see Annex on page 129) which was last modified in April 2011. Since then, new results from our own experiments and newly published work of other laboratories will require the adaptation of this manuscript. These new aspects are in part presented and discussed in the thesis and will be included later.

Saupe F.*, Gasser I.*, Jia Y.*, Heinke A., Kammerer M., Hussenet T., Marko M., Lefebvre O., van der Heyden M., Hegi M., Hlushchuk R., Kant J., Huang W., Feutz A-C., Simon-Assmann P., Kedinger M., Djonov V., Christofori G. and Orend G. Tenascin-C promotes tumor angiogenesis and metastasis through repression of Dickkopf-1. **Manuscript in preparation**. (* equal contribution).

Together with M. van der Heyden, I organized the mouse work and set up breeding and genotyping of the mice. I performed the glucose-tolerance test of Rip-hTNC and wildtype mice. Already obtained data in the RT2/hTNC model (tumor growth, proliferation, angiogenesis) were statistically reanalyzed and completed with new experiments. I set up sampling and analysis on 14 weeks old RT2/hTNC mice. qRT-PCR analysis on tumor, liver and lung tissue was performed together with M. Kammerer. I organized the backcrossing of 129/Sv TNC-/- mice into the C57BL6 background to generate a RT2/TNC-/- mouse colony in the C57BL6 mouse strain and I analyzed preliminary samples out of this colony.

Contributions to published articles during the thesis

Van Obberghen-Schilling E., Tucker R.P., **Saupe F.**, Gasser I., Cseh B. and Orend G. (**2011**). Fibronectin and Tenascin-C: Accomplices in Vascular Morphogenesis during Development and Tumor Growth. *Int J Dev Biol*., In press (doi: 10.1387/ijdb.103243eo).

I contributed to this review by summarizing published articles concerning the TNC knockout mouse models which had been generated in two different laboratories.

Lange K., Kammerer M., **Saupe F.**, Hegi M.E., Grotegut S., Fluri E., and Orend G. (**2008**). Combined lysophosphatic acid/platelet-derived growth factor signaling triggers glioma cell migration in a tenascin-C microenvironment. *Cancer Research 68*, 6942-6952.

During the first six months of the thesis I was implicated in the *in vitro* experiments showing that LPA/PDGF signaling initiates glioma cell spreading and migration through syndecan-4 independent activation of paxillin and FAK. I performed gene silencing in T98G cancer cells for paxillin and showed that paxillin function is essential for LPA/PDGF-induced cell spreading on a FN/TNC substratum and for syndesmos-triggered spreading on a FN/TNC substratum. I showed that TNC induced cell rounding is a general effect in several other cancer cell lines.

Contents

List of figures

List of tables

Abbreviations

Abbreviations and symbols

Ø	diameter
%	percentage
3D	three dimensional
BM	basement membrane
BMDC	bone marrow-derived cells
CAF	cancer-associated fibroblast
CAM	chick chorioallantoic membrane
cDNA	complementary deoxyribonucleic acid
ct	cycle threshold
DAPI	4',6-diamidino-2-phenylindole
DMEM	Dulbecco's modified eagle medium
EC	endothelial cells
ECM	extracellular matrix
EMT	epithelial mesenchymal transition
EPC	endothelial progenitor cells
FCS	fetal calf serum
FITC	fluorescein isothiocyanate
GBM	glioblastoma multiforme
GOI	gene of interest
H&E	hematoxylin and eosin
IF	immunofluorescence
IHC	immunohistochemistry
Mercox	methylmethacrylate
miR	microRNA
NGS	normal goat serum
PBS/T	phosphate buffered saline / tween
PCR	polymerase chain reaction
PFA	paraformaldehyde
qRT-PCR	quantitative reverse transcriptase polymerase chain reaction
Rip	rat insulin promoter
RNA	ribonucleic acid
SDS-PAGE	sodium dodecyl sulfate polyacrylamide gel electrophoresis
SEM	scanning electron microscopy
S.E.M.	standard error of the mean
TEM	transmission electron microscopy
vs.	versus
w	weeks

Abbreviations of gene and protein names

Ang1 / -2	angiopoietin-1 / -2
CD31	cluster of differentiation 31 alias Pecam1 (platelet endothelial cell adhesion molecule 1)
DKK1	Dickkopf related protein 1
Dll4	delta like ligand 4
E-cad	E-cadherin
EDNRA	endothelin receptor type A
EGFR	epidermal growth factor receptor
EphA2	ephrin type-A receptor
FGF	fibroblast growth factor
FN	fibronectin
GAPDH	glyceraldehyde-3-phosphate dehydrogenase
Glp1r	glucagon-like peptide 1 receptor
Hey1	hairy/enhancer-of-split related with YRPW motif protein 1
HIF	hypoxia inducible factor
Id2	inhibitor of DNA binding 2
Insm1	insulinoma-associated 1
Jag1	jagged 1
LM	laminins
Lgr5	leucine-rich repeat containing G protein-coupled receptor 5
Notch2	neurogenic locus notch homolog protein 2
PDGFRα	platelet-derived growth factor receptor, alpha polypeptide
PlGF	placental growth factor
PH3	phospho-histone-H3
RPL9	ribosomal protein 9
Slug	snail homolog 2
Sox4	SRY (sex determining region Y)-box 4
SV40 Tag	simian virus 40 large T-antigen
Syn	Synaptophysin
Tag	T antigen
TGF	transforming growth factor
Tie2	TEK tyrosine kinase
TBP	TATA box binding protein
TNC	tenascin-C
VEGFA	vascular endothelial growth factor A
VEGF-R	vascular endothelial growth factor receptor

Mouse models

Rip-hTNC	single-transgenic mice with transgenic expression of human TNC in pancreatic β-cells
RT2	Rip1-Tag2
RT2/hTNC	Rip1-Tag2 over-expressing human TNC
RT2/TNC-/-	Rip1-Tag2 with TNC knockout
RT2/TNC+/-	Rip1-Tag2 with one TNC gene
RT2/TNC+/+	Rip1-Tag2 with two TNC gene copies (wildtype TNC expression)

1 Introduction

Cancer is the uncontrolled growth of cells in a given tissue to a cell mass which, in some cases, spread throughout the body to form metastasis, leading to death. The oldest description of cancer can be found in the Egyptian Edwin Smith Papyrus and dates back to approximately 1600 before Christ (B.C.) depicting the surgical treatment of ulcers in the breast by cauterization (Greaves, 2000). The word 'cancer' dates back to 400 years B.C. to the Greek physician Hippocrates of Cos who was one of the first describing cancer as a specific disease. The term 'cancer' refers to the Greek word *carcinos* (crab), based on the crab-like appearance of blood vessels of the cut surface of a tumor. Nowadays, cancer is a leading cause of death with about 8 million of new diagnoses each year worldwide (WHO, 2008). This short historical summary shows that cancer is not a new disease of the modern and developing world but it had become a major health issue in all societies worldwide.

Cancer is a class of several diseases dependent on the cell type initially affected. The course of this pathology depends on many different factors including the affected tissue type, gender, genetic conditions and environmental influences. PubMed, the database for references on life science and biomedical topics, lists more than 2.5 million scientific articles for the keyword "cancer", demonstrating the deep interest of the scientific community to better understand the causes and incidences of individual cancers and the need to find new therapies. In most cases, cancer is not a hereditary disease but is primarily caused by environmental factors, which can explain the high diversity of cancer and the unique course of disease in individual patients. Metastasis, the spread of cancer to other organs, is the most frequent reason for death in cancer patients (Sporn, 1997).

Cancer is known and studied for long and many insights have been obtained, mainly thanks to technical advances during the last century. But the disease remains a mystery and an efficient therapy is still missing for many aggressive cancer types. In the last two decades several key steps have been defined which are necessary for the development of cancer whereas the tumor cells do not autonomously dictate tumor growth and formation of metastasis but also the tumor microenvironment plays a crucial role. One component of the tumor microenvironment is the extracellular matrix. Extracellular matrix (ECM) is the non-cellular and insoluble part of a tissue providing structural support but also playing a role in many other functions in normal tissues and in disease. The ECM molecule tenascin-C (TNC) is part of the microenvironment in the developing embryo and it reemerges in pathological situations including cancer.

In the following, the key components during tumor development will be introduced with focus on tumor angiogenesis and the role of the tumor microenvironment in cancer. Next, the implication of TNC in tumor progression will be summarized. Finally, the principal characteristics of the mouse model of pancreatic neuroendocrine cancer, which was used to study the role of TNC during tumor progression, will be described.

1.1 Key processes during cancer progression

Although cancer is a very complex disease it is now understood as a multi-step process following a minimum of principles that control the transformation of normal cells into malignant cancers. These acquired capabilities of cancer have been formulated about ten years ago by recapitulating the progress in cancer research (Hanahan and Weinberg, 2000) which was recently updated (Hanahan and Weinberg, 2011). These hallmarks are based on the modification of the normal molecular program of a cell, leading to uncontrolled cell growth and cell mass expansion, tumor growth, angiogenesis, tumor cell invasion and metastasis.

1.1.1 The first step toward cancer

The initial step of cancer requires an accumulation of gene mutations leading to uncontrolled cell growth. Genetic predisposition explains only 5-10% of cancer whereas most of the cases are caused by environmental factors such as smoking, diet, infections, radiation, stress or physical inactivity (Anand *et al.*, 2008). It is believed that a single mutation alone cannot induce cancer but that a sequential accumulation of several mutations is necessary which need to be passed to and kept by the daughter cells. For example, it was estimated in colon cancer that at least five genetic alterations are needed to develop cancer (Fearon and Vogelstein, 1990). Genetic alterations can affect oncogenes, tumor suppressor genes or so-called caretaker and gatekeeper genes. Normal functions of these genes are intracellular signaling, regulation of transcription, cell cycle progression or DNA repair. Gain-of-function mutations shift oncogenes to a permanent active state leading to enhanced cell division. Loss-of-function in tumor suppressor genes avoids their implication in slowing down cell division and triggering apoptosis. Caretaker genes are mainly implicated in DNA repair and known as stability genes. Gatekeeper genes act to prevent mutations in genes which lead to enhanced proliferation. But mutations in caretaker and gatekeeper genes alone cannot cause cancer. Beside direct genetic mutations which can include DNA mutations at nucleotide or chromosomal level, cancer genetics is much more complex than described here including epigenetic modifications, the effect of other genes which modify the effect of

the mutated genes, the interaction with other cell types and immune responses (Ponder, 2001).

1.1.2 Cell proliferation and tumor growth

The above described genetic mutations provoke changes in the normal cell program modifying the normal homeostasis between cell division, apoptosis and senescence. This allows division and amplification of tumor cells and the growth of a tumor cell mass. In normal tissues, this balance is sustained by signals from neighboring cells and by the release of growth factors from the pericellular space and the ECM. Three of the established hallmarks of cancer implicate the ability of cancer cells to sustain proliferative signaling, to evade growth suppressors and to resist cell death (Hanahan and Weinberg, 2011).

A cancer cell may regulate their own proliferation by stimulating normal neighboring cells to produce growth factors, by autocrine stimulation with growth factors produced on its own or by regulation of the implicated surface receptors. On the other hand, tumor cells need to escape growth suppressing mechanisms that would negatively regulate cell proliferation through the activity of tumor suppressors. The best known tumor suppressors are retinoblastoma-associated (RB) (Murphree and Benedict, 1984) and TP53 (Linzer and Levine, 1979). RB regulates entry into the cell cycle and functions as a break. TP53 controls DNA damages and can trigger DNA repair or apoptosis. TP53 is often mutated in various cancers but its mutation alone cannot trigger cancer. Apoptosis, programmed cell death, is tightly regulated by extrinsic or intrinsic signals to carry out the apoptotic program. This cellular program protects the organism from aberrant proliferation in normal conditions. Disturbance of the homeostasis between pro-survival and pro-apoptotic proteins is often oncogenic (Adams and Cory, 2007). But tumorigenic cells do not readily cause cancer if they are kept silent. This so-called state of “tumor dormancy” is largely determined by tissue homeostasis. Several mechanisms such as angiogenic dormancy, cellular dormancy or immunosurveillance determine if a small and non-invasive tumor lesion develops into a macroscopic tumor (Aguirre-Ghiso, 2007; Almog, 2010).

1.1.3 Angiogenesis

Vasculogenesis is the formation of new blood vessels during embryogenesis. In the adult, angiogenesis is the process of formation of new blood vessels from preexisting vessels through sprouting or non-sprouting angiogenesis. Sprouting angiogenesis (**Figure 1A**) is induced in endothelial cells (EC) through signals such as vascular endothelial growth factor (VEGF) (Wilting *et al.*, 1993). An EC forms a tip cell by developing filopodia and acquiring a

motile behavior, thus guiding the new vessel sprout. During sprout extension, tip cells will contact other vessels or other tip cells and establish new connections, form a lumen and convert into new blood-perfused vessels. Additional EC are generated by proliferation and new sprouting is initiated at other sites (**Figure 1A**). Non-sprouting angiogenesis is a mode of capillary formation by vessel splitting, also called intussusceptive angiogenesis (**Figure 1B**). This includes the following steps: 1) opposing capillary walls perform protrusion into the lumen and create a contact between the endothelial cells, 2) reorganization of intercellular junctions and central perforation of the endothelial bilayer, 3) formation of an interstitial pillar, 4) invasion by myofibroblasts or pericytes and deposition of matrix.

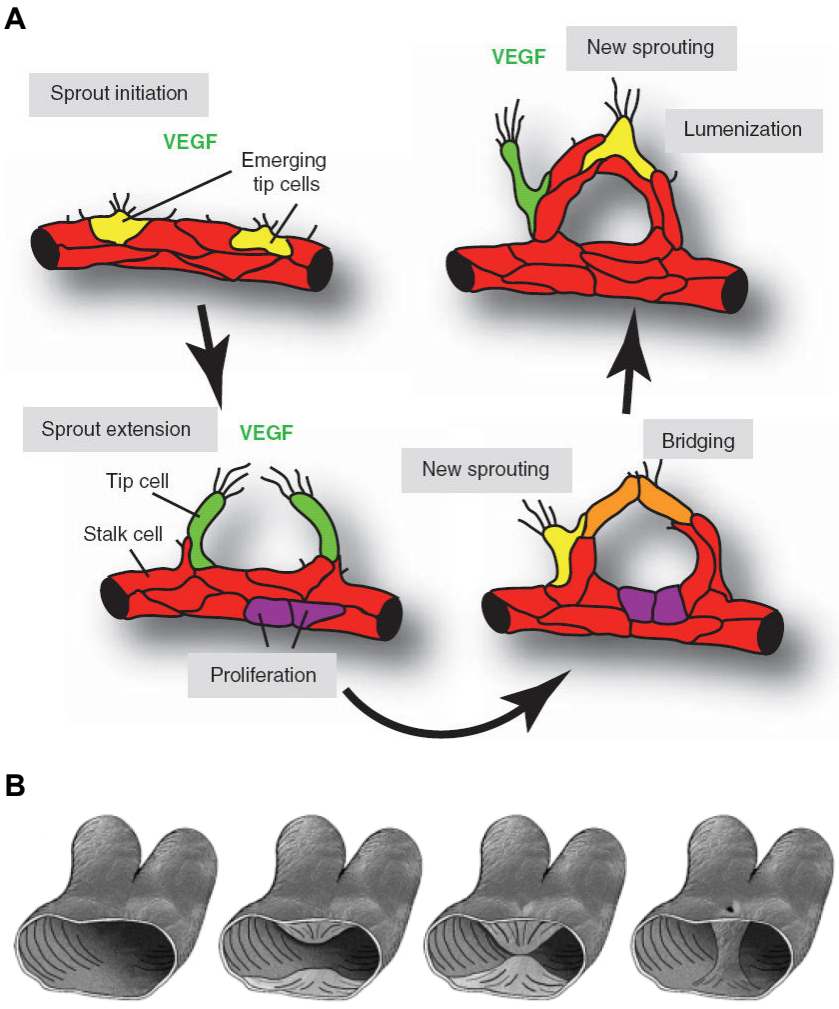

Figure 1: Principle steps of sprouting angiogenesis and intussusception angiogenesis

(A) Sprouting angiogenesis. Taken from (Adams and Eichmann, 2010)
(B) Intussusception angiogenesis. Taken from (Kurz *et al.*, 2003)

Both types of angiogenesis also occur during tumor angiogenesis but during the last decade several new concepts of vessel formation in tumors have been described (Carmeliet and Jain, 2011a). Vasculogenesis can be reactivated in cancer in the adult tissue (postnatal vasculogenesis) and involves vascular-wall-resident endothelial progenitor cells (EPC) or the

recruitment of bone marrow-derived cells (BMDC) (Dome *et al.*, 2007) (**Figure 2b**). By vessel co-option tumor cells compass existing vessels of the previously normal tissue (**Figure 2d**). This mode of angiogenesis can be observed for example during astrocytoma progression (Vajkoczy *et al.*, 2002). In vasculogenic mimicry, the plasticity of some cancer cells allows them to mimic the activity of EC and participate in the formation of neovessels and fluid-conducting networks (**Figure 2e**). This mode of tumor angiogenesis can be observed in melanomas (Maniotis *et al.*, 1999), in uveal carcinoma (Seftor *et al.*, 2002), in astrocytoma (Yue and Chen, 2005) and in many other cancer types (Hendrix *et al.*, 2003). Recently, it was described in brain tumors that tumor vascularization can occur via differentiation of stem cell-like tumor cells which gave rise to a tumor endothelium (Ricci-Vitiani *et al.*, 2010; Wang *et al.*, 2010) (**Figure 2f**). The molecular mechanisms which regulate the formation of new blood vessels in tumors by the different modes implicate classic molecules of the VEGF, PDGF and FGF family; the TGF-β or Ang/Tie signaling system, classic signaling pathways such as Notch and Wnt and the active interaction with the microenvironment mediated by integrins and proteases. The recently published review of Carmeliet and Jain gives a well summarized overview of these mechanisms and the implication in cancer (Carmeliet and Jain, 2011a).

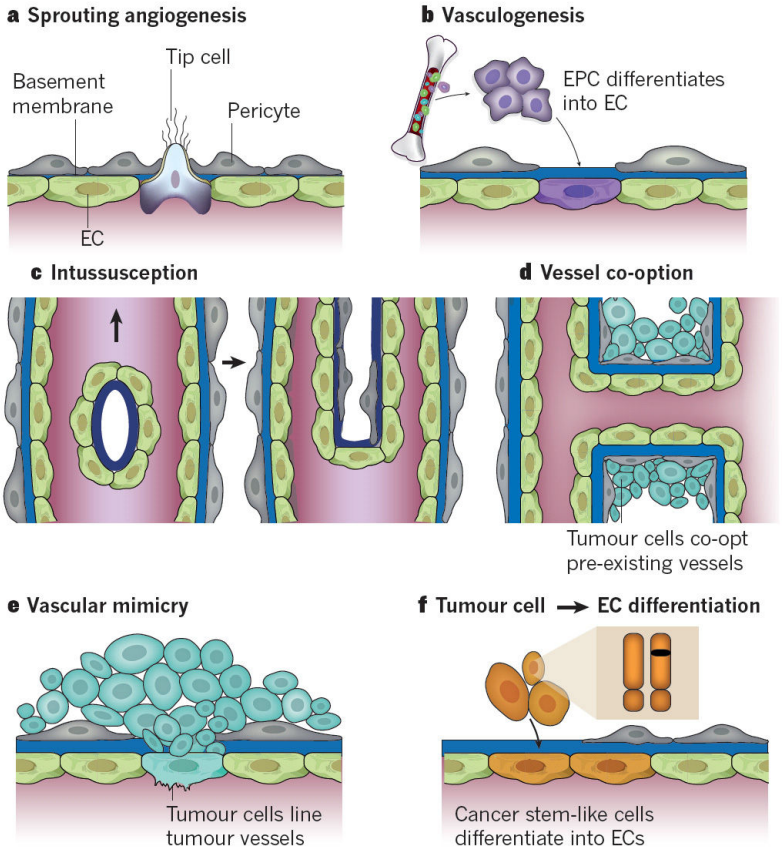

Figure 2: Modes of blood vessel formation

Modes of vessel formation in normal (a, b, c) or tumor (d, e, f) tissue. Taken from (Carmeliet and Jain, 2011a)

Whereas in the adult the normal tissue vasculature is quiescent, tumor growth requires a persistent growth of blood vessels for supplying the tumor with nutrients and oxygen as well as for evacuating metabolic waste. At one point during tumor progression sprouting of new blood vessels is initiated and remains activated. This discrete step during tumor development is called the “angiogenic switch” (Hanahan and Folkman, 1996) and is necessary to ensure exponential tumor growth. The angiogenic switch begins with perivascular detachment and vessel dilation, followed by angiogenic sprouting, new vessel formation and maturation and the recruitment of perivascular cells (**Figure 3**) (Bergers and Benjamin, 2003).

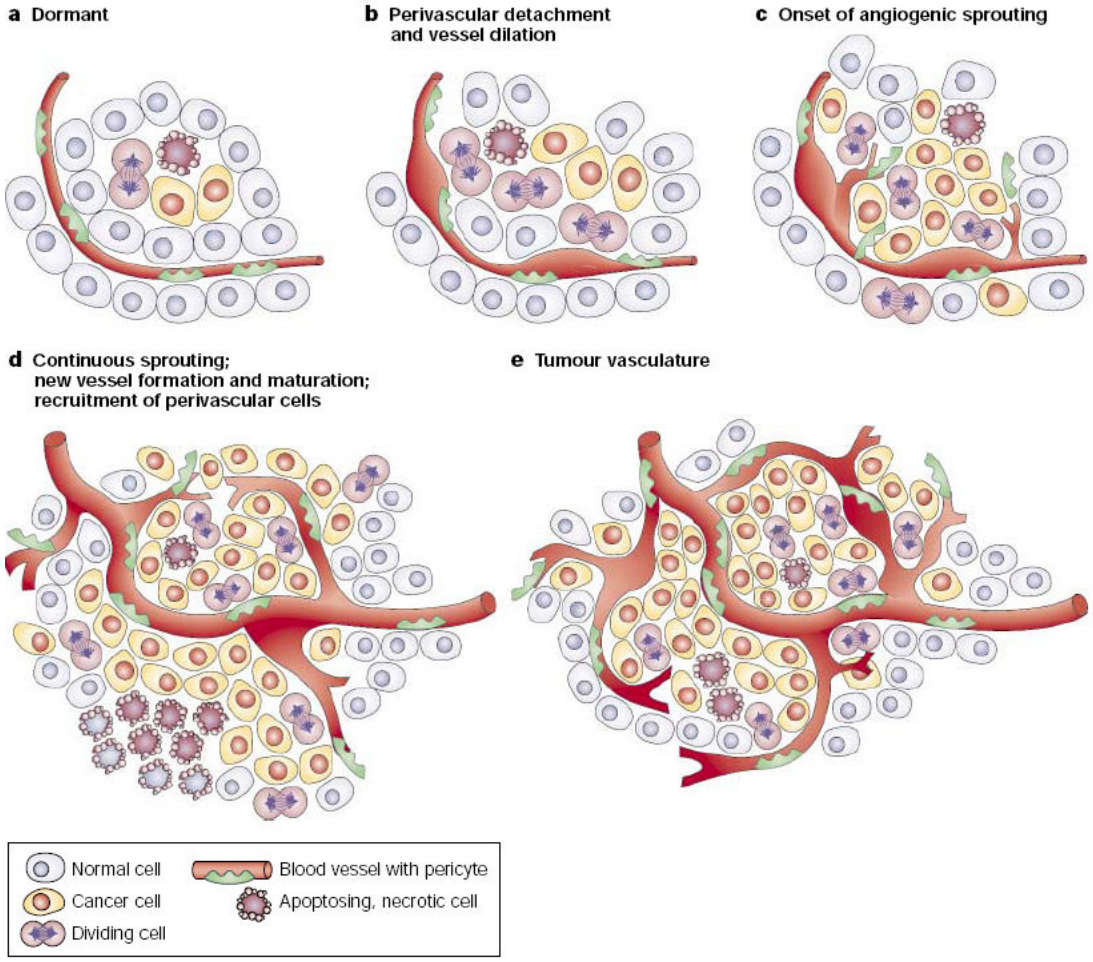

Figure 3: The angiogenic switch

Induction of angiogenesis in an avascular tumor nodule to ensure exponential tumor growth. Taken from (Bergers and Benjamin, 2003)

During the multi-stage development of tumors, angiogenesis is induced already early on during the premalignant phase of neoplastic progression (Hanahan and Weinberg, 2011) and stays chronically activated. In normal tissues, the vasculature shows a regular pattern. But tumor blood vessels appear abnormal by showing precocious capillary sprouting, irregular branching, enlarged vessels, erratic blood flow and leakiness which can lead to hypoxic regions (Baluk *et al.*, 2005; Carmeliet and Jain, 2011b) (**Figure 4**).

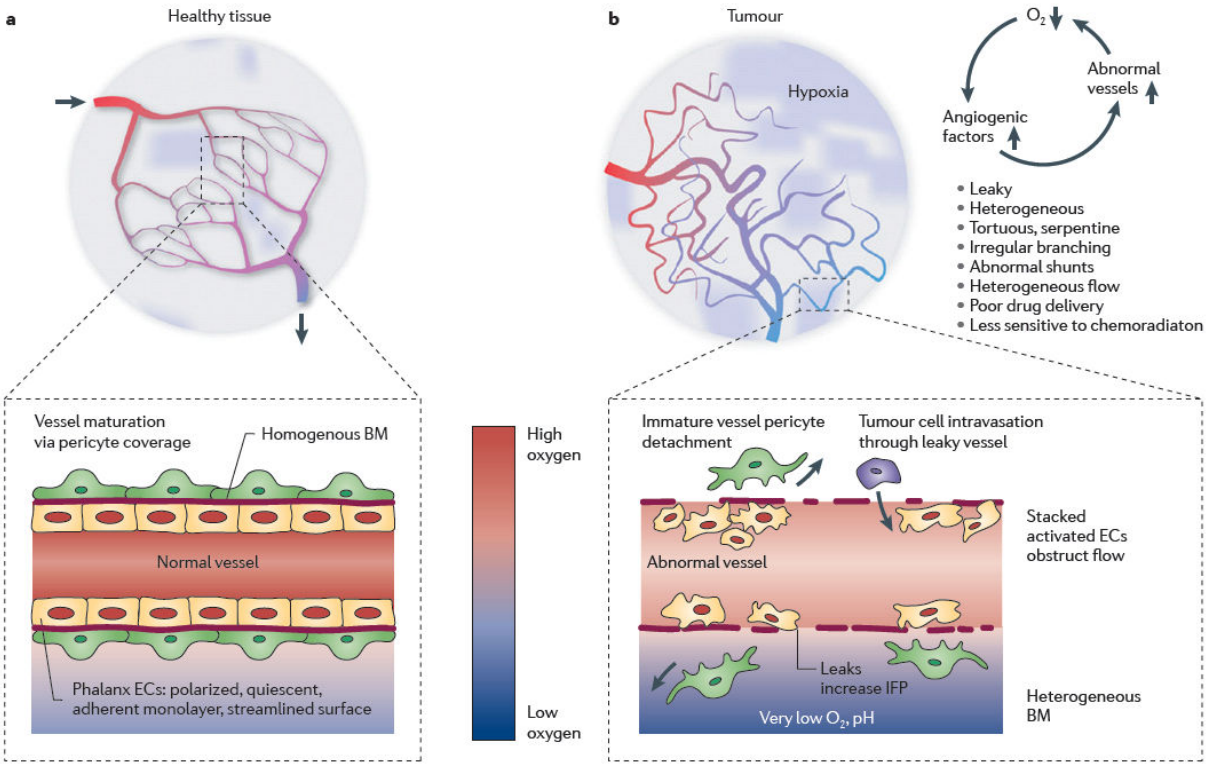

Figure 4: Abnormal structure and function of tumor vessels

Comparison of key characteristics between normal vasculature in healthy tissue (a) and the abnormal appearance of tumor blood vessels (b). Taken from (Carmeliet and Jain, 2011b)

1.1.4 Metastasis

Metastasis is the final step in the course of tumor progression where tumor cells leave the primary site to invade distant secondary organs. It is also a multi-step process including local tumor cell invasion, intravasation into blood or lymphatic vessels, adherence to the capillary wall in the secondary organ, extravasation from the blood vessel, the formation of small micrometastatic nodules and finally the growth into macroscopic tumors that destroy the targeted organ (Steeg, 2003) (**Figure** 5). Epithelial-mesenchymal transition (EMT) is a major developmental regulatory program which can be reactivated by cancer cells to enable invasion and metastasis. Cancer cells change their cell-to-cell and cell-to-ECM adhesive properties involving reorganization of the actin cytoskeleton and the formation of membrane protrusions to gain migratory and invasive characteristics (Yilmaz and Christofori, 2009). But colonization of tumor cells in secondary organs can take years to decades as disseminated cancer cells often drop into dormancy (Aguirre-Ghiso, 2007).

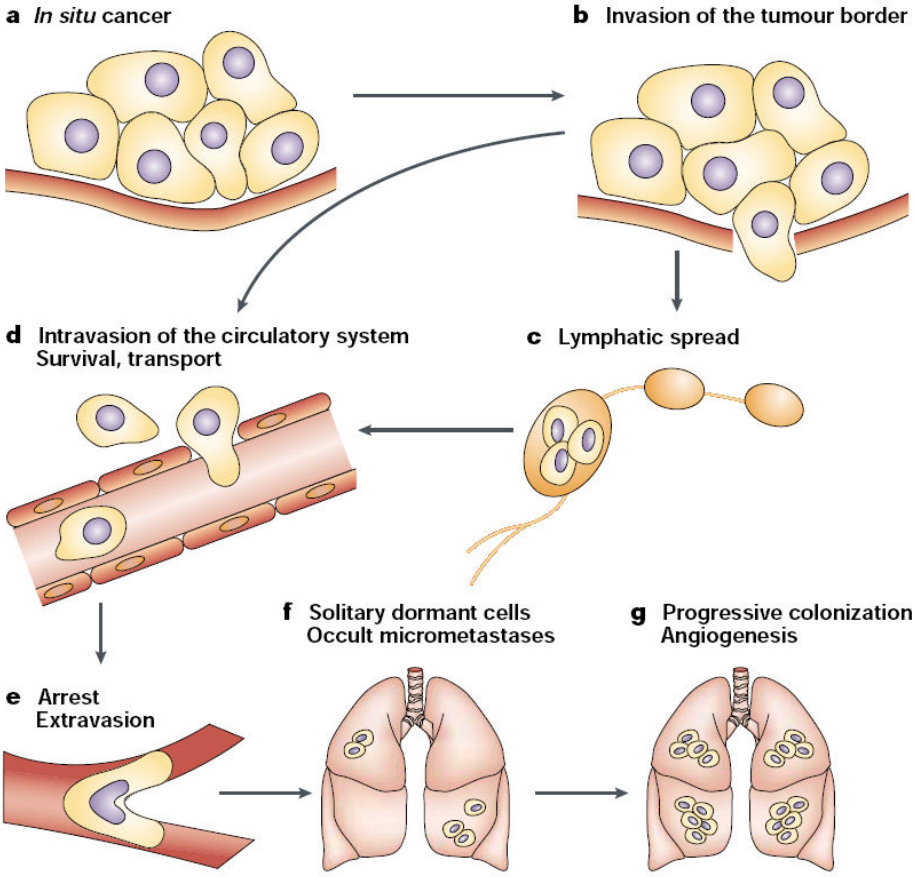

Figure 5: The multi-step process of metastasis

The process of metastasis formation where changes in and degradation of the basement membrane allows local invasion of metastasizing tumor cells into the lymphatic system or blood circulation. Surviving tumor cells may arrest at distant sites and extravasate of the circulatory system to colonize into secondary organs. Taken from (Steeg, 2003).

1.1.5 The Wnt signaling pathway

The Wnt signaling pathway plays an important role during embryo development and in normal tissue homeostasis in the adult. Non-canonical β-catenin independent pathways and the canonical β-catenin dependent pathway are the two major forms of Wnt signaling. Although there is growing evidence of the implication of non-canonical Wnt pathways in cancer, the canonical β-catenin dependent pathway has been described for long to play an important role in tumor progression. **Figure 6** illustrates the two principle states of canonical Wnt signaling. In the OFF-state (**Figure 6a**), Wnt antagonists such as soluble Frizzled-related proteins (SFRPs) and Wnt inhibitory factor (WIF) prevent binding of Wnt proteins to the transmembrane receptor Frizzled (FZD). β-catenin is recruited into a destruction complex, including APC, Axin and GSK3β, leading to proteasomal degradation. β-catenin levels are low, thus Wnt target genes are not transcribed. Likewise, interaction of the Wnt inhibitors of the DKK family with the transmembrane receptors circumvents activation of Wnt signaling by Wnt proteins. In the ON-state (**Figure 6b**), Wnt proteins bind FZD leading to

recruitment and phosphorylation of the LRP5/6 receptors. Interaction of Dishevelled (Dvl) and Axin with the FZD-LRP5/6 complex leads to inactivation of the destruction complex. Subsequently, β-catenin is stabilized in the cytoplasm and translocates to the nucleus. In the nucleus, β-catenin forms a complex with TCF and LEF transcription factors which leads to transcriptional activation of Wnt target genes such as Myc, cyclin D1 or Axin2 (**Figure 6b**). Many Wnt target genes have been identified in the meantime which are implicated in regulation of cell differentiation, cell adhesion, proliferation or in auto-regulation of this pathway.

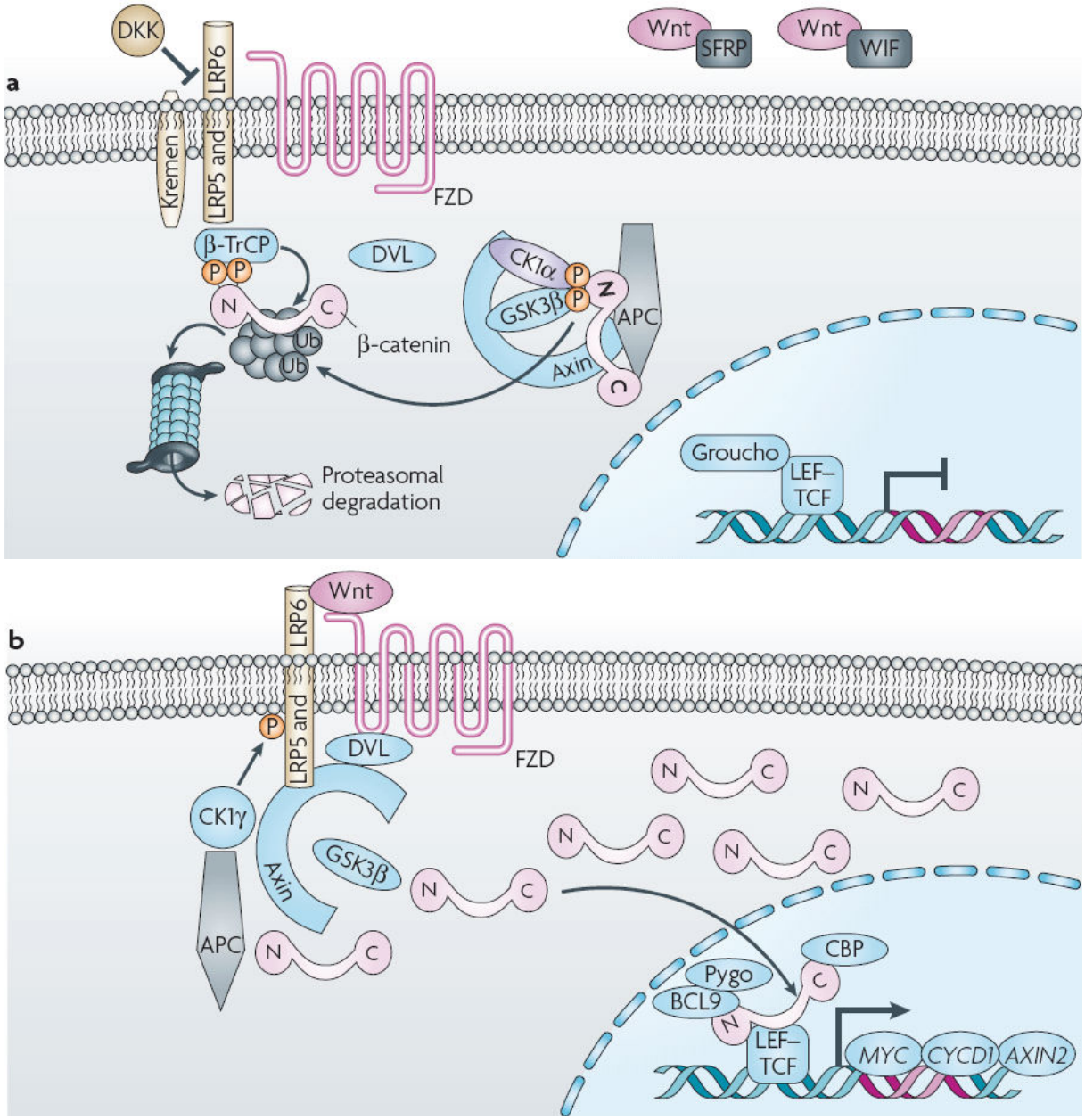

Figure 6: The canonical Wnt-β-catenin pathway

(a) inactive state (OFF) in the absence of Wnt ligands or (b) active (ON) state of Wnt signaling leading to activation of Wnt target genes. For more details see text. Taken from (Klaus and Birchmeier, 2008)

A first link of canonical Wnt signaling to cancer has been made by showing an interaction between the tumor suppressor APC and β-catenin (Rubinfeld *et al.*, 1993; Su *et al.*, 1993). Mutations in this negative regulator of the Wnt pathway and expression of a constitutively active form of β-catenin have been shown to induce hyperproliferation (Wong *et al.*, 1998) and are linked to human colorectal cancer (Sparks *et al.*, 1998). Since then, the Wnt signaling pathway has been extensively studied for its implication in cancer and has been considered as a therapeutic target in human cancer (Klaus and Birchmeier, 2008).

1.2 The tumor microenvironment

Already in 1889, Stephen Paget proposed the "seed and soil" hypothesis by saying that metastasis "*is not a matter of chance*" but that the 'soil', the microenvironment, determines the fate of the 'seed', the cancer cells (Paget, 1889). This hypothesis can be transferred to the primary tumor site, that the local tumor microenvironment actively influences tumor progression toward metastasis. The above very briefly described steps in cancer progression are driven by a complex interplay between cancer cells and the microenvironment in which the tumor cells are embedded. A tumor can actually be seen as a discrete organ, a complex tissue that involves the interaction with the entire organism (Egeblad *et al.*, 2010).

The tumor microenvironment is composed of the tumor stroma which consists of several components such as secreted growth factors, signaling molecules or enzymes. It also contains stromal cells recruited to the tumor such as cancer-associated fibroblasts (CAF), BMDC, EC or inflammatory cells, which actively participate in tumorigenesis (**Figure 7**). The extracellular matrix (ECM) is another major component of the tumor stroma in which cancer cells and the other components are embedded to form organized three-dimensional structures. Primarily, the ECM provides structural support to the tissue but also actively interacts with cells to regulate their behavior such as survival, migration, proliferation or shape. The major components of the ECM are proteoglycans, hyaluronic acid and fibrous glycoproteins such as collagens, fibronectins, laminins and tenascins (Erickson and Bourdon, 1989; Hay, 1981). These components together form the tumor microenvironment, the tumor bed, which plays a crucial role in cancer progression (Kalluri and Zeisberg, 2006).

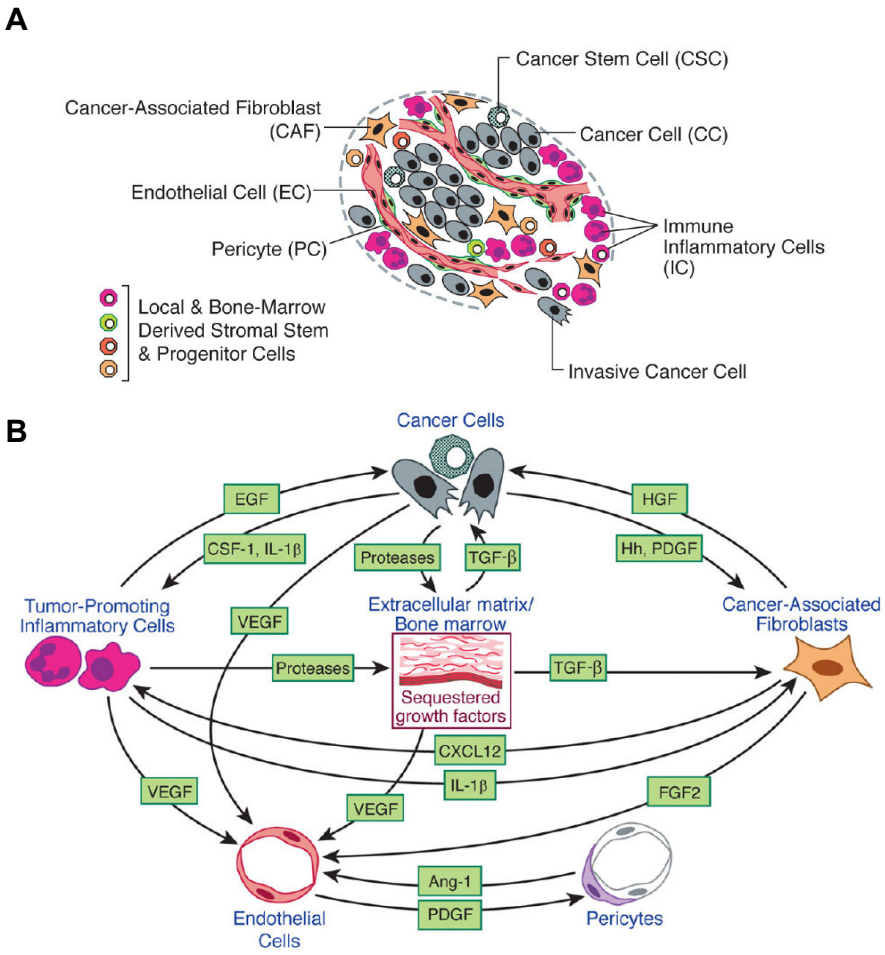

Figure 7: The tumor microenvironment

Presence of distinct cell types (A) of the tumor microenvironment and its signaling interactions (B) allowing tumor growth and progression. Taken from (Hanahan and Weinberg, 2011)

The tumor microenvironment was largely neglected in cancer research for long time but the knowledge about its specific role during tumor progression is growing. Within the tumor tissue, normal epithelial or myoepithelial cells rather inhibit malignant cell growth whereas fibroblasts, EC, BMDC or mesenchymal cells can promote proliferation, angiogenesis, invasion and the formation of metastasis (Egeblad *et al.*, 2010). An impact of the microenvironment on tumor dormancy and metastatic growth was recently summarized by Barkan and colleagues. Tumor cells may enter a state of dormancy when they fail to adhere to ECM. This might explain the development of metastasis in patients whose primary tumor site was successfully treated (Barkan *et al.*, 2010). Genetic and epigenetic alterations do not only affect gene products of cancer cells (see **1.1.1**) but can also cause gene alterations in stromal cells of the tumor microenvironment (Polyak *et al.*, 2009). Direct interactions of the ECM with cancer cells can also lead to tumor progression by inducing genomic instability or by enhanced matrix stiffness (e.g. fibrosis) which leads to clustering of cell-surface integrins and subsequent activation of cell proliferation and EMT (Comoglio and Trusolino, 2005).

Most anti-cancer therapies target exclusively tumor cells or only single, specific molecular pathways, originally thought to reduce nonspecific toxicity. But the different components of the microenvironment are mostly not yet considered. Now it is believed that components of the tumor microenvironment even constitute a barrier that protects against therapy and explains the development of resistance mechanisms in several therapeutic approaches. To prevent the development of adaptive resistance, several signaling pathways and components of the whole tumor microenvironment need to be targeted.

This is shortly exemplified by anti-angiogenic therapy as an anti-cancer treatment. Given the importance of the vascular network, targeting blood vessels promised to be a good cure for cancer by starving tumors to death and by blocking the route for tumor cell dissemination and to circumvent acquired resistance to common chemo- or radiotherapy which mainly target tumor cells (Kerbel, 1991). The most common clinically used anti-angiogenic drugs are Bevacizumab, Sorafenib and Sunitinib, all of them targeting the VEGF and/or PDFG signaling cascade. Now, there is accumulating evidence from cancer patients and from murine cancer models that a successful destruction of the tumor vasculature is not sufficient to eradicate cancer but that anti-angiogenic therapies can promote cancer progression and metastasis (Bergers and Hanahan, 2008; Ebos *et al.*, 2009; Paez-Ribes *et al.*, 2009). Modes of resistance to this therapy include intrinsic non-responsiveness or adaptive resistance provided by the tumor microenvironment. **Figure 8** illustrates the initiation of several mechanisms after anti-VEGF-induced tumor shrinkage by destruction of blood vessels. Vessel-deprived tumors can induce tolerance to hypoxia and EMT to escape oxygen deprivation, leading to enhanced tumor invasiveness. Cancer cells might also co-opt residual vessels and intravasate more easily into the circulation leading to enhanced metastasis (Loges *et al.*, 2009). Moreover, induction of pro-angiogenic factors and recruitment of BMDC facilitate tumor neovascularization after anti-angiogenic treatment (Bergers and Hanahan, 2008). Together, these mechanisms can result in enhanced tumor invasiveness and metastasis and tumor re-growth (**Figure 8D**).

It is evident that the tumor vasculature is abnormal compared to normal vessel networks (**Figure 4**). This leads to vessel malfunction and therefore continued tumor progression and resistance to classical anti-tumor treatment by hindering the proper distribution of therapeutic drugs to the tumor. These functional abnormalities also lead to regions of severe hypoxia in the tumor tissue. Hypoxia is a main driver of tumor angiogenesis. The transcriptional complex hypoxia inducible factor (HIF) is commonly activated within regions of solid tumors. In regions poor of oxygen, activation of HIF induces VEGF leading to stimulation of EC proliferation and therefore to induction of blood-vessel formation (Dor *et al.*, 2001; Maxwell *et al.*, 2001). Therefore, vessel normalization rather than

destruction is emerging as a complementary therapeutic concept to improve access of therapeutic agents to the tumor (Carmeliet and Jain, 2011b).

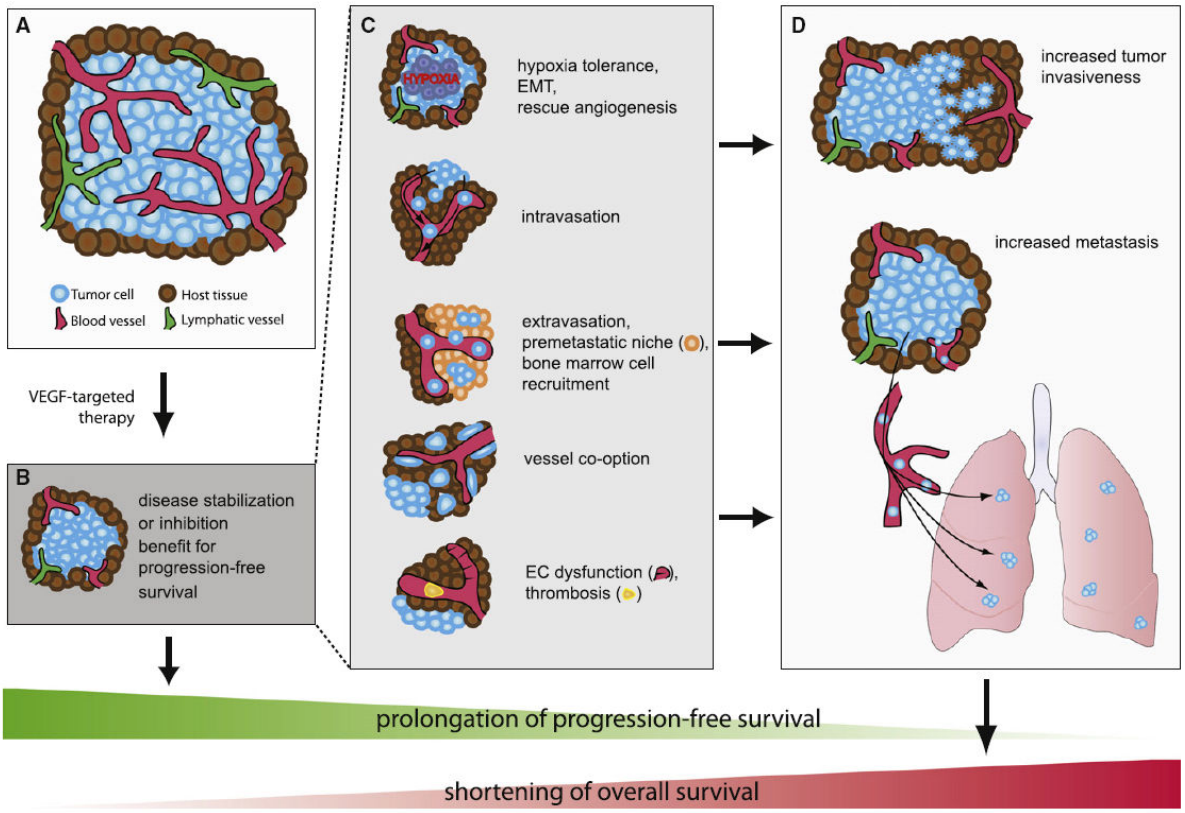

Figure 8: Modes of resistance at the example of anti-angiogenic therapy

Different modes of resistance of tumor cells at the example of anti-angiogenic therapy leading to reduced overall survival benefit. Taken from (Loges *et al.*, 2009)

1.3 The extracellular matrix molecule tenascin-C

During tumor progression, the constitution of the ECM is largely remodeled by degradation as well as by synthesis of new ECM components and helps to form a pro-tumorigenic microenvironment. In many human cancers, one major component of the remodeled tumor-specific ECM is tenascin-C (Orend and Chiquet-Ehrismann, 2006). Tenascin-C (TNC) is the founding member of the tenascin family which comprises four different members: TNC, tenascin-R, tenascin-W and tenascin-X (**Figure 9**) each having specific expression patterns (Chiquet-Ehrismann, 2004; Chiquet-Ehrismann and Tucker, 2011). TNC (Chiquet-Ehrismann *et al.*, 1986) was first described in the early 1980 and was earlier named glioma mesenchymal extracellular antigen (Bourdon *et al.*, 1983), myotendinous antigen (Chiquet and Fambrough, 1984), cytoactin (Grumet *et al.*, 1985) or J1 glycoprotein (Kruse *et al.*, 1985).

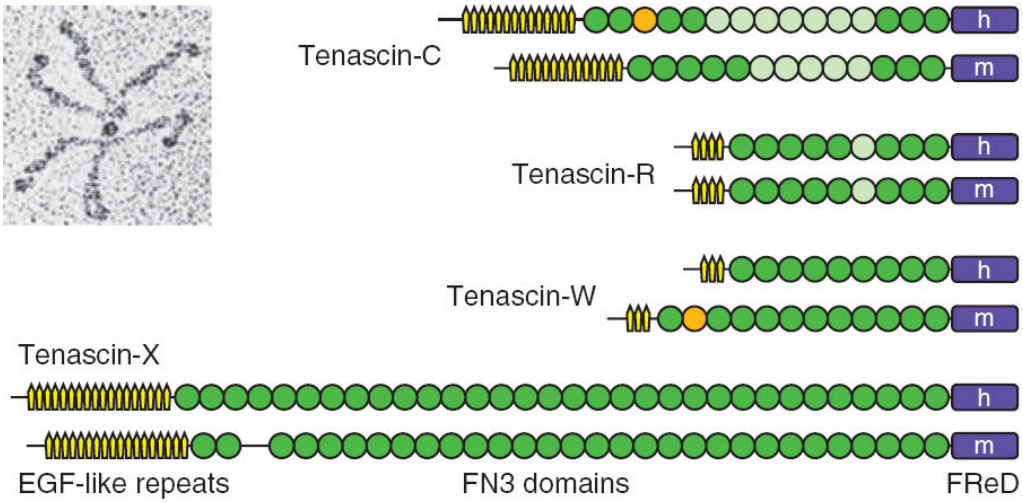

Figure 9: Structural models of the four members of the tenascin family

Domain models of each tenascin member are shown for human (h) and mouse (m) orthologs. Top left shows an electron micrograph of a TNC hexamer after rotary shadowing. Taken from (Chiquet-Ehrismann and Tucker, 2011)

The TNC monomer is a 300 kDa protein which is, on its way of secretion, assembled into a hexamer extracellularly (**Figure 9**). It is a multidomain-molecule which is composed of a N-terminal oligomerization domain followed by heptad- and EGF-like repeats, fibronectin type III repeats (constant and alternatively spliced domains) and a C-terminal fibrinogen-like globular domain. Via the different domains TNC interacts with cell surface receptors and other matrix molecules (**Figure 10**). The first described characteristics of TNC function is the modulation of cell adhesion which can further influence proliferation, migration and differentiation (Chiquet-Ehrismann *et al.*, 1986).

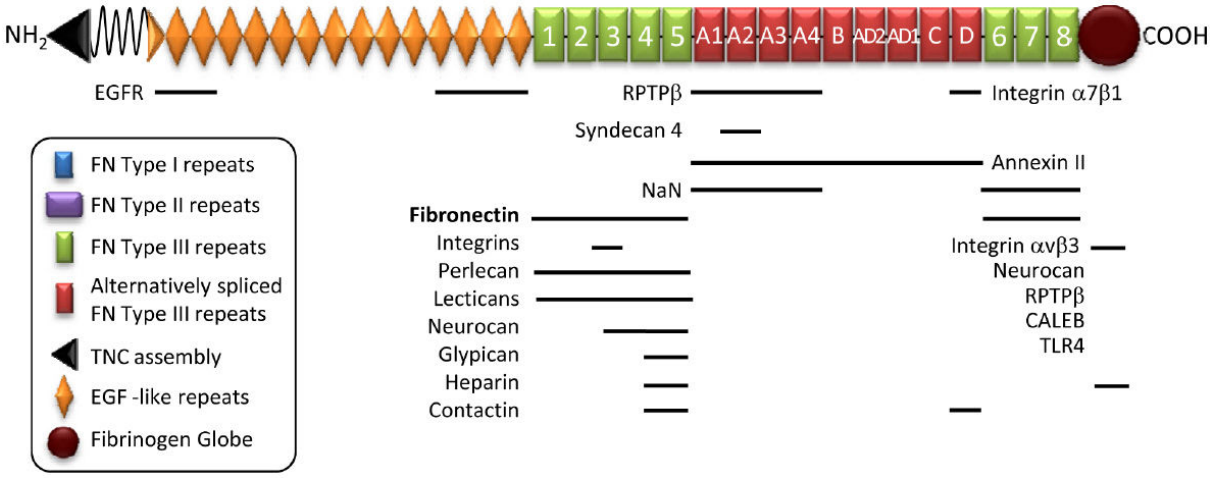

Figure 10: Domain structure of tenascin-C and potential binding partners

Modular composition of TNC including an oligomerization domain, EGF-L and FN type III (constant and alternate) repeats and a fibrinogen globe. Binding sites for interaction partners are indicated. Taken from (Van Obberghen-Schilling *et al.*, 2011).

1.3.1 The role of TNC in tumorigenesis

TNC is associated with tissue remodeling and is highly expressed during embryogenesis but in the adult tissues it is largely reduced or absent. Its expression is regained in several pathological situations such as wound healing, fibrosis, nerve regeneration (Chiquet-Ehrismann and Tucker, 2011), inflammation (Udalova *et al.*, 2011), tissue injury and tumorigenesis (Midwood and Orend, 2009; Orend and Chiquet-Ehrismann, 2006). The interaction of TNC with other ECM molecules and surface receptors of different cell types in the tumor microenvironment affects tissue architecture and initiates cellular responses relevant in cell proliferation, tumor growth, invasion, angiogenesis and metastasis (**Figure 11**) (Midwood and Orend, 2009; Orend and Chiquet-Ehrismann, 2006).

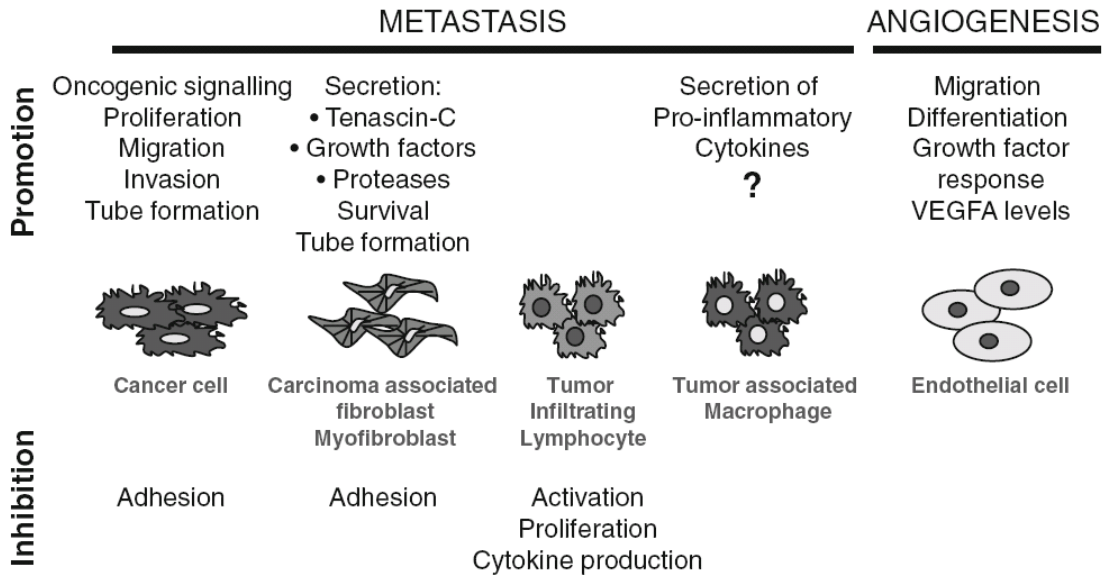

Figure 11: Overview of the role of tenascin-C in tumorigenesis

Interactions of tenascin-C with different cell types in the tumor environment and its cellular responses which may promote tumor angiogenesis and the formation of metastasis. Taken from (Midwood and Orend, 2009)

TNC is prominently expressed in the tumor microenvironment of several cancer types and plays a promoting role in malignant tumor progression and its high expression correlates with lymph node metastasis and poor prognosis (Midwood *et al.*, 2011; Orend and Chiquet-Ehrismann, 2006). TNC is linked to lung metastasis in experimental murine breast cancer models (Calvo *et al.*, 2008; Oskarsson *et al.*, 2011; Tavazoie *et al.*, 2008) and it is amongst a list of genes having a predictive value in human breast cancer metastasis to the lung (Minn *et al.*, 2005). High levels of TNC expression are linked to resistance to tamoxifen treatment in patients with estrogen receptor positive breast cancer (Helleman *et al.*, 2008). These reports demonstrate that TNC is a well established inducer of cancer progression but it is still not well understood by which mechanism of action TNC promotes tumor progression.

1.3.2 The source of TNC

In epithelial cancers such as breast or colon cancer, mostly tumor associated fibroblasts express TNC into a fibrous network around tumor cell clusters (Degen *et al.*, 2007; Degen *et al.*, 2008). In other cancers such as melanoma or glioblastoma multiforme (GBM), the tumor cells themselves secrete TNC (Herlyn *et al.*, 1991; Natali *et al.*, 1990; Sivasankaran *et al.*, 2009). Immunohistological analysis in brain cancer revealed that TNC is present in blood vessels and its expression correlated with desmin staining showing that pericytes might be the primary source (Martina *et al.*, 2010). Strong perivascular staining of TNC was also found to correlate with brain tumor malignancy suggesting it as a prognostic marker (Herold-Mende *et al.*, 2002). In a cancer model system, TNC produced by myofibroblasts *in vitro* had a pro-invasive impact on human colon cancer cells (De Wever *et al.*, 2004). In a three-dimensional co-culture system of stromal fibroblasts and cancer cells, imaging of cell invasion into a matrix revealed that the leading cell was a fibroblast preparing a track by deposition of matrix molecules which included TNC (Gaggioli *et al.*, 2007). These examples demonstrate again the importance of the tumor microenvironment and the active implication of non-tumorigenic cells in remodeling the ECM, including TNC.

1.3.3 Regulation of TNC expression

TNC is mainly expressed during embryo development and shows highly variable expression patterns depending on the developmental stage, regulated by intrinsic and extrinsic signals. It is also expressed in the adult skeleton and in the basement membrane of the intestine (Brellier *et al.*, 2009). The appearance of pathological situations can trigger TNC expression such as infection, inflammation or tumorigenesis (Chiquet-Ehrismann and Chiquet, 2003). TNC expression can be induced by mechanical strain (Asparuhova *et al.*, 2011; Chiquet-Ehrismann *et al.*, 1994; Sarasa-Renedo *et al.*, 2006) or by growth factors and cytokines (Orend and Chiquet-Ehrismann, 2006; Tucker and Chiquet-Ehrismann, 2009). Activation of signaling pathways such as ROS/NFkB, ERK, Wnt or Notch can lead to induction of TNC including positive or negative feedback loops (Chiquet-Ehrismann and Tucker, 2011). In normal human fibroblasts extracellular pH controlled alternative splicing of TNC (Borsi *et al.*, 1996). In the lung it was shown that pulmonary blood flow had an impact on TNC expression (Jones *et al.*, 2002). In a breast cancer context restoration of microRNA miR335 expression was shown to suppress lung metastasis formation in a mouse xenograft model through targeting TNC and Sox4 (Tavazoie *et al.*, 2008). The transcription factor Sox4 induced TNC expression in prostate cancer (Scharer *et al.*, 2009). Sox4 was already seen to be induced by TNC in GBM cells grown on a TNC substratum (Ruiz *et al.*, 2004) suggesting a positive feedback regulation of Sox4 and TNC. In patients with GBM, the Notch2 co-factor RBP Jk

protein was co-expressed with TNC and activation of Notch2 in cultured cells increased TNC expression (Sivasankaran *et al.*, 2009).

1.3.4 The role of TNC in vascular morphogenesis

In normal tissue, TNC expression is very restricted and mostly absent. Low levels of TNC can be found in large blood vessels of the skin (Lightner *et al.*, 1989). Its expression is largely induced in experimental models such as in arteries upon vascular injury, in neointimal hyperplasia upon abdominal aortotomy or during atherosclerosis (Midwood *et al.*, 2011). Furthermore, it was shown to regulate EC spreading and migration and cardiac allograft vascularization which failed in mice lacking TNC expression. Donor EC showed enhanced migration properties when cultured on TNC suggesting that TNC regulates early stages of angiogenesis by modulating EC adhesiveness and migration (Ballard *et al.*, 2006). The role of TNC in vascular remodeling in pathological situations, including cancer, was extensively reviewed recently (Midwood *et al.*, 2011; Midwood and Orend, 2009; Van Obberghen-Schilling *et al.*, 2011).

TNC had already been shown to act as a chemoattractant for EC and to play a role in the generation of tumor derived EC (Pezzolo *et al.*, 2011), to promote EC tube formation (Martina *et al.*, 2010; Schenk *et al.*, 1999) and to promote the selection of highly proliferative endothelial cells (Alves *et al.*, 2011). In tumors of GBM patients TNC is often localized in perivascular regions (Herold-Mende *et al.*, 2002). Melanoma cells grafted into mice lacking TNC expression displayed a reduced tumor angiogenesis that was linked to reduced VEGFA (Tanaka *et al.*, 2004). These reports demonstrate the importance of TNC as tumor promoter by stimulating angiogenesis.

TNC might also play an important role in alternative programs of angiogenesis and formation of tubular structures. During lung development the absence of TNC is associated with abnormal branching morphogenesis and with decreased vascularization (Roth-Kleiner *et al.*, 2004). TNC is also present in normal secondary lymphoid tissues such as in the thymus where it is found in reticular fibers, the so called thymic conduits (Drumea-Mirancea *et al.*, 2006). In malignant melanomas (Kaariainen *et al.*, 2006), in breast cancer (Degen *et al.*, 2007) and in colorectal carcinoma (Degen *et al.*, 2008) TNC is not homogenously expressed but organized in tube-like structures throughout the tumor. In melanoma TNC was found in tubular channels with a lumen that contained tumor cells (Kaariainen *et al.*, 2006). These observations suggest that TNC is implicated in the formation of matrix tracks. In a co-culture

experiment carcinoma-associated fibroblasts prepared TNC containing tracks which were used by tumor cells to invade (Gaggioli *et al.*, 2007).

Such matrix tracks might serve for tumor cells to metastasize but in parallel they also might reflect the alternative program of vasculogenic mimicry, the plasticity of cancer cells to mimic the activity of EC and participate in the formation of neovessels and fluid-conducting networks. These vessel-like structures were linked to metastasis in melanoma and are found in many other different tumor types including breast, prostate or lung cancer (Hendrix *et al.*, 2003) and were identified in brain cancer (Yue and Chen, 2005). Key signaling molecules in this process include VE-cadherin, EphA2 or remodeling of ECM by cleavage of LM5γ2 to pro-migratory fragments through MMP-2 amongst others (Paulis *et al.*, 2010). But the implication of TNC in this program is currently unknown.

1.3.5 Loss-of-function mouse models to study TNC functions

TNC knockout mice were generated in two different laboratories (Forsberg *et al.*, 1996; Saga *et al.*, 1992). In both studies the signal peptide and the heptad repeat sequences were disrupted. Saga and colleagues inserted a lacZ-neo construct just in front of the translational initiation codon in exon 2 of the TNC gene, deleting parts of the exon 2 and intron 2 and keeping the regulatory unit of the TNC gene for lacZ expression (Saga *et al.*, 1992). Since expression of a truncated TNC in these mice was detected (Mitrovic and Schachner, 1995), a second independent TNC knockout mouse was generated where a neomycin resistance cassette was inserted into exon 2 leading to two aberrant splice products of TNC in homozygous mice inducing a frameshift and translation stop after 99 and 18 nucleotides (Forsberg *et al.*, 1996). In both cases TNC knockout mice were alive and fertile and exhibited an apparently normal development and tissue organization which has been attributed to compensation (Orend and Chiquet-Ehrismann, 2006). It was noticed that in the subventricular zone of the brain, oligodendrocyte precursor cells respond differently to growth factors and proliferate less, but this appears to be compensated by a reduced apoptosis rate later on. Thus the number of oligodendrocytes ends up being similar in the TNC knockout and wildtype mouse (Garcion *et al.*, 2001). Later studies showed that the absence of TNC imposes problems for tissue homeostasis which is particularly evident during wound- or inflammation-associated tissue repair (Orend and Chiquet-Ehrismann, 2006). TNC knockout mice now present valuable tools for addressing the roles of TNC in development, angiogenesis, inflammation, heart failure and tumorigenesis. R. Chiquet-Ehrismann and R. Tucker have summarized the phenotype of the TNC knockout mouse published to date (Chiquet-Ehrismann and Tucker, 2011).

1.4 The RT2 mouse model of pancreatic neuroendocrine tumorigenesis

The modeling and study of human cancer in mice has a strong contribution to the understanding of cancer. It further allows investigating multiple steps of carcinogenesis at the same time. The Rip1-Tag2 (RT2) model is a mouse model of pancreatic islet β-cell tumors (Hanahan, 1985). In RT2 mice, simian virus 40 large T-antigen (SV40 Tag) is expressed under the control of the rat insulin II promoter. This allows a tissue-specific expression of the oncogene in the insulin-producing β-cells of the islets of Langerhans in the mouse pancreas. SV40 Tag complexes with the two tumor suppressor gene products p53 and pRb and represses their function (Ludlow, 1993). This induces proliferation in all β-cells and leads to hyperplasia of pancreatic islets and formation of solid tumors in a reproducible and sequential manner and recapitulates multi-stage tumorigenesis as observed in a large fraction of human cancer (Nevins, 2001; Pipas and Levine, 2001).

Figure 12 illustrates the multiple steps of RT2 tumorigenesis. The mouse pancreas comprises approximately 400 islets of Langerhans in which oncogenic expression of SV40 Tag is expressed from embryonic day 9 on persisting through adulthood (Alpert *et al.*, 1988). During the first three weeks of age, all islets show hyperplasia compared to normal wildtype islets. Then, approximately 50% of the islets become hyperproliferative and develop into hyperplastic lesions. A subpopulation of these islets (~20%) subsequently becomes angiogenic and of these a few progress into solid tumors. By passing through the four discrete stages of SV40 Tag induced islet progression, 2-10 solid tumors develop within 12 to 14 weeks of age in a RT2 mouse (**Figure 12**). RT2 mice in the most commonly C57BL6 background do not exhibit formation of metastasis to other organs, likely because they die about 12 to 14 weeks of age due to hypoglycemia (Hanahan, 1985).

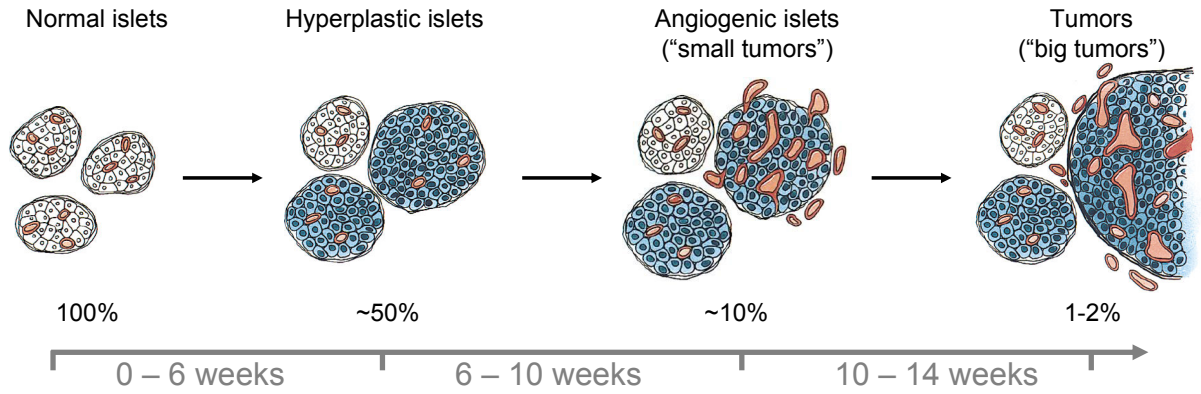

Figure 12: Multiple steps of tumorigenesis in the RT2 model system

Oncogene expression in all pancreatic islets induces hyperproliferation and the angiogenic switch in a subset of islet lesions which then further grow to solid insulinoma. Adapted from (Hanahan and Folkman, 1996).

In the RT2 model islet lesions and tumors are classified according to their size in diameter into normal islets (< 0.2 mm), hyperplastic islets (0.2 – 0.5 mm), angiogenic islets (> 0.5 – < 1 mm) and tumors (≥ 1 mm). Tumors can be classified into non-invasive adenomas and aggressive, invasive carcinomas. A more detailed classification of these insulinomas was established, including vascular morphology and invasiveness as additional criteria (Lopez and Hanahan, 2002). Although a detailed classification according to these criteria (for details see Table 1 in the article of Lopez and Hanahan) was not yet investigated quantitatively in the model systems that I will present in this thesis, I noticed after observation of some tissue sections that the classification of angiogenic islets according to their size is misleading. According to the literature, all islet lesions from 0.5 mm in diameter are considered as angiogenic. But some of the islets between 0.5 and 1 mm in diameter which I observed were non-angiogenic as they did not show any angiogenic signs such as dilated or tortuous vessels or the presence of hemorrhages. Therefore, I will use the classification of islet lesions and tumors according to their size as defined above. But the classes “angiogenic islets” and “tumors” will be defined here as “small tumors” (> 0.5 – < 1 mm) and “big tumors” (≥ 1 mm) respectively (**Figure 12**).

The use of the RT2 model system has several advantages compared to other mouse models using transplantation experiments in immune-deficient mice. In RT2 mice, tumorigenesis occurs spontaneously in a stochastic but defined and reproducible way. This model allows to study the impact of the immune system and tumor-promoting inflammation on tumor progression. Tumor progression occurs sequentially in multiple steps as it can be observed in many human cancers. These discrete steps can be analyzed in parallel as RT2 mice contain tumors at different stages from hyperplastic islets over angiogenic islets to invasive or non-invasive tumors at the same time. In most cases samples from cancer patients are not available from several tumor stages. The induction of angiogenesis in a subset of hyperplastic islets in the approximate time-frame between 5 to 10 weeks of age made RT2 mice to a reference model for the study of tumor angiogenesis and induction of the angiogenic switch (Parangi *et al.*, 1995). Despite the many advantages, RT2 mice do not develop macrometastasis and die early which complicates the analysis of late-stage tumor parameters and metastasis in this model.

2 Aims

The overall objective of the present thesis was to investigate the role of tenascin-C in tumor progression in the RT2 mouse model of pancreatic neuroendocrine tumorigenesis and to get a better mechanistic understanding of TNC actions in cancer progression.

The specific aims were:

1. To determine the role of tenascin-C in tumor progression in a mouse model mimicking high expression of tenascin-C in human cancers.

2. To establish a mouse model for investigating tumorigenesis in the absence of tenascin-C.

3. To identify molecular mechanisms of action downstream of tenascin-C.

4. To establish a method for studying the role of tenascin-C in blood vessel anatomy and tumor architecture.

3 Materials and Methods

3.1 Animal handling and *in vivo* experiments

All experimental procedures involving mice were done according to the guidelines of Inserm. β-cell tumorigenic mice were supplemented with 5% (w/v) glucose in drinking water beginning at 10 weeks of age to overcome hypoglycemia due to increased insulin production from developing insulinoma.

3.1.1 Generation of Rip-hTNC and RT2/hTNC mice and genotyping

Plasmid construction and the generation of transgenic Rip-hTNC mice with forced over-expression of human TNC in β-cells of the Langerhans islets is described in detail in Manuscript 1 (see Annex, **Manuscript 1 Supplemental Material and Methods**). In brief, the human TNC cDNA sequence (Gherzi *et al.*, 1995) containing the largest splice variant of TNC (most domains except AD1 and AD2) was removed from the HxBL.pBS plasmid (Aukhil *et al.*, 1993) and cloned into the Rip1 expression vector (Hanahan, 1985). The resulting Rip-hTNC expression vector contains the human TNC cDNA driven by the β-cell specific insulin promoter. Partial sequencing confirmed the presence of all 5' and 3' untranslated regions. The Rip-hTNC expression vector was used for injection into the pronucleus of fertilized oocytes of a mixed C57BL6 mouse strain giving rise to mice with stable transmission and expression of the transgene. Transgenic mice were identified by polymerase chain reaction (PCR) with primers "RipES/VD": 5'-TAA TGG GAC AAA CAG CAA AG-3' and "revP1 TNC": 5'-GAA AGA CAC CTG CCA ACA GC-3'. For generation of double-transgenic RT2/hTNC mice, single-transgenic Rip-hTNC mice were crossed with RT2 mice (Hanahan, 1985). The presence of the RT2 transgene was identified by PCR using primers "Tag1": 5'-GGA CAA ACC ACA ACT AGA ATG CAG-3' and "Tag2": 5'-CAG AGC AGA ATT GTG GAG TGG-3'. Genotyping was performed on mouse tail tissue digested with 200 µl DirectPCR buffer (Viagenbiotech) containing 10 µg proteinase K (Roche). Digestion mix was diluted to 1 ml with water and 1 µl was used for PCR using Red'y'Star mix (Eurogentech). Amplified products were visualized on a 2% agarose gel using GelRed nucleic acid stain (Biotinum).

3.1.2 Generation of RT2/TNC-/- mice lacking TNC expression

Mice lacking expression of a functional TNC gene (TNC-/-) were originally generated in the 129/Sv mouse strain (Forsberg et al., 1996). These mice have been backcrossed for ten generations into the C57BL6 strain in our lab. TNC+/- mice of generation 9 have been

crossed with C57BL6 RT2 mice (Hanahan, 1985) to generate RT2/TNC+/- mice in generation 10. These mice have been crossed with TNC+/- mice of generation 10 to create a RT2/TNC-/- colony in a C57BL6 background. This colony is maintained by crossing male RT2/TNC-/- with female TNC-/- mice. The presence of the wildtype or the deleted form of TNC was determined by PCR using primers “TNCKO_TNCup”: 5’-CTG CCA GGC ATC TTT CTA GC-3’, “TNCKO_TNCdown”: 5’-TTC TGC AGG TTG GAG GCA AC-3’ and “TNCKO_TNCNeoPA”: 5’-CTG CTC TTT ACT GAA GGC TC-3’ (**Figure 18B**).

Before availability of the C57BL6 RT2/TNC-/- colony, RT2/TNC-/- mice have been generated in generation 1 of backcrossing and mice were analyzed in comparison to RT2/TNC+/- littermates expressing only one allele of TNC. A second set of RT2/TNC-/- mice had been generated in generation 8 of backcrossing (99.6% C57BL6) and were analyzed in comparison to control RT2/TNC+/+ littermates with wildtype expression of TNC.

3.1.3 Oral glucose tolerance test

To test glucose metabolism female and male 12-14 weeks old mice were starved for 16-18 hours over night in clean cages and with free access to water. Tail vein blood glucose concentration was measured at time = 0 using Glucofix® sensor for Glucofix® mio (A. Menarini Diagnostics, Italy). 2 mg glucose per gram of body weight was orally administered by gavage (~35-60 mg/mouse). Blood glucose levels (mg/dL) were measured every 15 minutes for 1.5 hours. At the end of the experiment food was given to the mice.

3.2 Analysis of tumor parameters

3.2.1 Tumor incidence and tumor burden

In 12 weeks old mice tumor incidence was estimated by counting all visible macroscopic tumors ≥ 1 mm in diameter without destroying the tissue that was used for further analysis. Tumor diameter (d) was measured under a stereomicroscope using a ruler. In 14 weeks old mice each tumor ≥ 1 mm in diameter was dissected from the pancreas, measured and counted to determine the tumor incidence per mouse. Assuming a spherical shape of the tumors, the tumor volume V was calculated using the formula $V=1/6*\pi*d^3$. The tumor incidence represents the sum of all counted tumors and tumor burden represents the total tumor volume per mouse.

3.2.2 Tumor classification by size and tumor staging

The diameter of pancreatic islets was measured on hematoxilin and eosin (H&E) or 4',6-diamidino-2-phenylindole (DAPI) stained tissue sections (see **3.3**). The largest tumor dimension was measured on a Zeiss AxioImager.A1 (light microscope) or Zeiss Imager.Z2 microscope (light and fluorescence) using AxioVs40 software (version 4.8, Carl Zeiss Microimaging). Islets were classified according to their size into normal islets (< 0.2 mm), hyperplastic islets (0.2 to 0.5 mm), small tumors (> 0.5 to < 1 mm) and big tumors (≥ 1 mm). The data are presented as frequency (%) of all analyzed islets and statistical analysis was performed using the Chi-squared (χ^2) test. When data were pooled into two categories (≤ 0.5 mm and > 0.5 mm) Fisher's exact test was applied to determine if the distribution of islets into different categories is statistically different between the analyzed genotypes.

3.3 Tissue analysis by histology and immunofluorescence

Pancreata were isolated and either fixed in 4% paraformaldehyde (PFA) overnight followed by embedding in paraffin or fixed for 2 hours in 4% PFA at 4°C followed by immersion in 20% sucrose over night and embedded in Tissue-Tek O.C.T. (Sakura Finetek Europe B.V., Zoeterwoude, Netherlands). Freshly isolated pancreata were embedded in Tissue-Tek O.C.T. and frozen on dry ice. Staining by immunohistochemistry (IHC) was done on paraffin sections (5 µm) and immune labeling was developed by the Vectorstain system (Vector labs). Tissue sections were prepared using Cryostat Leica CM3050S and paraffin sliding microtome Leica RM2145. Staining by immunofluorescence (IF) was done on fresh frozen or fixed frozen cryosections (7 – 50 µm). Histological analysis (classification, staging) was done on sections stained with H&E. For IF staining tissue sections were incubated for 45 minutes with 5% NGS/PBS. Primary antibodies were diluted in 5% NGS/PBS and sections incubated in a humidified chamber at 4°C over night. After extensive washing with PBS appropriate secondary antibodies labeled with FITC, Cy3 or Cy5 produced in goat or donkey (Jackson ImmunoResearch) were incubated on the sections for 1.5 hours at room temperature. Cell nuclei were stained by incubation for 10 minutes with DAPI (1:30,000 dilution in water of a 10 mg/ml stock solution). After extensive washing slides were mounted using a glycerol based anti-fading solution (self-made by C. Arnold). Slides were stored at 4°C or at -20°C for long term. The name, reference and used dilutions for the applied primary antibodies are listed in **Table 1**.

The following microscopes and software were used for the different analysis presented in this thesis: Axioskop2 plus light microscope (Zeiss) with Axiovision 3.1 (Zeiss); Nikon Diaphot 300 immunofluorescence microscope (Nikon) with Openlab 3.1.7 software (Improvision);

Zeiss AxioImager.A1 (light microscope) or Zeiss Imager.Z2 microscope (light and fluorescence) equipped with the ApoTome module for three-dimensional (3D) imaging and with AxioVs40 software (version 4.8, Carl Zeiss Microimaging).

Table 1: List of primary antibodies used for immunohistological staining

Protein name	Species	Dilution	Reference
CD31	rat	1:50	BD Pharmingen (550274)
CD31	rat	1:50	Acris Antibodies GmbH (BM4086)
F4/80	rat	1:50	AbD Serotec (MCA497G)
Insulin	guinea pig	1:200	DakoCytomation (A0564)
KI67	rabbit	1:200	Thermo Scientific (RM-9106)
Laminin	rabbit	1:2000	P. Simon-Assmann (Simo et al., 1991)
PH3	rabbit	1:200	Upstate (06-570)
TNC (human)	mouse	1:50	B28.13 (Wagner et al., 2003)
TNC (mouse)	rat	1:100	MTn12 (Aufderheide and Ekblom, 1988)

3.3.1 Quantification of immunofluorescent signals

Quantification at histological level was done for several molecules by IF microscopy and analysis by using the ImageJ software (National Institutes of Health, USA). Staining protocols (fixation, blocking, antibody dilutions), settings for image acquisition (used microscope, lamp power, magnification, exposure time) and post-treatment of images by ImageJ (threshold to exclude background staining, contrast) were always kept constant for one set of experiments and performed at the same time.

For proliferation analysis, tissue sections were stained for phosphor-histone-H3 (PH3) or KI67 and DAPI. PH3-postivie nuclei were counted in defined fields (200x magnifications) and are presented as average of PH3-positive cells per analyzed tumor area. KI67-positive staining was quantified as area fraction per analyzed tumor area because cells with positive staining were too dense to count as single events. Several images per tumor were taken when not fitting in the 20x objective field to cover most of the tumor surface. In this case the average between the images per tumor was calculated. Data are presented as average area fraction (%) per tumor in all analyzed samples or in the defined subclasses.

Tumor angiogenesis was assessed by quantifying intra-tumor vessel density using CD31 as a blood vessel EC marker and DAPI staining. CD31-positive signals were quantified as area fraction per analyzed tumor area in images acquired at 200x magnifications.

3.3.2 Preparation of Mercox vascular casts for scanning electron microscopy

For preparation of vascular casts, anaesthetized RT2 and RT2/hTNC mice were perfused through the thoracic aorta with 0.9% sodium chloride containing 1% heparin and 1% procaine followed by freshly prepared Mercox solution (Vilene Company, Japan) containing 0.1 ml of accelerator per 5 ml of resin. One hour after perfusion, the pancreas was excised and kept in 7.5% potassium hydroxide for up to 3 weeks for tissue dissolution. Casts were then dehydrated in ethanol and dried in a vacuum dessicator. The samples were mounted on aluminum stubs, sputtered with gold to a thickness of 10 nm and examined in a Philips XL-30 SFEG scan electron microscope (SEM) (collaboration V. Djonov, Uni Bern, Switzerland).

3.3.3 Tissue preparation for transmission electron microscopy

For analysis by transmission electron microscopy (TEM), pancreata of RT2 and RT2/hTNC mice were excised and fixed in 2.5 % (v/v) glutaraldehyde and 2% PFA solution buffered with 0.1 M sodiumcacodylate buffer (pH 7.4; 350 mOsm). Samples were post-fixed in osmium tetroxide, stained in uranyl acetate and dehydrated in ethanol. After embedding in epoxy resin 90 nm ultrathin sections were prepared and mounted on copper grids coated with Formvar (polyvinyl formal; Fluka, Buchs, CH). Sections were stained with lead citrate and uranyl acetate prior to observation in a Philips EM-400 electron microscope. All images obtained by SEM and TEM analysis presented in this thesis were prepared by V. Djonov and R. Hlushchuk (University of Bern, CH) who are experienced in analyzing the vasculature of RT2 tumors.

3.3.4 Perfusion experiments using FITC-labeled molecules

For FITC-lectin and FITC-dextran perfusions, mice were anesthetized with phentobarbital (100 µl of a 5% solution), the chest was opened, and the vasculature was perfused by injection of either 150 µl FITC-conjugated tomato lectin (containing 150 µg *Lycopersicon esculentum*, Vector Laboratories, FL-1171) or 150 µl FITC-conjugated dextran (10 mg/150 µl PBS; 2000 kDa, FS2000S-100MG, Sigma, Schnelldorf, Germany) into the left heart chamber using a 0.5 ml insulin syringe (BD Micro-Fine, 324893). Circulation was allowed for at least 5 minutes before pancreas extraction, followed by fixation in 4% PFA for 2 hours, incubation in 20% sucrose over night, embedding into Tissue-Tek O.C.T and freezing. Tissue preparation and IF staining was performed as described above. Samples were analyzed by pseudo-confocal 3D microscopy using a Zeiss Imager.Z2 microscope equipped with the ApoTome module and AxioVs40 software with a 3D analysis tool.

3.4 RNA preparation and qRT-PCR analysis

Tissue from tumors, liver, lung and heart of 12 to 17 weeks old mice was isolated and immediately snap frozen in liquid nitrogen. Total ribonucleic acid (RNA) was extracted using NucleoSpin RNA II kit (Macherey-Nagel, Düren, Germany) according to the manufacturer's protocol. RNA from heart, liver (1 µg), tumor or lung (2 µg) was treated with DNase I (Invitrogen) and reverse transcribed using MultiScribe reverse transcriptase (Applied Biosystems, Fostercity, CA, USA). cDNA was diluted with water to 100 µl (liver, lung, heart) or 200 µl (tumors). Quantitative reverse transcriptase polymerase chain reaction (qRT-PCR) was performed on a 7500 Real Time PCR System (Applied Biosystems) using SYBR green (Applied Biosystems, Warrington, UK) or Taqman reaction mixtures (Applied Biosystems, Fostercity, CA, USA). Primers for SYBR green were designed using Roche Probefinder v2.45 or found in the database "RTPrimerDB" (http://medgen.ugent.be/rtprimerdb/). Taqman probes were obtained from Applied Biosystems. Sequences and references are listed in **Table 2**. Samples were analyzed in 10 µl reactions using 1-5 µl (tumors) or 2.5 µl (heart, liver, lung) cDNA. Data were normalized either to a centered reference of RPL9, TBP, GAPDH (tumors) or to TBP (heart, liver, lung). Relative expression of a certain gene of interest (GOI) between genotypes was calculated based on the mean ΔΔct-values in each group using following formulas:

$$\Delta ct\ [sample] = ct\ [GOI] - ct\ [reference]$$

$$\Delta\Delta ct\ [sample] = \Delta ct\ [sample] - \Delta ct\ [average\ all\ samples\ ctrl\ group]$$

$$Fold\text{-}change = 2^{(-\Delta\Delta ct\ [average\ all\ samples\ per\ group])}$$

Following this calculation the average ΔΔct in the control group is always 0 and therefore the fold change is 1. To facilitate reading of graphs qRT-PCR data are presented as negative ΔΔct showing same ±-directions as the fold changes are. Data are presented as Whiskers plots showing median, quartile, minimum and maximum of -ΔΔct-values per group.

Table 2: Primer list for qRT-PCR on mouse tissue

List containing all primer sequences (SYBR green) or references for Taqman primers used for qRT-PCR analysis on liver, lung, heart and tumor tissue and on isolated islets of mice.

Gene	Forward primer (or reference)	Reverse Primer
Ang1	CATTCTTCGCTGCCATTCTG	GCACATTGCCCATGTTGAATC
Ang2	TTAGCACAAAGGATTCGGACAAT	TTTTGTGGGTAGTACTGTCCATTCA
β-catenin	GCTGACCTGATGGAGTTGGA	GCTACTTGCTCTTGCGTGAA
CD31	GCTGGTGCTCTATGCAAGC	ATGGATGCTGTTGATGGTGA
CD44	GTCTGCATCGCGGTCAATAG	GGTCTCTGATGGTTCCTTGTTC
c-Myc	TGAGCCCCTAGTGCTGCAT	AGCCCGACTCCGACCTCTT
CyclinD1	CGCACTTTCTTTCCAGAGTCA	AAGGGCTTCAATCTGTTCCTG
CyclinD2	CACCGACAACTCTGTGAAGC	TCCACTTCAGCTTACCCAACA
DKK1	Taqman mDKK1 Mm00438422_m1	
DKK1	CCGGGAACTACTGCAAAAAT	CCAAGGTTTTCAATGATGCTT
Dll4	AGGTGCCACTTCGGTTACAC	GGGAGAGCAAATGGCTGATA
E-cad	CAGCCTTCTTTTCGGAAGACT	GGTAGACAGCTCCCTATGACTG
EDNRA	GGTGGCTCTTTGGGTTCT	GACGCTGTTTGAGGTGCT
EphA2	TACGAGAAGGTCGAGGATGC	TCAGATGCCTCAGACTTGAAGA
GAPDH	Taqman Mm99999915_g1	
Glp1r	CTGCCCAGCAACACCAGT	CAGTCGGCAGCCTAGAGAGT
Hey1	CATGAAGAGAGCTCACCCAGA	TTGGGGACATGGAACACAG
Id2	AAGACTTTTGTTATCAGCCATTTCACCA	GACGATCATCCTTAGTTTTCCTTCCGCTTTCTT
Insm1	GGTTTGCTCTGCCTACCAAT	TCACCCAAAACAACCCGTA
Insulin	TGGCTTCTTCTACACACCCAAG	ACAATGCCACGCTTCTGCC
Insulin	Taqman mIns1 Mm01259683_g1	
Lgr5	GGAAAGAAATGCTTTGATGGAC	AGTGGGGAATTCATCAAGGTT
PDGFRα	AAGACCTGGGCAAGAGGAAC	GAACCTGTCTCGATGGCACT
RPL9	ACCCTGGCCCGACGG	TACCCTTCCTCTTCCCTATGCC
Slug	GAAAAGCACATTGCATCTTTTCT	TGTTCCTTTGGTTGAAATGGT
Sox4	ACCGGTTTCCACCTTTCAA	ATTATGGTGCTGGGCTGAA
Syp	AACAACAAAGGGCCAATGAT	TAGCCACATGAAAGCGAACA
Tie2	GTATGGACTCTTTAGCCGGCTT	TTCGCCCATTCTCTGGTCAC
TBP	CCCCACAACTCTTCCATTCT	GCAGGAGTGATAGGGGTCAT
TNC (ms)	GCGCAGACACACACCCTAGC	TTTCCAGGTCGGGAAAAGCA
TNC (hu)	CCTTGCTGTAGAGGTCGTCA	CCAACCTCAGACACGGCTA
VEGF-A	GTACCTCCACCATGCCAAGT	TGGGACTTCTGCTCTCCTTC
VEGF-R1	GAGGAGGATGAGGGTGTCTATAGGT	GTGATCAGCTCCAGGTTTGACTT
VEGF-R2	GCCCTGCTGTGGTCTCACTAC	CAAAGCATTGCCCATTCGAT
VEGF-R3	TATGTCCGAAAGGGCAGTG	ACACCTTATCAAAGATGCTCTCG

3.5 Determination of micrometastasis

According to our own observations, mice of the RT2 model do not develop visible macrometastasis in liver and lung. Therefore, potentially arising micrometastasis to liver and lung were determined by qRT-PCR for insulin as a tumor cell specific marker. The biggest liver and lung lobe of tumor bearing mice was isolated immediately after sacrificing and snap frozen in liquid nitrogen. A few livers and lungs from wildtype and single-transgenic Rip-hTNC mice or heart tissue from wildtype or RT2 mice was analyzed as control tissues. Samples were prepared as described in section **3.4** and qRT-PCR was performed for TBP as reference gene and for insulin using a Taqman probe.

When analyzing samples of the RT2/hTNC model, a few heart and lung samples of control animals showed a weak background signal at cycle threshold later than 37 and was not always present in the duplicates. Therefore samples with ∆ct-values ≥ 12 were considered as undetermined and were removed from further calculations. For a subset of the analyzed mice the rest of liver and lung tissue was embedded in Tissue-Tek O.C.T. and frozen on dry ice. Histological sections were prepared of four distinct parts of the organs and stained for insulin and DAPI or for H&E. When analyzing liver and lung samples of the RT2/TNC-/- model in a mixed genetic background, control tissue of non-tumorigenic mice expressing one allele of TNC (TNC+/-) was analyzed and did not show a signal in liver or lung.

3.6 Mathematical and statistical analysis

Organization of original data, calculations of averages and relative expression levels were performed using the Microsoft Excel program. Graphical representation and statistical analysis was done on original data using GraphPad Prism 5.00. For significance of an association (contingency) Fisher's exact test or chi-square test was applied (islet/tumor staging, gene expression incidence, metastasis incidence). Statistical differences between two groups were analyzed by unpaired t-test (Gaussian distribution) or nonparametric Mann-Whitney U-test (no Gaussian distribution). Gaussian data sets with different variances were analyzed by unpaired t-test with Welch's correction. p-values ≤ 0.05 were considered as statistically significant. Data are represented as average values per group ± standard error of the mean (S.E.M.) or as Whiskers plot showing median, quartiles, minimum and maximum.

3.7 Preparation of murine pancreatic islets

Langerhans islets were isolated from adult male pancreata of 12 weeks old Rip-hTNC and wildtype mice or of 8 weeks old RT2/hTNC and RT2 mice (see **3.1.1**). Islets were isolated from the mouse pancreas by using Liberase RI (Roche). 3 ml Liberase RI solution was prepared for one mouse in ice-cold DMEM low glucose (Invitrogen, #31885) containing 0.82 Wünsch units per ml (175 µg/ml). Mice have been sacrificed by cervical dislocation and the bile duct was disconnected at its duodenal insertion by using a small bulldog clamp. The common bile duct was cannulated for injection of 2-3 ml Liberase RI solution. Only when the entire pancreas was inflated with Liberase RI, the organ was excised and kept on ice no longer than 60 minutes. Collected pancreata were digested at 37°C for 24 to 26 minutes. After several washing steps the digested pancreatic tissue was mixed with 10 ml Histopaque 1077 (Sigma) and covered with a layer of DMEM creating two phases. After centrifugation for 30 minutes at 1500 x g the islets accumulated at the interphase between Histopaque and

DMEM, were aspirated, washed once with fresh DMEM and transferred into islet culture medium (RPMI 1640 containing 11.1 mM glucose, 15% FCS, 1% penicillin/ streptomycin, 7.5% $NaHCO_3$, 66 µM β-mercaptoethanol). Islets were handpicked under a Leica MZ FLIII Stereomicroscope and placed into fresh islet culture medium. Only intact islets were kept. For Rip-hTNC and wildtype mice pools of at least 70 islets were prepared separately per mouse. For preparations of RT2 and RT2/hTNC mice, non-angiogenic and angiogenic islets were collected separately and were pooled from several mice of the same genotype to obtain at least 70 non-angiogenic or 25 angiogenic islets per sample. Non-angiogenic islets appeared completely whitish. Islets were considered as angiogenic as soon as they appeared reddish (see also **Figure 23A**). Islet pools were collected in sterile collection tubes, shortly centrifuged, medium removed, snap frozen in liquid nitrogen and kept at -80°C until RNA isolation.

3.8 Affymetrix® chip analysis

Total RNA of pools of isolated islets was extracted using the NucleoSpin RNA XS kit (Macherey-Nagel, Düren, Germany, #740902) according to the manufacturer's protocol. RNA was eluted from the columns in 15 µl pure water. 1 µl was used to determine RNA concentration on a NanoDrop ND-1000 spectrophotometer. 1.5 µl RNA was used for determining RNA integrity using RNA 6000 Nano Kit on a Agilent 2100 Bioanalyzer. The rest of the sample was transferred to the IGBMC microarray platform (Institute of Genetics and Molecular and Cellular Biology, IGBMC, Strasbourg) for performing Affymetrix® chip analysis. For each genotype at least 3 independent islet preparations were used. Rip-hTNC and wildtype islets were analyzed independent from the RT2 and RT2/hTNC preparations. 150 ng (Rip-hTNC or wildtype) or 200 ng (RT2 or RT2/hTNC) RNA was taken to prepare single strand cDNA according to the standard procedures of the IGBMC platform. Gene expression profiling was performed using GeneChip Mouse Gene 1.0ST Arrays. Data were provided as log2 values after normalization using the RMA (robust multi-array average) method (Irizarry *et al.*, 2003). Microsoft Excel was used for calculating fold-changes, for performing Student's t-test (assuming equal variances) and for filtering the data. Although the obtained data have not yet been analyzed in detail, preliminary filtering was performed to generate candidate genes lists (see Annex **8.2** *et seq.*).

4 Results

4.1 RT2 tumorigenesis upon forced expression of TNC

To determine the role of TNC in tumorigenesis, the RT2 mouse model of pancreatic neuroendocrine tumors was used to generate double transgenic mice with over-expression of human TNC mimicking high expression of TNC in human cancer. For the generation of single-transgenic Rip-hTNC mice, the cDNA of human TNC was cloned downstream of the rat insulin II promoter (Rip) (see Annex, **Manuscript 1 Suppl. Fig. 1**). Transgenic Rip-hTNC mice ectopically expressed the human TNC protein in Langerhans islets of the pancreas (**Figure 13A**), were healthy and fertile. Pancreatic islets displayed the typical pattern of glucagon-positive α-cells surrounding β-cells (Yundan Jia, not shown). To investigate whether ectopically expressed TNC had an impact on islet function, a glucose tolerance test was performed. This test showed that Rip-hTNC mice also exhibited normal blood glucose levels after starvation in comparison to wildtype control mice (**Figure 13B**). The maximal blood glucose levels at 15 minutes after glucose administration were slightly lower in Rip-hTNC mice but this difference was not statistically significant. Thus, ectopic expression of TNC did not interfere with the function of the endocrine pancreas in Rip-hTNC mice.

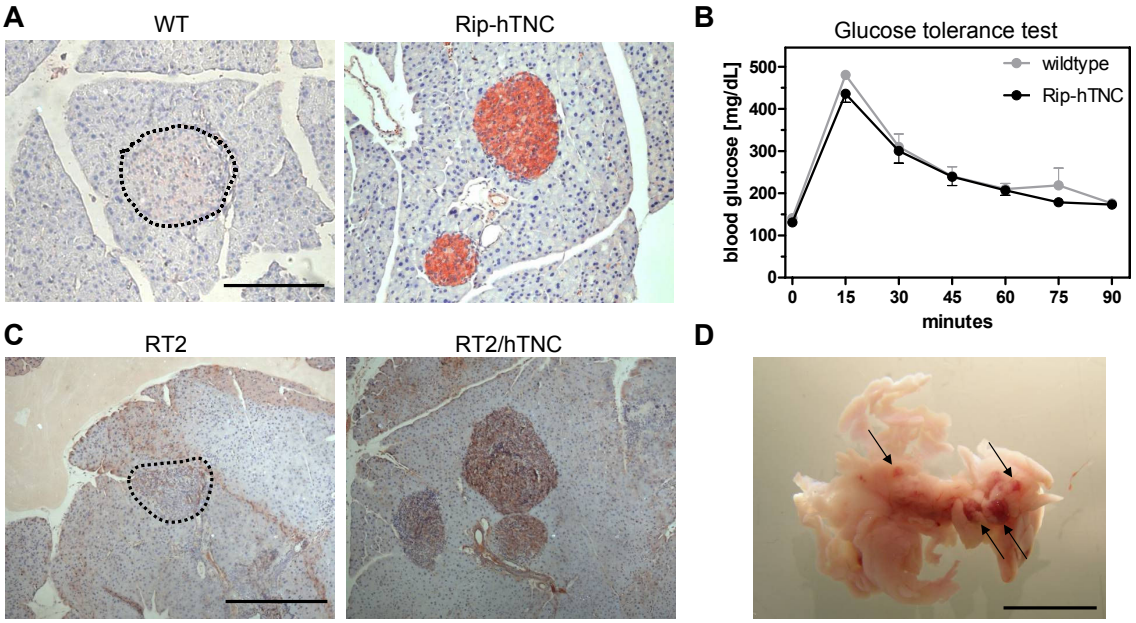

Figure 13: Generation of the RT2/hTNC model mimicking high TNC expression in human cancer

(A) IHC staining for human TNC expression in transgenic Rip-hTNC or wildtype control mice. Scale bar = 100 µm. (Staining performed by Yundan Jia).

(B) Blood glucose levels after an oral glucose tolerance test of transgenic Rip-hTNC (N = 14) and wildtype (N = 15) mice. Average ± S.E.M. is shown for each time point. Data from male and female mice were pooled as there was no gender-specific difference.

(C) IHC staining for human TNC in pancreata of double-transgenic RT2/hTNC or RT2 control mice. Scale bar = 500 µm. (Staining performed by Yundan Jia).

(D) Representative image of a 12 weeks old RT2 mouse pancreas. Few tumors ≥ 1 mm in diameter are visible (arrows). Scale bar = 1 cm.

RT2/hTNC double-transgenic mice were generated by breeding Rip-hTNC with RT2 mice. Tumors of double-transgenic animals expressed human TNC whereas control RT2 tumors showed no specific staining using the B28.13 antibody specific for human TNC (**Figure 13C**). **Figure 13D** shows an example of a pancreas dissected from a 12 weeks old RT2 mouse at macroscopic level. At that stage RT2 and RT2/hTNC mice usually develop several macroscopically visible tumors between 1 – 5 mm in diameter. In the following, different aspects of tumor progression will be presented which have been analyzed in the RT2/hTNC model system.

4.1.1 Impact of TNC on tumor growth and proliferation

First, a potential effect of TNC on tumor incidence and tumor burden was determined by counting tumor numbers and calculating tumor volume in RT2 and RT2/hTNC mice. When sacrificing 12 weeks old mice all macroscopically visible tumors (≥ 1 mm) were counted and the diameter was measured by a ruler to calculate the tumor volume. No difference in tumor incidence and tumor burden could be detected between RT2 and RT2/hTNC mice (**Figure 14A**). Note, by this method tumors located inside the pancreas are not taken into account, as the organ was embedded for further investigations.

To obtain a more precise measurement, 14 weeks old mice had been sacrificed and the size of each tumor was measured (≥ 1 mm). This revealed that whereas the tumor incidence was slightly elevated, surprisingly, the tumor burden was significantly reduced in double-transgenic RT2/hTNC mice compared to control RT2 mice (**Figure 14B**). This result suggests that ectopic expression of TNC rather inhibits tumor growth of bigger tumors. When classifying the tumors according to their size it turned out that RT2/hTNC mice developed significantly less huge tumors bigger than 3 mm in diameter (**Figure 14C**). This can explain the reduction of tumor volume as a single big tumor can have a substantial contribution to the total tumor volume per mouse. At the same time, 14 weeks old RT2/hTNC mice showed a tendency to develop more tumors smaller than 3 mm in diameter (**Figure 14C**), suggesting that TNC might have an effect on tumor onset.

Therefore, it was analyzed whether islet size, which correlates with the tumorigenic state, was different between RT2 and RT2/hTNC mice at 10 weeks of age where most of the islets are still smaller than 1 mm in diameter. The islet diameters were measured on tissue sections showing that the ratio of small and big tumors over that of normal and hyperplastic islets was higher in RT2/hTNC (0.8) than in RT2 control mice (0.4) and was close to statistical significance ($p = 0.064$ Fisher's exact test) (**Manuscript 1 Suppl. Table 1**). Since the sample size was too small it was not possible to get a more detailed information if there was a difference in each subclass between genotypes. Altogether, these data suggest that

ectopic expression of TNC in RT2 mice promotes tumor progression but does not support growth of established tumors.

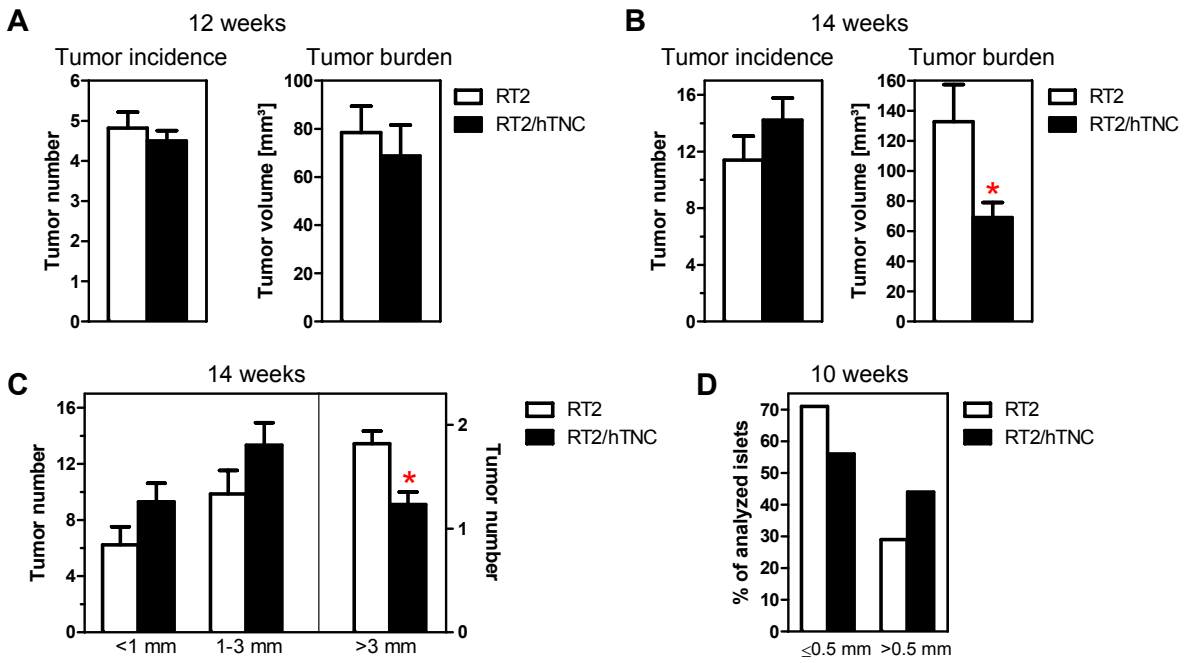

Figure 14: Impact of TNC on tumor growth

(A) Determination of tumor incidence and tumor burden per mouse by measuring the diameter of macroscopically visible tumors (Ø ≥1 mm) from 12 weeks old RT2 (33 mice; 156 tumors) and RT2/hTNC (26 mice; 117 tumors) mice. Data represent average values per mouse (± S.E.M.).

(B) Determination of tumor number and volume upon dissection and measurement of the tumor diameter (Ø ≥ 1 mm) in 14 weeks old RT2 (13 mice; 148 tumors) and RT2/hTNC (18 mice; 256 tumors) mice. Data represent average values per mouse (± S.E.M.). (* p = 0.0296).

(C) Quantification of tumors (same samples as in B) with a diameter <1 mm, 1-3 mm and >3 mm. For a subset of mice shown in (B) small tumors (Ø < 1 mm) were detectable (9 x RT2, 17 x RT2/hTNC). Data represent average values (± S.E.M.) (* p = 0.0055)

(D) Frequency of normal and hyperplastic islets (≤ 0.5 mm) or small tumors (>0.5 mm) in 10 weeks old RT2 and RT2/hTNC mice. Islets were classified according to diameter determined on tissue sections. Data represent percentage of all analyzed islets. The distribution of islets in the two subclasses of RT2 and RT2/hTNC mice was close to statistical significance (p = 0.0629, Fisher's exact test). Detailed data for all subclasses and sample number are shown in Manuscript 1 Suppl. Table 1 (see Annex).

Next, it was investigated if enhanced tumor progression correlates with enhanced proliferation. Therefore, it was addressed whether forced expression of TNC had an effect on cell proliferation. Histological sections of pancreata of 12 weeks old RT2 and RT2/hTNC mice were stained for the proliferation marker PH3 or KI67 (**Figure 15A**) and immuno-fluorescence signals were quantified. Tumors of RT2/hTNC mice exhibited 1.7-fold more proliferating cells than those from RT2 mice (**Figure 15B**). This was confirmed on a subset of the same samples by staining for KI67 where RT2/hTNC tumors showed 1.5-fold more proliferating cells than RT2 control mice (**Figure 15C**). A detailed analysis of the proliferation rate in different subclasses revealed that normal (1.7-fold) and hyperplastic (1.4-fold) islets

were more proliferative in RT2/hTNC than in RT2 mice whereas small and big tumors did not show a difference between genotypes (**Figure 15C**). To determine which cells are proliferative in the tumors, co-staining of KI67 with SV40 Tag or insulin (β-cell tumor cells), with F4/80 (macrophages) and with CD31 (endothelial cells) was performed. This analysis revealed that the proliferating cells were mostly tumor cells (data not shown). If over-expression of TNC had an impact on the proliferation rate of a specific cell type has not been addressed quantitatively.

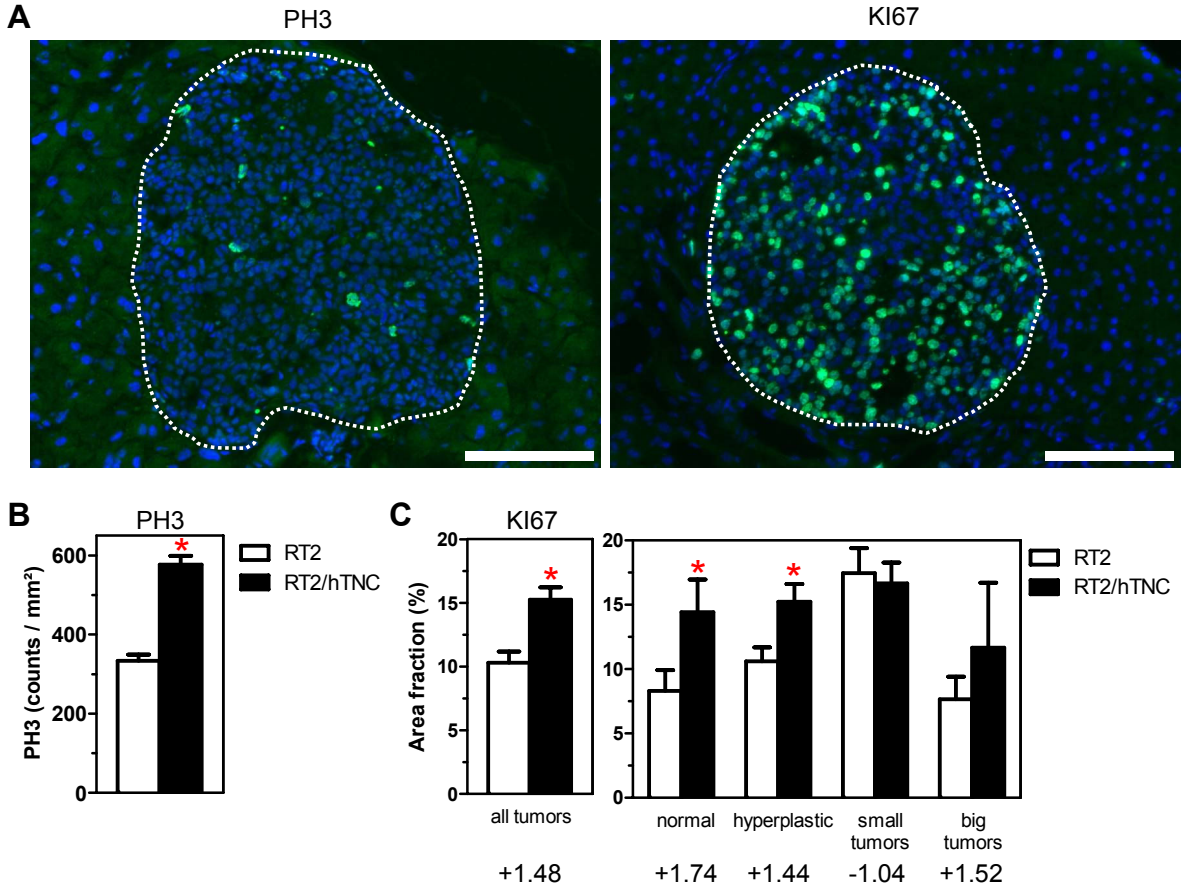

Figure 15: Impact of TNC on cell proliferation

(A) Representative pictures of DAPI, PH3 and KI67 staining of RT2 tumors. Dotted lines delineate the islet lesions. Scale bar = 100 µm.

(B) Quantification of proliferating cells in islets of 12 weeks old RT2 and RT2/hTNC mice. Tissue sections were stained for PH3 and quantified using the ImageJ software. Data are shown as number of PH3-positive cells per mm² (average ± S.E.M.). RT2 (13 mice, 199 sections), RT2/hTNC (24 mice, 176 sections). RT2/hTNC mice showed significant 1.7-fold more PH3 cells (* $p < 0.0001$).

(C) Subset of tissue sections analyzed in (B) of three RT2 mice (34 tumors) and one RT2/hTNC mouse (39 tumors) were stained for KI67 as proliferation marker and quantified. Data are presented as average area fraction per analyzed tumor (± S.E.M.). RT2/hTNC mice showed a significantly higher proliferation rate already in normal and hyperplastic islets. Fold-changes are indicated below each subclass (* $p \leq 0.05$).

In summary, these data indicate that enhanced expression of TNC had a very early effect on pancreatic islet tissue homeostasis which led to accelerated tumor onset in RT2/hTNC mice likely by increasing the proliferation rate in normal islets.

4.1.2 Impact of TNC on tumor angiogenesis

The role of TNC during tumor angiogenesis was addressed by quantification of the EC marker CD31 in tumor sections of RT2 and RT2/hTNC mice (**Figure 16A**). The area fraction of CD31-positive signals turned out to be 2.2-fold (10 weeks) and 2.5-fold (12 weeks) higher in tumors of RT2/hTNC mice than in tumors of RT2 controls (**Figure 16B**). This experiment suggests that ectopically expressed TNC promoted angiogenesis in spontaneously arising RT2 tumors.

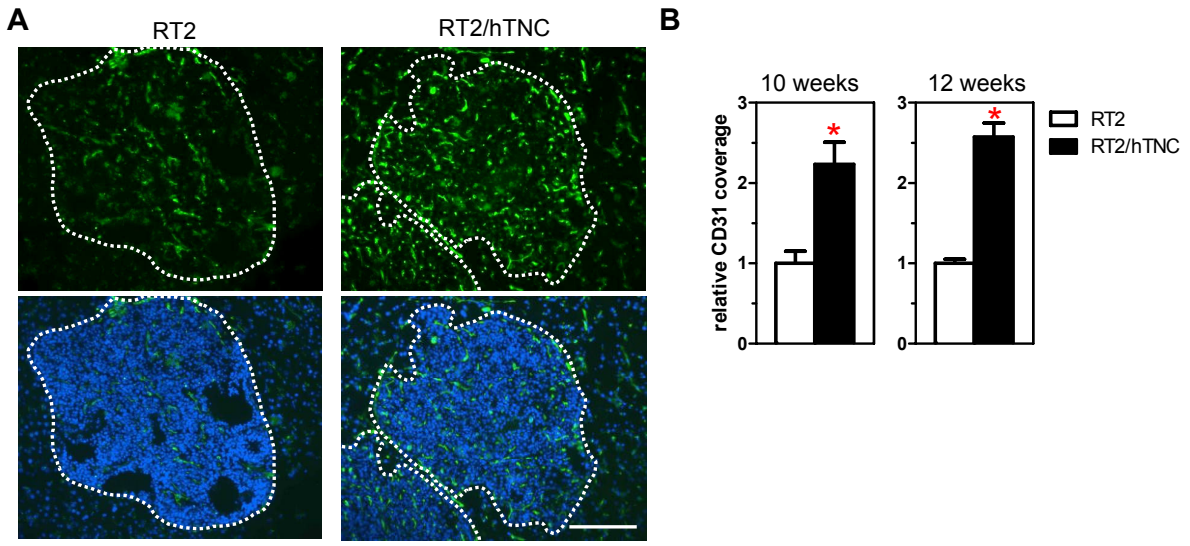

Figure 16: Impact of TNC on tumor angiogenesis

(A) Representative pictures of DAPI and CD31 staining of RT2 and RT2/hTNC tumors. Dotted lines delineate the islet lesions. Scale bar = 100 µm. (Staining performed by Yundan Jia).

(B) Quantification of CD31-positive IF signals in tumors of 10 week (left) or 12 week (right) old RT2 and RT2/hTNC mice. Area fraction per analyzed field was determined using the ImageJ software. RT2/hTNC mice showed significantly 2.23-fold (10 weeks, $p = 0.0017$) or 2.57-fold (12 weeks, $p < 0.001$) higher CD31. Data were normalized relative to control RT2 tumors.

4.1.3 Impact of TNC on invasion and metastasis formation

By determining the percentage of adenomas and invasive carcinomas it was shown that the ratio of carcinomas versus adenomas was higher in tumors of RT2/hTNC mice (1.8) than in RT2 controls (0.8) (**Manuscript 1 Fig. 1E and Suppl. Table 2**). A higher number of invasive tumors in double-transgenic mice suggests that they may also form more metastasis. Therefore, it was investigated if ectopic expression of TNC had an impact on the formation of liver and lung metastasis.

In a C57BL6 background, RT2 mice usually do not exhibit macrometastasis (Hanahan, 1985) and during this thesis I never observed macrometastasis to liver or lung in none of the experiments. Therefore, potentially arising micrometastasis in liver and lung were determined by qRT-PCR for insulin. Insulin expression was compared to heart tissue, which

is not a primary site for metastasis. In contrast to low background levels of insulin mRNA in a few lungs of control Rip-hTNC and wildtype mice and in hearts of RT2/hTNC mice (see **3.5**), a strong insulin-specific signal was observed in livers and lungs of RT2 (6 livers and 9 lungs from 24 mice) and RT2/hTNC mice (7 livers and 11 lungs from 24 mice). Yet, while insulin expression of micrometastatic β-tumor cells was indistinguishable between liver tissue of RT2 and RT2/hTNC mice, insulin levels in lungs of RT2/hTNC mice were 6.1-fold higher in comparison to lungs of RT2 mice which was statistically significant (**Figure 17A**).

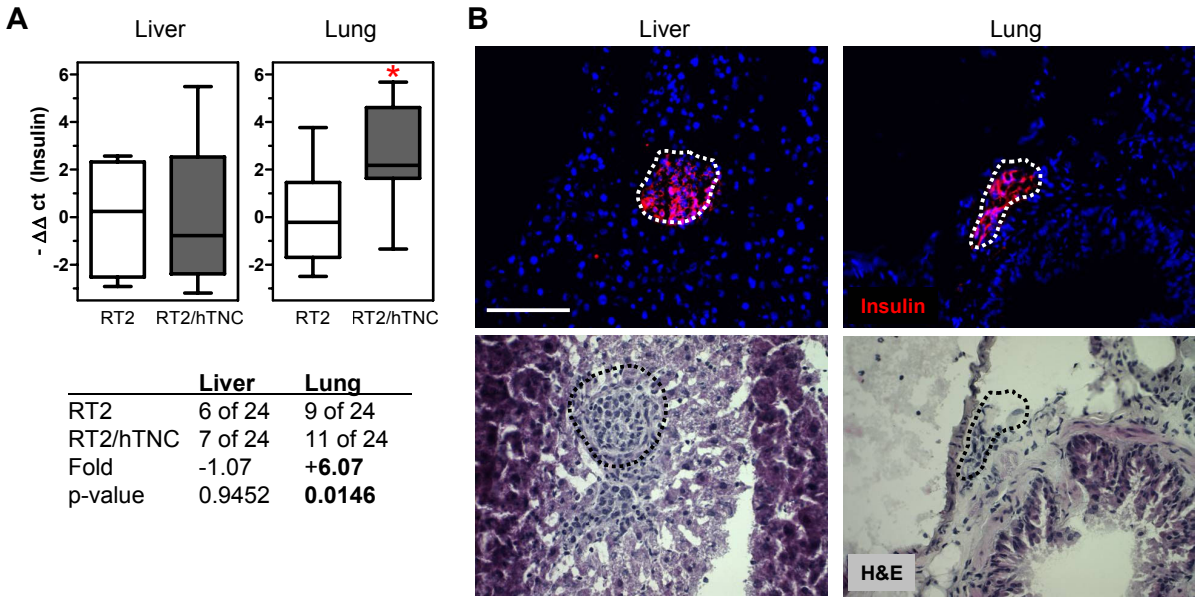

	Liver	Lung
RT2	6 of 24	9 of 24
RT2/hTNC	7 of 24	11 of 24
Fold	-1.07	**+6.07**
p-value	0.9452	**0.0146**

Figure 17: Impact of TNC on metastasis formation

(A) Quantification of micrometastasis in liver and lung tissue by qRT-PCR for insulin as a specific tumor marker. Not all samples exhibited insulin expression. Data are presented as -ΔΔct using Whiskers plot showing median, minimum and maximum of analyzed samples. The difference in signal intensity for lung tissue was statistically significant. There was no statistical difference in frequency detected in liver micrometastasis between genotypes.

(B) Representative images of liver and lung tissue stained for insulin (top) or H&E (down). Insulin-positive cell clusters (red) were found in sections adjacent to the H&E stained sample as dense cell clusters representing micrometastasis derived from the insulinoma. Scale bar = 50 µm (Staining performed by M. van der Heyden and C. Arnold).

To determine whether the insulin signal indeed derived from tumor cells that had colonized the liver and lung, tissue sections were stained by IF for insulin. Considerable numbers of insulinoma cells in small cell clusters could be detected within the liver and lung parenchyma which could likewise be recognized in adjacent sections stained for H&E (**Figure 17B**) and this, indeed represent micrometastasis. Lungs of 5 mice of each genotype were analyzed in more detail showing an insulin-specific signal in only a few samples which does not allow statistical analysis (**Table 3**). Yet, in lung samples which were negative or in the range of background expression by qRT-PCR, no insulin-positive signal could be detected by tissue staining. On the other hand, in samples with high insulin-specific RNA expression insulin-

positive cell clusters could easily be detected, which supports that insulin quantification by qRT-PCR is a valid approach for micrometastasis detection.

Table 3: Comparison of insulin expression analyses in lungs of RT2 and RT2/hTNC mice

Quantification of IF signal was performed using the ImageJ program after staining lung sections of 14 weeks old RT2 and RT2/hTNC mice for insulin and DAPI. 8 randomly chosen tissue sections from different regions of the lung were analyzed. The insulin positive surface area was normalized to the total analyzed area per section. Values represent the sum of normalized insulin area per mouse. At RNA level fold-changes were calculated relative to the sample with lowest signal (#96).

Mouse	**IF staining** (relative surface)	**qRT-PCR** (relative expression)
RT2 #93	negative	background
RT2 #96	**low** (160)	**1.0**
RT2 #99	negative	negative
RT2 #100	negative	negative
RT2 #112	**very high** (15900)	**11.8**
RT2/hTNC #71	**high** (5230)	**3.2**
RT2/hTNC #80	negative	negative
RT2/hTNC #91	negative	background
RT2/hTNC #94	**high** (510)	**34.3**
RT2/hTNC #116	very low (7)	background
control tissue	**negative**	**background**

By using insulin as a marker, only disseminated tumor cells can be detected which had maintained or had regained expression of insulin, but not those β-tumor cells that potentially had lost insulin expression. For an independent means of metastasis determination, the neuroendocrine-specific markers glucagon-like peptide-1 receptor (Wild *et al.*, 2006), insulinoma-associated antigen-1 (Breslin *et al.*, 2002; Garber *et al.*, 2001) and synaptophysin (Du *et al.*, 2007) have been tested by qRT-PCR. But their expression was either below the limit of detection or was already high in livers and lungs of control wildtype mice.

In summary, RT2 and RT2/hTNC do not develop visible macrometastasis in a C57BL6 genetic background. By using insulin as a β-tumor cell specific marker we were able to detect micrometastasis in liver and lung tissue in a subset of RT2 and RT2/hTNC mice. Quantification of the insulin signal by qRT-PCR suggests that ectopically expressed TNC enhanced lung but not liver metastasis.

By analyzing the effect of ectopic expression of human TNC in the RT2 model system it was observed that forced expression of TNC promoted cell proliferation, carcinoma progression, tumor invasion, angiogenesis and the formation of lung micrometastasis.

4.2 RT2 tumorigenesis in the absence of TNC

I had established the loss-of-function RT2/TNC-/- model to study whether the absence of TNC had an impact on tumorigenesis in the RT2 model. This will serve as a complementary model system to the already established transgenic RT2/hTNC model with forced over-expression of TNC. Mice lacking expression of a functional TNC gene (Forsberg et al., 1996) and RT2 mice (Hanahan, 1985) have originally been generated in different genetic mouse strains (see **3.1**). The C57BL6 RT2/TNC-/- colony was obtained only recently and therefore only a few preliminary results were already obtained in a mixed genetic background (generation 1, 50% C57BL6) or in an almost pure C57BL6 background (generation 8, 99.6% C57BL6) by comparing littermates.

4.2.1 Analysis of tumor growth and metastasis in RT2/TNC-/- mice in a mixed genetic background

When sacrificing mice in the mixed 129/Sv-C57BL6 background at 12 weeks of age, I observed that they did not develop macroscopically visible tumors (**Figure 18A**) which is in contrast to C57BL6 RT2 mice (**Figure 13D**). But later at 15 to 17 weeks, mice developed visible tumors with up to 16 mm in diameter. Sometimes the entire pancreas was a single big tumor (**Figure 18A**), an observation that has never been made in RT2 or RT2/hTNC mice in a C57BL6 background. In summary, in the mixed genetic background, RT2 tumorigenesis was delayed by ~4 weeks and tumor burden was highly increased compared to C57BL6 RT2 mice, which was independent on TNC expression levels.

In the same mixed genetic background, RT2/TNC+/- mice carrying one allele of TNC have been compared to RT2/TNC-/- mice at 15-17 weeks. The presence of the wildtype or the deleted form of TNC was determined by PCR (**Figure 18B**). For each genotype, protein extracts of two tumors were analyzed by Western Blot for TNC expression and no TNC was found in tumors of RT2/TNC-/- mice (**Figure 18C**). IF staining for TNC on fresh frozen tumor material confirmed the absence of TNC protein in RT2/TNC-/- tumors whereas tumors of RT2/TNC+/- mice showed deposition of TNC in the tumor microenvironment (**Figure 18D**).

To investigate the impact of the absence of TNC on tumor incidence and tumor burden, the total number and volume of tumors (≥ 1 mm) was determined for each mouse. This analysis revealed no statistically significant difference between mice of both genotypes but there was a tendency toward more tumors and a reduced total tumor volume in mice with one TNC allele in comparison to RT2 mice lacking TNC (**Figure 18E**).

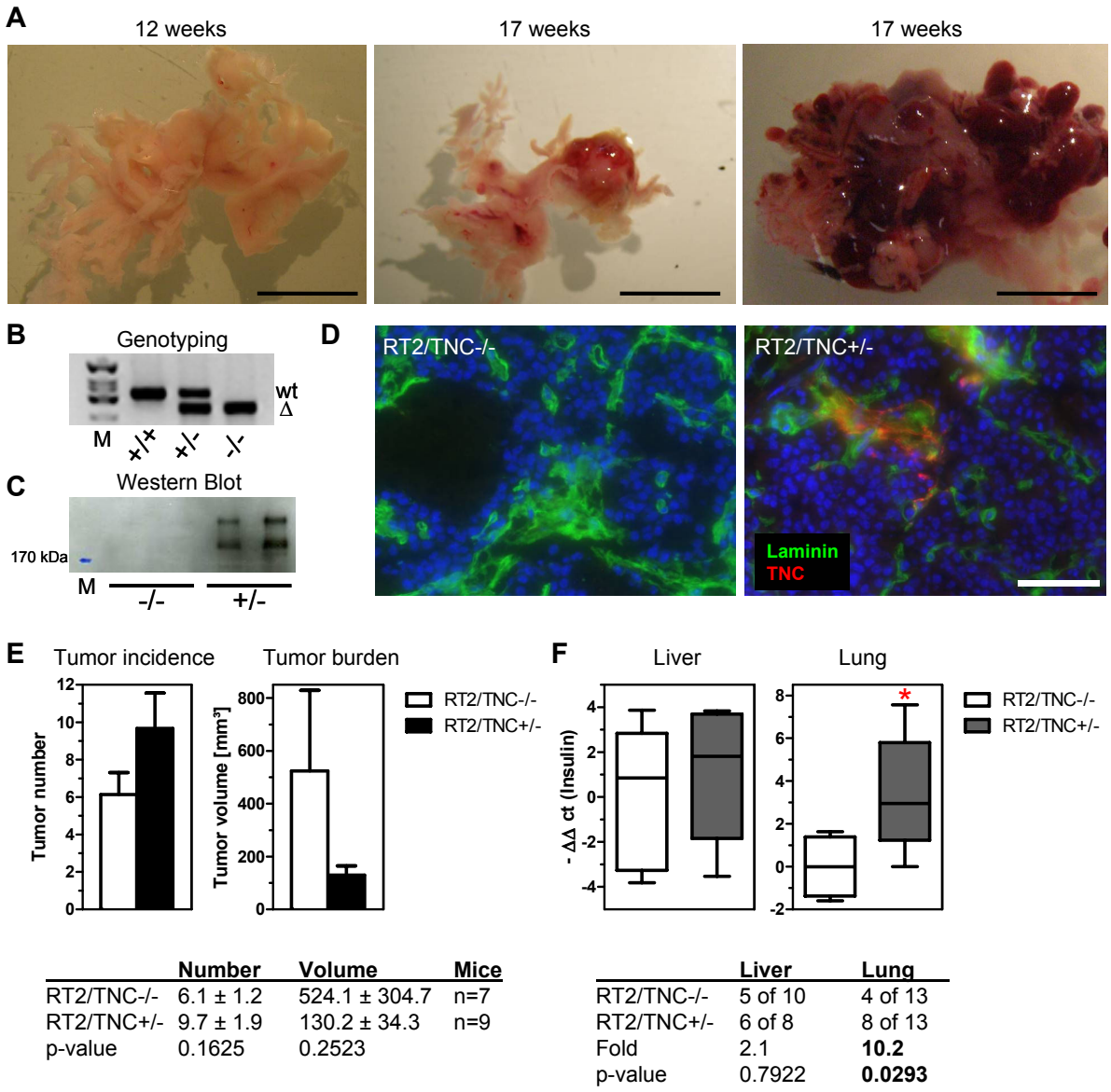

	Number	Volume	Mice
RT2/TNC-/-	6.1 ± 1.2	524.1 ± 304.7	n=7
RT2/TNC+/-	9.7 ± 1.9	130.2 ± 34.3	n=9
p-value	0.1625	0.2523	

	Liver	Lung
RT2/TNC-/-	5 of 10	4 of 13
RT2/TNC+/-	6 of 8	8 of 13
Fold	2.1	**10.2**
p-value	0.7922	**0.0293**

Figure 18: Effect of the absence of TNC on RT2 tumorigenesis in a mixed 129/Sv-C57BL6 genetic background

(A) Representative images of pancreata of RT2 mice with a 50-75% 129/Sv genome. At 12 weeks (left) pancreata showed no visible tumors but tumor mass increased massively in mice by 14 to 17 weeks of age. Scale bar = 1 cm.

(B) PCR of genomic DNA for the wildtype (wt) and the knockout TNC allele (Δ) in wildtype, heterozygous and homozygous mice.

(C) Western blot for TNC expression in RT2/TNC-/- and RT2/TNC+/- tumors. Total protein was extracted from isolated tumors, 50 µg were separated by 6% SDS-PAGE, and the blot was incubated with the MTn12 antibody.

(D) IF analysis of fresh frozen tumor material for TNC (red) and laminin (green) expression showing the absence of TNC in RT2/TNC-/- tumors. Nuclei were stained using DAPI (blue). Scale bar = 50 µm.

(E) Quantification of tumor number and volume (mm³) per mouse of macroscopically visible tumors ≥1 mm in diameter in RT2/TNC-/- and RT2/TNC+/- mice from the same breeding at ages between 16 to 17 weeks. Data are shown as average per mouse ± S.E.M. and are not statistically significant.

(F) Determination of micrometastasis in liver and lung by qRT-PCR for insulin as a specific tumor marker. Note that 4 of 13 (RT2/TNC-/-) and 8 of 13 (RT2/TNC+/-) mice exhibited detectable insulin expression in the lung. Analyzed organs were sampled from 15 to 17 weeks old mice. Data are presented as -ΔΔct using Whiskers plot with median, minimum and maximum of analyzed samples.

Whether the absence of TNC had an impact on formation of micrometastasis was further investigated by qRT-PCR for insulin. In organs with detectable insulin expression no difference was observed between livers of RT2/TNC-/- and RT2/TNC+/- mice whereas lungs of RT2 mice carrying one intact TNC allele displayed 10.2-fold higher insulin levels compared to lungs of RT2/TNC-/- mice (**Figure 18F**).

4.2.2 Analysis of tumor progression in RT2/TNC-/- mice in a C57BL6 background

To verify if the lack of visible tumors in 12 weeks old mice (**Figure 18A**) was due to the 129/Sv background, TNC+/- mice of generation 3, 6 and 8 have been bred with RT2 mice. Indeed, RT2 mice in generation 3 still showed a delayed tumor formation with development of huge tumors whereas RT2 mice in generation 6 and 8 developed visible tumors up to 4 mm in diameter in a time frame of 12 to 14 weeks (**Figure 19A**) that is comparable to a C57BL6 background (**Figure 13D**). Thus, the 129/Sv mouse strain has a strong impact on tumor incidence and tumor burden in the RT2 model system independent on TNC expression levels.

4.2.2.1 Tumor incidence and burden

A new set of mice was generated in an almost pure C57BL6 background (generation 8, 0.4% 129/Sv left) where mice lacking TNC expression (RT2/TNC-/-) were compared to mice from the same litter having both alleles of TNC (RT2/TNC+/+). 12 weeks old mice were sacrificed and tumor incidence and tumor burden were determined macroscopically. This analysis revealed that the lack of TNC had no impact on tumor formation as the average tumor number and tumor volume per mouse were equal in RT2/TNC-/- and RT2/TNC+/+ mice (**Figure 19B**). In a more detailed analysis the islet size was determined on tissue sections and revealed that the lack of TNC had indeed no effect on the frequency of normal islets, hyperplastic islets, small and big tumors (**Figure 19C**). This preliminary analysis including 3 mice of each genotype needs to be extended which is ongoing. To investigate the effect of TNC on tumor malignancy by grading other parameters such as the angiogenic and invasive stages needs to be included (Lopez and Hanahan, 2002). These experiments require paraffin embedded samples which are not available yet.

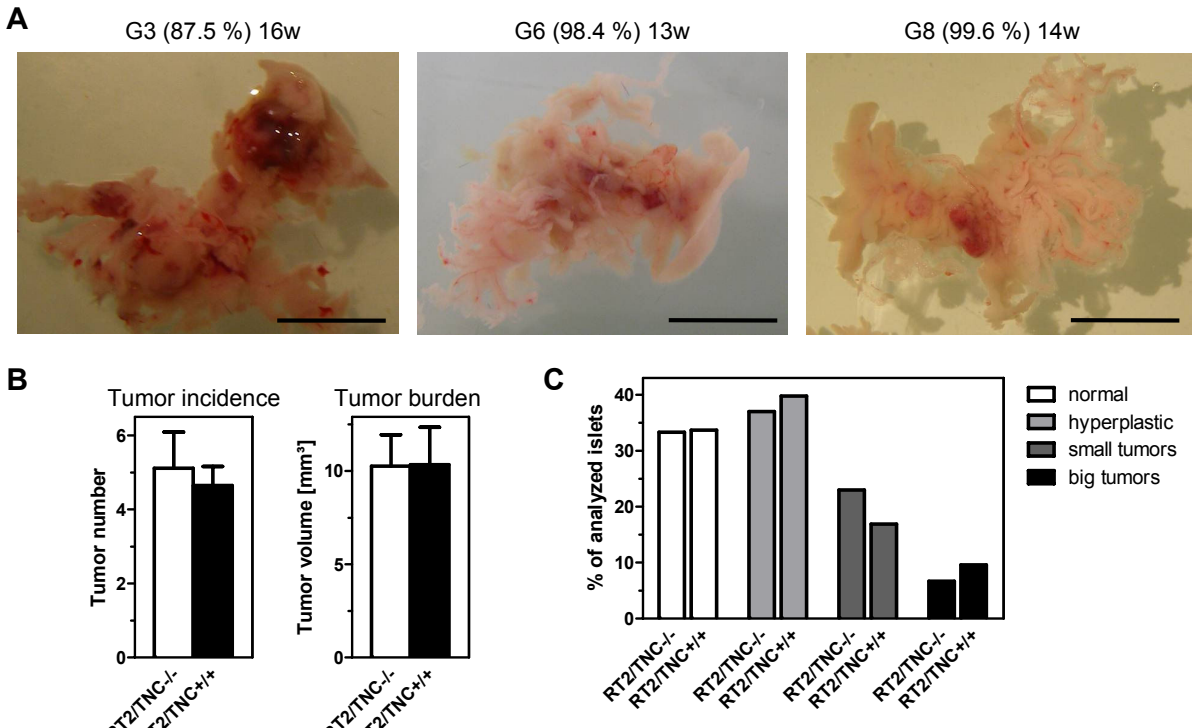

	Number	Volume	Mice
RT2/TNC-/-	5.1 ± 1.0	10.3 ± 1.7	n=9
RT2/TNC+/+	4.6 ± 0.5	10.3 ± 2.0	n=17
p-value	0.6463	0.9803	

	RT2/TNC-/-		RT2/TNC+/+	
	%	(#)	%	(#)
normal	**33.3**	(45)	**33.7**	(28)
hyperplastic	**37.0**	(50)	**39.8**	(33)
small tumors	**23.0**	(31)	**16.9**	(14)
big tumors	**6.7**	(9)	**9.6**	(8)
total	**100**	(135)	**100**	(83)

Figure 19: Effect of the absence of TNC on tumor growth in a C57BL6 background

(A) Representative images of pancreata of RT2 mice with different levels of the C57BL6 genome (in %) at the indicated time points after birth. RT2 mice in generation 6 and 8 of backcrossing into C57BL6 show a similar phenotype than RT2 mice in a pure C57BL6 background. Scale bar = 1 cm.

(B) Estimation of tumor incidence and tumor burden per mouse by measuring the diameter of macroscopically visible tumors (Ø ≥1 mm) from 12 weeks old RT2/TNC-/- (9 mice; 46 tumors) and RT2/TNC+/+ (17 mice; 79 tumors) mice from the same breeding. Data represent average values (± S.E.M.) per mouse.

(C) Quantification of subclasses of tumorigenic islets by size. Data are represented as percentage of all analyzed islets in 3 mice of each genotype. No statistical difference was found (χ^2-test p=0.6572). (normal: <0.2 mm, hyperplastic: 0.2-0.5 mm, small tumor: >0.5 mm - <1 mm, big tumor: ≥1 mm).

4.2.2.2 Tumor angiogenesis

Next, the effect of the absence of TNC on tumor angiogenesis was addressed by quantification of CD31-positive signals in tumor sections of both genotypes (**Figure 20A**). The CD31-positive area fraction turned out to be 1.57-fold higher in control tumors than in tumors of mice lacking TNC expression (**Figure 20B**). This supports our observation of the angiogenesis promoting effect of TNC in double-transgenic RT2/hTNC mice (see **4.1.2**). A more detailed analysis revealed that in RT2/TNC+/+ mice hyperplastic islets and small tumors showed enhanced angiogenesis in comparison to normal islets of the same mice. An increased angiogenesis could not be observed in samples of RT2/TNC-/- mice where levels

of CD31-positive signals remained similar in all subclasses of pancreatic islets (**Figure 20B**). This result confirms the angiogenesis promoting effect of TNC and indicates a promoting influence of TNC on the angiogenic switch.

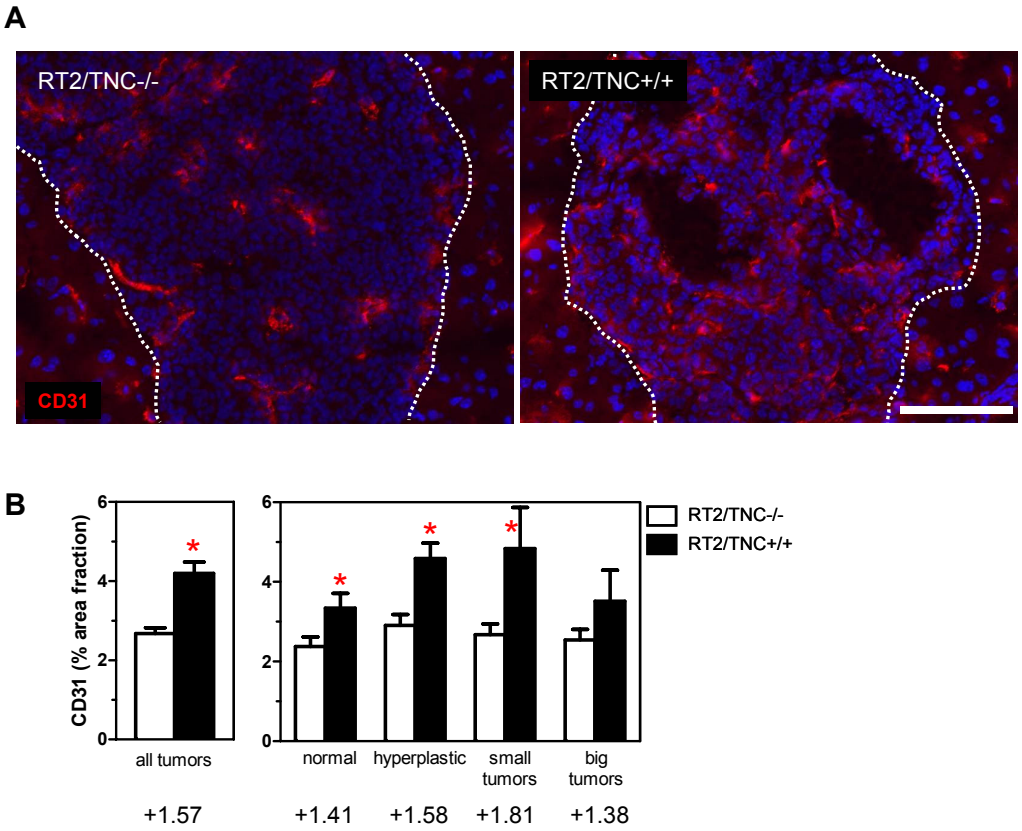

Figure 20: Tumor angiogenesis in tumors of RT2/TNC-/- and RT2/TNC+/+ mice

(A) Representative images for CD31 staining in RT2/TNC-/- and RT2/TNC+/+ tumors. Dotted lines delineate the tumor. Scale bar = 100 µm.

(B) Quantification of CD31 expression in tumors of 3 RT2/TNC-/- mice (111 tumors) and 3 RT2/TNC+/+ mice (71 tumors) of 12 weeks of age from the same breeding. CD31 is expressed as area fraction per tumor (average ± S.E.M.). Control RT2/TNC+/+ mice showed significantly higher angiogenesis already in normal and hyperplastic islets. Fold-changes compare RT2/TNC+/+ versus RT2/TNC-/- tumors and are indicated below each subclass (* $p < 0.026$).

4.2.2.3 Tenascin-C expression pattern

Furthermore, IF staining was performed to determine TNC expression levels during different tumor stages. This confirmed the absence of TNC in RT2/TNC-/- tumors (**Figure 21A**). In tumors of RT2/TNC+/+ littermates TNC expression levels were heterogeneous. Therefore, three different categories have been defined according to the TNC expression pattern. Whereas some tumors did not show a TNC positive signal (category 0) others locally expressed TNC at different intensity (category 1). Other tumors had a strong and widely distributed TNC signal in tube-like appearance (category 2) (**Figure 21A**). Correlation of the TNC expression pattern with tumor size revealed that TNC was not detected in normal islets but TNC was expressed in 50% of hyperplastic islets and 79% of small tumors whereas all

big tumors showed TNC expression (**Figure 21B**). This observation suggests that TNC might play a role during early and late events of tumorigenesis.

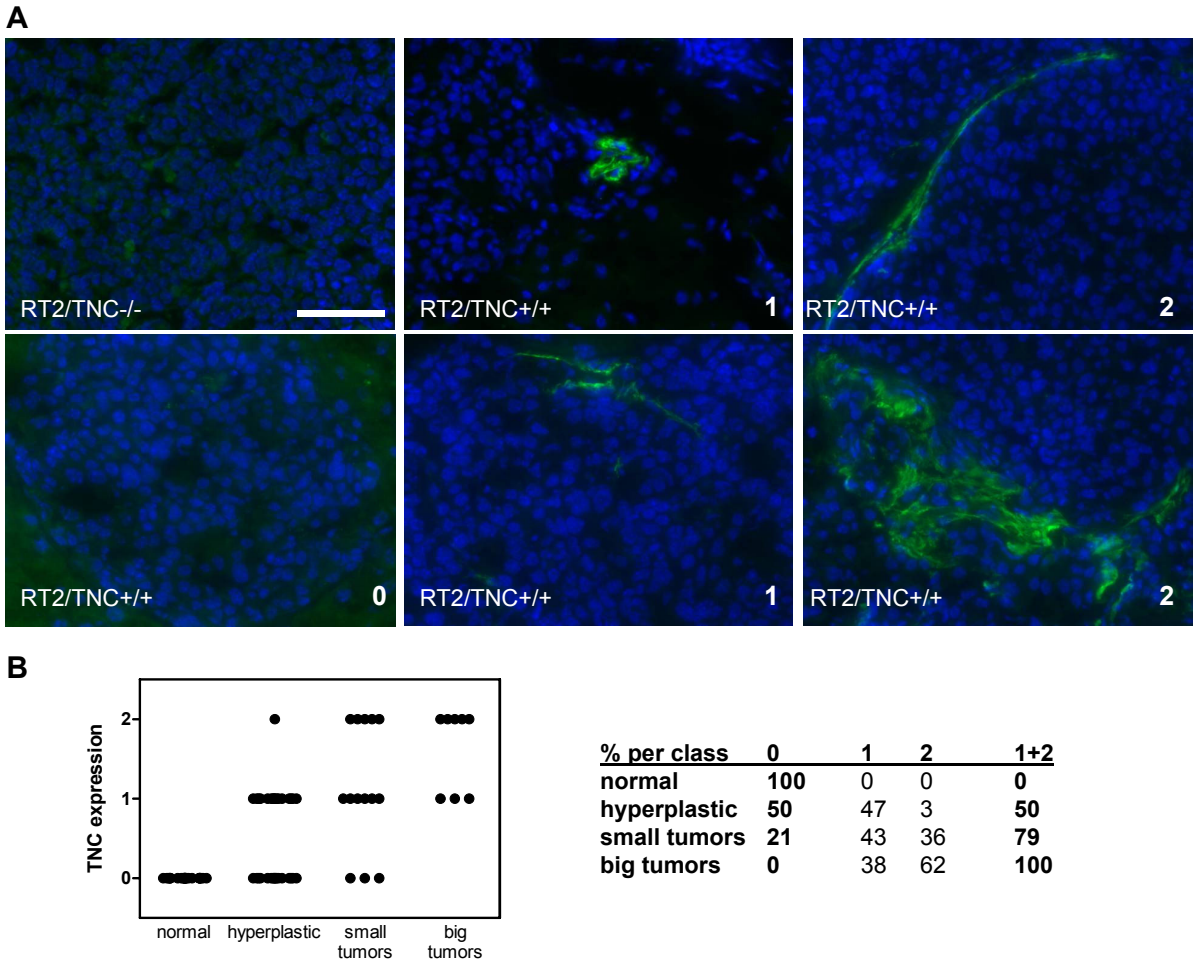

% per class	0	1	2	1+2
normal	**100**	0	0	**0**
hyperplastic	**50**	47	3	**50**
small tumors	**21**	43	36	**79**
big tumors	**0**	38	62	**100**

Figure 21: Correlation of TNC expression and tumor growth

(A) Representative images of TNC staining in a RT2/TNC-/- tumor and tumors of RT2/TNC+/+ mice with different TNC expression patterns. Mice were sacrifice at age of 12 weeks. The numbers indicate classification of TNC expression assessed by microscopy: 0 = no expression, 1 = local expression with variable intensity; 3 = strong, widely distributed expression in tube-like structures. Scale bar = 50 µm.

(B) Graphical representation of classifying the TNC expression pattern. Each dot represents one tumor according to its size and classification of TNC expression. The table summarizes the frequency of the TNC expression patterns in each subclass according to its size. Normal islets do not express TNC whereas all big tumors express TNC visualized by IF staining using the MTn12 antibody.

In conclusion, RT2 mice lacking TNC expression in a C57BL6 genetic background had been generated and showed a similar tumor development as RT2 and RT2/hTNC mice. TNC expression in samples of control RT2/TNC+/+ mice promoted angiogenesis compared to samples lacking TNC. A similar CD31-positive signal in all subclasses of islets of RT2/TNC-/- mice suggests an important role of TNC during the angiogenic switch. Moreover, normal RT2 islets did not show expression of TNC whereas hyperplastic islets and small and big tumors expressed TNC to a variable extent. In a mixed genetic background, using mice with only one allele of TNC the lack of TNC diminished the formation of lung micrometastasis.

4.3 Mechanism of TNC action in the RT2 model

4.3.1 Candidate gene expression analysis

In search for mechanisms of TNC action that could explain the above described impact of TNC on tumor progression in the RT2/hTNC model, expression levels of several candidate genes were determined by qRT-PCR on RNA extracted from isolated tumors (≥ 1 mm) of 14 weeks old RT2 and RT2/hTNC mice. Tumors were classified according to their size (1-3 mm or > 3 mm) and tumor stage. In the RT2 model, reduced insulin expression and loss of E-cadherin protein levels is a sign of tumor progression from adenoma to highly invasive carcinoma (Chun and Hanahan, 2010; Perl *et al.*, 1998). Therefore, gene expression levels for insulin and E-cadherin have been determined in all analyzed tumors (**Figure 22A**). Whereas most tumors showed high expression levels of both molecules, five tumors showed a strong reduction of insulin (~150-fold) and E-cadherin (~13-fold) expression. These tumors were considered as dedifferentiated and thus as invasive carcinomas. Expression levels of candidate genes have been compared between RT2 and RT2/hTNC tumors in the defined subclasses (**Figure 22A;** see Annex **Table 5**).

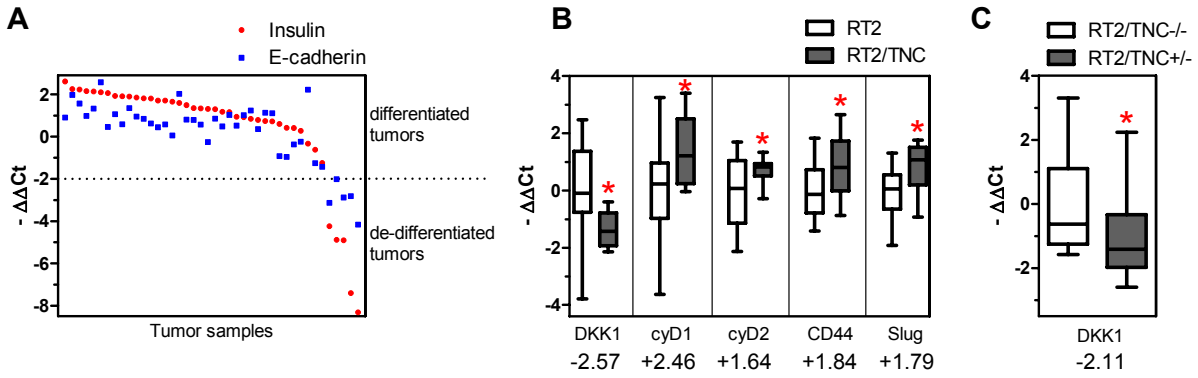

Figure 22: Gene expression analysis of candidate genes in tumors of 14 weeks old mice

(A) qRT-PCR of insulin and E-cadherin expression levels in RT2 and RT2/hTNC tumors. Data were calculated relative to average expression in all analyzed RT2 tumors and sorted by descending insulin expression. Dotted line: cutoff between "differentiated" (high levels) and "de-differentiated" (low levels) tumors.

(B) qRT-PCR on small and differentiated tumors from RT2 (n = 18) and RT2/hTNC mice (n = 11) for DKK1, cylinD1, cyclinD2, CD44 and Slug. Note, not all tumors expressed DKK1. Fold-changes are indicated. Data for all tumors are summarized in **Table 5**. (* $p \leq 0.05$).

(C) qRT-PCR for DKK1 expression in RT2/TNC-/- (n = 16) and RT2/TNC+/- (n = 15) tumors (* $p = 0.023$). Data show 2.1-fold reduced DKK1 expression levels in tumors from mice with one allele of TNC.

A potential link of TNC to Wnt signaling was investigated since the Wnt inhibitor DKK1 was strongly down-regulated in GBM cells cultured on a TNC substratum. At the same time, the transcription factors TCF1α/LEF1 and the Wnt target gene Id2 were significantly up-regulated (Ruiz *et al.*, 2004). Therefore DKK1 expression was determined by qRT-PCR in

tumors of single- and double-transgenic RT2 mice. In RT2/hTNC mice, 7-times more tumors (50%) lacked DKK1 expression as compared to RT2 mice (7.1%) (see Annex, **Manuscript 1 Fig. 5B**). In tumors with detectable DKK1 expression, the levels were 2.57-fold reduced in RT2/hTNC mice in comparison to RT2 controls. We also determined expression of some Wnt target genes and observed that expression of cyclin D1 (2.5-fold), cyclin D2 (1.6-fold), CD44 (1.8-fold) and Slug (1.8-fold) was significantly increased in small still differentiated tumors of RT2/hTNC mice over that in RT2 controls (**Figure 22B; Table 5**). This was in contrast to other Wnt target genes (c-Myc, Id2, Lgr5) with similar expression in tumors of both genotypes (**Table 5**). Moreover, in RT2 tumors with only one TNC allele DKK1 levels were significantly lower (-2.1-fold) than in RT2/TNC-/- tumors that completely lacked TNC (**Figure 22C**). This suggests that expression of TNC and DKK1 are inversely correlated. In order to investigate activation of Wnt signaling staining for β-catenin in tumors of RT2 and RT2/hTNC mice was performed (**Manuscript 1 Fig. 4C**). IF staining on PFA fixed tissue revealed cells with nuclear β-catenin in tumor tissue of RT2/hTNC mice (5 of 8) but not in RT2 mice (0 of 5). That the signal was indeed nuclear was confirmed by confocal microscopic analysis (**Manuscript 1 Fig. 4C, inlet**). Due to documentation of very few cases this observation could not be investigated at statistical level. Analysis of gene expression levels of β-catenin by qRT-PCR did not reveal a difference between tumors of the two genotypes in any of the tumor subclasses (**Table 5**). Together, qRT-PCR results indicated TNC-induced Wnt signaling due to loss of the Wnt inhibitor DKK1 and induction of potential Wnt target genes in adenomas of RT2/hTNC mice. At protein level non-membranous and eventual nuclear β-catenin was found which appeared to be a rare and local event.

It was also determined if angiogenic markers were affected at transcriptional level as an angiogenesis promoting effect was observed by over-expressing TNC in RT2/hTNC tumors (**Figure 16**). None of the tested markers (CD31, VEGFA, VEGF-R1/ -2/ -3, EDNRA, EphA2, Hey1, Dll4, Ang1, Ang2, Tie2) showed a significant induction in any of the subclasses or even a strong reduction in big tumors (VEGF-R2, EDNRA, EphA2, Hey1, Ang2) (**Table 5**). Well developed tumors (≥ 1 mm) isolated from 14 weeks old mice have been used for this analysis which typically have already passed the angiogenic switch. Thus, this analysis disregards potential effects of TNC on early tumor stages. In fact, we now have evidence that TNC has an impact on angiogenesis already in hyperplastic islets (**Figure 20B**). Quantification of IF CD31-signals in control RT2/TNC+/+ tumors of the RT2/TNC-/- model revealed that hyperplastic islets displayed enhanced CD31-positive signals compared to normal islets of the same mice.

In summary, expression analysis of candidate genes on isolated single tumors by qRT-PCR was useful to test a potential implication of known signaling pathways in tumorigenesis but did not reveal a potential involvement of TNC in promoting any of the tested pro-angiogenic pathways including VEGF, Ang-1/2, Notch and EDNRA. But we showed that the level of the Wnt inhibitor DKK1 and the TNC copy number are inversely expressed which suggests that they are functionally linked. Induction of CD44, cyclin D1, cyclin D2 and Slug in RT2/hTNC tumors, which had been shown to be activated by Wnt signaling (Lambertini *et al.*, 2010; Shtutman *et al.*, 1999; Wielenga *et al.*, 1999), could be interpreted as evidence for activation of the Wnt pathway by ectopically expressed TNC. Although angiogenesis was increased, classical angiogenic markers were not elevated in well established RT2/hTNC tumors at RNA level.

4.3.2 Selected candidate gene expression analysis in early tumorigenesis

Since CD31-positive signals were enhanced already in normal and hyperplastic islets of tumor mice with wildtype TNC levels in comparison to tumors of mice lacking TNC (**Figure 20B**) and since forced expression of TNC induced cell proliferation already in normal and hyperplastic islets (**Figure 15B**), it is possible that TNC plays a role in earlier events of tumorigenesis. To uncover molecular mechanisms of action downstream of TNC in early tumorigenesis, gene expression profiling was performed by using Affymetrix® gene chip arrays as a screening method. Langerhans islets have been isolated from 8 weeks old RT2 and RT2/hTNC mice where a subset of islets already had undergone the angiogenic switch as evidenced by a reddish color (Parangi *et al.*, 1995). **Figure 23A** shows an example of purified islets at histological level. Non-angiogenic (completely whitish) and angiogenic islets (red dots, or completely reddish) could easily be distinguished under a stereomicroscope. By determining the ratio of non-angiogenic and angiogenic islets between the genotypes, it was revealed that double transgenic RT2/hTNC mice developed 2.5-fold more angiogenic islets than control RT2 mice (**Figure 23B**). This goes in line with our observation that RT2/hTNC tumors comprised more CD31-positive signals and suggests that overexpression of TNC accelerates the angiogenic switch. For RT2 and RT2/hTNC mice, respectively 3 pools of non-angiogenic and 3 pools of angiogenic islets were analyzed using Affymetrix® gene profiling arrays.

First, the validity of the obtained data sets was assessed by comparing gene expression levels between angiogenic versus non-angiogenic islets of all analyzed samples, independent of the genotype. Data were filtered according to fold-changes of minimally ±1.2-fold or more with a significance value of $p \leq 0.05$. This revealed that around 1000 genes

were deregulated during the angiogenic switch (**Figure 23C**) mainly containing genes of the ECM (FN, collagens, periostin, laminins, SPARC), gene products being implicated in blood vessel development and morphogenesis (CD31/Pecam1, EDNRA) or genes implicated in signal transduction such as members of the Notch signaling pathway (Jag1, Hey1/2, Notch2/3) (see Annex **Table 6**).

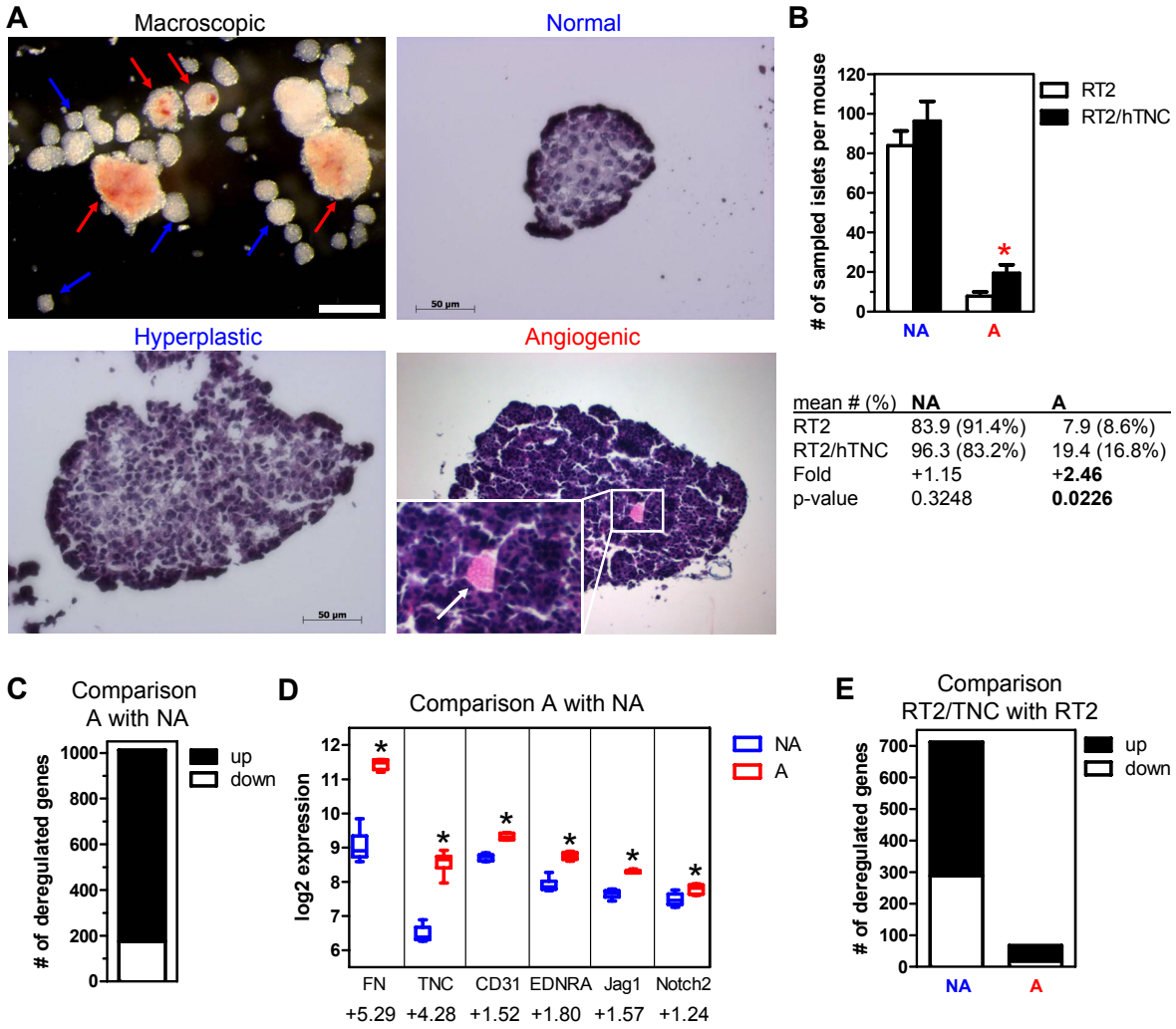

mean # (%)	NA	A
RT2	83.9 (91.4%)	7.9 (8.6%)
RT2/hTNC	96.3 (83.2%)	19.4 (16.8%)
Fold	+1.15	**+2.46**
p-value	0.3248	**0.0226**

Figure 23: Gene expression profiling of early RT2 tumors with over-expression of TNC

(A) Purified non-angiogenic (normal, hyperplastic; blue arrows) and angiogenic islets (red arrows) sampled from 8 weeks old RT2 and RT2/hTNC mice seen under the stereomicroscope (bar = 500 µm) or at histological level on H&E stained tissue sections (fresh frozen or paraffin). Inlet: magnification of the boxed region of the angiogenic islet indicating erythrocytes (white arrow).

(B) Quantification of average number of purified non-angiogenic (NA) and angiogenic (A) islets in 8 weeks old RT2 (N=9) and RT2/hTNC (N=7) mice. RT2/hTNC mice contained significantly more angiogenic islets than RT2 mice (2.5-fold, p = 0.023).

(C) Number of deregulated genes comparing angiogenic versus non-angiogenic islets in all analyzed samples. Statistically significant data ($p \leq 0.05$) with fold-changes of more than ±1.2-fold were considered. List of gene candidates see **Table 6**.

(D) Gene expression profiling data showing induction of TNC and selected genes upon comparison A with NA islets. Fold-changes as indicated were statistically significant ($p \leq 0.009$).

(E) Number of deregulated genes between genotypes comparing samples from RT2/hTNC with RT2 mice in either NA or A islets. List of gene candidates see **Table 7** and **Table 8**.

We first extracted data for the expression of CD31/Pecam1 and EDNRA, both key molecules implicated in blood vessel formation, and for FN and TNC which are highly up-regulated in vascular remodeling and cancer (Van Obberghen-Schilling *et al.*, 2011). When comparing angiogenic with non-angiogenic islets these molecules were significantly up-regulated between 5.3 and 1.5-fold (**Figure 23D**). We also looked at Jag1 and Notch2, key molecules of the Notch signaling pathway whose regulation is perturbed in many cancers (Ranganathan *et al.*, 2011) and which plays an important role in tumor angiogenesis (Bridges *et al.*, 2011; Rehman and Wang, 2006). Angiogenic islets showed enhanced expression levels for Jag1 (1.6-fold) and Notch2 (1.2-fold) (**Figure 23D**).

In summary, by analyzing gene expression levels during the angiogenic switch by comparing more advanced angiogenic islets versus early stage non-angiogenic islets we saw that ECM molecules and key molecules of angiogenesis and Notch signaling were significantly enhanced. The differential expression of well-known players in tumor progression in this experimental setup validates the relevance of the obtained data.

To uncover the mechanisms which are deregulated by enhanced TNC expression we then used an unbiased strategy by sorting the obtained data by fold-changes of minimum ±1.2-fold or more between the compared subgroups with a significance value of $p \leq 0.05$ as mathematical constraints. When comparing results for RT2/hTNC with those for RT2 islets we found that about 10 - times more genes were deregulated by TNC in non-angiogenic islets (~700 genes) than in angiogenic islets (~70 genes) (**Figure 23E**) whereas the majority of them (~60-70%) were up-regulated upon TNC overexpression. This suggests that overexpression of TNC plays an important role in early events of tumor progression even before the angiogenic switch takes place.

For the moment, the obtained gene lists with potentially TNC dependent expression levels were not further analyzed. Only the above mentioned few molecules were also compared between genotypes but did not show a difference in islets with enhanced TNC expression levels neither in non-angiogenic nor in angiogenic islet pools. Only Notch2 was weakly, but significantly enhanced by about 1.2-fold in non-angiogenic and angiogenic islets of RT2/hTNC mice (**Table 7**). At first glance classical markers of angiogenesis and Notch and Wnt signaling do not seem to be linked to enhanced TNC expression levels. The lists for non-angiogenic (**Table 7**) and angiogenic gene candidates (**Table 8**) can be found in the Annex at the end of this thesis.

In summary, purification of islets for gene expression profiling confirmed a promoting role of TNC in tumor angiogenesis as we observed more angiogenic islets in RT2/hTNC mice. Furthermore, well established players of tumor progression are up-regulated during the angiogenic switch proving the relevance of the analyzed model system. Moreover, more genes were deregulated by enhanced expression of TNC in non-angiogenic islets indicating a promoting role of TNC on tumor onset.

In the future, the generated data set will be used for screening to discover potential candidate genes being implicated in TNC-dependent RT2 tumor onset and angiogenesis. As this analysis is still at the beginning, defined constraints and specific software tools will be applied to generate gene candidate lists. Differential expression of these genes will be confirmed by qRT-PCR and validated on tissue sections at protein level.

4.4 Role of TNC in enhancing angiogenesis upon over-expression in pancreatic islets

Under normal conditions, TNC is only weakly expressed or undetectable in the ECM of the quiescent vasculature but is highly up-regulated following vessel injury or at sites of vascular remodeling in cancer and in diseases not related to cancer (Van Obberghen-Schilling *et al.*, 2011). A potential angiogenesis-promoting effect of TNC had been addressed in the laboratory by J. Kant (Kant, Master thesis 2008) in the chick chorioallantoic membrane (CAM) assay. This experiment showed that purified TNC enhanced angiogenesis during chick embryo development (see Annex, **Manuscript 1 Fig. 2E**). If the forced expression of TNC in single-transgenic Rip-hTNC mice had potentially already an effect on angiogenesis under normal conditions was addressed by quantification of CD31-positive signals in islets of wildtype and Rip-hTNC mice. This preliminary experiment on a low number of samples showed a tendency of 1.5-fold more CD31-positive blood vessels in normal pancreatic islets of Rip-hTNC compared to wildtype mice but the difference was not statistically significant (Yundan Jia, not shown).

Therefore, to address the underlying mechanisms of TNC-induced angiogenesis, a gene expression profiling was performed on Langerhans islets isolated from transgenic Rip-hTNC and wildtype control mice. Compared to non-angiogenic islets of RT2 mice at 8 weeks of age, an advantage of this experiment might be that Langerhans islets from non-tumorigenic mice are less heterogeneous and thus potentially will give robust results.

Pools of Rip-hTNC (N = 3) and wildtype (N = 4) pancreatic islets have been analyzed by Affymetrix® chip analysis. As for the above described gene expression profiling using RT2 mice, the obtained data set was not yet analyzed in detail. However, the data were screened for potential deregulated gene products and the gene list was filtered for a minimal fold-change of ±1.2 with a p-value ≤ 0.100. A list of 582 deregulated genes was obtained whereas 64% of the deregulated genes were up-regulated upon forced expression of TNC (see Annex **Table 9**). This list contained many cytokines and chemokines of the CC- and CXC-family. This indicates that ectopic expression of TNC potentially activated an immune and/or inflammatory signature in the islets which needs to be addressed in more detail. Moreover, plexin A3 and placental growth factor (PlGF) were up-regulated in Rip-hTNC islets. Plexin receptors are crucial for semaphorin-signaling which is implicated in several cancer-related aspects including angiogenesis (Gaur *et al.*, 2009). The VEGF homolog PlGF is a key molecule in angiogenesis during embryonic development and is affected in angiogenesis in cancer and other diseases (Carmeliet *et al.*, 2001). This result indicates that ectopically expressed TNC plays a role in angiogenesis already in a normal

situation. Likewise, the list contained gene products implicated in cell cycle and transcriptional regulation indicating a potential effect on cell proliferation and growth. Moreover, several genes encoding RNA binding proteins were significantly down-regulated which suggests a profound effect of TNC on cellular physiology (see Annex **Table 9**). This needs to be investigated in more detail in the future.

Together, the obtained data are promising for a better understanding the mechanism of TNC in cell proliferation and induction of angiogenesis in pancreatic islets of Rip-hTNC mice and to uncover genes downstream of TNC in a non-tumorigenic context. These changes in normal conditions might also play a role in a tumor context further inducing angiogenesis (or other pro-tumorigenic parameters) in an indirect manner, possibly via induction of inflammation. Candidates will be investigated for a potential role in very early events in tumorigenesis in the RT2 model system with different TNC expression levels (knockout, wildtype, over-expression). Preferably, islet tissue should be analyzed at a time point before the angiogenic switch, such as 5 weeks of age.

4.5 The role of TNC in blood vessel anatomy and tumor architecture

Tumor vessels are abnormal compared to normal blood vessels exhibiting a disorganized network, loosely attached pericytes and an altered basement membrane (McDonald and Choyke, 2003). We have shown in the RT2 model system that tumor angiogenesis is higher in dependence on the TNC gene copy number (**Figure 16B, Figure 20**) suggesting that TNC promotes angiogenesis.

4.5.1 Tumor vessel anatomy in double-transgenic RT2/hTNC mice

To determine a potential effect of TNC on vessel anatomy we investigated vascular casts by scanning electron microscopy (SEM) upon perfusion of RT2 and RT2/hTNC mice with the Mercox compound. This work was done in collaboration with V. Djonov (University of Bern, CH). This analysis revealed that tumors of double-transgenic RT2/hTNC mice were different to that of RT2 control tumors. The vascular network appeared more disorganized and highly branched compared to a control RT2 tumor (**Figure 24A**). By having a look at a higher magnification the vessel surface appeared rough and the blood vessels showed potential branching points (white arrows) in a RT2/hTNC tumor. This was in contrast to the RT2 vasculature that appeared smooth without showing branching points (**Figure 24B**). In another region of the same RT2/hTNC tumor, blood vessels also appeared leaky as indicated by Mercox escaping the vessels at multiple sites (black arrows) which was in contrast to the RT2 vasculature that did not exhibit similar Mercox leakage sites (**Figure 24C**).

A more detailed analysis by transmission electron microscopy (TEM) revealed that in contrast to vessels with a basement membrane and EC as observed in a RT2 tumor (**Figure 25A**), several structures in RT2/hTNC tumors were filled with and lined by matrix which contained nucleated cells (**Figure 25B, C**). Such structures are atypical for the observed control RT2 tumors (V. Djonov, personal communication). They were not normal blood vessels as they lacked EC and a basement membrane (BM). In contrast, these structures exhibited a prominent and thick matrix-lining representing a separating border to the surrounding tumor cells (**Figure 25B**). In the following, these structures will be called “conduits”. Attached tumor cells (AtTu) which were lining them seemed to have a reduced number of insulin secretory granules (**Figure 25B, C**). Erythrocytes (Er) were observed in conduits of RT2/hTNC tumors suggesting a functional connection with the vascular system (**Figure 25B, C**). This was supported by documenting a connection between a blood vessel, characterized by a BM and lining EC, and a matrix conduit lacking these characteristics but exhibiting a lumen and adjacent tumor cells with few granular vesicles (**Figure 25D**).

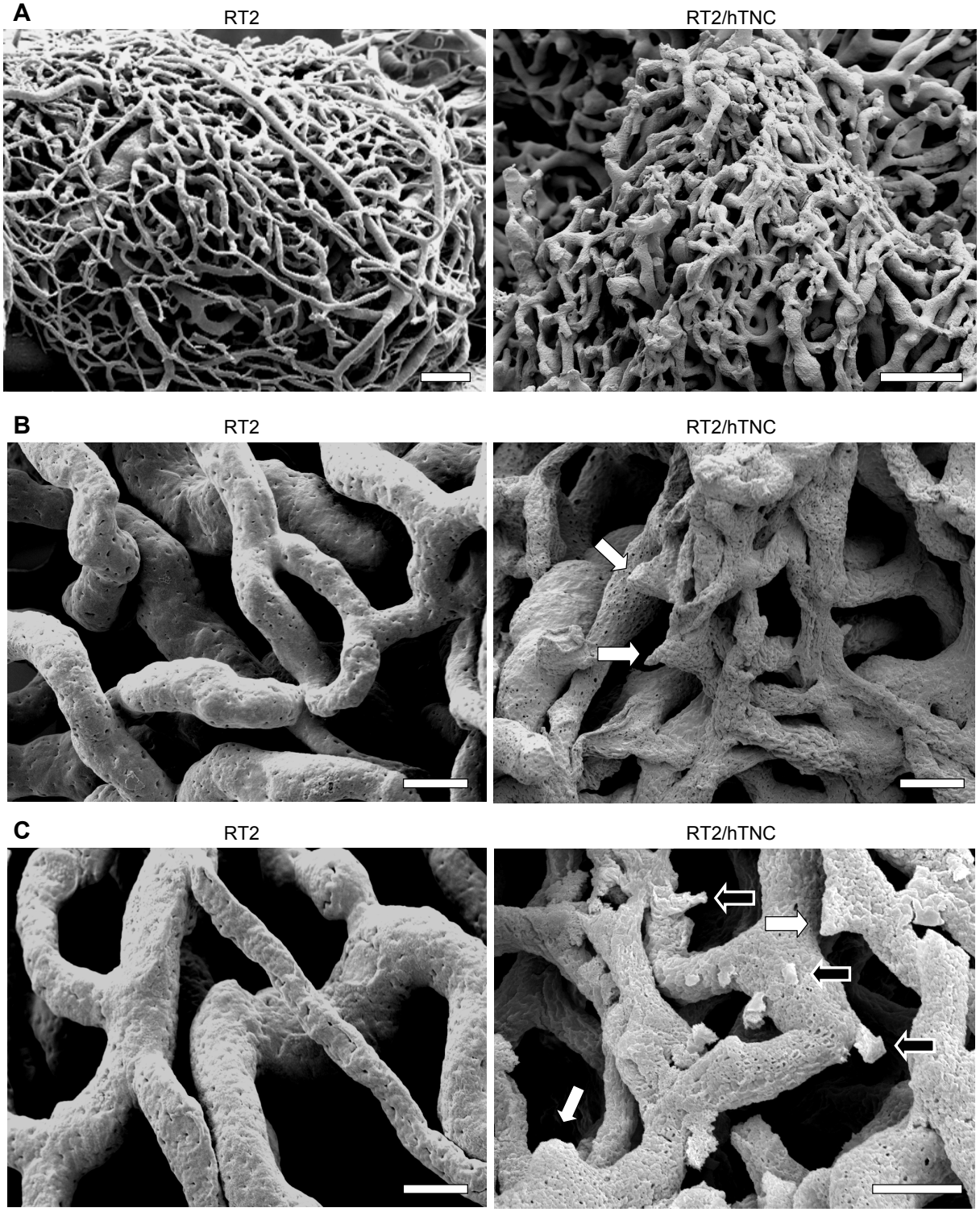

Figure 24: Vessel anatomy in tumors of RT2 and RT2/hTNC mice

(A) Reproduction of the vasculature in tumors of 12 weeks old RT2 and RT2/hTNC mice in vascular casts upon Mercox perfusion. Scale bar = 50 µm.

(B, C) Higher magnification of the tumors shown in (A). White arrows indicate potential branching points. Black arrows indicate leakage site. Scale bars = 10 µm.

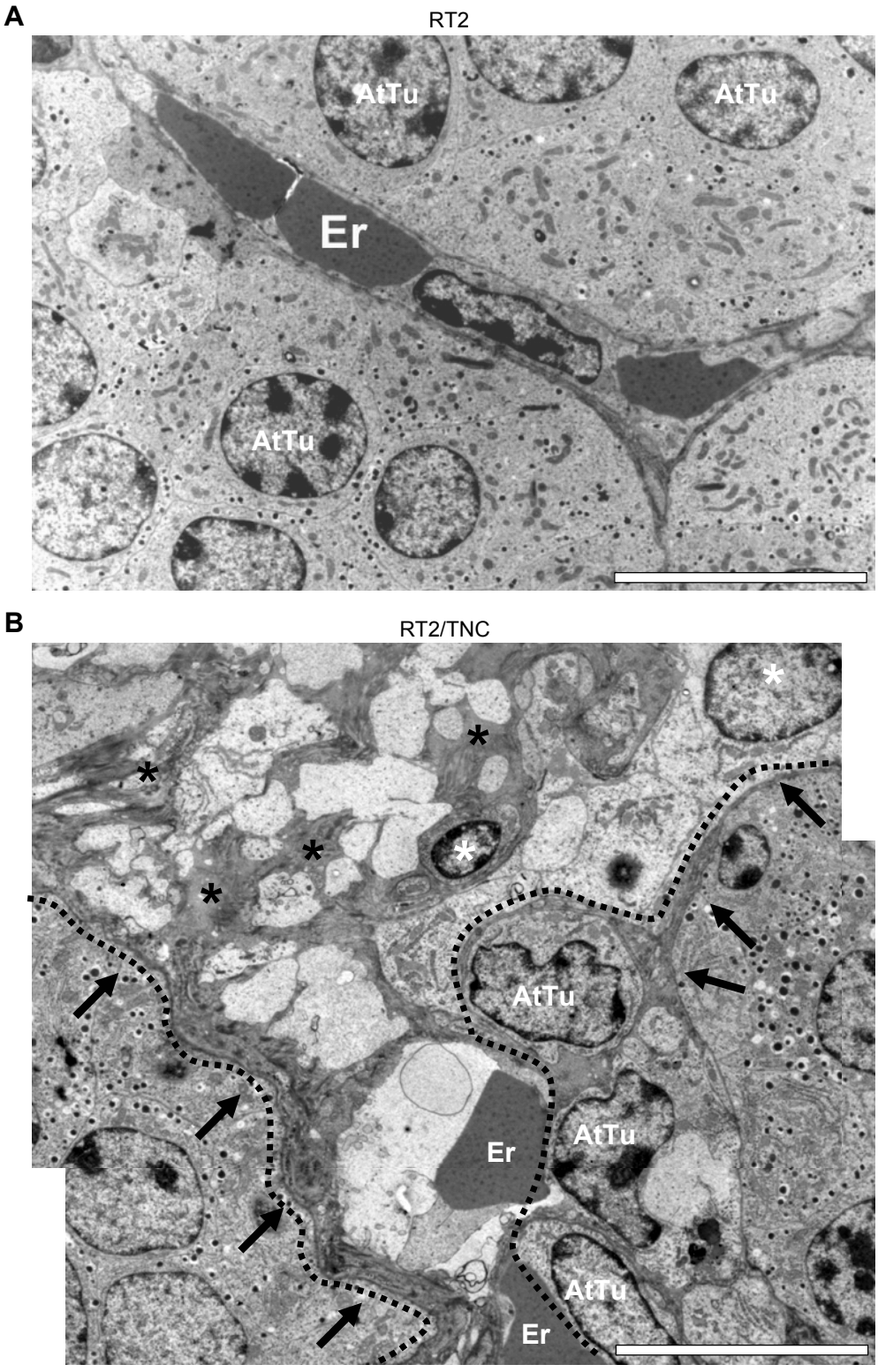
A
RT2
AtTu
AtTu
Er
AtTu
B
RT2/TNC
AtTu
Er
AtTu
AtTu
Er

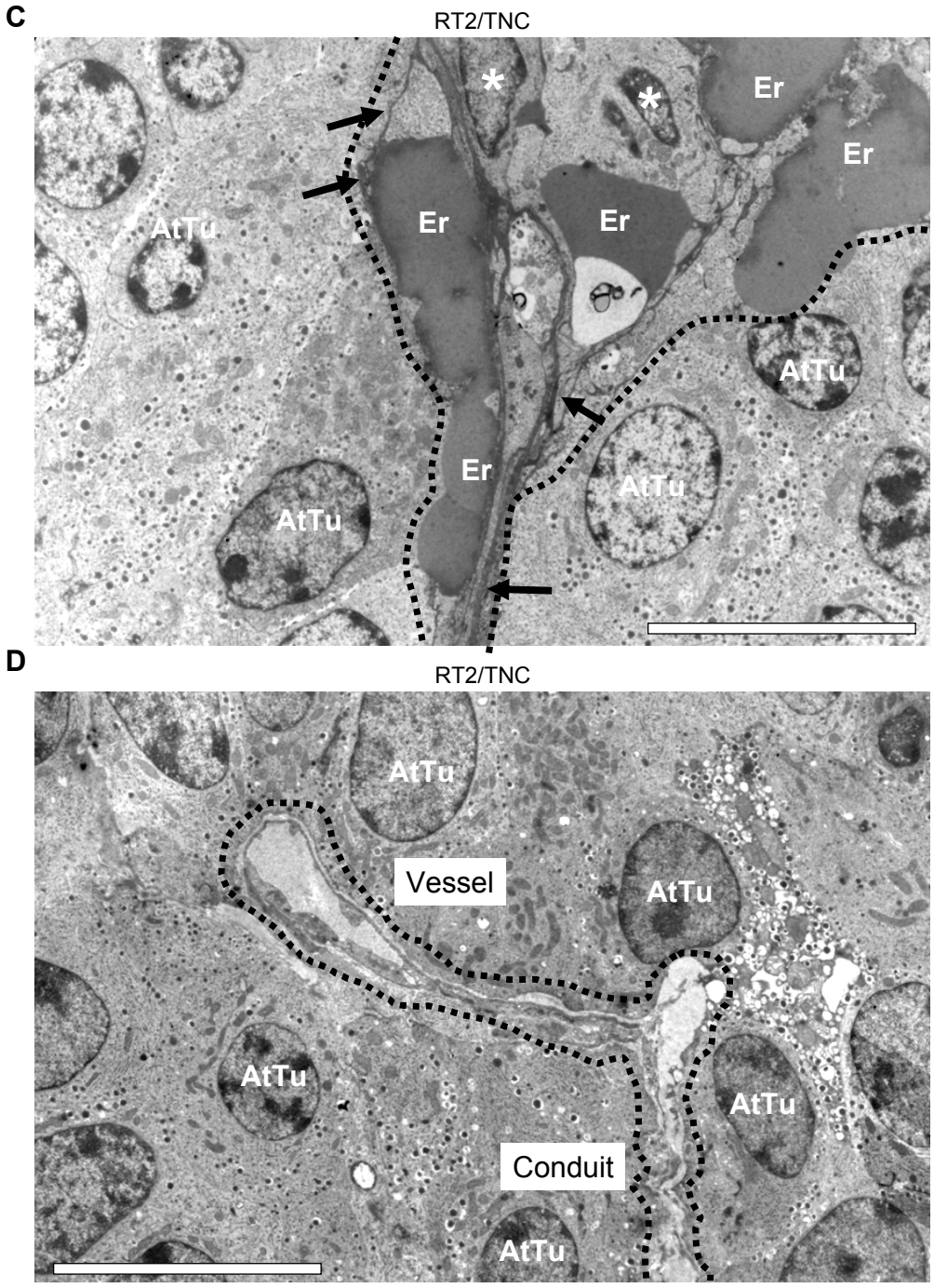

Figure 25: Transmission electron micrographs of tumor vessels and matrix conduits in RT2 tumors

(A) TEM picture of a RT2 tumor vessel containing erythrocytes (Er) and surrounded by attached tumor cells (AtTu). Scale bar = 10 µm.

(B, C) TEM pictures representing different examples of matrix conduits in RT2/hTNC tumors delineated by dotted lines. Black arrows indicate matrix deposits that are lined by AtTu. Black asterisks indicate matrix inside the conduit. Erythrocytes (Er) and nucleated cells (white asterisks) are present within the structures. Scale bar = 10 µm.

(D) TEM picture of a RT2/hTNC tumor showing a continuum (dotted line) between a blood vessel characterized by a BM and EC and a potential matrix conduit that exhibits a lumen and is lined by AtTu but not by BM and EC. Scale bar = 10 µm.

4.5.2 Establishment of a method to study the structural organization of TNC in the RT2 model

To determine where in RT2 tumors TNC is located and to prove that the described conduits are indeed connected to the blood circulation I established perfusion experiments using fluorescence-labeled molecules and performed IF co-staining for TNC or CD31. FITC-conjugated tomato lectin (*Lycopersicon Esculentum*) was used to directly label blood vessel EC. FITC-conjugated dextran was used to determine which of the different structures (blood vessels, matrix conduits) are perfusable and therefore connected to a functional circulation. Thick tissue sections were prepared of the perfused tumor tissue and were analyzed by pseudo-confocal 3D microscopy.

In principle, pancreata of RT2 mice could be perfused with FITC-lectin to directly label tumor blood vessels (**Figure 26A**) or with FITC-dextran to visualize perfusable structures inside the tumor which are connected to the circulation (**Figure 27**). For both molecules, I tried different techniques to get a good distribution in the entire pancreas and also for good conservation of the tissue and the fluorophore. Whereas injecting molecules directly into the heart of anaesthetized mice may lead to good results, it is time consuming and not a reproducible technique with high failure rates. FITC-conjugated molecules are now applied via tail vein injection into non-anaesthetized mice which will be sacrificed 15 minutes after circulation. By using this technique mostly all pancreatic tumors of a mouse showed FITC positive signals (not shown, analysis in progress). Samples being kept at -20 °C, as tissue-blocks or as prepared slices, are stable for more than one year and FITC does not fade. The following presented examples were obtained on heart-perfused tissue using a not yet optimal protocol and are therefore preliminary results. New material needs to be analyzed which has already been generated.

Figure 26A shows a hyperplastic islet of a RT2 mouse which was perfused with FITC-conjugated lectin and histological sections were co-stained for CD31. In this example, FITC-lectin co-localized with CD31 proving that lectin indeed binds EC and therefore is a valid marker for blood vessels in the perfused mouse pancreas. A 50 µm thick FITC-lectin perfused tumor section was analyzed after co-staining for TNC by 3D-microscopy (**Figure 26B**). FITC-lectin shows the presence of several blood vessels inside the tumor which appeared either normal (asterisks, 5-10 µm) or dilated (arrowhead, ~20 µm) which do not co-stain for TNC at the same time. On the other hand, the tumor contained TNC positive tube-like structures (arrows) which were not labeled by FITC-lectin and did not show the shape of a blood vessel. This structure might be a matrix conduit, as observed by TEM.

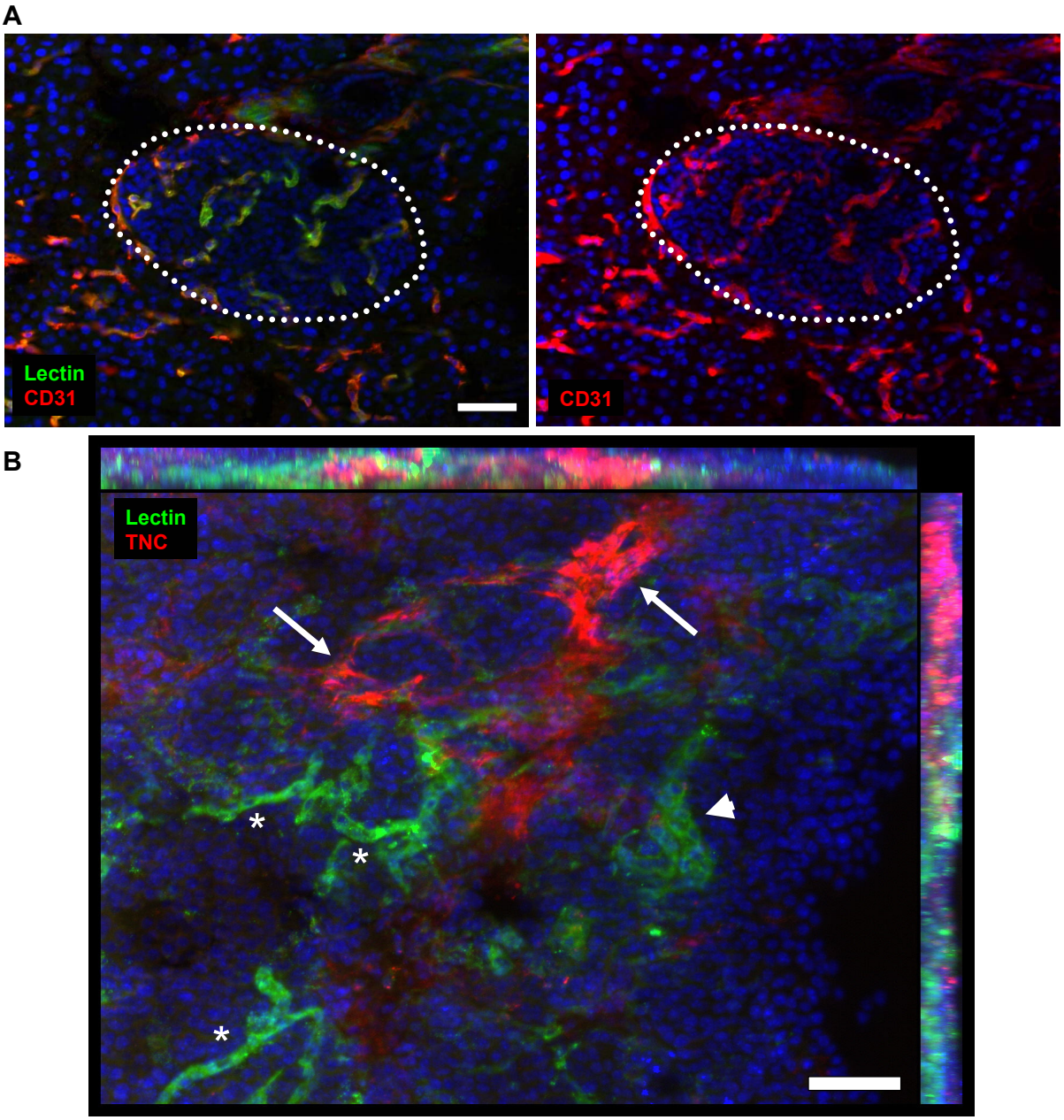

Figure 26: Perfusion experiments using FITC-conjugated lectin

(A) IF analysis of a hyperplastic islet of a RT2 mouse after perfusion with FITC-lectin (green) and co-staining with CD31 (red) and DAPI (blue). Left image shows all channels merged, right image DAPI and CD31 staining. Dotted lines delineate the islet. Scale bar = 50 µm.

(B) Example of lectin perfused RT2 tumor. Frozen tumor sections (50 µm thick) were co-stained for DAPI (blue) and TNC (red). Merged image of 48 acquired z-stack images is shown. Lectin (green) indicates normal tumor blood vessels (asterisks) or a vessel appearing possibly dilated (arrowhead). Arrows indicate TNC positive matrix conduits. Top and right bars show IF signal in z-orientation. Scale bar = 50 µm.

To address whether TNC containing matrix conduits were functional and connected to the circulation as indicated by TEM analysis (**Figure 25D**), tumor-bearing mice were perfused with FITC-dextran and tissue sections were stained for TNC and laminin (LM) before 3D-reconstruction of the images. **Figure 27** shows three different regions of one tumor in which dextran was distributed.

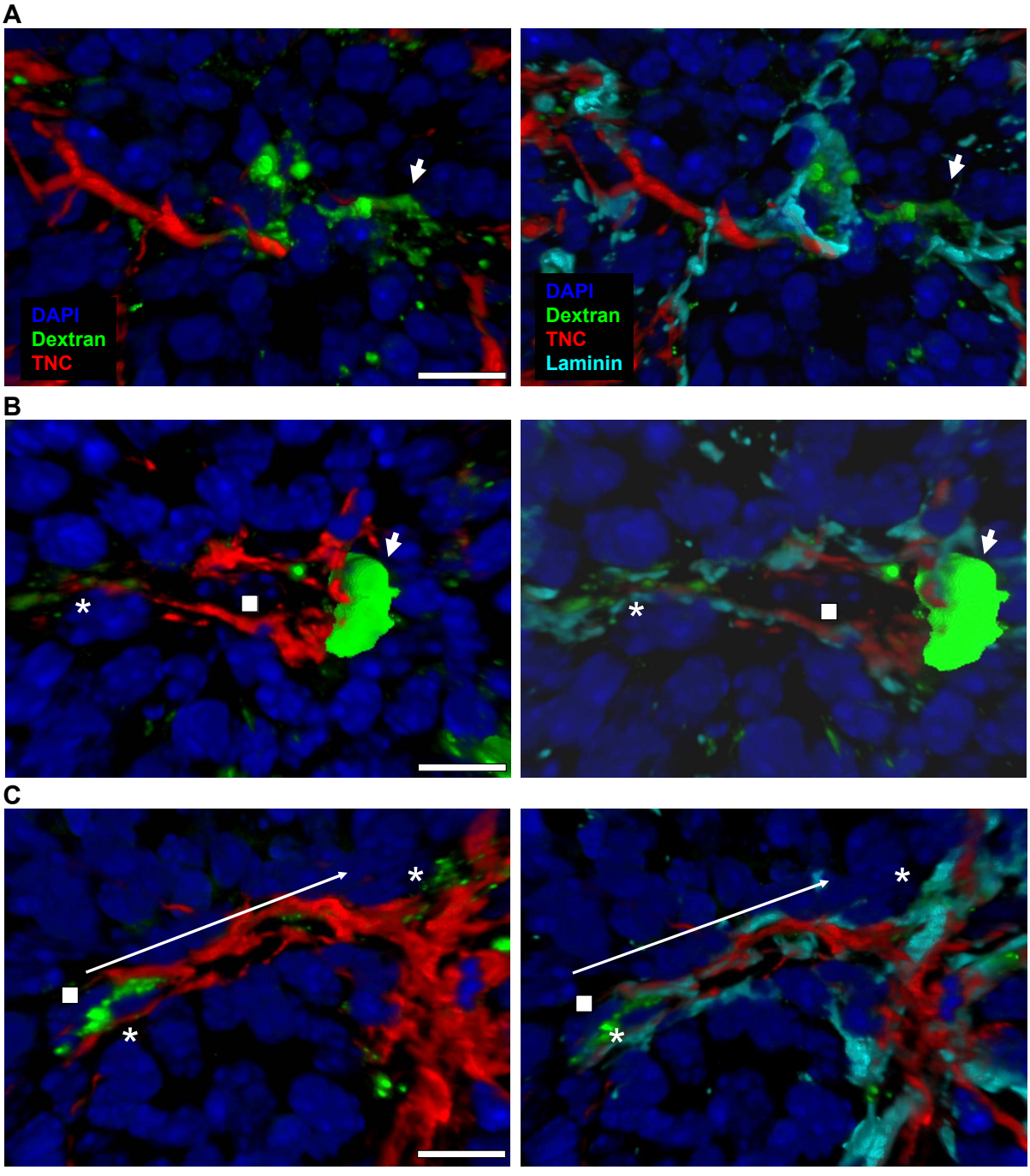

Figure 27: Perfusion experiments using FITC-conjugated dextran

(A, B, C) 3D reconstruction microscopy. Magnifications of different regions of a dextran-perfused RT2 tumor after co-staining with DAPI (dark blue), TNC (red) and laminin (light blue). Left images show the same as right images but without laminin. Dextran (green) is distributed throughout the tumor in different regions. Arrowheads (A, B) indicate vessel-shaped dextran containing structures. Asterisks (B, C) indicate dextran containing structures with conduit-like appearance. Some of the structures contain nucleated cells (rectangle). Arrows in (C) indicate connection between a vessel-like structure ending in a potential matrix conduit.

By having a closer look on the distribution and co-localization of dextran, TNC and LM, dextran molecules could be found in vessel-shaped structures which did not stain for TNC nor LM (arrowheads in **Figure 27A, B**). This suggests that this might be an abnormal blood vessel without BM, as LM is a marker for blood vessel BM. In some structures TNC and LM were intermingled in an unorganized manner with some dextran distribution inside (asterisks in **Figure 27B, C**). These might represent TNC containing matrix conduits that we had seen by TEM. But they could also be blood vessels lined by a BM. The final proof that these conduits are not blood vessels is still missing and need to be analyzed by co-staining for EC markers. However, the distribution in structures different than blood vessels proved their connection to the vascular circulation. In **Figure 27C** dextran seems to reach a vessel-like structure which was lined by LM and by an additional layer of TNC and which contained a cell inside (rectangle). This structure seems to continue and then end in a less organized matrix conduit (direction indicated by an arrow) where TNC and LM intermingle in an unorganized manner and which is perfusable since dextran can be found inside.

In summary, tumor-bearing mice could successfully be perfused with FITC-conjugated molecules to directly visualize blood vessels or matrix conduits in tumors. Dextran could also be found in structures which did not have blood vessel-like appearance suggesting that they are connected to the vasculature supporting the observation made by TEM. Now, a deeper analysis of newly prepared samples according to an optimized protocol as well as co-staining for different molecules needs to be done to further characterize the identified structures. Co-injection of lectin and dextran which are labeled with different fluorophores will be performed to directly distinguish blood vessels and perfusable matrix conduits in the tumor tissue. Similar vessel analysis of tumor mice lacking TNC will give more precise answers about the importance of TNC in matrix conduit and blood vessel formation.

In conclusion, our data suggest a complex organization of the tumor-specific TNC matrix into conduits that can form a lumen and a connection to the circulation thus providing a continuum between conduits and the vasculature. The presence of nucleated cells inside these structures suggests that TNC matrix conduits might serve as guiding cue and niche for different cell types, an aspect which will be analyzed in the laboratory in the future.

5 Discussion and Perspectives

TNC is a major component of the tumor microenvironment and plays an instrumental role in cancer progression including cell proliferation, tumor cell migration and invasion, tumor angiogenesis and the formation of lung metastasis (see **Introduction**). The first objective of the presented work was to investigate the role of the extracellular matrix molecule TNC in cancer progression in an immune-competent stochastic cancer model. Therefore, gain and loss-of-function strategies were used to investigate the role of TNC in the RT2 model where mice develop pancreatic neuroendocrine tumors. First, the double-transgenic RT2/hTNC model was generated mimicking high expression of TNC in human cancer and different aspects of tumor progression have been investigated in more detail. Second, the loss of TNC function model RT2/TNC-/- was newly established as part of this thesis and first preliminary results have been obtained in a small cohort of mice. Gene expression profiling was performed to obtain preliminary insight into the molecular mechanisms of action downstream of TNC.

In the following, the above presented effects of TNC on tumor progression in the RT2 model will be discussed in comparison to the literature and to other experiments performed in our laboratory. Last, the role of TNC on tumor angiogenesis and the formation of matrix-conduits and its possible implication in tumor progression will be discussed.

5.1 The effect of TNC on tumor growth and proliferation

In the RT2 model system mice develop several macroscopic visible tumors (bigger than 1 mm) at the age of 12 weeks. In both model systems using gain and loss of TNC function strategies the tumor incidence and tumor burden was determined macroscopically but no difference in tumor number nor tumor volume could be detected in 12 weeks old mice with different levels of TNC expression (**Figure 14A, Figure 19B**). In contrast, by isolating each tumor and measuring tumor diameter in 14 weeks old mice, a significant reduction of the tumor burden in RT2/hTNC mice was observed suggesting that ectopically expressed TNC did not support or potentially inhibited growth of established tumors (**Figure 14B**). This reduction can be explained by the reduced number of tumors bigger than 3 mm. But the same mice showed a tendency toward more tumors smaller than 3 mm suggesting that TNC potentially promoted tumor initiation and tumor growth but that established tumors did not expand which points at a problem with supply of oxygen and nutrients.

In both models, the analysis of the tumor burden and incidence showed a tendency toward more tumors smaller 3 mm in diameter suggesting that TNC supports tumor initiation. These analyses were done at the end of the lifespan of RT2 mice and it is possible that differences are more evident at earlier time points of tumorigenesis. Therefore, the tumor size was investigated at histological level in 10 weeks old RT2 and RT2/hTNC mice by measuring tumor diameter followed by sub-classification of islets (**Figure 14D**). This indeed showed that enhanced expression of TNC promoted the formation of tumors in RT2/hTNC mice. These observations suggest that TNC has an impact on early tumorigenesis resulting in an accelerated tumor growth in the RT2 model system leading to a slightly enhanced tumor number in 14 weeks old RT2/hTNC mice.

In the RT2/TNC-/- model in a C57BL6 background the tumor size was assessed at histological level which did not show a difference in the frequency of the different islet lesions between the genotypes. The distribution of islet lesions per mouse in dependence on TNC is currently assessed at histological level in a bigger cohort of 12 weeks old mice in both model systems (RT2/hTNC and RT2/TNC-/-).

In a mouse model of spontaneous mammary tumors the absence of TNC did not have an effect on the appearance of palpable tumors nor tumor size (Talts *et al.*, 1999) indicating that TNC did not play a role during spontaneous tumor development in the breast. The drawback of this model is that the size can only be assessed when the tumors are big enough and had reached a certain size masking a potential early effect of TNC on tumor formation. Another study using orthotopic injection of breast cancer cells with knockdown for TNC into the mammary fat pad also did not show a difference in primary tumor formation compared to control cancer cells (Oskarsson *et al.*, 2011; Tavazoie *et al.*, 2008). But this model system is based on grafting experiments in an immune-compromised mouse lacking spontaneous tumor formation. A subcutaneous transplantation experiment of human melanoma cells into BALB/cA mice lacking TNC expression had shown that these tumors grew more slowly compared to tumors injected into wildtype mice (Tanaka *et al.*, 2004) which supports our observation that in an immune-competent setting TNC has a negative effect on tumor expansion.

To my knowledge, there is no other study published that investigated the effect of TNC on tumor growth by mimicking enhanced TNC expression levels in human cancer. But this might be necessary as the basal TNC expression could be too low compared to a knockout situation and a strong over-expression of TNC correlates with tumor progression in several human cancers (Orend and Chiquet-Ehrismann, 2006). In our laboratory we established several cancer cell lines with different TNC expression levels (knockdown, wildtype, over-expression) which will be used for grafting experiments in immune-competent

mice with wildtype TNC or no TNC expression (I. Gasser and G. Orend, unpublished). These experiments will help to better understand the growth-promoting effect of TNC and will further characterize the specific role of tumor-cell and host-cell derived TNC.

Many *in vitro* studies show the supporting effect of TNC on cell proliferation (Orend and Chiquet-Ehrismann, 2000). The tendency toward a higher number of tumors in 14 weeks old RT2/hTNC mice and the observation that tumors are more frequent on sections of 10 weeks old RT2/hTNC mice suggests that in these mice tumor cells are more proliferative. Therefore cell proliferation was analyzed in RT2 and RT2/hTNC tumors by quantifying PH3 and KI67 staining which showed an overall enhanced proliferation rate in tumors with ectopic TNC expression (**Figure 15**). Preliminary results on a small cohort of tumors assessing the KI67 signal in islet lesions after classification according to size revealed an enhanced proliferation rate in dependence on TNC already in normal and hyperplastic islets. This observation can explain the presence of more tumors in RT2/hTNC mice. One possible explanation is that TNC triggers the hyperplastic switch in normal islets in early RT2 tumorigenesis. In the RT2 model only a subset of normal islets (~50%) are triggered to proliferate and develop into hyperplastic islets (Hanahan *et al.*, 1996). If this fraction is indeed increased by ectopically expressed TNC needs to be addressed in more mice and in RT2 mice at a younger age of 3 to 5 weeks, before islet lesions perform the angiogenic switch (Parangi *et al.*, 1995).

It would be interesting to know which mechanisms are triggering the hyperplastic switch and are increasing the proliferation rate. qRT-PCR analysis on tumors of 14 weeks old mice revealed that the cell cycle proteins cyclinD1 and cyclinD2 are significantly induced in RT2/hTNC tumors (**Table 5**) which correlates with our observation of higher proliferation rates in RT2/hTNC tumors. We also performed gene expression profiling on tumor preparations of 8 weeks old mice which revealed that ~700 gene products are deregulated in non-angiogenic islet by ectopic TNC expression. If this gene list contains candidates which could explain our observations still needs to be analyzed. Another gene expression profiling on non-tumorigenic Rip-hTNC islets revealed that some cell cycle and transcriptional regulating genes are induced. TNC dependent expression of the candidates needs to be further addressed. This indicates at a potential effect of TNC on cell proliferation and DNA replication already under normal conditions. If these TNC-induced changes in a normal situation potentially play a role in a tumor context needs to be analyzed on early tumor samples of our model system exhibiting differential TNC expression levels.

In conclusion, whereas in a breast cancer context TNC does not seem to have an obvious impact on tumor growth, our data obtained in the RT2 model system indicate that enhanced

expression of TNC had an effect on very early tumor growth by accelerating the hyperplastic switch and subsequent enhanced tumor formation in RT2/hTNC mice likely by increasing the proliferation rate in early islet lesions. Analysis in mice at early time points of RT2 tumorigenesis will be performed in both model systems to evaluate this observation further.

Another process which is important to be analyzed in the future is apoptosis. In the RT2 model, the apoptotic index increases with size in the premalignant islet lesions but drops down again in tumors (Naik *et al.*, 1996). It was shown that down-regulation of apoptosis can be a critical regulator of RT2 tumorigenesis and tumor growth, whereas the proliferative index did not change at the same time (Naik *et al.*, 1994; Naik *et al.*, 1996; Parangi *et al.*, 1996). In an experimental murine breast cancer model, knockdown of TNC showed an increase in apoptosis suggesting that TNC exhibits anti-apoptotic properties (Oskarsson *et al.*, 2011). Although we could show that ectopic expression of TNC enhanced the proliferative index, it might be possible that down-regulation of the programmed cell death in parallel supports tumor growth. This aspect will be investigated in the future.

5.2 The effect of TNC on tumor invasion and metastasis

In the RT2 model system a subset of islet lesions undergo the angiogenic switch allowing the further development into solid non-invasive tumors or invasive carcinoma and dissemination of β-tumor cells into distant organs. In patients with GBM, high levels of TNC in tumors are associated with invasion of this aggressive tumor type and stromal TNC expression correlates with shorter survival (Leins *et al.*, 2003; Sivasankaran *et al.*, 2009). In cell culture experiments GBM cells grown on a TNC containing matrix were less adhesive and showed enhanced growth factor induced tumor cell migration (Lange *et al.*, 2008) illustrating the pro-migratory properties of TNC on cancer cells. We had determined the percentage of adenomas and invasive carcinomas and observed that RT2/hTNC mice with ectopic expression of TNC developed more invasive tumors than RT2 control mice (**Manuscript 1 Fig. 1E**) suggesting that they are prone to form metastasis. A potential impact of TNC on the formation of micrometastasis to liver and lung was investigated by qRT-PCR for insulin expression. This experiment revealed that a subset of mice developed micrometastasis to liver and lung which could be confirmed at histological level by staining for insulin. Whereas different TNC expression levels had no impact on liver micrometastasis, higher TNC expression correlated with enhanced lung micrometastasis in both model systems (**Figure 17, Figure 18F**).

RT2 mice in a C57BL6 background normally lack visible macrometastasis but can develop macrometastasis for example to liver, kidney, intestine and local lymph nodes under certain conditions as e.g. upon pericyte dysfunction. But no lung metastasis was observed under these conditions (Xian *et al.*, 2006). Therefore we did not expect to see primarily an effect in the lung but rather in the liver. However, these results reflect what was published in other studies where TNC is directly linked to lung metastasis in experimental murine breast cancer (Calvo *et al.*, 2008; Minn *et al.*, 2005; Tavazoie *et al.*, 2008) and melanoma (Fukunaga-Kalabis *et al.*, 2010). In breast cancer patients high TNC expression in primary tumors correlated with reduced lung metastasis-free survival, and cancer cells with high basal TNC expression had a selective advantage in the lung microenvironment compared to cells with knockdown for TNC (Oskarsson *et al.*, 2011).

These reports show that TNC is associated with lung metastagenicity in several model systems and in cancer patients suggesting a specific mechanism behind. First mechanistic insight for the pro-metastatic effect of TNC has been obtained in a xenograft model where the microRNA miR335 suppressed lung metastasis by down-regulation of Sox4 and TNC (Tavazoie *et al.*, 2008) and TNC has been described as a direct target of Sox4 in prostate cancer (Scharer *et al.*, 2009). Sox4 had already turned out to be induced by TNC in GBM cells on a TNC substratum (Ruiz *et al.*, 2004). Recently, the stem cell markers Msi1 and Lgr5 were linked to induction of Notch- and Wnt signaling and TNC in oncospheres and metastatic breast cancer cells (Oskarsson *et al.*, 2011). In patients with GBM the Notch2 co-factor RBP Jk protein was co-expressed with TNC and activated Notch2 in cultured cells that had increased TNC expression (Sivasankaran *et al.*, 2009).

To address whether TNC had an effect on Sox4 in RT2/hTNC tumors, expression was determined by qRT-PCR, but no increase was observed in comparison to RT2 tumors (**Table 5**). In cultured cells on a TNC substratum, no induction of Lgr5 was observed in GBM and osteosarcoma cells (A. Heinke, personal communication). Understanding of the role of TNC on invasion and metastasis in the RT2/hTNC model might be hampered by the fact that we had analyzed expression in tumors which were still differentiated with high expression of insulin and E-cadherin and are therefore most likely not invasive (Chun and Hanahan, 2010; Perl *et al.*, 1998). Moreover, the analysis in tumors of 14 weeks old mice is presumably too late to detect early events. Furthermore, it is believed that tumor cells need to invade lymphatic vessels or the blood circulation to disseminate and colonize other organs. Therefore a potential effect of TNC expression levels on the formation of regional lymph node metastasis will be addressed in RT2 mice with the different TNC expression levels.

5.3 Mechanisms of TNC action in the RT2 model system

Several aspects in search of a mechanistic explanation of TNC actions in the RT2 model system have already been discussed above, including Notch signaling which plays an important role in cancer (Ranganathan *et al.*, 2011) and tumor angiogenesis (Bridges *et al.*, 2011). Notch signaling is likely not affected by forced expression of TNC in the RT2 model system since the Notch pathway genes Hey1 and Dll4 are not induced, but expression of more genes of this pathway needs to be tested in the future. Wnt signaling is another well described pathway that promotes tumor progression toward metastasis (MacDonald *et al.*, 2009; Polakis, 2000), which is associated with tumor invasion and accumulation of nuclear β-catenin as for example in colorectal cancer (Hlubek *et al.*, 2007) and which plays an important role in angiogenesis (Franco *et al.*, 2009).

5.3.1 TNC represses the Wnt inhibitor DKK1 thus potentially activating Wnt signaling

In the RT2/hTNC model activation of Wnt signaling was investigated by staining for β-catenin in tumors of RT2 and RT2/hTNC mice (**Manuscript 1 Fig. 4C**). IF staining documented a few cases of strong, eventual nuclear β-catenin in tumors of RT2/hTNC but not in RT2 control mice. At RNA level qRT-PCR for β-catenin did not reveal a difference between tumors of the two genotypes (**Table 5**). In GBM cells cultured on a TNC substratum, the Wnt inhibitor DKK1 was strongly down-regulated (Ruiz *et al.*, 2004). Therefore, we also performed qRT-PCR for DKK1 on isolated tumors showing that the TNC gene copy number correlated inversely with DKK1 expression levels suggesting a functional link and a potential activation of Wnt signaling by TNC (**Figure 22B, C**). In the RT2/hTNC model several Wnt target genes (cyclinD1, cyclinD2, CD44, Slug) were induced in adenomas. Further, several cancer cell lines grown on a TNC substratum showed loss of DKK1 expression and induction of several Wnt target genes in T98G GBM and KRIB osteosarcoma cells (**Manuscript 1 Fig. 6C, D, Suppl. Table 4**). Altogether, the data suggest a potential activation of Wnt signaling due to the loss of DKK1 but the proof of a robust Wnt signaling activation by TNC in tumor cells or tumor associated cells is still missing.

Likely, TNC acts locally within the tumor in a non-tumor cell autonomous manner which complicates quantification in whole tumors at RNA level. Enhanced expression of the cell cycle components cyclin D1 and cyclin D2 by TNC could explain the increased proliferation rate in tumors of RT2/hTNC mice. Enhanced levels of CD44 is also described to be involved in other cancer-associated processes such as metastasis and cell survival (Ponta *et al.*, 2003) and Slug is linked to EMT and anti-apoptotic activities (Thiery and Chopin, 1999) and

therefore could have played a role in TNC-associated enhanced carcinoma formation and formation of lung micrometastasis.

There are several points that argue against a direct activation of Wnt signaling by TNC in tumor cells: no compelling evidence for an effect of TNC knockdown on Wnt3a mediated induction of Lgr5 in breast cancer cells (Oskarsson *et al.*, 2011), a Wnt independent tumor progression by the loss of E-cadherin in the RT2 model (Herzig *et al.*, 2007) and the absence of a Wnt signature in dependence of TNC in non-angiogenic and angiogenic islets of RT2 mice (this study). But it is possible that low DKK1 levels act in a non-tumor cell specific manner on other cells within the tumor. This hypothesis is supported by subcutaneous grafting experiments of KRIB osteosarcoma cells that had been engineered to ectopically express high DKK1 (KRIB:DKK1). Whereas DKK1 did not affect proliferation of the cells in culture, xenografted KRIB:DKK1 cells generated small poorly vascularized tumors which was in contrast to the parental KRIB cells that formed big well vascularized tumors (**Manuscript 1 Fig. 7**). This suggests that TNC-induced repression of DKK1 in tumor cells exerts a paracrine effect on the tumor microenvironment, potentially on EC, CAF or other pro-angiogenic cells. Whether reduction of DKK1 in tumor cells can potentiate Wnt signaling in non-tumorigenic cells in a TNC-dependent manner is currently investigated *in vitro* in co-culture assays (A. Heinke, PhD student).

5.3.2 TNC-induced tumor angiogenesis and mechanisms

Angiogenesis is indispensable for supplying the tumor cells with nutrients and oxygen as well as for evacuating metabolic waste and is therefore crucial for tumor growth but also for metastasis as blood vessels serve as routes for cancer cells to colonize secondary organs. We used CD31 as a marker of angiogenesis and could show that tumors with forced TNC expression demonstrated significantly more blood vessel EC than control RT2 tumors (**Figure 16**). The same analysis was performed in a preliminary small set of tumors lacking TNC expression (**Figure 20**). These results showed that the extent of angiogenesis correlated with the TNC copy number and suggests that TNC promotes tumor angiogenesis. Invasive tumor cells might have a higher probability to get into the blood circulation which could explain that RT2 mice with higher TNC expression showed enhanced lung micrometastasis in both analyzed model systems.

We had also addressed the impact of TNC on the normal islet vasculature by quantification of CD31-positive cells in single-transgenic Rip-hTNC mice and revealed that normal non-tumorigenic islets of Rip-hTNC mice exhibited a tendency of 1.5-fold stronger CD31 staining

which was not statistically significant presumably due to the small sample size (not shown). This suggests that TNC might promote the expansion of EC already under normal conditions. A potential angiogenesis-promoting effect of TNC had been addressed in the laboratory by J. Kant (Kant, 2008) in the chick chorioallantoic membrane (CAM) assay showing that TNC induced EC sprouting *in vivo* (**Manuscript 1 Fig. 2E**).

In vitro TNC had already been shown to act as a chemoattractant for EC and to play a role in the generation of tumor derived EC (Pezzolo *et al.*, 2011), to promote EC tube formation (Martina *et al.*, 2010; Schenk *et al.*, 1999) and to promote the selection of highly proliferative endothelial cells (Alves *et al.*, 2011). Furthermore, it was shown to regulate EC spreading and migration and cardiac allografts failed to vascularize in mice lacking TNC expression (Ballard *et al.*, 2006).

Melanoma cells grafted into mice lacking TNC expression displayed a reduced tumor angiogenesis that was linked to reduced VEGFA (Tanaka *et al.*, 2004). TNC was shown to induce pro-angiogenic factors *in vitro* such as EDNRA and PDGFRα in a GBM cell line (Ruiz *et al.*, 2004). To investigate which angiogenic factors were affected by TNC in RT2 tumors, RNA expression levels of pro-angiogenic molecules were determined in well developed 14 weeks tumors but none of the tested markers (VEGFA, VEGF-R1/2/3, EDNRA, PDGFRα, EphA2, Hey1, Dll4) were significantly enhanced. The differences might also be local within the tumor and therefore difficult to detect at RNA level. In addition, the tested tumors had already passed the angiogenic switch and therefore, this analysis disregards potential early effects of TNC on tumor angiogenesis.

Indeed, quantifying CD31 levels in the different subclasses of tumors in the RT2/TNC-/- model revealed that already normal and hyperplastic islets showed enhanced angiogenesis in control tumors with TNC expression (**Figure 20B**) indicating that in control RT2 mice more hyperplastic islets perform the angiogenic switch and therefore develop more tumors. But quantification of the number of islets in the subgroups by size did not reveal a higher number of tumors in RT2/TNC+/+ tumors (**Figure 19C**) but this analysis needs to be repeated on a bigger sample size and at histological level.

In the same sample set, CD31 levels in tumors lacking TNC expression from RT2/TNC-/- mice remained at the same level independent on the islet size whereas in mice with TNC expression CD31 levels increased gradually from normal islets to tumors (**Figure 20B**). This suggests that RT2/TNC-/- mice might lack the angiogenic switch. In the RT2 model the angiogenic switch is necessary for growth of islet lesions into tumors (Hanahan and

Folkman, 1996) but tumors were observed in RT2/TNC-/- mice. One explanation could be that the angiogenic switch is delayed in tumors lacking TNC expression. To conclude alone from a certain level of CD31 expression that the angiogenic switch has been performed or not is misleading. At histological level, other angiogenic parameters such as formation of hemorrhages or the presence of dilated vessels needs to be included as proposed by Lopez and Hanahan (Lopez and Hanahan, 2002). This requires analysis of paraffin embedded tissue. However, the hypothesis that TNC could affect the chronology of the angiogenic switch in RT2 mice was supported by an observation in the RT2/hTNC model. When collecting pancreatic islets of 8 weeks old animals, mice with forced TNC expression contained twice as many angiogenic islets than control RT2 mice (**Figure 23B**). If the angiogenic switch is indeed accelerated needs to be investigated in 5 weeks old mice where tumors normally did not yet have performed the angiogenic switch. The same analysis will be done in the RT2/TNC-/- model which may give more conclusive results.

One could also speculate that TNC is necessary for priming EC that they respond to mitogenic stimuli which is necessary during sprouting angiogenesis. According to this hypothesis, EC priming might be defective or reduced in RT2/TNC-/- tumors lacking TNC. In consequence, sprouting angiogenesis is not induced. In perspectives, the angiogenic activity of islets from RT2 mice with different TNC levels will be tested in an *in vitro* 3D assay (Folkman *et al.*, 1989) to test a potential effect of TNC on the attraction of EC to angiogenic islets.

In search for mechanism of TNC on tumor angiogenesis and tumor progression, a gene transcription analysis was performed of non-angiogenic and angiogenic islets from RT2 and RT2/hTNC mice at early tumor stage. This experiment showed that key molecules of angiogenesis (CD31, EDNRA, Notch signaling) were enhanced in angiogenic compared to non-angiogenic islets independent of TNC expression. At a first glance, classical pro-angiogenic markers do not seem to be linked to enhanced TNC expression when comparing between the genotypes, but a detailed analysis of the data including independent validation by qRT-PCR and at tissue level has not been performed yet. Interestingly, TNC was highly up-regulated in the angiogenic islets (see Annex **Table 6**). This analysis is hampered by the possibility that the TNC expression level in RT2/hTNC islets is not high enough to reach the critical level necessary for the angiogenic switch. This possibility needs to be addressed in the future.

Further, pro-angiogenic processes in non-angiogenic islets might already be activated in 8 weeks old mice suggesting that events in very early islet lesions initiate pro-angiogenic programs. In the gene expression profiling of normal pancreatic islets of

Rip-hTNC mice, classical angiogenic factors such as VEGFs and their receptors were not up-regulated. However, the pro-angiogenic VEGF homologue PlGF was induced in islets with forced expression of TNC suggesting that it might regulate angiogenesis in the normal pancreas (see Annex **Table 9**). Loss of PlGF impaired angiogenesis in pathological conditions including cancer (Carmeliet *et al.*, 2001) and forced expression of PlGF in β-cells in Rip-PlGF mice induced formation of highly dilated vessels (Schomber *et al.*, 2007). Furthermore, the induction of pro-inflammatory chemokines in Rip-hTNC islets suggests that a potential recruitment of bone marrow-derived myeloid cells such as neutrophils or macrophages contributed to TNC-induced angiogenesis. In the RT2 model, neutrophils were shown to mediate the angiogenic switch (Nozawa *et al.*, 2006) and anti-Bv8-treated RT2 mice inhibited mobilization of myeloid cells in early islet lesions and subsequently exhibited reduced tumor angiogenesis (Shojaei *et al.*, 2008). Although such a signature could not be found in non-angiogenic islets of 8 weeks old RT2/hTNC mice it will be interesting to investigate if enhanced angiogenesis by TNC in normal and hyperplastic islets correlates with a higher number of neutrophils and/or other immune cells in the tissue. This aspect will be investigated at tissue level in RT2 mice with different TNC expression levels (knockout, wildtype, over-expression) in mice at the age of 5 weeks which did not yet have performed the angiogenic switch.

Together, high TNC expression levels correlated with enhanced angiogenesis in the RT2 model system already in early islet lesions. Furthermore, ectopic expression of TNC in RT2/hTNC mice showed that more islets had performed the angiogenic switch. Whereas classical pro-angiogenic mechanisms do not seem to be activated in this system, angiogenesis is presumably affected indirectly, possibly via induction of inflammation or via recruitment of bone-marrow derived cells. These possibilities will be addressed in the future.

Another possibility for the increase of angiogenesis by TNC could involve repression of the Wnt inhibitor DKK1. According to the literature, the role of DKK1 in normal and tumor angiogenesis is not clear. Whereas DKK1 appears to mobilize pro-angiogenic EC progenitor cells (Aicher *et al.*, 2008; Smadja *et al.*, 2010) and induced angiogenesis in DKK1 treated mesenteric tissue *in vivo* (Glaw *et al.*, 2010) it suppressed VEGFA-induced angiogenesis in a matrigel plug assay (Min *et al.*, 2011) and perturbed vascular development in isolated embryonic lung explants (De Langhe *et al.*, 2005).

In xenograft experiments, we observed that over-expression of DKK1 in osteosarcoma cells blocked tumor growth, presumably by inhibiting tumor angiogenesis. This suggests an inverse correlation between DKK1 and angiogenesis. In the RT2 model low DKK1 levels in tumors of RT2/hTNC mice could be linked to enhanced tumor angiogenesis in

mice with high TNC expression levels. *In vitro*, DKK1 levels were largely reduced in GBM, osteosarcoma and other tumor cells grown on a TNC substratum (A. Heinke, personal communication). Our experiments suggest that TNC-induced loss of DKK1 promotes tumor angiogenesis.

Possible explanations for the different effects of DKK1 may be found in the different experimental systems and settings used and the influence of non-canonical Wnt signaling pathways involving c-Jun N-terminal kinases (Pandur *et al.*, 2002; Thudi *et al.*, 2010) or could be explained by not well understood Wnt-independent functions of DKK1 (Mikheev *et al.*, 2004). Furthermore, DKK1 is differentially regulated upon cancer-specific contexts (Niehrs, 2006) suggesting an organ specific role of DKK1.

In summary, using the RT2 model system it was demonstrated that TNC expression affects tumor progression by determining the extent of angiogenesis and metastasis in an immune-competent tumorigenesis model. For a mechanistic explanation, based on yet undefined signaling events, it is likely that loss of the Wnt inhibitor DKK1 triggered several events leading to enhanced cell proliferation, tumor cell invasion, angiogenesis and finally to formation of more lung micrometastasis. Whereas a tumor cell-autonomous activation of Wnt signaling by the loss of DKK1 is unlikely, it is possible that a down-regulation of DKK1 in tumor cells causes a paracrine effect on other cell types in the microenvironment, further inducing angiogenesis or recruitment of other cell types to the tumor which then would promote tumor angiogenesis and tumor progression resulting in metastasis. In perspectives, the detailed analysis of data obtained by gene expression profiling of islets of Rip-hTNC mice and tumorigenic islets of RT2/hTNC mice will give a deeper insight into the mechanistic actions of TNC on tumor angiogenesis and progression.

5.3.3 Tumor vessel architecture and alternative mechanisms in RT2 tumor angiogenesis

Many *in vivo* studies and clinical investigations on cancer patients demonstrated the importance of TNC during tumor angiogenesis and its link to enhanced tumor malignancy and some mechanistic insight has been obtained at the cellular level and in a few mouse model systems (see **Introduction**). One objective of this thesis was to get a better understanding of the role of TNC in the tumor vessel architecture.

First, vascular casts were analyzed by SEM to investigate vessel anatomy in tumors from RT2 and RT2/hTNC mice. This experiment revealed that over-expression of TNC trans-formed the tumor blood vessels into a highly disorganized network showing increased vessel

branching and leakiness (**Figure 24**). This raises the question of how functional these vessels are. Although quantification was not finished yet, the analysis of RT2 tumor vessels for pericyte coverage using NG2 as a maker suggested that tumors with ectopic expression of TNC showed less pericyte coverage (I. Gasser, personal communication). Coverage of blood vessels with mural cells, such as pericytes, is important for blood vessel maturation and stability as they regulate capillary proliferation and blood flow (Crocker *et al.*, 1970; Darland and D'Amore, 1999; Kutcher and Herman, 2009). A potential substantial loss of pericytes in tumor vessels of RT2/hTNC tumors might explain the aberrant tumor vasculature observed in vascular casts. It is possible that in RT2/hTNC mice the supply of such tumors is disturbed which can inhibit their growth beyond a certain size. This can explain that RT2/hTNC mice develop less huge tumors bigger than 3 mm in diameter, compared to control RT2 mice. Moreover, disruption of the crosstalk between pericytes and EC resulted in enhanced leakiness and reduced vessel stability (Fuxe *et al.*, 2011) promoting tumor cell dissemination and metastasis formation. A link between the vessel quality and the formation of metastasis will be addressed in the future.

Further, tumors of RT2 and RT2/hTNC mice were analyzed in detail by transmission electron microscopy. This revealed that tumors of RT2/hTNC mice comprised matrix-rich tubular structures which contained nucleated cells and erythrocytes but lacked blood vessel properties such as EC-lining and the presence of a BM and therefore were named conduits. A connection between conduits and a blood vessel was further documented (**Figure 25**). These observations motivated us to investigate the location and organization of TNC in tumor tissue in particular in blood vessels and, likely, in matrix conduits. *In vivo* perfusion experiments were developed using fluorescence-labeled molecules to directly visualize perfusable structures inside the tumor for analysis at three-dimensional microscopic level. Although only a few preliminary results prove the principal benefit of the developed technique and the optimal protocol was only recently established, some first interesting insights into the architectural organization of TNC in the tumor tissue could be observed.

Visualization of the tumor vasculature by perfusion with lectin and co-staining for TNC showed that blood vessels of either normal or increased size did not show TNC expression. Instead, TNC was strongly expressed in a loop-like structure which did not show lectin staining and therefore was not a blood vessel (**Figure 26B**). These structures might represent what was determined as matrix conduits by TEM. To show a possible connection between the vasculature and matrix conduits, RT2 mice were perfused with FITC-dextran and co-staining performed by IF for TNC and LM (**Figure 27**). Analysis by 3D microscopy revealed that TNC matrix conduits were very heterogeneous even within one tumor. Some

structures were lined by LM, indicating a BM, and had an additional inner layer of TNC. Other structures showed exclusively either TNC or LM staining. Some of these TNC matrix conduits were positive for dextran as well as for nucleated cells but others were not able to transport dextran molecules. These observations indicate that some of the matrix conduits were connected to the blood circulation and are able to transport molecules and cells.

Although a detailed analysis of the described TNC containing matrix conduits is still missing it is intriguing to speculate which function these structures may have and how they affect tumor progression. In melanomas TNC expression was found in tubular channels with a lumen that contained tumor cells (Kaariainen *et al.*, 2006). In three-dimensional co-culture experiments carcinoma-associated fibroblasts prepared TNC containing tracks which were used by tumor cells to invade (Gaggioli *et al.*, 2007). Nucleated cells in the identified TNC containing matrix conduits in RT2/hTNC tumors might be such fibroblasts forming the tubular structures or might represent tumor cells that had disseminated. This could facilitate metastasis because of the connection of the conduits to the circulation.

Another possibility is that matrix conduits serve as a scaffold for angiogenesis comparable to the angiogenic alternative program of vasculogenic mimicry. Vasculogenic mimicry is the formation of blood transporting tubes by differentiated tumor cells showing EC-like characteristics but lack classical EC-lining. Such structures were identified in several cancer types and were linked to metastasis in melanoma (Hendrix *et al.*, 2003). To date, the implication of TNC in this process is unknown but it is intriguing to speculate that TNC is crucial for the formation of matrix tracks in tumors as an alternative vasculogenesis/ tubulogenesis program which in parallel supports the formation of metastasis. By TEM we observed that some of the tumor cells which were next to the matrix conduits had lost their insulin-containing granular vesicles. This might be an indication of a dedifferentiation of these tumor cells, maybe into cells with EC-like character or it might indicate the activation of other cellular processes leading to a pro-angiogenic environment. In the future, a detailed analysis of lectin- and dextran-perfused tumors combined with co-staining for different marker needs to be performed. Furthermore, the performed gene expression profiling might point at TNC induced signaling pathways important in vasculogenic mimicry such as VE-cadherin, EphA2, MMP2 or HIF-2α (Paulis *et al.*, 2010). Together, this will assess if TNC matrix conduits represent vasculogenic mimicry or a different tubulogenesis program. It is also possible that cells secrete TNC to form a scaffold and a pro-angiogenic environment. Later, proteases might degrade TNC forming a lumen which can be colonized by different cell types, for example EC progenitor cells to form a neovasculature.

It is also possible that the observed TNC conduits represent the result of an extensive pruning. This possibility is supported by the observation that bigger tumors exhibited less EC than smaller tumors. The EC number increased from angiogenic to small tumorigenic islets in RT2 mice but did not further increase in established tumors. Moreover, in established RT2/hTNC tumors there was a pronounced absence of an angiogenic signature noticed.

Is there any indication of how the TNC conduits may have formed? Therefore it is worth to have a look at TNC structures found in non-pathological tissues. TNC is expressed in reticular fibers of secondary lymphoid tissues such as the thymus where they are called thymic conduits and where TNC is surrounding an inner core of LM and collagens. These structures are believed to play a role in antigen maturation and as guiding cue for immune cells (Drumea-Mirancea *et al.*, 2006). We also observed co-expression of TNC and LM in matrix conduits in a layered and non-layered fashion. It is intriguing to speculate that a genetic program for reticular fibers is turned on in cancer and that the resulting conduits exhibit similar functions (Midwood *et al.*, 2011; Midwood and Orend, 2009). Therefore, it is possible that TNC matrix conduits represent lymphoid tissue-like structures that could help tumor cells to evade host immunity, a process termed “tumor immune evasion” (Zindl and Chaplin, 2010). This could be achieved by decreasing the expression of certain cell surface antigens or by secretion of factors which inhibit T-cell actions. Such a mechanism was recently described by Shields and colleagues (Shields *et al.*, 2010). CCL21 expression in melanoma cells was linked to recruitment of lymphoid tissue inducer cells to the tumor. This resulted in reorganization of the tumor stroma and recruitment of T regulatory cells and myeloid-derived suppressor cells preparing an immune tolerant tumor environment (Shields *et al.*, 2010; Zindl and Chaplin, 2010). A potential role of TNC in this process was not addressed, but it would be interesting to investigate, if TNC matrix-conduits in RT2 tumors provide such an environment. This possibility is supported by the obtained gene profiling data showing a potential induction of an immune signature in Rip-hTNC islets (see Annex **Table 9**). Moreover, F4/80 positive macrophages had highly infiltrated RT2/hTNC tumors where they were in close contact with TNC (Gasser *et al.*, in preparation). If tumor immune evasion is promoted by TNC needs to be addressed in the future.

In **Table 4** key features of the mentioned types of matrix tube formation in comparison to tumor blood vessels and to the matrix conduits described in this study are summarized. It is obvious that more work is needed to determine the key characteristics of TNC matrix conduits and to understand their role in tumor angiogenesis and cancer progression. Because of the presence and absence of several of these characteristics in the same tumors, one could hypothesize that it is likely that not only one of the presented processes

occurs but rather several of them which are activated simultaneously in a TNC dependent manner in the RT2 tumor model which would promote progression into malignant tumors and metastasis. If the presence of TNC is crucial in the formation and function of matrix conduits needs to be investigated in the future in the newly established RT2 model lacking TNC expression. In parallel, three dimensional co-culture experiments need to be established to model matrix conduit formation in dependence on TNC and to investigate the underlying molecular mechanisms.

Table 4: Comparison of key characteristics of matrix tube formation versus RT2 matrix conduits

Table showing absence (-) or presence (+) of key characteristics for the specific alternative tube formation according to published literature (Dome *et al.*, 2007; Folberg *et al.*, 2000; Hendrix *et al.*, 2003; Kaariainen *et al.*, 2006; Maniotis *et al.*, 1999) in comparison with matrix conduits observed in RT2 tumors. Observations combined from SEM, TEM and IF analysis. AtTu: atypical tumor cells, BM: basement membrane, EC: endothelial cells, ECM: extracellular matrix. LM: laminin, n.d.: not determined, PAS: Periodic acid-Schiff, TEC: thymic EC, TEM: transmission electron microscopy.

Feature	Tumor vessels	Vasculogenic mimicry	Melanoma matrix channels	Thymic conduits	RT2 TNC matrix conduits
EC lining	+	-	-	TEC	- (TEM)
BM lining	+	+	-	+	-
Tumor cell lining	-	+	n.d.	-	+
Erythrocytes	+	+	+	-	+
Nucleated cells	-	+	+	-	+
CD31	+	-	-	-	+ / -
PAS	+	+	n.d.	n.d.	+
Pan-LM / LM5γ2	+	+ / +	- / -	+ / +	+ / -
Collagen IV	+	+	-	+	+ / -
Tube formed by	EC	TC	ECM	ECM	ECM, AtTu cells
Size (diameter)	5 – 15 µm	variable	variable	~2 µm	~2 up to more than 30 µm
Lumen	+	+	n.d.	+	+ / -
Tenascin-C	+	unknown	+	+	+
Proposed functions	Angiogenesis Metastasis	Angiogenesis Metastasis	Metastasis	Immune Evasion	Angiogenesis Metastasis Immune evasion

6 Conclusion

The objectives of this thesis were to investigate the role of TNC in tumor progression in the RT2 mouse model of pancreatic neuroendocrine tumorigenesis and to get a better mechanistic understanding of TNC actions in cancer progression.

Here, the first model system copying TNC actions in human cancer in an immune-competent spontaneous tumorigenesis model is presented. In this model, ectopic expression of TNC promoted cell proliferation, carcinoma progression, tumor invasion, tumor angiogenesis and the formation of lung micrometastasis. Second, a loss-of-function model was developed to study the invalidation of TNC in RT2 tumorigenesis in a complementary approach. The promoting effect of ectopically expressed TNC on tumor angiogenesis and the formation of lung micrometastasis could be validated in this model.

Interestingly, several lines of evidence suggest that TNC has a strong impact on early events in tumor progression: 1) a detailed analysis of cell proliferation revealed that already normal islets had a similar proliferation index than hyperplastic islets suggesting that ectopic expression of TNC accelerates the hyperplastic switch. 2) TNC induced angiogenesis already in normal and hyperplastic islets of the RT2/TNC-/- model and ectopic expression of TNC in RT2/hTNC mice presumably accelerated the angiogenic switch. 3) Gene expression profiling of non-angiogenic and angiogenic islets from eight weeks old RT2 and RT2/hTNC mice revealed that ectopic expression of TNC had an impact on gene expression by largely deregulating gene expression in early non-angiogenic islets. These observations indicate that TNC plays an important role in key steps of early RT2 tumorigenesis, during the hyperplastic and the angiogenic switch. In this model, these steps are required for the development of solid tumors.

In search for mechanisms of TNC actions in RT2 tumorigenesis, gene expression analysis was performed on isolated tumors. This showed that the TNC gene copy number is inversely linked to expression levels of the Wnt inhibitor DKK1 and to induction of potential Wnt target genes but a tumor cell autonomous activation of Wnt signaling has not been shown. Additional experiments performed in the laboratory rather suggest a link between DKK1 and angiogenesis, as enhanced expression of DKK1 in tumors formed by osteosarcoma cells inhibited tumor growth and angiogenesis.

Another objective of this thesis was to get a better understanding of the structural role of TNC in the tumor vessel architecture. Perfusion experiments, electron microscopy and immunofluorescence 3D reconstruction microscopy were performed and revealed that

ectopic expression of TNC transformed the tumor vessel network in a highly disorganized network showing increased vessel branching and leakiness. This suggests that TNC affects tumor vessel functionality and therefore interferes with tumor growth beyond a certain size. We also discovered TNC matrix conduits which were not blood vessels but showed characteristics of vasculogenic mimicry including matrix tube formation. It is possible that matrix conduits play an important role as alternative angiogenic program and thus facilitate tumor cell dissemination or provide an immune tolerant microenvironment.

Taken together, two model systems had been generated to investigate the role of TNC on tumorigenesis using gain- and loss-of-function strategies. The data obtained in these models show that TNC has a signaling and a structural function and plays an important role in tumor onset and the angiogenic switch. The implication of the Wnt inhibitor DKK1 provides a mechanistic basis for the described TNC actions. TNC also had a structural function by perturbing the vessel architecture and by formation of matrix conduits which may promote tumor malignancy. These findings are summarized in **Figure 28**. The newly established RT2 model lacking TNC expression provides a valuable tool to investigate where TNC is essential for driving tumor onset, angiogenesis and lung metastasis. Based on these observations, TNC presents an attractive target for blocking tumor angiogenesis and tumor cell dissemination. Therefore, the presented model systems with different TNC expression could serve as an excellent preclinical model for evaluating the efficacy of drugs targeting TNC.

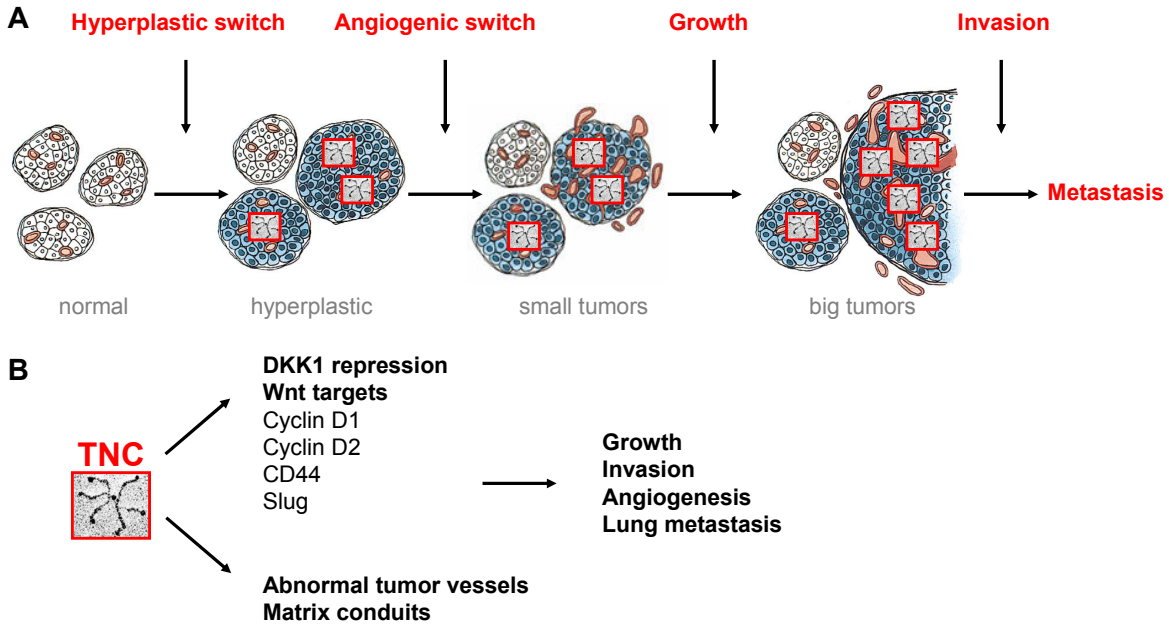

Figure 28: Impact of the extracellular matrix molecule tenascin-C on RT2 tumorigenesis

Summary scheme illustrating the promoting role of TNC on key steps in cancer progression of the RT2 model (adapted from Hahahan and Folkman, 1996) **(A)**. TNC has a signaling role by repressing DKK1 expression thus promoting tumor progression. TNC has also a structural role by formation of matrix conduits which may promote tumor malignancy **(B)**. Insert: Electron micrograph of a TNC hexamer visualized after rotary shadowing (Chiquet-Ehrisman and Chiquet 2003).

7 Summary

1. Forced over-expression of TNC enhances cell proliferation, accelerates tumor progression, increases angiogenesis and promotes the formation of lung micrometastasis in the RT2 model system.

2. The lack of TNC in the RT2 model correlates with reduced tumor angiogenesis and lung micrometastasis.

3. Over-expressed TNC induces very early events during RT2 tumor progression such as hyperproliferation and the angiogenic switch.

4. The TNC gene copy number inversely correlates with expression of the Wnt inhibitor DKK1 which is presumably linked to altered signaling that promotes tumor angiogenesis and tumor progression by TNC.

5. TNC is organized into matrix conduits which are connected to the circulation and which might represent an alternative program for angiogenesis and tumor cell dissemination.

8 Annex

8.1 Candidate gene expression by qRT-PCR

Table 5: Candidate gene expression by qRT-PCR on isolated tumors in the RT2/hTNC model

Relative gene expression of candidate genes (alphabetical order) in RT2/hTNC tumors versus RT2 tumors is based on ΔΔct values that were determined by qRT-PCR on RNA isolated from 14 weeks old RT2 (N = 11 mice, n = 28 tumors) and RT2/hTNC mice (N = 3, n = 14). Data are presented for **all** tumors (All), **small** tumors (Small, 1 - 3 mm, RT2 (n = 20), RT2/hTNC (n = 11)), **small and differentiated** tumors (Small diff., RT2 (n = 18), RT2/hTNC (n = 11)), **big** tumors (Big >3 mm, RT2 (n = 8), RT2/hTNC (n = 3)), **big and differentiated** tumors (Big diff., RT2 (n = 5), RT2/hTNC (n = 3)), **differentiated tumors** (Diff., high expression of insulin and E-cadherin, RT2 (n = 23), RT2/hTNC (n = 14). Bold numbers represent statistically significant data ($p \leq 0.05$); n.a.: not applicable due to too small sample number with detectable expression.

Candidate gene	Tumor class	ΔΔCt RT2/TNC versus RT2	p-value	Relative expression
Angiopoietin-1	All	-0.27	0.46	1.20
	Small	-0.25	0.54	1.19
	Small + Diff	-0.32	0.42	1.25
	Big	-0.18	0.83	1.13
	Big + Diff	-0.16	0.88	1.11
	Diff	-0.28	0.44	1.22
Angiopoietin-2	All	**0.90**	**0.01**	**-1.89**
	Small	0.50	0.15	-1.41
	Small + Diff	0.57	0.10	-1.49
	Big	**2.31**	**0.02**	**-5.00**
	Big + Diff	**2.73**	**0.02**	**-6.67**
	Diff	**1.04**	**0.01**	**-2.04**
β-Catenin	All	0.02	0.95	-1.01
	Small	-0.07	0.83	1.05
	Small + Diff	-0.10	0.77	1.07
	Big	0.20	0.60	-1.15
	Big + Diff	0.20	0.62	-1.15
	Diff	-0.04	0.90	1.03
CD31	All	0.11	0.957	-1.08
	Small	0.20	0.984	-1.15
	Small + Diff	0.11	0.805	-1.08
	Big	0.01	0.776	-1.01
	Big + Diff	0.19	0.368	-1.14
	Diff	0.12	0.863	-1.09
CD44	All	-0.46	0.22	1.38
	Small	-0.54	0.19	1.45
	Small + Diff	**-0.88**	**0.03**	**1.84**
	Big	0.71	0.11	-1.64
	Big + Diff	0.71	0.11	-1.64
	Diff	-0.54	0.15	1.46

Candidate gene	Tumor class	ΔΔCt RT2/TNC versus RT2	p-value	Relative expression
cMyc	All	0.34	0.07	-1.27
	Small	0.21	0.27	-1.16
	Small + Diff	0.13	0.47	-1.10
	Big	**0.91**	**0.03**	**-1.89**
	Big + Diff	0.70	0.11	-1.61
	Diff	0.25	0.19	-1.19
Cyclin D1	All	-0.77	0.13	1.70
	Small	-1.02	0.11	2.02
	Small + Diff	**-1.30**	**0.03**	**2.46**
	Big	0.13	0.86	-1.10
	Big + Diff	0.51	0.50	-1.43
	Diff	-0.91	0.07	1.88
Cyclin D2	All	-0.38	0.29	1.30
	Small	-0.50	0.14	1.42
	Small + Diff	**-0.71**	**0.03**	**1.64**
	Big	0.43	0.37	-1.35
	Big + Diff	0.67	0.21	-1.59
	Diff	-0.41	0.21	1.33
DKK1	All	**1.71**	**<0.01**	**-3.23**
	Small	**1.61**	**0.02**	**-3.03**
	Small Diff	**1.36**	**0.02**	**-2.57**
	Big	1.88	n.a.	-3.70
	Big Diff	0.74	n.a.	-1.67
	Diff Only	**1.22**	**0.01**	**-2.33**
	Diff	n.a.	n.a.	n.a.
DLL4	All	-0.44	0.28	1.35
	Small	-0.20	0.66	1.15
	Small + Diff	-0.04	0.93	1.03
	Big	-0.93	0.25	1.90
	Big + Diff	-0.53	0.50	1.45
	Diff	-0.15	0.70	1.11
EDNRA	All	0.41	0.21	-1.33
	Small	-0.19	0.45	1.14
	Small + Diff	-0.25	0.27	1.19
	Big	**2.29**	**0.02**	**-4.76**
	Big + Diff	1.72	0.11	-3.33
	Diff	0.18	0.54	-1.12
EphA2	All	0.43	0.23	-1.35
	Small	0.20	0.92	-1.15
	Small + Diff	0.20	0.86	-1.15
	Big	**1.23**	**0.01**	**-2.34**
	Big + Diff	**0.98**	**0.04**	**-1.97**
	Diff	0.37	0.31	-1.29
Hey1	All	0.35	0.12	-1.27
	Small	-0.03	0.89	1.02
	Small + Diff	-0.10	0.66	1.07
	Big	**1.60**	**<0.01**	**-3.03**
	Big + Diff	**1.41**	**0.02**	**-2.63**
	Diff	0.22	0.32	-1.16
Id2	All	**0.87**	**0.03**	**-1.82**
	Small	0.22	0.54	-1.16
	Small + Diff	0.02	0.96	-1.01
	Big	**2.82**	**0.02**	**-7.14**
	Big + Diff	2.04	0.41	-4.17
	Diff	0.41	0.20	-1.33

Candidate gene	Tumor class	ΔΔCt RT2/TNC versus RT2	p-value	Relative expression
Lgr5	All	0.38	0.84	-1.30
	Small	-0.46	0.32	1.37
	Small + Diff	-0.56	0.25	1.48
	Big	2.71	0.28	-6.53
	Big + Diff	1.31	0.79	-2.47
	Diff	-0.16	0.30	1.12
PDGFRα	All	**0.86**	**0.02**	**-1.82**
	Small	0.75	0.06	-1.67
	Small + Diff	0.50	0.12	-1.41
	Big	**1.50**	**0.02**	**-2.86**
	Big + Diff	1.17	0.06	-2.22
	Diff	**0.64**	**0.04**	**-1.56**
Slug	All	-0.25	0.43	1.19
	Small	**-0.72**	**0.04**	**1.64**
	Small + Diff	**-0.84**	**0.02**	**1.79**
	Big	1.29	0.05	-2.44
	Big + Diff	1.00	0.19	-2.00
	Diff	-0.44	0.18	1.36
Sox4	All	0.46	0.05	-1.37
	Small	0.47	0.13	-1.39
	Small + Diff	0.44	0.17	-1.35
	Big	0.47	0.07	-1.39
	Big + Diff	0.50	0.10	-1.41
	Diff	0.45	0.08	-1.37
Tie2	All	0.01	0.97	-1.01
	Small	-0.04	0.89	1.03
	Small + Diff	-0.09	0.76	1.06
	Big	0.49	0.36	-1.41
	Big + Diff	0.83	0.10	-1.79
	Diff	0.10	0.71	-1.08
VEGF-A	All	0.19	0.48	-1.14
	Small	0.33	0.19	-1.25
	Small + Diff	**0.50**	**0.02**	**-1.41**
	Big	-0.07	0.92	1.05
	Big + Diff	0.39	0.59	-1.32
	Diff	**0.48**	**0.03**	**-1.39**
VEGF-R1	All	-0.11	0.82	1.08
	Small	-0.29	0.51	1.22
	Small + Diff	-0.23	0.65	1.17
	Big	0.87	0.29	-1.82
	Big + Diff	1.21	0.21	-2.33
	Diff	0.08	0.88	-1.05
VEGF-R2	All	0.51	0.16	-1.43
	Small	0.47	0.25	-1.39
	Small + Diff	0.51	0.24	-1.43
	Big	0.89	0.19	-1.85
	Big + Diff	**1.47**	**0.02**	**-2.78**
	Diff	0.71	0.05	-1.64
VEGF-R3	All	-0.47	0.07	1.39
	Small	-0.57	0.05	1.48
	Small + Diff	-0.40	0.12	1.32
	Big	-0.07	0.90	1.05
	Big + Diff	0.35	0.44	-1.28
	Diff	-0.24	0.28	1.18

8.2 Affymetrix chip analysis – RT2 and RT2/hTNC mice (I)

Table 6: Gene expression between angiogenic and non-angiogenic islet pools from 8 weeks old RT2 and RT2/hTNC mice

Affymetrix chip analysis of angiogenic and non-angiogenic islet pools of 8 weeks old RT2 and RT2/hTNC mice. Fold-changes were compared between angiogenic and non-angiogenic samples, independent on the genotype. Data were filtered for fold-changes of minimally ±1.2-fold or more with a significance value of $p \leq 0.05$. List contains 1013 gene candidates. Data were screened by searching for the keywords “extracellular matrix”, “blood vessel development”, “angiogenesis” and “Notch” in the GO biological process or GO cellular component terms and are highlighted in bold. Gene products mentioned in the text are highlighted in grey. Data are sorted according descending fold-changes.

Annex Table 6 - Angiogenic versus non-angiogenic (RT2 and RT2/hTNC)

Probe Set ID	Gene Symbol	Gene Description	Fold-change	p-value
10411082	**Thbs4**	**thrombospondin 4**	**6.54**	**0.000**
10355403	**Fn1**	**fibronectin 1**	**5.29**	**0.000**
10458894	**Lox**	**lysyl oxidase**	**5.11**	**0.000**
10513739	**Tnc**	**tenascin C**	**4.28**	**0.000**
10598976	**Timp1**	**tissue inhibitor of metalloproteinase 1**	**3.72**	**0.000**
10440091	**Col8a1**	**collagen, type VIII, alpha 1**	**3.51**	**0.000**
10492021	**Postn**	**periostin, osteoblast specific factor**	**3.43**	**0.000**
10467124	Acta2	actin, alpha 2, smooth muscle, aorta	3.31	0.000
10541496	**Mfap5**	**microfibrillar associated protein 5**	**3.23**	**0.000**
10365983	**Lum**	**lumican**	**3.19**	**0.000**
10487040	**Fbn1**	**fibrillin 1**	**3.09**	**0.000**
10435641	Fstl1	follistatin-like 1	3.05	0.000
10435948	**Ccdc80**	**coiled-coil domain containing 80**	**2.92**	**0.000**
10573924	**Mmp2**	**matrix metallopeptidase 2**	**2.88**	**0.000**
10536220	**Col1a2**	**collagen, type I, alpha 2**	**2.88**	**0.000**
10380419	**Col1a1**	**collagen, type I, alpha 1**	**2.86**	**0.000**
10600169	**Bgn**	**biglycan**	**2.66**	**0.000**
10375051	Hba-a1	hemoglobin alpha, adult chain 1	2.66	0.000
10581013	Cdh11	cadherin 11	2.65	0.000
10375058	Hba-a2	hemoglobin alpha, adult chain 2	2.64	0.000
10572897	**Hmox1**	**heme oxygenase (decycling) 1**	**2.64**	**0.000**
10349947	**Fmod**	**fibromodulin**	**2.50**	**0.000**
10362201	**Ctgf**	**connective tissue growth factor**	**2.48**	**0.000**
10362495	**Col10a1**	**collagen, type X, alpha 1**	**2.43**	**0.004**
10513208	Svep1	sushi, von Willebrand factor type A, EGF and pentraxin domain containing 1	2.41	0.000
10566258	Hbb-b1	hemoglobin, beta adult major chain	2.40	0.001
10601659	Srpx2	sushi-repeat-containing protein, X-linked 2	2.39	0.000
10566254	Hbb-b1	hemoglobin, beta adult major chain	2.33	0.001
10356520	**Col6a3**	**collagen, type VI, alpha 3**	**2.33**	**0.000**
10375751	**Adamts2**	**a disintegrin-like and metallopeptidase (reprolysin type) with thrombospc**	**2.31**	**0.000**
10534667	**Serpine1**	**serine (or cysteine) peptidase inhibitor, clade E, member 1**	**2.31**	**0.000**
10388430	**Serpinf1**	**serine (or cysteine) peptidase inhibitor, clade F, member 1**	**2.25**	**0.000**
10548879	**Mgp**	**matrix Gla protein**	**2.23**	**0.000**
10466606	Anxa1	annexin A1	2.22	0.000
10542355	Emp1	epithelial membrane protein 1	2.19	0.000
10595211	**Col12a1**	**collagen, type XII, alpha 1**	**2.17**	**0.000**
10456046	Pdgfrb	platelet derived growth factor receptor, beta polypeptide	2.13	0.000
10556509	**Spon1**	**spondin 1, (f-spondin) extracellular matrix protein**	**2.12**	**0.000**
10424140	**Col14a1**	**collagen, type XIV, alpha 1**	**2.11**	**0.000**
10351293	**Dpt**	**dermatopontin**	**2.11**	**0.001**
10412207	Gpx8	glutathione peroxidase 8 (putative)	2.10	0.000
10534862	Pcolce	procollagen C-endopeptidase enhancer protein	2.10	0.000
10365559	Igf1	insulin-like growth factor 1	2.09	0.000
10403584	**Nid1**	**nidogen 1**	**2.06**	**0.000**
10417212	Itgbl1	integrin, beta-like 1	2.06	0.000
10586357	**Cilp**	**cartilage intermediate layer protein, nucleotide pyrophosphohydrolase**	**2.06**	**0.000**
10425161	**Lgals1**	**lectin, galactose binding, soluble 1**	**2.05**	**0.000**
10405063	**Ogn**	**osteoglycin**	**2.05**	**0.000**
10458906	Ppic	peptidylprolyl isomerase C	2.04	0.000
10594066	**Loxl1**	**lysyl oxidase-like 1**	**2.04**	**0.000**
10376778	**Mfap4**	**microfibrillar-associated protein 4**	**2.03**	**0.000**
10355984	Serpine2	serine (or cysteine) peptidase inhibitor, clade E, member 2	2.00	0.000
10473444	Aplnr	apelin receptor	2.00	0.000
10447951	**Thbs2**	**thrombospondin 2**	**1.99**	**0.000**
10594044	Islr	immunoglobulin superfamily containing leucine-rich repeat	1.98	0.000
10405047	**Aspn**	**asporin**	**1.98**	**0.000**
10411229	F2r	coagulation factor II (thrombin) receptor	1.98	0.000
10401527	Ltbp2	latent transforming growth factor beta binding protein 2	1.97	0.000
10474700	**Thbs1**	**thrombospondin 1**	**1.97**	**0.000**
10415052	**Mmp14**	**matrix metallopeptidase 14 (membrane-inserted)**	**1.97**	**0.000**
10541605	Clec4n	C-type lectin domain family 4, member n	1.97	0.000
10358339	Cfh	complement component factor h	1.97	0.000
10365974	**Dcn**	**decorin**	**1.95**	**0.003**
10459335	Fam38b	family with sequence similarity 38, member B	1.95	0.000
10368289	Enpp1	ectonucleotide pyrophosphatase/phosphodiesterase 1	1.94	0.000
10491970	Lhfp	lipoma HMGIC fusion partner	1.94	0.000
10469457	Plxdc2	plexin domain containing 2	1.93	0.000
10381122	Fkbp10	FK506 binding protein 10	1.93	0.000
10386058	**Sparc**	**secreted acidic cysteine rich glycoprotein**	**1.93**	**0.000**
10477920	Myl9	myosin, light polypeptide 9, regulatory	1.92	0.000
10459353	Fam38b	family with sequence similarity 38, member B	1.91	0.000
10504775	**Col15a1**	**collagen, type XV, alpha 1**	**1.91**	**0.000**
10401673	**Tgfb3**	**transforming growth factor, beta 3**	**1.90**	**0.000**
10346015	**Col3a1**	**collagen, type III, alpha 1**	**1.88**	**0.000**
10362538	**Lama4**	**laminin, alpha 4**	**1.87**	**0.000**
10570957	Sfrp1	secreted frizzled-related protein 1	1.87	0.001
10560190	Ehd2	EH-domain containing 2	1.85	0.000
10370210	**Col6a1**	**collagen, type VI, alpha 1**	**1.83**	**0.000**
10396476	Rhoj	ras homolog gene family, member J	1.83	0.000

10381898	Mrc2	mannose receptor, C type 2	1.83	0.000
10445293	Pla2g7	phospholipase A2, group VII (platelet-activating factor acetylhydrolase, plasma	1.83	0.000
10359624	Prrx1	paired related homeobox 1	1.81	0.000
10357870	**Prelp**	**proline arginine-rich end leucine-rich repeat**	**1.81**	**0.000**
10352905	Cd34	CD34 antigen	1.81	0.000
10527158	Fscn1	fascin homolog 1, actin bundling protein (Strongylocentrotus purpuratus)	1.81	0.000
10579812	**Ednra**	**endothelin receptor type A**	**1.80**	**0.000**
10574438	Cdh5	cadherin 5	1.80	0.000
10351463	Rgs5	regulator of G-protein signaling 5	1.80	0.000
10370180	**Col6a2**	**collagen, type VI, alpha 2**	**1.79**	**0.000**
10398075	Serpina3n	serine (or cysteine) peptidase inhibitor, clade A, member 3N	1.78	0.003
10412298	Itga1	integrin alpha 1	1.77	0.000
10488382	Cd93	CD93 antigen	1.77	0.000
10574471	Cmtm3	CKLF-like MARVEL transmembrane domain containing 3	1.77	0.000
10375360	Ebf1	early B-cell factor 1	1.77	0.000
10569017	Ifitm3	interferon induced transmembrane protein 3	1.76	0.000
10469322	Vim	vimentin	1.76	0.000
10351455	Rgs5	regulator of G-protein signaling 5	1.75	0.000
10374083	Aebp1	AE binding protein 1	1.75	0.000
10586744	**Anxa2**	**annexin A2**	**1.75**	**0.000**
10546725	Pdzrn3	PDZ domain containing RING finger 3	1.74	0.000
10368409	**Lama2**	**laminin, alpha 2**	**1.73**	**0.000**
10514088	**Frem1**	**Fras1 related extracellular matrix protein 1**	**1.73**	**0.000**
10492682	Fam198b	family with sequence similarity 198, member B	1.73	0.000
10565794	Serpinh1	serine (or cysteine) peptidase inhibitor, clade H, member 1	1.73	0.000
10467258	Myof	myoferlin	1.73	0.000
10565456	Prss23	protease, serine, 23	1.72	0.000
10433114	Itga5	integrin alpha 5 (fibronectin receptor alpha)	1.72	0.000
10547740	C1s	complement component 1, s subcomponent	1.72	0.001
10511180	Mxra8	matrix-remodelling associated 8	1.72	0.000
10459363	Fam38b	family with sequence similarity 38, member B	1.71	0.000
10570068	**Col4a2**	**collagen, type IV, alpha 2**	**1.71**	**0.000**
10500808	Olfml3	olfactomedin-like 3	1.71	0.000
10554789	Ctsc	cathepsin C	1.71	0.000
10502778	Lphn2	latrophilin 2	1.71	0.000
10440258	Epha3	Eph receptor A3	1.71	0.000
10410931	**Vcan**	**versican**	**1.71**	**0.000**
10547100	**Plxnd1**	**plexin D1**	**1.70**	**0.000**
10598507	Slc38a5	solute carrier family 38, member 5	1.70	0.000
10521759	Slit2	slit homolog 2 (Drosophila)	1.69	0.000
10555174	Lrrc32	leucine rich repeat containing 32	1.69	0.000
10466210	Ms4a6d	membrane-spanning 4-domains, subfamily A, member 6D	1.69	0.002
10561104	Axl	AXL receptor tyrosine kinase	1.69	0.000
10372648	Lyz2	lysozyme 2	1.68	0.000
10585214	Cryab	crystallin, alpha B	1.68	0.000
10501608	Vcam1	vascular cell adhesion molecule 1	1.67	0.000
10379727	Gm11428	predicted gene 11428	1.67	0.000
10364593	Cnn2	calponin 2	1.67	0.000
10496727	**Ddah1**	**dimethylarginine dimethylaminohydrolase 1**	**1.66**	**0.000**
10441003	Runx1	runt related transcription factor 1	1.65	0.000
10436727	ORF63	open reading frame 63	1.65	0.000
10531931	**Sparcl1**	**SPARC-like 1**	**1.64**	**0.000**
10555297	Kcne3	potassium voltage-gated channel, Isk-related subfamily, gene 3	1.64	0.000
10445758	Treml4	triggering receptor expressed on myeloid cells-like 4	1.64	0.000
10534927	Pilra	paired immunoglobin-like type 2 receptor alpha	1.63	0.000
10458663	Dpysl3	dihydropyrimidinase-like 3	1.63	0.000
10360391	Ifi203	interferon activated gene 203	1.63	0.000
10577164	Gas6	growth arrest specific 6	1.63	0.001
10593123	Tagln	transgelin	1.63	0.000
10555736	Olfr558	olfactory receptor 558	1.62	0.001
10532711	Cmklr1	chemokine-like receptor 1	1.62	0.000
10350516	Ptgs2	prostaglandin-endoperoxide synthase 2	1.62	0.013
10351206	Selp	selectin, platelet	1.62	0.004
10523451	Anxa3	annexin A3	1.62	0.000
10554945	Prcp	prolylcarboxypeptidase (angiotensinase C)	1.62	0.000
10587733	**Ctsh**	**cathepsin H**	**1.61**	**0.000**
10576973	**Col4a1**	**collagen, type IV, alpha 1**	**1.61**	**0.000**
10461869	Prune2	prune homolog 2 (Drosophila)	1.61	0.002
10360382	Ifi204	interferon activated gene 204	1.61	0.000
10493820	S100a6	S100 calcium binding protein A6 (calcyclin)	1.61	0.000
10360406	Ifi205	interferon activated gene 205	1.61	0.029
10478048	Lbp	lipopolysaccharide binding protein	1.61	0.002
10467139	Lipa	lysosomal acid lipase A	1.60	0.000
10425287	Kdelr3	KDEL (Lys-Asp-Glu-Leu) endoplasmic reticulum protein retention receptor 3	1.60	0.000
10354309	**Col5a2**	**collagen, type V, alpha 2**	**1.60**	**0.000**
10502780	Lphn2	latrophilin 2	1.60	0.000
10371662	Spic	Spi-C transcription factor (Spi-1/PU.1 related)	1.59	0.001
10531407	Cxcl9	chemokine (C-X-C motif) ligand 9	1.59	0.012
10436487	Vgll3	vestigial like 3 (Drosophila)	1.59	0.000
10467420	Pdlim1	PDZ and LIM domain 1 (elfin)	1.59	0.000
10422728	Dab2	disabled homolog 2 (Drosophila)	1.59	0.000

10458314	Tmem173	transmembrane protein 173	1.58	0.000
10381096	Igfbp4	insulin-like growth factor binding protein 4	1.58	0.002
10419578	Ndrg2	N-myc downstream regulated gene 2	1.58	0.000
10488060	**Jag1**	**jagged 1**	**1.57**	**0.000**
10584674	Mcam	melanoma cell adhesion molecule	1.57	0.000
10485466	Cat	catalase	1.57	0.000
10476321	Prnd	prion protein dublet	1.57	0.000
10418506	Stab1	stabilin 1	1.56	0.000
10363070	Gp49a	glycoprotein 49 A	1.56	0.001
10471486	**Eng**	**endoglin**	**1.56**	**0.000**
10494817	Ngf	nerve growth factor	1.55	0.000
10600836	Msn	moesin	1.55	0.000
10514054	Nfib	nuclear factor I/B	1.55	0.000
10520452	Il6	interleukin 6	1.55	0.006
10440522	**Adamts1**	**a disintegrin-like and metallopeptidase (reprolysin type) with thrombospc**	**1.55**	**0.000**
10446282	Emr1	EGF-like module containing, mucin-like, hormone receptor-like sequence 1	1.55	0.000
10548892	Arhgdib	Rho, GDP dissociation inhibitor (GDI) beta	1.55	0.001
10567297	Itpripl2	inositol 1,4,5-triphosphate receptor interacting protein-like 2	1.55	0.000
10401238	Zfp36l1	zinc finger protein 36, C3H type-like 1	1.55	0.000
10407337	Hcn1	hyperpolarization-activated, cyclic nucleotide-gated K+ 1	1.55	0.001
10483353	Scn7a	sodium channel, voltage-gated, type VII, alpha	1.54	0.003
10360070	Fcer1g	Fc receptor, IgE, high affinity I, gamma polypeptide	1.54	0.000
10360377	AI607873	expressed sequence AI607873	1.54	0.004
10501586	**S1pr1**	**sphingosine-1-phosphate receptor 1**	**1.54**	**0.000**
10393364	Cygb	cytoglobin	1.53	0.000
10568668	Adam12	a disintegrin and metallopeptidase domain 12 (meltrin alpha)	1.53	0.000
10571840	Hpgd	hydroxyprostaglandin dehydrogenase 15 (NAD)	1.53	0.004
10588037	Rbp1	retinol binding protein 1, cellular	1.53	0.000
10554752	Nox4	NADPH oxidase 4	1.53	0.000
10389231	Ccl3	chemokine (C-C motif) ligand 3	1.53	0.006
10498018	Pcdh18	protocadherin 18	1.53	0.001
10347583	Des	desmin	1.53	0.000
10440534	**Adamts5**	**a disintegrin-like and metallopeptidase (reprolysin type) with thrombospc**	**1.52**	**0.000**
10395163	**Lamb1-1**	**laminin B1 subunit 1**	**1.52**	**0.000**
10392221	**Pecam1**	**platelet/endothelial cell adhesion molecule 1**	**1.52**	**0.000**
10540085	**Fbln2**	**fibulin 2**	**1.52**	**0.000**
10482448	Zeb2	zinc finger E-box binding homeobox 2	1.51	0.000
10440019	Tmem45a	transmembrane protein 45a	1.51	0.000
10493114	Nes	nestin	1.51	0.000
10517513	C1qc	complement component 1, q subcomponent, C chain	1.51	0.000
10590031	Itga9	integrin alpha 9	1.51	0.000
10466190	Ms4a14	membrane-spanning 4-domains, subfamily A, member 14	1.51	0.000
10463070	Entpd1	ectonucleoside triphosphate diphosphohydrolase 1	1.51	0.000
10363082	Lilrb4	leukocyte immunoglobulin-like receptor, subfamily B, member 4	1.51	0.000
10505954	**Tek**	**endothelial-specific receptor tyrosine kinase**	**1.51**	**0.000**
10531560	Antxr2	anthrax toxin receptor 2	1.50	0.000
10502791	Ifi44	interferon-induced protein 44	1.50	0.001
10522503	Pdgfra	platelet derived growth factor receptor, alpha polypeptide	1.50	0.001
10358816	**Lamc1**	**laminin, gamma 1**	**1.50**	**0.000**
10485198	Tspan18	tetraspanin 18	1.50	0.000
10511835	Fhl5	four and a half LIM domains 5	1.50	0.000
10508663	Laptm5	lysosomal-associated protein transmembrane 5	1.49	0.000
10498024	Slc7a11	solute carrier family 7 (cationic amino acid transporter, y+ system), member 11	1.49	0.000
10471555	Angptl2	angiopoietin-like 2	1.49	0.001
10461587	Ms4a4a	membrane-spanning 4-domains, subfamily A, member 4A	1.49	0.000
10379511	Ccl2	chemokine (C-C motif) ligand 2	1.49	0.000
10355536	Tns1	tensin 1	1.49	0.000
10573939	Lpcat2	lysophosphatidylcholine acyltransferase 2	1.49	0.000
10359929	Ddr2	discoidin domain receptor family, member 2	1.49	0.000
10502776	Lphn2	latrophilin 2	1.48	0.000
10584628	**Thy1**	**thymus cell antigen 1, theta**	**1.48**	**0.000**
10360028	Fcgr2b	Fc receptor, IgG, low affinity IIb	1.48	0.000
10566358	Trim30	tripartite motif-containing 30	1.48	0.000
10580382	Neto2	neuropilin (NRP) and tolloid (TLL)-like 2	1.48	0.016
10583008	Casp12	caspase 12	1.48	0.000
10606016	Il2rg	interleukin 2 receptor, gamma chain	1.48	0.003
10402211	Fbln5	fibulin 5	1.48	0.000
10373223	Lrp1	low density lipoprotein receptor-related protein 1	1.47	0.000
10423109	**Adamts12**	**a disintegrin-like and metallopeptidase (reprolysin type) with thrombospc**	**1.47**	**0.000**
10551883	Tyrobp	TYRO protein tyrosine kinase binding protein	1.47	0.000
10367591	Myct1	myc target 1	1.47	0.000
10375175	Slit3	slit homolog 3 (Drosophila)	1.47	0.000
10388902	Lgals9	lectin, galactose binding, soluble 9	1.47	0.000
10605256	Flna	filamin, alpha	1.46	0.000
10534343	**Eln**	**elastin**	**1.46**	**0.000**
10434229	Cldn5	claudin 5	1.46	0.000
10529875	Ldb2	LIM domain binding 2	1.46	0.000
10586865	**Aldh1a2**	**aldehyde dehydrogenase family 1, subfamily A2**	**1.46**	**0.000**
10551185	**Tgfb1**	**transforming growth factor, beta 1**	**1.46**	**0.000**
10517508	C1qb	complement component 1, q subcomponent, beta polypeptide	1.46	0.000
10351551	**Adamts4**	**a disintegrin-like and metallopeptidase (reprolysin type) with thrombospc**	**1.46**	**0.000**

10446965	Rasgrp3	RAS, guanyl releasing protein 3	1.46	0.000
10591139	Naalad2	N-acetylated alpha-linked acidic dipeptidase 2	1.46	0.000
10405587	**Tgfbi**	**transforming growth factor, beta induced**	**1.46**	**0.000**
10453747	Colec12	collectin sub-family member 12	1.45	0.000
10358434	Pla2g4a	phospholipase A2, group IVA (cytosolic, calcium-dependent)	1.45	0.000
10370259	**Col18a1**	**collagen, type XVIII, alpha 1**	**1.45**	**0.000**
10399148	Rapgef5	Rap guanine nucleotide exchange factor (GEF) 5	1.45	0.000
10483081	Fap	fibroblast activation protein	1.45	0.001
10566454	Prkcdbp	protein kinase C, delta binding protein	1.45	0.000
10469358	Mrc1	mannose receptor, C type 1	1.45	0.000
10527332	Nptx2	neuronal pentraxin 2	1.45	0.006
10412921	**Nid2**	**nidogen 2**	**1.45**	**0.000**
10419744	Oxa1l	oxidase assembly 1-like	1.45	0.000
10379518	Ccl7	chemokine (C-C motif) ligand 7	1.45	0.000
10466200	Ms4a7	membrane-spanning 4-domains, subfamily A, member 7	1.45	0.000
10521678	Cd38	CD38 antigen	1.45	0.004
10603151	Gpm6b	glycoprotein m6b	1.45	0.001
10512372	Ccl19	chemokine (C-C motif) ligand 19	1.45	0.003
10568392	Rgs10	regulator of G-protein signalling 10	1.44	0.001
10456071	Csf1r	colony stimulating factor 1 receptor	1.44	0.000
10584288	**Robo4**	**roundabout homolog 4 (Drosophila)**	**1.44**	**0.000**
10509280	**Hspg2**	**perlecan (heparan sulfate proteoglycan 2)**	**1.44**	**0.000**
10347335	Slc11a1	solute carrier family 11 (proton-coupled divalent metal ion transporters), memb	1.44	0.000
10366476	**Ptprb**	**protein tyrosine phosphatase, receptor type, B**	**1.44**	**0.000**
10461614	Ms4a6c	membrane-spanning 4-domains, subfamily A, member 6C	1.44	0.000
10489759	Sulf2	sulfatase 2	1.44	0.000
10582376	Fam38a	family with sequence similarity 38, member A	1.44	0.000
10502748	Lphn2	latrophilin 2	1.44	0.000
10438445	Klhl6	kelch-like 6 (Drosophila)	1.44	0.000
10498284	Wwtr1	WW domain containing transcription regulator 1	1.44	0.000
10539263	Loxl3	lysyl oxidase-like 3	1.44	0.000
10490159	Pmepa1	prostate transmembrane protein, androgen induced 1	1.43	0.000
10381371	Aoc3	amine oxidase, copper containing 3	1.43	0.000
10545707	Actg2	actin, gamma 2, smooth muscle, enteric	1.43	0.000
10404606	Ly86	lymphocyte antigen 86	1.43	0.001
10504159	Ccl19	chemokine (C-C motif) ligand 19	1.43	0.003
10512322	Ccl19	chemokine (C-C motif) ligand 19	1.43	0.003
10413609	Mustn1	musculoskeletal, embryonic nuclear protein 1	1.43	0.000
10562192	Fxyd5	FXYD domain-containing ion transport regulator 5	1.43	0.000
10582958	Gucy1a2	guanylate cyclase 1, soluble, alpha 2	1.43	0.000
10579525	Plvap	plasmalemma vesicle associated protein	1.42	0.000
10414102	**Mmrn2**	**multimerin 2**	**1.42**	**0.000**
10587829	Plod2	procollagen lysine, 2-oxoglutarate 5-dioxygenase 2	1.42	0.000
10398665	**Tnfaip2**	**tumor necrosis factor, alpha-induced protein 2**	**1.42**	**0.000**
10475890	Mertk	c-mer proto-oncogene tyrosine kinase	1.42	0.000
10523128	Ppbp	pro-platelet basic protein	1.42	0.000
10484371	Calcrl	calcitonin receptor-like	1.42	0.000
10399540	Pqlc3	PQ loop repeat containing	1.42	0.001
10436304	**Abi3bp**	**ABI gene family, member 3 (NESH) binding protein**	**1.42**	**0.002**
10445268	Gpr116	G protein-coupled receptor 116	1.42	0.000
10505143	Akap2	A kinase (PRKA) anchor protein 2	1.42	0.000
10461622	Ms4a6b	membrane-spanning 4-domains, subfamily A, member 6B	1.41	0.016
10458303	**Ecscr**	**endothelial cell-specific chemotaxis regulator**	**1.41**	**0.000**
10427744	Rai14	retinoic acid induced 14	1.41	0.000
10496872	Eltd1	EGF, latrophilin seven transmembrane domain containing 1	1.41	0.000
10346843	Nrp2	neuropilin 2	1.41	0.000
10360040	Fcgr3	Fc receptor, IgG, low affinity III	1.41	0.000
10555510	Pde2a	phosphodiesterase 2A, cGMP-stimulated	1.41	0.001
10547657	C3ar1	complement component 3a receptor 1	1.41	0.000
10487613	Pdyn	prodynorphin	1.41	0.035
10398907	Pld4	phospholipase D family, member 4	1.41	0.001
10437885	Myh11	myosin, heavy polypeptide 11, smooth muscle	1.41	0.000
10587383	Cd109	CD109 antigen	1.41	0.000
10561212	**Ltbp4**	**latent transforming growth factor beta binding protein 4**	**1.41**	**0.000**
10536499	Cav1	caveolin 1, caveolae protein	1.41	0.000
10585588	**Cspg4**	**chondroitin sulfate proteoglycan 4**	**1.41**	**0.000**
10537146	Akr1b8	aldo-keto reductase family 1, member B8	1.41	0.001
10372807	Msrb3	methionine sulfoxide reductase B3	1.41	0.000
10582303	Cyba	cytochrome b-245, alpha polypeptide	1.41	0.000
10504188	Ccl19	chemokine (C-C motif) ligand 19	1.40	0.004
10395103	**Pxdn**	**peroxidasin homolog (Drosophila)**	**1.40**	**0.000**
10379615	Slfn5	schlafen 5	1.40	0.000
10491721	Spry1	sprouty homolog 1 (Drosophila)	1.40	0.000
10461629	Ms4a4d	membrane-spanning 4-domains, subfamily A, member 4D	1.40	0.007
10492689	Pdgfc	platelet-derived growth factor, C polypeptide	1.40	0.000
10424543	Wisp1	WNT1 inducible signaling pathway protein 1	1.40	0.001
10405179	S1pr3	sphingosine-1-phosphate receptor 3	1.40	0.000
10405033	**Ecm2**	**extracellular matrix protein 2, female organ and adipocyte specific**	**1.40**	**0.001**
10544583	Gimap6	GTPase, IMAP family member 6	1.40	0.000
10554599	Adamtsl3	ADAMTS-like 3	1.40	0.000
10563077	Rcn3	reticulocalbin 3, EF-hand calcium binding domain	1.40	0.003

10452633	Tgif1	TGFB-induced factor homeobox 1	1.40	0.001
10350630	Fam129a	family with sequence similarity 129, member A	1.40	0.001
10530841	Igfbp7	insulin-like growth factor binding protein 7	1.39	0.000
10570855	Plat	plasminogen activator, tissue	1.39	0.000
10473880	Lrp4	low density lipoprotein receptor-related protein 4	1.39	0.000
10580033	Cd97	CD97 antigen	1.39	0.000
10354374	Slc40a1	solute carrier family 40 (iron-regulated transporter), member 1	1.39	0.002
10582337	Fam38a	family with sequence similarity 38, member A	1.39	0.000
10355500	Igfbp5	insulin-like growth factor binding protein 5	1.39	0.003
10507840	**Heyl**	**hairy/enhancer-of-split related with YRPW motif-like**	**1.39**	**0.000**
10487645	Cpxm1	carboxypeptidase X 1 (M14 family)	1.39	0.001
10351509	Fcgr4	Fc receptor, IgG, low affinity IV	1.39	0.002
10422164	Ednrb	endothelin receptor type B	1.39	0.000
10501063	Cd53	CD53 antigen	1.39	0.004
10509163	Id3	inhibitor of DNA binding 3	1.38	0.001
10583044	**Mmp13**	**matrix metallopeptidase 13**	**1.38**	**0.003**
10503098	Lyn	Yamaguchi sarcoma viral (v-yes-1) oncogene homolog	1.38	0.000
10367673	Plekhg1	pleckstrin homology domain containing, family G (with RhoGef domain) membe	1.38	0.000
10567580	Igsf6	immunoglobulin superfamily, member 6	1.38	0.000
10420488	D14Ertd668e	DNA segment, Chr 14, ERATO Doi 668, expressed	1.38	0.000
10584142	Ets1	E26 avian leukemia oncogene 1, 5' domain	1.38	0.000
10429568	Ly6c1	lymphocyte antigen 6 complex, locus C1	1.38	0.000
10540472	Bhlhe40	basic helix-loop-helix family, member e40	1.38	0.003
10358408	Rgs1	regulator of G-protein signaling 1	1.38	0.003
10528207	Cd36	CD36 antigen	1.38	0.012
10471721	Ptgs1	prostaglandin-endoperoxide synthase 1	1.38	0.001
10496324	Slc39a8	solute carrier family 39 (metal ion transporter), member 8	1.38	0.030
10355514	Tns1	tensin 1	1.38	0.000
10398319	Dlk1	delta-like 1 homolog (Drosophila)	1.38	0.008
10548829	Gucy2c	guanylate cyclase 2c	1.37	0.003
10458843	Sema6a	sema domain, transmembrane domain (TM), and cytoplasmic domain, (semap	1.37	0.000
10347948	Sp100	nuclear antigen Sp100	1.37	0.001
10563085	Fcgrt	Fc receptor, IgG, alpha chain transporter	1.37	0.000
10538126	Gimap4	GTPase, IMAP family member 4	1.37	0.000
10527441	Arpc1b	actin related protein 2/3 complex, subunit 1B	1.37	0.001
10451710	Rftn1	raftlin lipid raft linker 1	1.37	0.000
10410547	Nkd2	naked cuticle 2 homolog (Drosophila)	1.37	0.000
10548375	Clec7a	C-type lectin domain family 7, member a	1.37	0.003
10393559	**Timp2**	**tissue inhibitor of metalloproteinase 2**	**1.37**	**0.000**
10553301	Ldha	lactate dehydrogenase A	1.37	0.001
10564713	**Mfge8**	**milk fat globule-EGF factor 8 protein**	**1.37**	**0.001**
10416437	Lcp1	lymphocyte cytosolic protein 1	1.37	0.001
10494262	Ctsk	cathepsin K	1.37	0.012
10363173	Gja1	gap junction protein, alpha 1	1.37	0.000
10453057	Cyp1b1	cytochrome P450, family 1, subfamily b, polypeptide 1	1.36	0.006
10543239	Tcfec	transcription factor EC	1.36	0.000
10549108	Abcc9	ATP-binding cassette, sub-family C (CFTR/MRP), member 9	1.36	0.000
10517165	Cd52	CD52 antigen	1.36	0.009
10603551	Cybb	cytochrome b-245, beta polypeptide	1.36	0.000
10489204	**Tgm2**	**transglutaminase 2, C polypeptide**	**1.36**	**0.005**
10369388	Unc5b	unc-5 homolog B (C. elegans)	1.36	0.000
10550332	Slc1a5	solute carrier family 1 (neutral amino acid transporter), member 5	1.36	0.000
10344897	Sulf1	sulfatase 1	1.36	0.000
10498273	Tm4sf1	transmembrane 4 superfamily member 1	1.36	0.000
10458999	**Fbn2**	**fibrillin 2**	**1.36**	**0.000**
10435961	Gm10808	predicted gene 10808	1.36	0.000
10607870	Tlr7	toll-like receptor 7	1.36	0.000
10591739	Acp5	acid phosphatase 5, tartrate resistant	1.36	0.001
10435565	Hcls1	hematopoietic cell specific Lyn substrate 1	1.36	0.000
10539517	Dysf	dysferlin	1.36	0.000
10458183	Gfra3	glial cell line derived neurotrophic factor family receptor alpha 3	1.36	0.008
10547752	Gm5077	predicted gene 5077	1.36	0.000
10396402	Prkch	protein kinase C, eta	1.35	0.000
10601385	Tlr13	toll-like receptor 13	1.35	0.000
10520950	Pdlim1	PDZ and LIM domain 1 (elfin)	1.35	0.000
10512470	Cd72	CD72 antigen	1.35	0.004
10473809	Sfpi1	SFFV proviral integration 1	1.35	0.000
10455961	Iigp1	interferon inducible GTPase 1	1.35	0.000
10597518	Tgfbr2	transforming growth factor, beta receptor II	1.35	0.000
10378334	Tax1bp3	Tax1 (human T-cell leukemia virus type I) binding protein 3	1.35	0.002
10461721	Mpeg1	macrophage expressed gene 1	1.35	0.001
10566543	Dchs1	dachsous 1 (Drosophila)	1.35	0.000
10460541	Cd248	CD248 antigen, endosialin	1.35	0.000
10548118	Prmt8	protein arginine N-methyltransferase 8	1.35	0.015
10429564	Ly6a	lymphocyte antigen 6 complex, locus A	1.35	0.004
10472440	Tax1bp3	Tax1 (human T-cell leukemia virus type I) binding protein 3	1.35	0.002
10560709	Pvr	poliovirus receptor	1.35	0.002
10500276	BC028528	cDNA sequence BC028528	1.35	0.005
10441093	Erg	avian erythroblastosis virus E-26 (v-ets) oncogene related	1.35	0.000
10347928	Sp110	Sp110 nuclear body protein	1.35	0.001
10582874	Sp110	Sp110 nuclear body protein	1.35	0.001

10588263	Slco2a1	solute carrier organic anion transporter family, member 2a1	1.35	0.000
10606609	Tspan6	tetraspanin 6	1.35	0.014
10538187	Gpnmb	glycoprotein (transmembrane) nmb	1.35	0.002
10548817	Plbd1	phospholipase B domain containing 1	1.35	0.004
10552824	Rras	Harvey rat sarcoma oncogene, subgroup R	1.35	0.000
10607738	Car5b	carbonic anhydrase 5b, mitochondrial	1.35	0.003
10541683	C1rb	complement component 1, r subcomponent B	1.35	0.011
10406928	Cd180	CD180 antigen	1.35	0.005
10355534	Tns1	tensin 1	1.35	0.000
10427471	Osmr	oncostatin M receptor	1.34	0.001
10370766	Gamt	guanidinoacetate methyltransferase	1.34	0.001
10502655	**Cyr61**	**cysteine rich protein 61**	**1.34**	**0.001**
10604763	Arpc1b	actin related protein 2/3 complex, subunit 1B	1.34	0.001
10517967	Fblim1	filamin binding LIM protein 1	1.34	0.000
10392522	Abca8a	ATP-binding cassette, sub-family A (ABC1), member 8a	1.34	0.002
10375145	Lcp2	lymphocyte cytosolic protein 2	1.34	0.000
10505120	Palm2	paralemmin 2	1.34	0.000
10497265	Fabp4	fatty acid binding protein 4, adipocyte	1.34	0.003
10603099	**Figf**	**c-fos induced growth factor**	**1.34**	**0.000**
10449775	**Notch3**	**Notch gene homolog 3 (Drosophila)**	**1.34**	**0.000**
10391332	Ptrf	polymerase I and transcript release factor	1.34	0.000
10406434	**Mef2c**	**myocyte enhancer factor 2C**	**1.34**	**0.000**
10586477	Ppib	peptidylprolyl isomerase B	1.34	0.009
10461423	Fads3	fatty acid desaturase 3	1.34	0.000
10571142	Gpr124	G protein-coupled receptor 124	1.34	0.000
10554808	Fzd4	frizzled homolog 4 (Drosophila)	1.34	0.001
10588942	**Lamb2**	**laminin, beta 2**	**1.33**	**0.000**
10358577	Hmcn1	hemicentin 1	1.33	0.021
10379190	**Vtn**	**vitronectin**	**1.33**	**0.002**
10358633	Hmcn1	hemicentin 1	1.33	0.000
10407211	Ppap2a	phosphatidic acid phosphatase type 2A	1.33	0.005
10494271	Ctss	cathepsin S	1.33	0.000
10429295	Kcnk9	potassium channel, subfamily K, member 9	1.33	0.011
10365482	**Timp3**	**tissue inhibitor of metalloproteinase 3**	**1.33**	**0.001**
10536216	Gng11	guanine nucleotide binding protein (G protein), gamma 11	1.33	0.000
10447649	Fndc1	fibronectin type III domain containing 1	1.33	0.002
10597743	**Cx3cr1**	**chemokine (C-X3-C) receptor 1**	**1.33**	**0.001**
10583021	Pdgfd	platelet-derived growth factor, D polypeptide	1.33	0.000
10362073	Sgk1	serum/glucocorticoid regulated kinase 1	1.33	0.001
10461558	Slc15a3	solute carrier family 15, member 3	1.33	0.000
10344837	Prex2	phosphatidylinositol-3,4,5-trisphosphate-dependent Rac exchange factor 2	1.33	0.000
10576051	**Foxc2**	**forkhead box C2**	**1.32**	**0.000**
10578241	Dlc1	deleted in liver cancer 1	1.32	0.000
10416700	Pcdh17	protocadherin 17	1.32	0.002
10490212	**Ctsz**	**cathepsin Z**	**1.32**	**0.000**
10420413	Lats2	large tumor suppressor 2	1.32	0.000
10415885	Sox7	SRY-box containing gene 7	1.32	0.000
10370510	Syde1	synapse defective 1, Rho GTPase, homolog 1 (C. elegans)	1.32	0.000
10504132	Ccl19	chemokine (C-C motif) ligand 19	1.32	0.007
10521667	Bst1	bone marrow stromal cell antigen 1	1.32	0.001
10594661	Tpm1	tropomyosin 1, alpha	1.32	0.000
10387536	Cd68	CD68 antigen	1.32	0.000
10484503	Lrrc55	leucine rich repeat containing 55	1.32	0.000
10472050	Tnfaip6	tumor necrosis factor alpha induced protein 6	1.32	0.002
10375402	Adam19	a disintegrin and metallopeptidase domain 19 (meltrin beta)	1.32	0.000
10422760	Fyb	FYN binding protein	1.32	0.002
10568553	Chst15	carbohydrate (N-acetylgalactosamine 4-sulfate 6-O) sulfotransferase 15	1.31	0.000
10510700	Gpr153	G protein-coupled receptor 153	1.31	0.000
10358533	Hmcn1	hemicentin 1	1.31	0.025
10575976	**Crispld2**	**cysteine-rich secretory protein LCCL domain containing 2**	**1.31**	**0.000**
10474671	Spred1	sprouty protein with EVH-1 domain 1, related sequence	1.31	0.000
10402268	Lgmn	legumain	1.31	0.000
10587616	Prss35	protease, serine, 35	1.31	0.010
10416974	**Gpc6**	**glypican 6**	**1.31**	**0.000**
10461979	Aldh1a1	aldehyde dehydrogenase family 1, subfamily A1	1.31	0.006
10523766	Lrrc8c	leucine rich repeat containing 8 family, member C	1.31	0.001
10425092	Cyth4	cytohesin 4	1.31	0.002
10566574	Gvin1	GTPase, very large interferon inducible 1	1.31	0.002
10546432	**Adamts9**	**a disintegrin-like and metallopeptidase (reprolysin type) with thrombospc**	**1.31**	**0.001**
10505132	Akap2	A kinase (PRKA) anchor protein 2	1.31	0.000
10499168	Kirrel	kin of IRRE like (Drosophila)	1.31	0.000
10562709	Cd33	CD33 antigen	1.31	0.000
10531286	Vdac2	voltage-dependent anion channel 2	1.30	0.004
10375515	Ifi47	interferon gamma inducible protein 47	1.30	0.003
10489569	Pltp	phospholipid transfer protein	1.30	0.001
10351679	Cd84	CD84 antigen	1.30	0.008
10526566	Ephb4	Eph receptor B4	1.30	0.000
10394593	Fam49a	family with sequence similarity 49, member A	1.30	0.002
10357472	Cxcr4	chemokine (C-X-C motif) receptor 4	1.30	0.000
10368647	Dse	dermatan sulfate epimerase	1.30	0.000
10435345	Mylk	myosin, light polypeptide kinase	1.30	0.000

10407126	Plk2	polo-like kinase 2 (Drosophila)	1.30	0.001
10372652	Lyz1	lysozyme 1	1.30	0.003
10469695	Apbb1ip	amyloid beta (A4) precursor protein-binding, family B, member 1 interacting pr	1.30	0.000
10515771	**Tie1**	**tyrosine kinase with immunoglobulin-like and EGF-like domains 1**	**1.30**	**0.000**
10569335	H19	H19 fetal liver mRNA	1.30	0.002
10425116	Cdc42ep1	CDC42 effector protein (Rho GTPase binding) 1	1.30	0.000
10541910	**Vwf**	**Von Willebrand factor homolog**	**1.30**	**0.009**
10555235	Arrb1	arrestin, beta 1	1.29	0.000
10362596	Fyn	Fyn proto-oncogene	1.29	0.000
10379389	Adap2	ArfGAP with dual PH domains 2	1.29	0.000
10607868	Tlr8	toll-like receptor 8	1.29	0.000
10560624	Apoe	apolipoprotein E	1.29	0.005
10564377	Lrrk1	leucine-rich repeat kinase 1	1.29	0.000
10575844	Cdh13	cadherin 13	1.29	0.000
10484201	Ccdc141	coiled-coil domain containing 141	1.29	0.001
10514049	Nfib	nuclear factor I/B	1.29	0.000
10352143	Kif26b	kinesin family member 26B	1.29	0.000
10600901	Ar	androgen receptor	1.29	0.001
10582378	Fam38a	family with sequence similarity 38, member A	1.29	0.000
10541564	Clec4a3	C-type lectin domain family 4, member a3	1.29	0.004
10412667	Ptprg	protein tyrosine phosphatase, receptor type, G	1.29	0.000
10439312	Cd86	CD86 antigen	1.29	0.007
10366052	Kitl	kit ligand	1.29	0.003
10522712	Rest	RE1-silencing transcription factor	1.29	0.000
10383756	Ifitm2	interferon induced transmembrane protein 2	1.29	0.000
10514275	Ptplad2	protein tyrosine phosphatase-like A domain containing 2	1.29	0.000
10496592	Gbp2	guanylate binding protein 2	1.29	0.023
10414333	Samd4	sterile alpha motif domain containing 4	1.29	0.001
10569014	Ifitm2	interferon induced transmembrane protein 2	1.29	0.000
10493798	S100a16	S100 calcium binding protein A16	1.29	0.000
10604375	Apln	apelin	1.29	0.000
10461594	Ms4a4c	membrane-spanning 4-domains, subfamily A, member 4C	1.29	0.024
10539135	Capg	capping protein (actin filament), gelsolin-like	1.28	0.000
10394978	Rrm2	ribonucleotide reductase M2	1.28	0.017
10391762	Gjc1	gap junction protein, gamma 1	1.28	0.001
10381588	Grn	granulin	1.28	0.000
10605437	Pls3	plastin 3 (T-isoform)	1.28	0.001
10596148	Trf	transferrin	1.28	0.047
10546450	**Adamts9**	**a disintegrin-like and metallopeptidase (reprolysin type) with thrombospc**	**1.28**	**0.009**
10397633	Flrt2	fibronectin leucine rich transmembrane protein 2	1.28	0.001
10542319	Apold1	apolipoprotein L domain containing 1	1.28	0.001
10603583	Srpx	sushi-repeat-containing protein	1.28	0.000
10606600	Pcdh19	protocadherin 19	1.28	0.000
10502772	Lphn2	latrophilin 2	1.28	0.045
10500204	**Ecm1**	**extracellular matrix protein 1**	**1.28**	**0.002**
10418702	Sh3bp5	SH3-domain binding protein 5 (BTK-associated)	1.28	0.001
10487447	Mall	mal, T-cell differentiation protein-like	1.28	0.002
10397645	Gpr65	G-protein coupled receptor 65	1.28	0.003
10360344	Darc	Duffy blood group, chemokine receptor	1.28	0.004
10556297	Adm	adrenomedullin	1.28	0.006
10543959	**Ptn**	**pleiotrophin**	**1.28**	**0.004**
10582862	Arhgef12	Rho guanine nucleotide exchange factor (GEF) 12	1.28	0.016
10563441	Emp3	epithelial membrane protein 3	1.28	0.000
10557960	Tgfb1i1	transforming growth factor beta 1 induced transcript 1	1.28	0.000
10578623	Wwc2	WW, C2 and coiled-coil domain containing 2	1.28	0.000
10471882	**Olfml2a**	**olfactomedin-like 2A**	**1.28**	**0.000**
10387890	Cxcl16	chemokine (C-X-C motif) ligand 16	1.28	0.000
10385504	Gm5431	predicted gene 5431	1.28	0.025
10403871	Aoah	acyloxyacyl hydrolase	1.28	0.000
10601519	Klhl4	kelch-like 4 (Drosophila)	1.28	0.000
10579347	Ifi30	interferon gamma inducible protein 30	1.28	0.000
10439442	Pla1a	phospholipase A1 member A	1.28	0.000
10380067	Septin4	septin 4	1.27	0.002
10455954	Gm4951	predicted gene 4951 // predicted gene 4951	1.27	0.004
10457071	Cyb5	cytochrome b-5	1.27	0.003
10425945	**Fbln1**	**fibulin 1**	**1.27**	**0.011**
10389894	Abcc3	ATP-binding cassette, sub-family C (CFTR/MRP), member 3	1.27	0.000
10501734	Palmd	palmdelphin	1.27	0.003
10597531	Rbms3	RNA binding motif, single stranded interacting protein	1.27	0.001
10419261	**Bmp4**	**bone morphogenetic protein 4**	**1.27**	**0.002**
10521972	Pcdh7	protocadherin 7	1.27	0.000
10568436	**Fgfr2**	**fibroblast growth factor receptor 2**	**1.27**	**0.001**
10470562	Gm10134	predicted gene 10134	1.27	0.002
10557895	Itgax	integrin alpha X	1.27	0.004
10606369	Itm2a	integral membrane protein 2A	1.27	0.011
10510129	Dhrs3	dehydrogenase/reductase (SDR family) member 3	1.27	0.014
10546434	**Adamts9**	**a disintegrin-like and metallopeptidase (reprolysin type) with thrombospc**	**1.27**	**0.001**
10462442	Il33	interleukin 33	1.27	0.008
10542953	Tfpi2	tissue factor pathway inhibitor 2	1.27	0.000
10467578	Pik3ap1	phosphoinositide-3-kinase adaptor protein 1	1.27	0.000
10346960	Ccnyl1	cyclin Y-like 1	1.27	0.020

10534935	Pilrb1	paired immunoglobin-like type 2 receptor beta 1	1.27	0.002
10469151	Itih5	inter-alpha (globulin) inhibitor H5	1.27	0.043
10408928	Hspb1	heat shock protein 1	1.27	0.027
10409876	Ctla2a	cytotoxic T lymphocyte-associated protein 2 alpha	1.27	0.013
10553299	Ifitm2	interferon induced transmembrane protein 2	1.27	0.000
10558961	Tspan4	tetraspanin 4	1.27	0.001
10477717	Procr	protein C receptor, endothelial	1.27	0.000
10514221	Plin2	perilipin 2	1.27	0.000
10355530	Tns1	tensin 1	1.27	0.002
10564527	Nr2f2	nuclear receptor subfamily 2, group F, member 2	1.27	0.001
10522208	Uchl1	ubiquitin carboxy-terminal hydrolase L1	1.27	0.008
10413047	**Plau**	**plasminogen activator, urokinase**	**1.27**	**0.003**
10429573	Ly6c2	lymphocyte antigen 6 complex, locus C2	1.27	0.002
10496359	Emcn	endomucin	1.27	0.000
10356262	Csprs	component of Sp100-rs	1.27	0.004
10500666	Ptgfrn	prostaglandin F2 receptor negative regulator	1.27	0.001
10467136	Ch25h	cholesterol 25-hydroxylase	1.27	0.003
10350146	Phlda3	pleckstrin homology-like domain, family A, member 3	1.27	0.000
10558345	Dock1	dedicator of cytokinesis 1	1.27	0.000
10466127	AW112010	expressed sequence AW112010	1.26	0.016
10578222	Dlc1	deleted in liver cancer 1	1.26	0.000
10392825	Gm11711	predicted gene 11711	1.26	0.000
10508770	Gm13033	prostaglandin-endoperoxide synthase 2 pseudogene	1.26	0.007
10584317	Esam	endothelial cell-specific adhesion molecule	1.26	0.000
10408850	Nedd9	neural precursor cell expressed, developmentally down-regulated gene 9	1.26	0.001
10498952	Gucy1a3	guanylate cyclase 1, soluble, alpha 3	1.26	0.001
10545101	Hpgds	hematopoietic prostaglandin D synthase	1.26	0.000
10473384	Slc43a3	solute carrier family 43, member 3	1.26	0.039
10372410	Glipr1	GLI pathogenesis-related 1 (glioma)	1.26	0.002
10502774	Lphn2	latrophilin 2	1.26	0.001
10526410	Hspb1	heat shock protein 1	1.26	0.032
10400510	Clec14a	C-type lectin domain family 14, member a	1.26	0.000
10518408	Plod1	procollagen-lysine, 2-oxoglutarate 5-dioxygenase 1	1.26	0.000
10366043	Dusp6	dual specificity phosphatase 6	1.26	0.001
10367982	Gpr126	G protein-coupled receptor 126	1.26	0.008
10499189	Fcrls	Fc receptor-like S, scavenger receptor	1.26	0.002
10437687	Litaf	LPS-induced TN factor	1.26	0.002
10353844	Neurl3	neuralized homolog 3 homolog (Drosophila)	1.26	0.000
10399005	Crip1	cysteine-rich protein 1 (intestinal)	1.26	0.003
10345777	Il1rl2	interleukin 1 receptor-like 2	1.26	0.002
10457587	Zfp521	zinc finger protein 521	1.26	0.000
10514177	Bnc2	basonuclin 2	1.26	0.002
10375065	Sh3pxd2b	SH3 and PX domains 2B	1.26	0.001
10452815	Xdh	xanthine dehydrogenase	1.26	0.014
10384223	Igfbp3	insulin-like growth factor binding protein 3	1.26	0.005
10558769	Ifitm1	interferon induced transmembrane protein 1	1.26	0.000
10392834	Gm11711	predicted gene 11711	1.26	0.000
10560242	C5ar1	complement component 5a receptor 1	1.26	0.000
10585778	Sema7a	sema domain, immunoglobulin domain (Ig), and GPI membrane anchor, (sema	1.26	0.001
10517169	Sh3bgrl3	SH3 domain binding glutamic acid-rich protein-like 3	1.26	0.001
10414360	**Lgals3**	**lectin, galactose binding, soluble 3**	**1.25**	**0.000**
10374197	Ramp3	receptor (calcitonin) activity modifying protein 3	1.25	0.001
10536472	Mdfic	MyoD family inhibitor domain containing	1.25	0.000
10450325	Cfb	complement factor B	1.25	0.003
10447317	**Epas1**	**endothelial PAS domain protein 1**	**1.25**	**0.002**
10543791	Podxl	podocalyxin-like	1.25	0.000
10464529	Tcirg1	T-cell, immune regulator 1, ATPase, H+ transporting, lysosomal V0 protein A3	1.25	0.000
10436456	Pros1	protein S (alpha)	1.25	0.001
10420891	Scara3	scavenger receptor class A, member 3	1.25	0.000
10427336	Nckap1l	NCK associated protein 1 like	1.25	0.006
10568568	Oat	ornithine aminotransferase	1.25	0.008
10472820	Itga6	integrin alpha 6	1.25	0.002
10484389	Tfpi	tissue factor pathway inhibitor	1.25	0.007
10482059	Ggta1	glycoprotein galactosyltransferase alpha 1, 3	1.25	0.002
10382106	Gm885	predicted gene 885	1.25	0.003
10498367	P2ry13	purinergic receptor P2Y, G-protein coupled 13	1.25	0.001
10452485	Rab31	RAB31, member RAS oncogene family	1.25	0.000
10526743	Cops6	COP9 (constitutive photomorphogenic) homolog, subunit 6 (Arabidopsis thaliar	1.25	0.020
10446986	Crim1	cysteine rich transmembrane BMP regulator 1 (chordin like)	1.25	0.001
10582997	Casp4	caspase 4, apoptosis-related cysteine peptidase	1.25	0.002
10395409	**Meox2**	**mesenchyme homeobox 2**	**1.25**	**0.001**
10569618	Ano1	anoctamin 1, calcium activated chloride channel	1.25	0.002
10369615	Srgn	serglycin	1.25	0.017
10573747	Adcy7	adenylate cyclase 7	1.24	0.001
10498935	Gucy1b3	guanylate cyclase 1, soluble, beta 3	1.24	0.001
10467508	Blnk	B-cell linker	1.24	0.002
10526783	BC055004	cDNA sequence BC055004	1.24	0.002
10416181	Stc1	stanniocalcin 1	1.24	0.010
10592251	Pknox2	Pbx/knotted 1 homeobox 2	1.24	0.004
10369932	Susd2	sushi domain containing 2	1.24	0.001
10546454	**Adamts9**	**a disintegrin-like and metallopeptidase (reprolysin type) with thrombospc**	**1.24**	**0.014**

10516735	Tinagl1	tubulointerstitial nephritis antigen-like 1	1.24	0.001
10473125	Itga4	integrin alpha 4	1.24	0.001
10566583	Gm8995	predicted gene 8995	1.24	0.002
10594540	Plekho2	pleckstrin homology domain containing, family O member 2	1.24	0.000
10583586	Slc44a2	solute carrier family 44, member 2	1.24	0.000
10561431	Plekhg2	pleckstrin homology domain containing, family G (with RhoGef domain) membe	1.24	0.000
10593198	Fam55b	family with sequence similarity 55, member B	1.24	0.002
10362091	Raet1d	retinoic acid early transcript delta	1.24	0.007
10391504	Meox1	mesenchyme homeobox 1	1.24	0.001
10592067	Fli1	Friend leukemia integration 1	1.24	0.002
10506031	Nfia	nuclear factor I/A	1.24	0.001
10351477	Sh2d1b1	SH2 domain protein 1B1	1.24	0.025
10593219	Nnmt	nicotinamide N-methyltransferase	1.24	0.004
10375578	Flt4	FMS-like tyrosine kinase 4	1.24	0.001
10348244	Inpp5d	inositol polyphosphate-5-phosphatase D	1.24	0.003
10484463	Serping1	serine (or cysteine) peptidase inhibitor, clade G, member 1	1.24	0.000
10586079	Itga11	integrin alpha 11	1.24	0.000
10570434	Ifitm1	interferon induced transmembrane protein 1	1.24	0.002
10495054	Rhoc	ras homolog gene family, member C	1.24	0.005
10458555	Spry4	sprouty homolog 4 (Drosophila)	1.24	0.000
10506488	**Ppap2b**	**phosphatidic acid phosphatase type 2B**	**1.24**	**0.000**
10456513	Mc5r	melanocortin 5 receptor	1.24	0.039
10482030	Stom	stomatin	1.24	0.001
10368556	**Hey2**	**hairy/enhancer-of-split related with YRPW motif 2**	**1.24**	**0.011**
10416371	Lpar6	lysophosphatidic acid receptor 6	1.24	0.000
10409464	Dbn1	drebrin 1	1.24	0.000
10505517	Tlr4	toll-like receptor 4	1.24	0.000
10451953	Lrg1	leucine-rich alpha-2-glycoprotein 1	1.24	0.000
10578264	Msr1	macrophage scavenger receptor 1	1.24	0.000
10491699	**Fgf2**	**fibroblast growth factor 2**	**1.24**	**0.000**
10594840	Gcom1	GRINL1A complex locus	1.24	0.000
10348451	Cxcr7	chemokine (C-X-C motif) receptor 7	1.24	0.006
10494595	**Notch2**	**Notch gene homolog 2 (Drosophila)**	**1.24**	**0.009**
10499216	Pear1	platelet endothelial aggregation receptor 1	1.23	0.000
10402347	Ifi27l2a	interferon, alpha-inducible protein 27 like 2A	1.23	0.003
10595718	Chst2	carbohydrate sulfotransferase 2	1.23	0.000
10460603	**Efemp2**	**epidermal growth factor-containing fibulin-like extracellular matrix protei**	**1.23**	**0.001**
10499639	Cks1b	CDC28 protein kinase 1b	1.23	0.002
10470283	**Egfl7**	**EGF-like domain 7**	**1.23**	**0.003**
10581992	Maf	avian musculoaponeurotic fibrosarcoma (v-maf) AS42 oncogene homolog	1.23	0.005
10424676	Ly6e	lymphocyte antigen 6 complex, locus E	1.23	0.000
10376513	Nlrp3	NLR family, pyrin domain containing 3	1.23	0.004
10602372	Alas2	aminolevulinic acid synthase 2, erythroid	1.23	0.002
10520521	Cenpa	centromere protein A	1.23	0.007
10481845	Fam125b	family with sequence similarity 125, member B	1.23	0.001
10385770	Olfr1372-ps1	olfactory receptor 1372, pseudogene 1	1.23	0.001
10485070	Mdk	midkine	1.23	0.001
10351491	**Olfml2b**	**olfactomedin-like 2B**	**1.23**	**0.047**
10506050	Nfia	nuclear factor I/A	1.23	0.009
10430968	A4galt	alpha 1,4-galactosyltransferase	1.23	0.001
10438753	Leprel1	leprecan-like 1	1.23	0.040
10432439	Fmnl3	formin-like 3	1.23	0.000
10432640	Bin2	bridging integrator 2	1.23	0.001
10495416	**Vav3**	**vav 3 oncogene**	**1.23**	**0.000**
10593050	Il10ra	interleukin 10 receptor, alpha	1.23	0.000
10576235	Dpep1	dipeptidase 1 (renal)	1.23	0.049
10490838	Fabp5	fatty acid binding protein 5, epidermal	1.23	0.000
10565962	P2ry2	purinergic receptor P2Y, G-protein coupled 2	1.23	0.001
10392815	AF251705	cDNA sequence AF251705	1.23	0.002
10541587	Clec4a2	C-type lectin domain family 4, member a2	1.23	0.000
10436048	Prdx1	peroxiredoxin 1	1.23	0.003
10568536	Cpxm2	carboxypeptidase X 2 (M14 family)	1.23	0.014
10465132	Sipa1	signal-induced proliferation associated gene 1	1.23	0.001
10573583	Man2b1	mannosidase 2, alpha B1	1.23	0.001
10554574	Tm6sf1	transmembrane 6 superfamily member 1	1.23	0.000
10517517	C1qa	complement component 1, q subcomponent, alpha polypeptide	1.23	0.002
10576639	**Nrp1**	**neuropilin 1**	**1.23**	**0.000**
10399691	Id2	inhibitor of DNA binding 2	1.23	0.022
10531724	Plac8	placenta-specific 8	1.23	0.035
10438708	Masp1	mannan-binding lectin serine peptidase 1	1.23	0.003
10456005	Cd74	CD74 antigen (invariant polypeptide of major histocompatibility complex, class	1.23	0.034
10579925	Gab1	growth factor receptor bound protein 2-associated protein 1	1.23	0.001
10585699	Fabp5	fatty acid binding protein 5, epidermal	1.23	0.000
10580191	Nfix	nuclear factor I/X	1.23	0.002
10487506	Gm14005	predicted gene 14005	1.23	0.023
10436369	Filip1l	filamin A interacting protein 1-like	1.23	0.000
10465005	Banf1	barrier to autointegration factor 1	1.23	0.003
10358224	Ptprc	protein tyrosine phosphatase, receptor type, C	1.22	0.035
10519324	Cdk6	cyclin-dependent kinase 6	1.22	0.001
10351658	Cd48	CD48 antigen	1.22	0.002
10429128	Sla	src-like adaptor	1.22	0.008

10523175	**Ereg**	**epiregulin**	**1.22**	**0.001**
10525419	P2rx7	purinergic receptor P2X, ligand-gated ion channel, 7	1.22	0.000
10402783	Ahnak2	AHNAK nucleoprotein 2	1.22	0.001
10347933	Sp140	Sp140 nuclear body protein	1.22	0.042
10583669	AB124611	cDNA sequence AB124611	1.22	0.001
10383025	C1qtnf1	C1q and tumor necrosis factor related protein 1	1.22	0.005
10583056	**Mmp12**	**matrix metallopeptidase 12**	**1.22**	**0.046**
10366293	Csrp2	cysteine and glycine-rich protein 2	1.22	0.000
10515744	Cdc20	cell division cycle 20 homolog (S. cerevisiae)	1.22	0.022
10541555	Clec4a1	C-type lectin domain family 4, member a1	1.22	0.007
10485711	Fibin	fin bud initiation factor homolog (zebrafish)	1.22	0.010
10355214	Idh1	isocitrate dehydrogenase 1 (NADP+), soluble	1.22	0.024
10388532	Nxn	nucleoredoxin	1.22	0.013
10379524	**Ccl11**	**chemokine (C-C motif) ligand 11**	**1.22**	**0.019**
10392808	Cd300ld	CD300 molecule-like family member d	1.22	0.010
10527638	Alox5ap	arachidonate 5-lipoxygenase activating protein	1.22	0.035
10590909	Endod1	endonuclease domain containing 1	1.22	0.002
10375614	Gfpt2	glutamine fructose-6-phosphate transaminase 2	1.22	0.011
10593449	Layn	layilin	1.22	0.000
10344981	Pi15	peptidase inhibitor 15	1.22	0.008
10567299	Itpripl2	inositol 1,4,5-triphosphate receptor interacting protein-like 2	1.22	0.001
10497689	Gnb4	guanine nucleotide binding protein (G protein), beta 4	1.21	0.003
10599562	Arhgap36	Rho GTPase activating protein 36	1.21	0.021
10580782	Dok4	docking protein 4	1.21	0.001
10383731	Smtn	smoothelin	1.21	0.001
10566578	Gm8979	very large inducible GTPase 1 pseudogene	1.21	0.005
10508465	Marcksl1	MARCKS-like 1	1.21	0.003
10355115	Prelid1	PRELI domain containing 1	1.21	0.031
10469936	Nrarp	Notch-regulated ankyrin repeat protein	1.21	0.001
10582985	Casp1	caspase 1	1.21	0.007
10531952	Abcg3	ATP-binding cassette, sub-family G (WHITE), member 3	1.21	0.000
10423654	Osr2	odd-skipped related 2 (Drosophila)	1.21	0.008
10521616	C1qtnf7	C1q and tumor necrosis factor related protein 7	1.21	0.001
10566585	Gm1966	predicted gene 1966	1.21	0.009
10525016	**Tbx3**	**T-box 3**	**1.21**	**0.001**
10403727	**Gli3**	**GLI-Kruppel family member GLI3**	**1.21**	**0.000**
10394558	Rpl29	ribosomal protein L29	1.21	0.000
10384985	Rhbdf1	rhomboid family 1 (Drosophila)	1.21	0.001
10581813	Mlkl	mixed lineage kinase domain-like	1.21	0.003
10362245	Epb4.1l2	erythrocyte protein band 4.1-like 2	1.21	0.000
10360173	Slamf7	SLAM family member 7	1.21	0.001
10572861	F2rl3	coagulation factor II (thrombin) receptor-like 3	1.21	0.024
10361234	Hsd11b1	hydroxysteroid 11-beta dehydrogenase 1	1.21	0.001
10514939	**Podn**	**podocan**	**1.21**	**0.001**
10360684	Ephx1	epoxide hydrolase 1, microsomal	1.21	0.045
10538247	Npy	neuropeptide Y	1.21	0.001
10423599	**Matn2**	**matrilin 2**	**1.21**	**0.022**
10537410	Tbxas1	thromboxane A synthase 1, platelet	1.21	0.002
10533929	Scarb1	scavenger receptor class B, member 1	1.21	0.000
10505090	Rpl29	ribosomal protein L29	1.21	0.000
10550906	Plaur	plasminogen activator, urokinase receptor	1.21	0.018
10483199	Slc38a11	solute carrier family 38, member 11	1.21	0.035
10450501	Tnf	tumor necrosis factor	1.21	0.001
10487508	Gm14005	predicted gene 14005	1.21	0.002
10604576	**Gpc3**	**glypican 3**	**1.21**	**0.021**
10566132	Rhog	ras homolog gene family, member G	1.21	0.000
10454709	Kif20a	kinesin family member 20A	1.21	0.013
10443949	**Adamts10**	**a disintegrin-like and metallopeptidase (reprolysin type) with thrombospc**	**1.21**	**0.000**
10519270	**Agrn**	**agrin**	**1.21**	**0.001**
10508734	Ptafr	platelet-activating factor receptor	1.21	0.002
10408613	Tubb2b	tubulin, beta 2B	1.21	0.008
10532741	Tmem119	transmembrane protein 119	1.21	0.000
10508182	Psmb2	proteasome (prosome, macropain) subunit, beta type 2	1.21	0.008
10533345	Aldh2	aldehyde dehydrogenase 2, mitochondrial	1.21	0.015
10566571	Gm8979	very large inducible GTPase 1 pseudogene	1.21	0.003
10436865	Ifngr2	interferon gamma receptor 2	1.21	0.005
10521824	**Sod3**	**superoxide dismutase 3, extracellular**	**1.20**	**0.001**
10542575	Pde3a	phosphodiesterase 3A, cGMP inhibited	1.20	0.016
10439483	Arhgap31	Rho GTPase activating protein 31	1.20	0.000
10599962	Mamld1	mastermind-like domain containing 1	1.20	0.002
10405427	Prelid1	PRELI domain containing 1	1.20	0.043
10355893	Epha4	Eph receptor A4	1.20	0.000
10462922	Plce1	phospholipase C, epsilon 1	1.20	0.002
10385118	Dock2	dedicator of cyto-kinesis 2	1.20	0.023
10486102	Gpr176	G protein-coupled receptor 176	1.20	0.000
10358529	Hmcn1	hemicentin 1	1.20	0.028
10586491	Dapk2	death-associated protein kinase 2	1.20	0.000
10458498	Arap3	ArfGAP with RhoGAP domain, ankyrin repeat and PH domain 3	1.20	0.001
10595668	Ankrd34c	ankyrin repeat domain 34C	1.20	0.002
10607467	Sat1	spermidine/spermine N1-acetyl transferase 1	1.20	0.048
10556113	Rbm3	RNA binding motif protein 3	1.20	0.040

10458382	Cd14	CD14 antigen	1.20	0.026
10451549	Gm4945	predicted gene 4945	1.20	0.000
10495405	Slc25a24	solute carrier family 25 (mitochondrial carrier, phosphate carrier), member 24	1.20	0.027
10356880	St8sia4	ST8 alpha-N-acetyl-neuraminide alpha-2,8-sialyltransferase 4	1.20	0.000
10475414	B2m	beta-2 microglobulin	1.20	0.000
10532984	Dynll1	dynein light chain LC8-type 1	1.20	0.000
10548875	Art4	ADP-ribosyltransferase 4	1.20	0.001
10530421	Gabra4	gamma-aminobutyric acid (GABA) A receptor, subunit alpha 4	1.20	0.024
10390186	Abi3	ABI gene family, member 3	1.20	0.010
10523281	Septin11	septin 11	1.20	0.000
10354741	Rftn2	raftlin family member 2	1.20	0.000
10516765	Serinc2	serine incorporator 2	1.20	0.002
10507612	**Lepre1**	**leprecan 1**	**1.20**	**0.000**
10430201	Myh9	myosin, heavy polypeptide 9, non-muscle	1.20	0.000
10450038	**Angptl4**	**angiopoietin-like 4**	**1.20**	**0.010**
10425880	Prr5	proline rich 5 (renal)	1.20	0.002
10561702	Kcnk6	potassium inwardly-rectifying channel, subfamily K, member 6	1.20	0.014
10444291	H2-Ab1	histocompatibility 2, class II antigen A, beta 1	1.20	0.027
10581569	Rpl29 // Rpl29	ribosomal protein L29 // ribosomal protein L29	1.20	0.000
10495651	Alg14	asparagine-linked glycosylation 14 homolog (yeast)	1.20	0.017
10584047	**Adamts8**	**a disintegrin-like and metallopeptidase (reprolysin type) with thrombospc**	**1.20**	**0.004**
10509901	**Mfap2**	**microfibrillar-associated protein 2**	**1.20**	**0.001**
10430743	Rpl29	ribosomal protein L29	1.20	0.000
10590808	Yap1	yes-associated protein 1	1.20	0.000
10367292	Cs	citrate synthase	1.20	0.010
10443494	Pi16	peptidase inhibitor 16	1.20	0.001
10482920	Cd302	CD302 antigen	1.20	0.002
10518300	Tnfrsf1b	tumor necrosis factor receptor superfamily, member 1b	1.20	0.001
10357242	Dbi	diazepam binding inhibitor	1.20	0.007
10360920	**Tgfb2**	**transforming growth factor, beta 2**	**1.20**	**0.005**
10529485	Htra3	HtrA serine peptidase 3	1.20	0.002

10406111	Slc12a7	solute carrier family 12, member 7	-1.20	0.002
10395692	Arhgap5	Rho GTPase activating protein 5	-1.20	0.005
10391555	Ppy	pancreatic polypeptide	-1.20	0.004
10499655	Il6ra	interleukin 6 receptor, alpha	-1.20	0.000
10445338	Enpp5	ectonucleotide pyrophosphatase/phosphodiesterase 5	-1.20	0.000
10352980	Sntg1	syntrophin, gamma 1	-1.20	0.003
10511817	Klhl32	kelch-like 32 (Drosophila)	-1.20	0.019
10457787	Klhl14	kelch-like 14 (Drosophila)	-1.20	0.008
10484261	Cerkl	ceramide kinase-like	-1.20	0.010
10429203	Fam135b	family with sequence similarity 135, member B	-1.20	0.014
10485580	Cstf3	cleavage stimulation factor, 3' pre-RNA, subunit 3	-1.20	0.006
10457942	Syt4	synaptotagmin IV	-1.20	0.005
10463263	Lztfl1	leucine zipper transcription factor-like 1	-1.20	0.025
10384504	**Meis1**	**Meis homeobox 1**	**-1.20**	**0.001**
10530666	Lnx1	ligand of numb-protein X 1	-1.20	0.001
10483324	Scn9a	sodium channel, voltage-gated, type IX, alpha	-1.20	0.007
10443110	Syngap1	synaptic Ras GTPase activating protein 1 homolog (rat)	-1.20	0.041
10407445	Akr1c12	aldo-keto reductase family 1, member C12	-1.20	0.006
10582941	Cwf19l2	CWF19-like 2, cell cycle control (S. pombe)	-1.20	0.002
10489522	Wfdc16	WAP four-disulfide core domain 16	-1.20	0.021
10349184	Cdh7	cadherin 7, type 2	-1.21	0.001
10380109	Hsf5	heat shock transcription factor family member 5	-1.21	0.034
10463104	Cc2d2b	coiled-coil and C2 domain containing 2B	-1.21	0.010
10533844	Rilpl2	Rab interacting lysosomal protein-like 2	-1.21	0.014
10458424	Taf7	TAF7 RNA polymerase II, TATA box binding protein (TBP)-associated factor	-1.21	0.001
10406423	Mblac2	metallo-beta-lactamase domain containing 2	-1.21	0.027
10507015	Agbl4	ATP/GTP binding protein-like 4	-1.21	0.016
10399146	Mir153	microRNA 153	-1.21	0.017
10434733	Eif4a2	eukaryotic translation initiation factor 4A2	-1.21	0.003
10509596	Rnf186	ring finger protein 186	-1.21	0.001
10449991	Zfp81	zinc finger protein 81	-1.21	0.020
10445638	Ubr2	ubiquitin protein ligase E3 component n-recognin 2	-1.21	0.001
10444332	BC051142	cDNA sequence BC051142	-1.21	0.029
10606530	Mir361	microRNA 361	-1.21	0.029
10368159	Slc35d3	solute carrier family 35, member D3	-1.21	0.001
10434758	St6gal1	beta galactoside alpha 2,6 sialyltransferase 1	-1.21	0.000
10582180	Fam92b	family with sequence similarity 92, member B	-1.21	0.005
10565193	Hdgfrp3	hepatoma-derived growth factor, related protein 3	-1.21	0.002
10564220	Gkap1	G kinase anchoring protein 1	-1.21	0.022
10429491	Arc	activity regulated cytoskeletal-associated protein	-1.21	0.017
10430649	Cbx7	chromobox homolog 7	-1.21	0.002
10432032	Vdr	vitamin D receptor	-1.21	0.003
10381474	Arl4d	ADP-ribosylation factor-like 4D	-1.21	0.000
10502816	Gipc2	GIPC PDZ domain containing family, member 2	-1.22	0.049
10553537	Luzp2	leucine zipper protein 2	-1.22	0.015
10368486	Rnf146	ring finger protein 146	-1.22	0.018
10368356	Akap7	A kinase (PRKA) anchor protein 7	-1.22	0.003
10413255	Duxbl	double homeobox B-like	-1.22	0.025

10413265	Duxbl	double homeobox B-like	-1.22	0.025
10358457	Bex4	brain expressed gene 4	-1.22	0.013
10588203	Ky	kyphoscoliosis peptidase	-1.22	0.004
10421577	Gm9779	predicted gene 9779	-1.22	0.002
10499108	Glt28d2	glycosyltransferase 28 domain containing 2	-1.22	0.001
10417510	Gm10044	predicted gene 10044	-1.22	0.002
10410364	Zfp738	zinc finger protein 738	-1.22	0.018
10551421	Zfp60	zinc finger protein 60	-1.22	0.026
10363921	Pcdh15	protocadherin 15	-1.22	0.013
10463082	Cc2d2b	coiled-coil and C2 domain containing 2B	-1.22	0.003
10490755	Hnf4g	hepatocyte nuclear factor 4, gamma	-1.22	0.003
10443108	Syngap1	synaptic Ras GTPase activating protein 1 homolog (rat)	-1.22	0.015
10407012	Sfrs12ip1	SFRS12-interacting protein 1	-1.22	0.002
10439362	Stxbp5l	syntaxin binding protein 5-like	-1.22	0.003
10437205	Pcp4	Purkinje cell protein 4	-1.22	0.013
10429114	Tmem71	transmembrane protein 71	-1.22	0.010
10451818	Sult1c2	sulfotransferase family, cytosolic, 1C, member 2	-1.22	0.035
10363773	Rhobtb1	Rho-related BTB domain containing 1	-1.22	0.000
10472136	Galnt13	UDP-N-acetyl-alpha-D-galactosamine:polypeptide N-acetylgalactosaminyltrans	-1.23	0.008
10398340	Rtl1	retrotransposon-like 1	-1.23	0.012
10556828	Anks4b	ankyrin repeat and sterile alpha motif domain containing 4B	-1.23	0.038
10496438	Adh1	alcohol dehydrogenase 1 (class I)	-1.23	0.008
10429100	Lrrc6	leucine rich repeat containing 6 (testis)	-1.23	0.007
10479726	Pcmtd2	protein-L-isoaspartate (D-aspartate) O-methyltransferase domain containing 2	-1.23	0.001
10435112	Muc4	mucin 4	-1.23	0.000
10522127	Klb	klotho beta	-1.23	0.010
10514713	Wdr78	WD repeat domain 78	-1.23	0.021
10417561	Fam107a	family with sequence similarity 107, member A	-1.23	0.001
10605522	Gm7173	predicted gene 7173	-1.23	0.004
10404250	Dcdc2a	doublecortin domain containing 2a	-1.23	0.008
10601459	Pou3f4	POU domain, class 3, transcription factor 4	-1.23	0.006
10355312	Ikzf2	IKAROS family zinc finger 2	-1.23	0.002
10398334	Mir337	microRNA 337	-1.23	0.014
10409660	Gkap1	G kinase anchoring protein 1	-1.23	0.010
10410362	Zfp738	zinc finger protein 738	-1.24	0.042
10598575	Lancl3	LanC lantibiotic synthetase component C-like 3 (bacterial)	-1.24	0.000
10430365	Sstr3	somatostatin receptor 3	-1.24	0.001
10426081	Fam19a5	family with sequence similarity 19, member A5	-1.24	0.003
10582427	Cbfa2t3	core-binding factor, runt domain, alpha subunit 2, translocated to, 3 (human)	-1.24	0.000
10489909	Ube2v1	ubiquitin-conjugating enzyme E2 variant 1	-1.24	0.024
10465963	Lrrc10b	leucine rich repeat containing 10B	-1.24	0.004
10401309	Cox16	COX16 cytochrome c oxidase assembly homolog (S. cerevisiae)	-1.24	0.031
10411223	S100z	S100 calcium binding protein, zeta	-1.24	0.019
10398350	Mir341	microRNA 341	-1.24	0.005
10399677	Cox7a2l	cytochrome c oxidase subunit VIIa polypeptide 2-like	-1.24	0.038
10557124	Scnn1b	sodium channel, nonvoltage-gated 1 beta	-1.24	0.000
10564539	Mctp2	multiple C2 domains, transmembrane 2	-1.24	0.001
10423024	Capsl	calcyphosine-like	-1.25	0.003
10571207	Dusp26	dual specificity phosphatase 26 (putative)	-1.25	0.001
10534395	Cldn4	claudin 4	-1.25	0.005
10484307	Frzb	frizzled-related protein	-1.25	0.003
10449000	Msln	mesothelin	-1.25	0.003
10578986	Psd3	pleckstrin and Sec7 domain containing 3	-1.25	0.006
10490845	Chmp4c	chromatin modifying protein 4C	-1.26	0.005
10383564	Fn3k	fructosamine 3 kinase	-1.26	0.000
10517646	Pla2g2f	phospholipase A2, group IIF	-1.26	0.001
10607658	Reps2	RALBP1 associated Eps domain containing protein 2	-1.26	0.000
10377673	Cldn7	claudin 7	-1.26	0.008
10368527	Hint3	histidine triad nucleotide binding protein 3	-1.26	0.000
10384044	Myl7	myosin, light polypeptide 7, regulatory	-1.26	0.022
10601874	Tceal3	transcription elongation factor A (SII)-like 3	-1.26	0.004
10348917	Fam174a	family with sequence similarity 174, member A	-1.27	0.002
10368343	Arg1	arginase, liver	-1.27	0.002
10511416	Tox	thymocyte selection-associated high mobility group box	-1.27	0.000
10548105	Ccnd2	cyclin D2	-1.28	0.005
10473058	Osbpl6	oxysterol binding protein-like 6	-1.28	0.000
10424113	Mal2	mal, T-cell differentiation protein 2	-1.28	0.001
10524684	Msi1	Musashi homolog 1(Drosophila)	-1.28	0.001
10428619	Enpp2	ectonucleotide pyrophosphatase/phosphodiesterase 2	-1.28	0.028
10414269	Bnip3	BCL2/adenovirus E1B interacting protein 3	-1.29	0.000
10436636	Ncam2	neural cell adhesion molecule 2	-1.29	0.010
10455647	Tnfaip8	tumor necrosis factor, alpha-induced protein 8	-1.29	0.002
10354031	Tsga10	testis specific 10	-1.29	0.000
10366446	Tspan8	tetraspanin 8	-1.29	0.002
10362147	Taar1	trace amine-associated receptor 1	-1.29	0.004
10572461	Gm16486	predicted gene 16486	-1.29	0.043
10453254	Cox7a2l	cytochrome c oxidase subunit VIIa polypeptide 2-like	-1.29	0.006
10411945	Fam159b	family with sequence similarity 159, member B	-1.30	0.002
10580282	Junb	Jun-B oncogene	-1.30	0.003
10503376	Gm11818	predicted gene 11818	-1.30	0.006
10582973	Kbtbd3	kelch repeat and BTB (POZ) domain containing 3	-1.30	0.000

10491319	Kcnmb2	potassium large conductance calcium-activated channel, subfamily M, beta me	-1.31	0.008
10510413	Gm572	predicted gene 572	-1.31	0.000
10493555	Kcnn3	potassium intermediate/small conductance calcium-activated channel, subfami	-1.31	0.005
10391561	Pyy	peptide YY	-1.31	0.004
10362701	Ddo	D-aspartate oxidase	-1.31	0.000
10472396	Scn2a1	sodium channel, voltage-gated, type II, alpha 1	-1.32	0.004
10427253	Map3k12	mitogen-activated protein kinase kinase kinase 12	-1.32	0.018
10495878	Ndst4	N-deacetylase/N-sulfotransferase (heparin glucosaminyl) 4	-1.32	0.011
10453256	Kcng3	potassium voltage-gated channel, subfamily G, member 3	-1.32	0.002
10479165	Edn3	endothelin 3	-1.32	0.001
10595298	Filip1	filamin A interacting protein 1	-1.33	0.006
10406782	Fam169a	family with sequence similarity 169, member A	-1.33	0.002
10347364	Vil1	villin 1	-1.33	0.001
10472707	Gad1	glutamic acid decarboxylase 1	-1.33	0.007
10352916	Mir29b-2	microRNA 29b-2	-1.33	0.045
10383891	Cabp7	calcium binding protein 7	-1.33	0.000
10354141	Lonrf2	LON peptidase N-terminal domain and ring finger 2	-1.34	0.001
10495794	Pde5a	phosphodiesterase 5A, cGMP-specific	-1.34	0.032
10402360	Serpina10	serine (or cysteine) peptidase inhibitor, clade A (alpha-1 antiproteinase, antitry	-1.34	0.009
10472398	Scn2a1	sodium channel, voltage-gated, type II, alpha 1	-1.34	0.005
10467744	Sfrp5	secreted frizzled-related sequence protein 5	-1.35	0.003
10543017	Pdk4	pyruvate dehydrogenase kinase, isoenzyme 4	-1.35	0.001
10383409	Gcgr	glucagon receptor	-1.35	0.000
10573198	Dnajb1	DnaJ (Hsp40) homolog, subfamily B, member 1	-1.35	0.000
10566993	Galntl4	UDP-N-acetyl-alpha-D-galactosamine:polypeptide N-acetylgalactosaminyltrans	-1.35	0.019
10572949	Nr3c2	nuclear receptor subfamily 3, group C, member 2	-1.36	0.000
10551025	Cd79a	CD79A antigen (immunoglobulin-associated alpha)	-1.36	0.007
10553450	Nell1	NEL-like 1 (chicken)	-1.36	0.000
10549842	Zfp667	zinc finger protein 667	-1.38	0.001
10519268	Mir200b	microRNA 200b	-1.38	0.011
10590071	Mir26a-1	microRNA 26a-1	-1.39	0.035
10505163	Zkscan16	zinc finger with KRAB and SCAN domains 16	-1.42	0.001
10472400	Scn2a1	sodium channel, voltage-gated, type II, alpha 1	-1.44	0.001
10531034	Ugt2b34	UDP glucuronosyltransferase 2 family, polypeptide B34	-1.44	0.009
10474361	Mpped2	metallophosphoesterase domain containing 2	-1.44	0.000
10472235	Dapl1	death associated protein-like 1	-1.45	0.020
10511333	Plag1	pleiomorphic adenoma gene 1	-1.48	0.000
10438730	Sst	somatostatin	-1.48	0.000
10531100	Sult1d1	sulfotransferase family 1D, member 1	-1.50	0.005
10503416	Calb1	calbindin 1	-1.52	0.001
10352918	Mir29c	microRNA 29c	-1.52	0.021
10506454	C8b	complement component 8, beta polypeptide	-1.54	0.000
10439660	Gm609	predicted gene 609	-1.57	0.000
10603066	Ace2	angiotensin I converting enzyme (peptidyl-dipeptidase A) 2	-1.63	0.001
10570741	Defb1	defensin beta 1	-1.71	0.000

8.3 Affymetrix chip analysis – RT2 and RT2/hTNC mice (II)

Table 7: Gene expression between RT2 and RT2/hTNC mice from non-angiogenic islet pools

Affymetrix chip analysis of non-angiogenic islet pools of 8 weeks old RT2 and RT2/hTNC mice. Fold-changes were compared between non-angiogenic RT2/hTNC and non-angiogenic RT2 islet pools. Data were filtered for fold-changes of minimally ±1.2-fold or more with a significance value of $p \leq 0.05$. List contains 689 gene candidates. Data were screened by searching for the keywords “extracellular matrix”, “blood vessel”, “angiogenesis” and “Notch” in the GO biological process or GO cellular component terms and are highlighted in bold. Gene products mentioned in the text are highlighted in grey. Data are sorted according descending fold-changes.

Annex Table 7 - RT2/hTNC versus RT2 (non-angiogenic)

Probe Set ID	Gene Symbol	Gene Description	Fold-change	p-value
10564207	Snord116	small nucleolar RNA, C/D box 116 cluster	2.64	0.025
10356269	Sp140	Sp140 nuclear body protein	1.85	0.004
10354732	Hspd1	heat shock protein 1 (chaperonin)	1.76	0.012
10523058	Eif5a	eukaryotic translation initiation factor 5A	1.69	0.000
10404063	Hist1h2ab	histone cluster 1, H2ab	1.66	0.027
10376201	Gpx3	glutathione peroxidase 3	1.60	0.049
10438690	Rfc4	replication factor C (activator 1) 4	1.56	0.002
10559233	Mrpl23	mitochondrial ribosomal protein L23	1.53	0.016
10503214	**Chd7**	**chromodomain helicase DNA binding protein 7**	**1.53**	**0.014**
10483786	Mrpl23	mitochondrial ribosomal protein L23	1.52	0.015
10601326	Uprt	uracil phosphoribosyltransferase (FUR1) homolog (S. cerevisiae)	1.51	0.033
10419532	Osgep	O-sialoglycoprotein endopeptidase	1.51	0.008
10596543	Rad54l2	RAD54 like 2 (S. cerevisiae)	1.51	0.009
10400395	Ppp2r3c	protein phosphatase 2, regulatory subunit B'', gamma	1.51	0.002
10440564	Rnf160	ring finger protein 160	1.50	0.015
10518774	Park7	Parkinson disease (autosomal recessive, early onset) 7	1.50	0.011
10601328	Uprt	uracil phosphoribosyltransferase (FUR1) homolog (S. cerevisiae)	1.49	0.020
10449452	Fkbp5	FK506 binding protein 5	1.49	0.010
10490665	Stmn3	stathmin-like 3	1.49	0.031
10581069	Gm9853	predicted gene 9853	1.49	0.027
10466210	Ms4a6d	membrane-spanning 4-domains, subfamily A, member 6D	1.46	0.025
10389795	Stxbp4	syntaxin binding protein 4	1.46	0.014
10443463	Cdkn1a	cyclin-dependent kinase inhibitor 1A (P21)	1.45	0.021
10512443	Stoml2	stomatin (Epb7.2)-like 2	1.44	0.000
10364696	Atp5d	ATP synthase, H+ transporting, mitochondrial F1 complex, delta subunit	1.44	0.002
10467319	Rbp4	retinol binding protein 4, plasma	1.44	0.020
10494832	Sike1	suppressor of IKBKE 1	1.44	0.003
10575616	Gabarapl2	gamma-aminobutyric acid (GABA) A receptor-associated protein-like 2	1.43	0.003
10427199	Pfdn5	prefoldin 5	1.42	0.015
10393573	**Lgals3bp**	**lectin, galactoside-binding, soluble, 3 binding protein**	**1.42**	**0.036**
10593497	Zc3h12c	zinc finger CCCH type containing 12C	1.42	0.018
10457959	Sft2d3	SFT2 domain containing 3	1.42	0.003
10441813	Snora20	small nucleolar RNA, H/ACA box 20	1.40	0.012
10503176	**Chd7**	**chromodomain helicase DNA binding protein 7**	**1.40**	**0.010**
10535095	Zfand2a	zinc finger, AN1-type domain 2A	1.40	0.026
10578619	Cdkn2aip	CDKN2A interacting protein	1.40	0.000
10440562	Rnf160	ring finger protein 160	1.40	0.050
10493995	S100a10	S100 calcium binding protein A10 (calpactin)	1.39	0.005
10587733	Ctsh	cathepsin H	1.39	0.019
10503216	**Chd7**	**chromodomain helicase DNA binding protein 7**	**1.38**	**0.024**
10535979	Rfc3	replication factor C (activator 1) 3	1.38	0.000
10586477	Ppib	peptidylprolyl isomerase B	1.37	0.009
10498168	Exosc8	exosome component 8	1.37	0.002
10458044	Osgep	O-sialoglycoprotein endopeptidase	1.37	0.007
10502791	Ifi44	interferon-induced protein 44	1.37	0.023
10398394	Mir494	microRNA 494	1.37	0.033
10369295	Anapc16	anaphase promoting complex subunit 16	1.36	0.006
10477543	Cbfa2t2	core-binding factor, runt domain, alpha subunit 2, translocated to, 2 (human)	1.36	0.017
10450519	Tcf19	transcription factor 19	1.35	0.000
10481920	Psmd5	proteasome (prosome, macropain) 26S subunit, non-ATPase, 5	1.35	0.009
10445558	BC048355	cDNA sequence BC048355	1.35	0.023
10392259	Smurf2	SMAD specific E3 ubiquitin protein ligase 2	1.35	0.002
10560260	Sae1	SUMO1 activating enzyme subunit 1	1.35	0.001
10394978	Rrm2	ribonucleotide reductase M2	1.35	0.022
10368881	Armc2	armadillo repeat containing 2	1.35	0.016
10503212	**Chd7**	**chromodomain helicase DNA binding protein 7**	**1.35**	**0.013**
10443527	Pim1	proviral integration site 1	1.35	0.036
10546760	Ddx3x	DEAD/H (Asp-Glu-Ala-Asp/His) box polypeptide 3, X-linked	1.35	0.025
10515257	Rad54l	RAD54 like (S. cerevisiae)	1.34	0.006
10414693	Tox4	TOX high mobility group box family member 4	1.34	0.024
10457463	Nutf2	nuclear transport factor 2	1.34	0.004
10468531	Nutf2	nuclear transport factor 2	1.34	0.004
10514779	Prkaa2	protein kinase, AMP-activated, alpha 2 catalytic subunit	1.34	0.045
10472372	Scn2a1	sodium channel, voltage-gated, type II, alpha 1	1.33	0.043
10354404	Dnajb6	DnaJ (Hsp40) homolog, subfamily B, member 6	1.33	0.029
10453214	Nutf2	nuclear transport factor 2	1.33	0.006
10405781	Mir27b	microRNA 27b	1.33	0.005
10505270	Slc31a2	solute carrier family 31, member 2	1.33	0.013
10503178	**Chd7**	**chromodomain helicase DNA binding protein 7**	**1.33**	**0.002**
10388154	Med31	mediator of RNA polymerase II transcription, subunit 31 homolog (yeast)	1.32	0.010
10511269	Sdf4	stromal cell derived factor 4	1.32	0.002
10447349	Cript	cysteine-rich PDZ-binding protein	1.32	0.001
10478447	Stk4	serine/threonine kinase 4	1.32	0.014
10519234	B3galt6	UDP-Gal:betaGal beta 1,3-galactosyltransferase, polypeptide 6	1.32	0.032
10393620	Cbx4	chromobox homolog 4 (Drosophila Pc class)	1.32	0.041
10355115	Prelid1	PRELI domain containing 1	1.32	0.009
10378334	Tax1bp3	Tax1 (human T-cell leukemia virus type I) binding protein 3	1.32	0.009
10351347	Creg1	cellular repressor of E1A-stimulated genes 1	1.32	0.038
10461334	Mta2	metastasis-associated gene family, member 2	1.32	0.005

10399691	Id2	inhibitor of DNA binding 2	1.32	0.026
10391207	Dhx58	DEXH (Asp-Glu-X-His) box polypeptide 58	1.32	0.002
10451481	BC032203	cDNA sequence BC032203	1.31	0.019
10472440	Tax1bp3	Tax1 (human T-cell leukemia virus type I) binding protein 3	1.31	0.012
10600485	Dkc1	dyskeratosis congenita 1, dyskerin homolog (human)	1.31	0.041
10518735	Spsb1	splA/ryanodine receptor domain and SOCS box containing 1	1.31	0.046
10607475	Prdx4	peroxiredoxin 4	1.31	0.034
10458960	Aldh7a1	aldehyde dehydrogenase family 7, member A1	1.31	0.007
10385504	Gm5431	predicted gene 5431	1.31	0.040
10487622	Snrpb	small nuclear ribonucleoprotein B	1.31	0.006
10437174	Wrb	tryptophan rich basic protein	1.31	0.048
10378855	Ssh2	slingshot homolog 2 (Drosophila)	1.31	0.049
10405427	Prelid1	PRELI domain containing 1	1.31	0.001
10585599	Imp3	IMP3, U3 small nucleolar ribonucleoprotein, homolog (yeast)	1.30	0.042
10492174	Tm4sf4	transmembrane 4 superfamily member 4	1.30	0.002
10586484	Fam96a	family with sequence similarity 96, member A	1.30	0.017
10606001	Snx12	sorting nexin 12	1.30	0.015
10560624	Apoe	apolipoprotein E	1.30	0.018
10518679	Nmnat1	nicotinamide nucleotide adenylyltransferase 1	1.30	0.014
10399710	Rsad2	radical S-adenosyl methionine domain containing 2	1.30	0.006
10491385	Actl6a	actin-like 6A	1.30	0.013
10568040	Ppp4c	protein phosphatase 4, catalytic subunit	1.30	0.001
10384378	Ddc	dopa decarboxylase	1.30	0.004
10442629	Spsb3	splA/ryanodine receptor domain and SOCS box containing 3	1.30	0.006
10489038	Scand1	SCAN domain-containing 1	1.30	0.001
10474596	Aven	apoptosis, caspase activation inhibitor	1.30	0.016
10410124	Ctsl	cathepsin L	1.30	0.009
10531286	Vdac2	voltage-dependent anion channel 2	1.30	0.013
10433088	Cbx5	chromobox homolog 5 (Drosophila HP1a)	1.30	0.005
10407042	Dimt1	DIM1 dimethyladenosine transferase 1-like (S. cerevisiae)	1.30	0.008
10453429	Pigf	phosphatidylinositol glycan anchor biosynthesis, class F	1.30	0.007
10406852	Cnn3	calponin 3, acidic	1.30	0.022
10430778	Phf5a	PHD finger protein 5A	1.30	0.000
10413710	Nt5dc2	5'-nucleotidase domain containing 2	1.29	0.005
10359713	Sft2d2	SFT2 domain containing 2	1.29	0.006
10546725	Pdzrn3	PDZ domain containing RING finger 3	1.29	0.027
10597627	Oxsr1	oxidative-stress responsive 1	1.29	0.007
10506154	Alg6	asparagine-linked glycosylation 6 homolog (yeast, alpha-1,3,-glucosyltransfera	1.29	0.026
10497817	Anxa5	annexin A5	1.29	0.011
10514924	Tomm22	translocase of outer mitochondrial membrane 22 homolog (yeast)	1.29	0.019
10409322	Thoc3	THO complex 3	1.29	0.001
10450367	Hspa1a	heat shock protein 1A	1.29	0.017
10528482	BC050254	cDNA sequence BC050254	1.29	0.011
10517508	C1qb	complement component 1, q subcomponent, beta polypeptide	1.29	0.021
10533090	Rfc5	replication factor C (activator 1) 5	1.29	0.004
10475293	Tubgcp4	tubulin, gamma complex associated protein 4	1.29	0.003
10489246	Mafb	v-maf musculoaponeurotic fibrosarcoma oncogene family, protein B (avian)	1.29	0.013
10358064	Ipo9	importin 9	1.29	0.001
10445894	Erh	enhancer of rudimentary homolog (Drosophila)	1.29	0.006
10548563	Ptp4a1	protein tyrosine phosphatase 4a1	1.29	0.034
10381250	Tubg1	tubulin, gamma 1	1.29	0.003
10430020	Vps28	vacuolar protein sorting 28 (yeast)	1.28	0.029
10415074	Rem2	rad and gem related GTP binding protein 2	1.28	0.015
10489204	**Tgm2**	**transglutaminase 2, C polypeptide**	**1.28**	**0.027**
10372082	Nudt4	nudix (nucleoside diphosphate linked moiety X)-type motif 4	1.28	0.006
10440556	Rnf160	ring finger protein 160	1.28	0.028
10513592	Wdr31	WD repeat domain 31	1.28	0.048
10495405	Slc25a24	solute carrier family 25 (mitochondrial carrier, phosphate carrier), member 24	1.28	0.038
10607952	Vamp7	vesicle-associated membrane protein 7	1.28	0.031
10440414	Fau	Finkel-Biskis-Reilly murine sarcoma virus (FBR-MuSV) ubiquitously expressed	1.28	0.005
10439762	Ahcy	S-adenosylhomocysteine hydrolase	1.28	0.012
10507218	Mknk1	MAP kinase-interacting serine/threonine kinase 1	1.28	0.004
10495659	Cnn3	calponin 3, acidic	1.28	0.000
10409190	Cenpp	centromere protein P	1.28	0.023
10462618	Ifit3	interferon-induced protein with tetratricopeptide repeats 3	1.28	0.048
10508479	Ptp4a2	protein tyrosine phosphatase 4a2	1.28	0.000
10384145	H2afv	H2A histone family, member V	1.28	0.009
10536996	Klhdc10	kelch domain containing 10	1.28	0.030
10472058	Rif1	Rap1 interacting factor 1 homolog (yeast)	1.27	0.001
10511739	Cpne3	copine III	1.27	0.031
10508042	Meaf6	MYST/Esa1-associated factor 6	1.27	0.015
10444436	Fkbpl	FK506 binding protein-like	1.27	0.004
10504398	Serf2	small EDRK-rich factor 2	1.27	0.016
10374453	Glul	glutamate-ammonia ligase (glutamine synthetase)	1.27	0.002
10522368	Nipal1	NIPA-like domain containing 1	1.27	0.005
10506134	Atg4c	autophagy-related 4C (yeast)	1.27	0.032
10396177	Actr10	ARP10 actin-related protein 10 homolog (S. cerevisiae)	1.27	0.015
10510462	Trmt112	tRNA methyltransferase 11-2 homolog (S. cerevisiae)	1.27	0.043
10517287	Man1c1	mannosidase, alpha, class 1C, member 1	1.27	0.040
10538590	Herc5	hect domain and RLD 5	1.27	0.033
10505623	D4Bwg0951e	DNA segment, Chr 4, Brigham & Women's Genetics 0951 expressed	1.27	0.000

10577623	Gins4	GINS complex subunit 4 (Sld5 homolog)	1.27	0.015
10402730	Ppp1r13b	protein phosphatase 1, regulatory (inhibitor) subunit 13B	1.27	0.023
10345357	Imp4	IMP4, U3 small nucleolar ribonucleoprotein, homolog (yeast)	1.27	0.001
10567171	Snord14a	small nucleolar RNA, C/D box 14A	1.27	0.032
10346105	Rpl23a	ribosomal protein L23a	1.26	0.047
10550169	Phf20	PHD finger protein 20	1.26	0.013
10517328	Tmem50a	transmembrane protein 50A	1.26	0.020
10395976	Dnajb6	DnaJ (Hsp40) homolog, subfamily B, member 6	1.26	0.032
10401781	Sptlc2	serine palmitoyltransferase, long chain base subunit 2	1.26	0.014
10494306	Mcl1	myeloid cell leukemia sequence 1	1.26	0.042
10439634	Gtpbp8	GTP-binding protein 8 (putative)	1.26	0.009
10584752	Rps25	ribosomal protein S25	1.26	0.013
10463068	Ptp4a1	protein tyrosine phosphatase 4a1	1.26	0.033
10575693	Vat1l	vesicle amine transport protein 1 homolog-like (T. californica)	1.26	0.050
10531284	Trmt112	tRNA methyltransferase 11-2 homolog (S. cerevisiae)	1.26	0.042
10557405	Rabep2	rabaptin, RAB GTPase binding effector protein 2	1.26	0.005
10456423	Seh1l	SEH1-like (S. cerevisiae	1.26	0.009
10535477	Usp42	ubiquitin specific peptidase 42	1.26	0.006
10344713	Ahcy	S-adenosylhomocysteine hydrolase	1.26	0.030
10541307	Usp18	ubiquitin specific peptidase 18	1.26	0.025
10455108	Pcdhb16	protocadherin beta 16	1.26	0.017
10475280	Adal	adenosine deaminase-like	1.26	0.008
10519488	Tubb2c	tubulin, beta 2C	1.26	0.002
10524169	Pole	polymerase (DNA directed), epsilon	1.26	0.014
10472289	Tank	TRAF family member-associated Nf-kappa B activator	1.25	0.040
10554156	Fam174b	family with sequence similarity 174, member B	1.25	0.016
10434804	Mir28	microRNA 28	1.25	0.038
10359078	Cep350	centrosomal protein 350	1.25	0.035
10488722	Commd7	COMM domain containing 7	1.25	0.005
10608422	Rmi1	RMI1, RecQ mediated genome instability 1, homolog (S. cerevisiae)	1.25	0.018
10558248	Bub3	budding uninhibited by benzimidazoles 3 homolog (S. cerevisiae)	1.25	0.044
10583034	Dcun1d5	DCN1, defective in cullin neddylation 1, domain containing 5 (S. cerevisiae)	1.25	0.005
10524436	Usp30	ubiquitin specific peptidase 30	1.25	0.003
10467162	Pank1	pantothenate kinase 1	1.25	0.022
10440560	Rnf160	ring finger protein 160	1.25	0.004
10350684	Arpc5	actin related protein 2/3 complex, subunit 5	1.25	0.002
10474064	Trp53i11	transformation related protein 53 inducible protein 11	1.25	0.023
10444927	Nrm	nurim (nuclear envelope membrane protein)	1.25	0.006
10381395	Rundc1	RUN domain containing 1	1.25	0.003
10348866	Atg4b	autophagy-related 4B (yeast)	1.25	0.022
10382516	Kctd2	potassium channel tetramerisation domain containing 2	1.25	0.004
10596277	Dnajc13	DnaJ (Hsp40) homolog, subfamily C, member 13	1.25	0.001
10388310	Rap1gap2	RAP1 GTPase activating protein 2	1.25	0.004
10453544	Mettl4	methyltransferase like 4	1.25	0.033
10359334	Cacybp	calcyclin binding protein	1.25	0.003
10375240	Hspd1	heat shock protein 1 (chaperonin)	1.25	0.005
10474902	Rad51	RAD51 homolog (S. cerevisiae)	1.25	0.004
10585417	Idh3a	isocitrate dehydrogenase 3 (NAD+) alpha	1.25	0.033
10415714	Fam123a	family with sequence similarity 123, member A	1.25	0.012
10594501	Ptplad1	protein tyrosine phosphatase-like A domain containing 1	1.25	0.005
10605740	Eif2s3x	eukaryotic translation initiation factor 2, subunit 3, structural gene X-linked	1.25	0.011
10450605	Tubb5	tubulin, beta 5	1.25	0.009
10513141	Ptpn3	protein tyrosine phosphatase, non-receptor type 3	1.25	0.041
10399430	Ddx1	DEAD (Asp-Glu-Ala-Asp) box polypeptide 1	1.25	0.007
10480628	Tubb2c	tubulin, beta 2C	1.25	0.002
10356339	Pde6d	phosphodiesterase 6D, cGMP-specific, rod, delta	1.25	0.020
10435075	Tfrc	transferrin receptor	1.25	0.000
10486710	Lcmt2	leucine carboxyl methyltransferase 2	1.24	0.041
10375926	Ppp2ca	protein phosphatase 2 (formerly 2A), catalytic subunit, alpha isoform	1.24	0.000
10598994	Atp1b3	ATPase, Na+/K+ transporting, beta 3 polypeptide	1.24	0.001
10407946	Stard3nl	STARD3 N-terminal like	1.24	0.004
10484227	Sestd1	SEC14 and spectrin domains 1	1.24	0.006
10539894	Mgll	monoglyceride lipase	1.24	0.007
10403052	Gm9238	transcription elongation factor B (SIII), polypeptide 2 pseudogene	1.24	0.001
10350024	Klhl12	kelch-like 12 (Drosophila)	1.24	0.021
10356329	Snora75	small nucleolar RNA, H/ACA box 75	1.24	0.033
10522668	Paics	phosphoribosylaminoimidazole carboxylase, phosphoribosylaminoribosylaminc	1.24	0.004
10389865	Nme1	non-metastatic cells 1, protein (NM23A) expressed in	1.24	0.018
10518532	Tardbp	TAR DNA binding protein	1.24	0.012
10374035	Xbp1	X-box binding protein 1	1.24	0.039
10398451	Rps25	ribosomal protein S25	1.24	0.016
10603254	Larp4	La ribonucleoprotein domain family, member 4	1.24	0.018
10440558	Rnf160	ring finger protein 160	1.24	0.021
10396064	Txndc9	thioredoxin domain containing 9	1.24	0.042
10543460	Tmem229a	transmembrane protein 229A	1.24	0.010
10461614	Ms4a6c	membrane-spanning 4-domains, subfamily A, member 6C	1.24	0.012
10476620	Snrpb2	U2 small nuclear ribonucleoprotein B	1.24	0.030
10564805	Pex11a	peroxisomal biogenesis factor 11 alpha	1.24	0.033
10358726	Tsen15	tRNA splicing endonuclease 15 homolog (S. cerevisiae)	1.24	0.022
10539632	Alms1	Alstrom syndrome 1 homolog (human)	1.24	0.046
10600324	Rpl3	ribosomal protein L3	1.24	0.034

10458823	Tmed7	transmembrane emp24 protein transport domain containing 7	1.23	0.016
10475610	Dut	deoxyuridine triphosphatase	1.23	0.010
10407955	Epdr1	ependymin related protein 1 (zebrafish)	1.23	0.008
10582649	Pgbd5	piggyBac transposable element derived 5	1.23	0.033
10363905	Zwint	ZW10 interactor	1.23	0.008
10383233	Rnf213	ring finger protein 213	1.23	0.021
10462796	Kif11	kinesin family member 11	1.23	0.003
10579828	Rps25	ribosomal protein S25	1.23	0.022
10526520	Plod3	procollagen-lysine, 2-oxoglutarate 5-dioxygenase 3	1.23	0.004
10605319	Ubl4	ubiquitin-like 4	1.23	0.037
10461878	Prune2	prune homolog 2 (Drosophila)	1.23	0.014
10526853	Fam20c	family with sequence similarity 20, member C	1.23	0.003
10503551	Usp45	ubiquitin specific petidase 45	1.23	0.001
10494595	**Notch2**	**Notch gene homolog 2 (Drosophila)**	**1.23**	**0.016**
10357371	Tmem163	transmembrane protein 163	1.23	0.040
10398665	**Tnfaip2**	**tumor necrosis factor, alpha-induced protein 2**	**1.23**	**0.014**
10440388	Hspa13	heat shock protein 70 family, member 13	1.23	0.008
10384138	Tmed4	transmembrane emp24 protein transport domain containing 4	1.23	0.028
10413803	Btd	biotinidase	1.23	0.032
10347106	Rpe	ribulose-5-phosphate-3-epimerase	1.23	0.005
10554281	Fanci	Fanconi anemia, complementation group I	1.23	0.003
10473547	Srp9	signal recognition particle 9	1.23	0.001
10388532	Nxn	nucleoredoxin	1.23	0.007
10369531	Tspan15	tetraspanin 15	1.23	0.008
10428534	Trps1	trichorhinophalangeal syndrome I (human)	1.23	0.023
10466423	Cep78	centrosomal protein 78	1.23	0.013
10538150	Tmem176a	transmembrane protein 176A	1.23	0.031
10445601	Mea1	male enhanced antigen 1	1.22	0.039
10461568	Prpf19	PRP19/PSO4 pre-mRNA processing factor 19 homolog (S. cerevisiae)	1.22	0.002
10508182	Psmb2	proteasome (prosome, macropain) subunit, beta type 2	1.22	0.015
10572449	Lsm4	LSM4 homolog, U6 small nuclear RNA associated (S. cerevisiae)	1.22	0.004
10595070	Fam83b	family with sequence similarity 83, member B	1.22	0.037
10595793	Atp1b3	ATPase, Na+/K+ transporting, beta 3 polypeptide	1.22	0.002
10368886	Foxo3	forkhead box O3	1.22	0.015
10404700	Ubxn2a	UBX domain protein 2A	1.22	0.021
10415662	Rcbtb1	regulator of chromosome condensation (RCC1) and BTB (POZ) domain contai	1.22	0.041
10403352	Klf6	Kruppel-like factor 6	1.22	0.043
10383214	Rnf213	ring finger protein 213	1.22	0.010
10483822	Ttc30a2	tetratricopeptide repeat domain 30A2	1.22	0.041
10351035	Gas5	growth arrest specific 5	1.22	0.027
10468489	Xpnpep1	X-prolyl aminopeptidase (aminopeptidase P) 1, soluble	1.22	0.010
10485280	Gm13889	predicted gene 13889	1.22	0.026
10398601	Rcor1	REST corepressor 1	1.22	0.002
10489904	Spata2	spermatogenesis associated 2	1.22	0.025
10539640	Alms1	Alstrom syndrome 1 homolog (human)	1.22	0.040
10472350	Gca	grancalcin	1.22	0.045
10365749	Lta4h	leukotriene A4 hydrolase	1.22	0.010
10423346	Zfp622	zinc finger protein 622	1.22	0.007
10556581	Gm10589	predicted gene 10589	1.22	0.016
10497399	Pde7a	phosphodiesterase 7A	1.22	0.007
10449386	D17Wsu92e	DNA segment, Chr 17, Wayne State University 92, expressed	1.22	0.002
10434467	Psmd2	proteasome (prosome, macropain) 26S subunit, non-ATPase, 2	1.22	0.015
10458569	Nr3c1	nuclear receptor subfamily 3, group C, member 1	1.22	0.002
10484402	Ctnnd1	catenin (cadherin associated protein), delta 1	1.22	0.013
10419354	Map1lc3b	microtubule-associated protein 1 light chain 3 beta	1.22	0.042
10595404	Fam46a	family with sequence similarity 46, member A	1.22	0.024
10479063	Rab22a	RAB22A, member RAS oncogene family	1.22	0.009
10561842	Capns1	calpain, small subunit 1	1.22	0.043
10442454	Pgp	phosphoglycolate phosphatase	1.22	0.008
10382243	**Gna13**	**guanine nucleotide binding protein, alpha 13**	**1.22**	**0.001**
10417664	Rpl19	ribosomal protein L19	1.22	0.020
10397179	Dnalc1	dynein, axonemal, light chain 1	1.22	0.049
10466087	Tmem109	transmembrane protein 109	1.21	0.001
10357124	Tsn	translin	1.21	0.004
10492671	Ppid	peptidylprolyl isomerase D (cyclophilin D)	1.21	0.002
10530421	Gabra4	gamma-aminobutyric acid (GABA) A receptor, subunit alpha 4	1.21	0.047
10458808	Fem1c	fem-1 homolog c (C.elegans)	1.21	0.009
10595109	Lrrc1	leucine rich repeat containing 1	1.21	0.048
10605431	Rab39b	RAB39B, member RAS oncogene family	1.21	0.031
10380859	Cdk12	cyclin-dependent kinase 12	1.21	0.044
10360957	Kctd3	potassium channel tetramerisation domain containing 3	1.21	0.021
10436428	Mina	myc induced nuclear antigen	1.21	0.045
10543067	Asns	asparagine synthetase	1.21	0.031
10410173	Hiatl1	hippocampus abundant transcript-like 1	1.21	0.014
10406782	Fam169a	family with sequence similarity 169, member A	1.21	0.024
10542722	Rps25	ribosomal protein S25	1.21	0.024
10409557	H2afy	H2A histone family, member Y	1.21	0.015
10497285	Impa1	inositol (myo)-1(or 4)-monophosphatase 1	1.21	0.021
10371321	Slc41a2	solute carrier family 41, member 2	1.21	0.040
10482323	Ppp6c	protein phosphatase 6, catalytic subunit	1.21	0.008
10405753	Me1	malic enzyme 1, NADP(+)-dependent, cytosolic	1.21	0.031

10431266	Cerk	ceramide kinase	1.21	0.031
10470948	Slc39a1	solute carrier family 39 (zinc transporter), member 1	1.21	0.032
10565873	Ppme1	protein phosphatase methylesterase 1	1.21	0.006
10546079	Cnbp	cellular nucleic acid binding protein	1.21	0.000
10454332	Elp2	elongation protein 2 homolog (S. cerevisiae)	1.21	0.025
10406598	Serinc5	serine incorporator 5	1.21	0.024
10432404	Tuba1a	tubulin, alpha 1A	1.21	0.010
10488816	Ahcy	S-adenosylhomocysteine hydrolase	1.21	0.029
10489413	Tomm34	translocase of outer mitochondrial membrane 34	1.21	0.001
10365005	Dapk3	death-associated protein kinase 3	1.21	0.002
10578145	Erh	enhancer of rudimentary homolog (Drosophila)	1.21	0.004
10596893	Dag1	dystroglycan 1	1.21	0.034
10458293	Dnajc18	DnaJ (Hsp40) homolog, subfamily C, member 18	1.21	0.026
10599612	Phf6	PHD finger protein 6	1.21	0.032
10400742	L2hgdh	L-2-hydroxyglutarate dehydrogenase	1.21	0.046
10430032	Nfkbil2	nuclear factor of kappa light polypeptide gene enhancer in B-cells inhibitor-like	1.21	0.003
10365590	Ccdc53	coiled-coil domain containing 53	1.21	0.030
10355996	Slc25a5	solute carrier family 25 (mitochondrial carrier, adenine nucleotide translocator),	1.21	0.025
10578069	Gtpbp10	GTP-binding protein 10 (putative)	1.21	0.015
10590325	**Ctnnb1**	**catenin (cadherin associated protein), beta 1**	**1.21**	**0.001**
10447167	Mta3	metastasis associated 3	1.21	0.030
10432511	Racgap1	Rac GTPase-activating protein 1	1.21	0.006
10463997	Pdcd4	programmed cell death 4	1.21	0.039
10388476	Rph3al	rabphilin 3A-like (without C2 domains)	1.20	0.009
10605674	Pola1	polymerase (DNA directed), alpha 1	1.20	0.002
10583326	Slc36a4	solute carrier family 36 (proton/amino acid symporter), member 4	1.20	0.036
10360225	Timm23	translocase of inner mitochondrial membrane 23 homolog (yeast)	1.20	0.015
10416069	Timm23	translocase of inner mitochondrial membrane 23 homolog (yeast)	1.20	0.015
10388238	Tmem93	transmembrane protein 93	1.20	0.046
10412036	Apoo-ps	apolipoprotein O, pseudogene	1.20	0.007
10534990	Taf6	TAF6 RNA polymerase II, TATA box binding protein (TBP)-associated factor	1.20	0.002
10530434	Commd8	COMM domain containing 8	1.20	0.031
10504743	Nans	N-acetylneuraminic acid synthase (sialic acid synthase)	1.20	0.027
10400336	Snx6	sorting nexin 6	1.20	0.022
10376685	Alkbh5	alkB, alkylation repair homolog 5 (E. coli)	1.20	0.001
10584572	Hspa8	heat shock protein 8	1.20	0.006
10472994	Mtx2	metaxin 2	1.20	0.025
10452228	Khsrp	KH-type splicing regulatory protein	1.20	0.002
10404187	Tdp2	tyrosyl-DNA phosphodiesterase 2	1.20	0.017
10585956	Myo9a	myosin IXa	1.20	0.031
10431014	Vkorc1l1	vitamin K epoxide reductase complex, subunit 1-like 1	1.20	0.050
10533633	Diablo	diablo homolog (Drosophila)	1.20	0.022
10378668	Pitpna	phosphatidylinositol transfer protein, alpha	1.20	0.037
10360460	Chml	choroideremia-like	1.20	0.016
10426110	Pim3	proviral integration site 3	1.20	0.018
10408032	Zfp187	zinc finger protein 187	1.20	0.014
10450103	H2-Ke6	H2-K region expressed gene 6	1.20	0.019
10431722	Gxylt1	glucoside xylosyltransferase 1	1.20	0.008
10537246	Nup205	nucleoporin 205	1.20	0.007
10533246	Oas1g	2'-5' oligoadenylate synthetase 1G	1.20	0.026
10388938	Wsb1	WD repeat and SOCS box-containing 1	1.20	0.004
10395227	Cog5	component of oligomeric golgi complex 5	1.20	0.001
10570764	Alg11	asparagine-linked glycosylation 11 homolog (yeast, alpha-1,2-mannosyltransfe	1.20	0.005
10592535	Sorl1	sortilin-related receptor, LDLR class A repeats-containing	1.20	0.035
10361110	Dtl	denticleless homolog (Drosophila)	1.20	0.022
10485979	Gjd2	gap junction protein, delta 2	1.20	0.034
10364361	Icosl	icos ligand	1.20	0.013
10486172	Fam82a2	family with sequence similarity 82, member A2	1.20	0.003
10582474	Chmp1a	chromatin modifying protein 1A	1.20	0.039
10396108	Arf6	ADP-ribosylation factor 6	1.20	0.003
10575074	Tmco7	transmembrane and coiled-coil domains 7	1.20	0.003
10500295	Plekho1	pleckstrin homology domain containing, family O member 1	1.20	0.020
10421188	R3hcc1	R3H domain and coiled-coil containing 1	1.20	0.026
10546944	Tmem111	transmembrane protein 111	1.20	0.003
10376950	Pmp22	peripheral myelin protein 22	1.20	0.011
10386636	Usp22	ubiquitin specific peptidase 22	1.20	0.009
10553336	Zdhhc13	zinc finger, DHHC domain containing 13	1.20	0.028
10590245	Slc25a38	solute carrier family 25, member 38	1.20	0.047
10469575	Gm13363	protein tyrosine phosphatase 4a1-like	1.20	0.046
10351414	Aldh9a1	aldehyde dehydrogenase 9, subfamily A1	1.20	0.009
10541279	Bcl2l13	BCL2-like 13 (apoptosis facilitator)	1.20	0.010
10406203	Stoml2	stomatin (Epb7.2)-like 2	1.20	0.044
10604175	Fam70a	family with sequence similarity 70, member A	1.20	0.043
10505187	Ugcg	UDP-glucose ceramide glucosyltransferase	1.20	0.045
10518385	Mfn2	mitofusin 2	1.20	0.018
10448424	Pdpk1	3-phosphoinositide dependent protein kinase-1	1.20	0.010
10581575	Gm1943	WD repeat domain 70 pseudogene	1.20	0.037
10359816	Pogk	pogo transposable element with KRAB domain	1.20	0.040
10347417	Bcs1l	BCS1-like (yeast)	1.20	0.019

10455707	Zfp474	zinc finger protein 474	-1.20	0.003
10445158	Olfr124	olfactory receptor 124	-1.20	0.008
10470166	Lcn10	lipocalin 10	-1.20	0.021
10365714	Sec61g	SEC61, gamma subunit	-1.20	0.013
10460704	Gm10814	predicted gene 10814	-1.20	0.011
10592330	Nrgn	neurogranin	-1.20	0.016
10491229	Mir551b	microRNA 551b	-1.20	0.028
10542376	Rpl36al	ribosomal protein L36A-like	-1.20	0.000
10447188	Mta3	metastasis associated 3	-1.20	0.047
10368027	Nmbr	neuromedin B receptor	-1.20	0.019
10512901	Mrpl50	mitochondrial ribosomal protein L50	-1.20	0.010
10444637	D17H6S56E-3	DNA segment, Chr 17, human D6S56E 3	-1.20	0.021
10540287	Gm10009	predicted gene 10009	-1.20	0.039
10359826	Uqcr11	ubiquinol-cytochrome c reductase, complex III subunit XI	-1.20	0.045
10344799	Cspp1	centrosome and spindle pole associated protein 1	-1.20	0.002
10375547	Olfr10	olfactory receptor 10	-1.20	0.029
10604078	Upf3b	UPF3 regulator of nonsense transcripts homolog B (yeast)	-1.20	0.002
10436662	Mir155	microRNA 155	-1.20	0.015
10452854	Srd5a2	steroid 5 alpha-reductase 2	-1.20	0.002
10379200	Sebox	SEBOX homeobox	-1.20	0.012
10505071	Tmem38b	transmembrane protein 38B	-1.20	0.019
10539700	Rps28	ribosomal protein S28	-1.20	0.046
10500347	BC107364	cDNA sequence BC107364	-1.20	0.003
10397068	Rbm25	RNA binding motif protein 25	-1.20	0.008
10513912	Aldoart1	aldolase 1 A retrogene 1	-1.20	0.018
10373630	Olfr801	olfactory receptor 801	-1.20	0.002
10409449	F12	coagulation factor XII (Hageman factor)	-1.20	0.036
10515708	Szt2	seizure threshold 2	-1.20	0.009
10559446	Lilrb3	leukocyte immunoglobulin-like receptor, subfamily B (with TM and ITIM domair	-1.20	0.004
10437205	Pcp4	Purkinje cell protein 4	-1.20	0.018
10546339	**Wnt7a**	**wingless-related MMTV integration site 7A**	**-1.20**	**0.012**
10371981	Snrpf	small nuclear ribonucleoprotein polypeptide F	-1.20	0.003
10546180	Gm839	predicted gene 839	-1.20	0.019
10350864	Sec16b	SEC16 homolog B (S. cerevisiae)	-1.20	0.041
10348910	Neu4	sialidase 4	-1.20	0.036
10543921	Slc13a4	solute carrier family 13 (sodium/sulfate symporters), member 4	-1.20	0.010
10534718	Trip6	thyroid hormone receptor interactor 6	-1.20	0.010
10511486	4930448K20Rik	glyceraldehyde-3-phosphate dehydrogenase pseudogene	-1.20	0.005
10450508	Lta	lymphotoxin A	-1.20	0.041
10428809	Klhl38	kelch-like 38 (Drosophila)	-1.20	0.046
10450767	H2-M10.1	histocompatibility 2, M region locus 10.1	-1.20	0.026
10403973	Pom121l2	POM121 membrane glycoprotein-like 2 (rat)	-1.20	0.033
10599274	Rhox4c	reproductive homeobox 4C	-1.20	0.040
10541494	Rps27a	ribosomal protein S27A	-1.20	0.011
10468239	Cyp17a1	cytochrome P450, family 17, subfamily a, polypeptide 1	-1.20	0.025
10566377	Olfr655	olfactory receptor 655	-1.20	0.013
10450496	Lst1	leukocyte specific transcript 1	-1.20	0.023
10548295	Clec2j	C-type lectin domain family 2, member J	-1.20	0.049
10362166	Taar7f	trace amine-associated receptor 7F	-1.20	0.022
10367471	Olfr9	olfactory receptor 9	-1.20	0.049
10384183	Nacad	NAC alpha domain containing	-1.20	0.000
10440279	Csnka2ip	casein kinase 2, alpha prime interacting protein	-1.20	0.004
10600718	Sec61g	SEC61, gamma subunit	-1.20	0.012
10394283	Cenpo	centromere protein O	-1.20	0.028
10536494	Cav2	caveolin 2	-1.20	0.030
10525397	Arpc3	actin related protein 2/3 complex, subunit 3	-1.20	0.025
10491952	Mgst2	microsomal glutathione S-transferase 2	-1.20	0.032
10469239	Mir669c	microRNA 669c	-1.20	0.007
10561153	Cyp2b23	cytochrome P450, family 2, subfamily b, polypeptide 23	-1.20	0.038
10560614	Apoc4	apolipoprotein C-IV	-1.20	0.000
10552451	Ceacam18	carcinoembryonic antigen-related cell adhesion molecule 18	-1.21	0.001
10558450	Gm10578	predicted gene 10578	-1.21	0.022
10562152	Mag	myelin-associated glycoprotein	-1.21	0.006
10479556	BC051628	cDNA sequence BC051628	-1.21	0.013
10532267	Vmn2r9	vomeronasal 2, receptor 9	-1.21	0.025
10500042	Zfp687	zinc finger protein 687	-1.21	0.026
10390919	Krtap4-1	keratin associated protein 4-1	-1.21	0.016
10559399	Oscar	osteoclast associated receptor	-1.21	0.031
10400639	Rpl36al	ribosomal protein L36A-like	-1.21	0.002
10381514	Cd300lg	CD300 antigen like family member G	-1.21	0.045
10390831	Krt10	keratin 10	-1.21	0.006
10465224	Gm10815	predicted gene 10815	-1.21	0.020
10411456	Tmem174	transmembrane protein 174	-1.21	0.003
10558436	BC005624	cDNA sequence BC005624	-1.21	0.018
10500009	Rpl31	ribosomal protein L31	-1.21	0.014
10427991	Trio	triple functional domain (PTPRF interacting)	-1.21	0.017
10549748	Zfp524	zinc finger protein 524	-1.21	0.016
10586602	Gm10647	predicted gene 10647	-1.21	0.008
10362892	Magmas	mitochondria-associated protein involved in granulocyte-macrophage colony-st	-1.21	0.025
10587501	Rps27a	ribosomal protein S27A	-1.21	0.007
10501489	Hectd1	HECT domain containing 1	-1.21	0.033

10601874	Tceal3	transcription elongation factor A (SII)-like 3	-1.21	0.039
10390328	Tbx21	T-box 21	-1.21	0.018
10564220	Gkap1	G kinase anchoring protein 1	-1.21	0.001
10601882	BC065397	cDNA sequence BC065397	-1.21	0.016
10559270	Tssc4	tumor-suppressing subchromosomal transferable fragment 4	-1.21	0.033
10390897	Krtap1-5	keratin associated protein 1-5	-1.21	0.007
10552570	Klk1b11	kallikrein 1-related peptidase b11	-1.21	0.036
10538123	Gimap9	GTPase, IMAP family member 9	-1.21	0.025
10421908	Rps3a	ribosomal protein S3A	-1.21	0.025
10547073	Snora7a	small nucleolar RNA, H/ACA box 7A	-1.21	0.030
10409660	Gkap1	G kinase anchoring protein 1	-1.21	0.015
10604612	Mir503	microRNA 503	-1.21	0.025
10515712	Szt2	seizure threshold 2	-1.21	0.032
10392135	Gh	growth hormone	-1.21	0.038
10543052	Rps27a	ribosomal protein S27A	-1.21	0.011
10419999	Jph4	junctophilin 4	-1.21	0.017
10505879	Ifna7	interferon alpha 7	-1.21	0.033
10566231	Olfr622	olfactory receptor 622	-1.21	0.020
10498323	Fam194a	family with sequence similarity 194, member A	-1.21	0.049
10464594	BC021614	cDNA sequence BC021614	-1.21	0.030
10543442	Ndufa5	NADH dehydrogenase (ubiquinone) 1 alpha subcomplex, 5	-1.21	0.009
10584862	Scn4b	sodium channel, type IV, beta	-1.21	0.039
10534384	Wbscr28	Williams-Beuren syndrome chromosome region 28 (human)	-1.21	0.025
10416732	Snora30	small nucleolar RNA, H/ACA box 30	-1.21	0.033
10557703	Snora30	small nucleolar RNA, H/ACA box 30	-1.21	0.033
10499861	S100a9	S100 calcium binding protein A9 (calgranulin B)	-1.21	0.019
10545479	Tmsb10	thymosin, beta 10	-1.21	0.047
10405741	Gm3338	predicted gene 3338	-1.21	0.023
10561474	Il28a	interleukin 28A	-1.21	0.029
10402383	Serpina1f	serine (or cysteine) peptidase inhibitor, clade A, member 1F	-1.21	0.041
10389882	Luc7l3	LUC7-like 3 (S. cerevisiae)	-1.21	0.027
10406622	Cmya5	cardiomyopathy associated 5	-1.21	0.005
10521088	Slbp	stem-loop binding protein	-1.22	0.025
10375543	Olfr1393	olfactory receptor 1393	-1.22	0.044
10482135	Olfr362	olfactory receptor 362	-1.22	0.010
10557587	Zfp771	zinc finger protein 771	-1.22	0.000
10606178	Xist	inactive X specific transcripts	-1.22	0.003
10511368	Impad1	inositol monophosphatase domain containing 1	-1.22	0.047
10440333	Speer2	spermatogenesis associated glutamate (E)-rich protein 2	-1.22	0.003
10584356	Olfr876	olfactory receptor 876	-1.22	0.009
10588075	Gm6406	predicted gene 6406	-1.22	0.010
10558919	Snora52	small nucleolar RNA, H/ACA box 52	-1.22	0.028
10604124	Rhox4f	reproductive homeobox 4F	-1.22	0.004
10599269	Rhox4b	reproductive homeobox 4B	-1.22	0.019
10567211	Gm9197	predicted gene 9197	-1.22	0.037
10516658	Ccdc28b	coiled coil domain containing 28B	-1.22	0.001
10516081	Ppie	peptidylprolyl isomerase E (cyclophilin E)	-1.22	0.010
10408593	Serpinb6c	serine (or cysteine) peptidase inhibitor, clade B, member 6c	-1.22	0.037
10606831	Tmsb15a	thymosin beta 15a	-1.22	0.004
10603833	Usmg5	upregulated during skeletal muscle growth 5	-1.22	0.017
10426284	Acr	acrosin prepropeptide	-1.22	0.027
10599281	Rhox4d	reproductive homeobox 4D	-1.22	0.019
10368077	Ect2l	epithelial cell transforming sequence 2 oncogene-like	-1.22	0.022
10566091	Chrna10	cholinergic receptor, nicotinic, alpha polypeptide 10	-1.22	0.013
10443215	Snrpc	U1 small nuclear ribonucleoprotein C	-1.22	0.003
10443089	Syngap1	synaptic Ras GTPase activating protein 1 homolog (rat)	-1.22	0.002
10520371	Rbm33	RNA binding motif protein 33	-1.22	0.002
10591612	Dock6	dedicator of cytokinesis 6	-1.22	0.017
10346668	Fam117b	family with sequence similarity 117, member B	-1.22	0.019
10578763	Sap30	sin3 associated polypeptide	-1.22	0.010
10557488	Tbx6	T-box 6	-1.22	0.041
10464612	Cabp4	calcium binding protein 4	-1.22	0.027
10505630	Snapc3	small nuclear RNA activating complex, polypeptide 3	-1.22	0.005
10377516	Kcnab3	potassium voltage-gated channel, shaker-related subfamily, beta member 3	-1.23	0.041
10474689	Fam98b	family with sequence similarity 98, member B	-1.23	0.006
10469774	Il1f8	interleukin 1 family, member 8	-1.23	0.029
10591224	Zfp560	zinc finger protein 560	-1.23	0.027
10487506	Gm14005	predicted gene 14005	-1.23	0.010
10551009	Tmsb10	thymosin, beta 10	-1.23	0.037
10465045	Drap1	Dr1 associated protein 1 (negative cofactor 2 alpha)	-1.23	0.009
10601854	Wbp5	WW domain binding protein 5	-1.23	0.005
10601272	Pin4	protein (peptidyl-prolyl cis/trans isomerase) NIMA-interacting, 4 (parvulin)	-1.23	0.001
10360046	Sdhc	succinate dehydrogenase complex, subunit C, integral membrane protein	-1.23	0.022
10515710	Szt2	seizure threshold 2	-1.23	0.006
10481496	Gm14488	predicted gene 14488	-1.23	0.005
10355312	Ikzf2	IKAROS family zinc finger 2	-1.23	0.005
10599291	Rhox4e	reproductive homeobox 4E	-1.23	0.027
10468419	D19Ertd652e	DNA segment, Chr 19, ERATO Doi 652, expressed	-1.23	0.038
10535329	Papolb	poly (A) polymerase beta (testis specific)	-1.23	0.037
10408762	Eef1e1	eukaryotic translation elongation factor 1 epsilon 1	-1.23	0.005
10474123	Commd9	COMM domain containing 9	-1.23	0.029

10366951	Ndufa4l2	NADH dehydrogenase (ubiquinone) 1 alpha subcomplex, 4-like 2	-1.23	0.012
10499873	Prr9	proline rich 9	-1.23	0.002
10366541	Lrrc10	leucine rich repeat containing 10	-1.23	0.005
10478114	Arhgap40	Rho GTPase activating protein 40	-1.23	0.010
10596263	Dnajc13	DnaJ (Hsp40) homolog, subfamily C, member 13	-1.23	0.001
10598359	Syp	synaptophysin	-1.23	0.005
10515841	Gm12866	predicted gene 12866	-1.24	0.037
10553115	Lmtk3	lemur tyrosine kinase 3	-1.24	0.000
10493498	Dcst1	DC-STAMP domain containing 1	-1.24	0.046
10585410	Sh2d7	SH2 domain containing 7	-1.24	0.023
10565858	Gm5115	predicted gene 5115	-1.24	0.027
10515696	Szt2	seizure threshold 2	-1.24	0.003
10401289	Slc10a1	solute carrier family 10 (sodium/bile acid cotransporter family), member 1	-1.24	0.015
10421418	Epb4.9	erythrocyte protein band 4.9	-1.24	0.003
10412555	Gm10044	predicted gene 10044	-1.24	0.012
10542156	Clec2d	C-type lectin domain family 2, member d	-1.24	0.043
10485597	Depdc7	DEP domain containing 7	-1.24	0.002
10484818	Olfr1238	olfactory receptor 1238	-1.24	0.004
10605315	Lage3	L antigen family, member 3	-1.24	0.030
10455824	Gm10536	predicted gene 10536	-1.24	0.033
10345556	Vwa3b	von Willebrand factor A domain containing 3B	-1.24	0.024
10578786	Galntl6	UDP-N-acetyl-alpha-D-galactosamine:polypeptide N-acetylgalactosaminyltrans	-1.24	0.035
10447897	Wtap	Wilms' tumour 1-associating protein	-1.24	0.033
10405892	Gm10767	predicted gene 10767	-1.25	0.005
10529953	Gm10048	predicted gene 10048	-1.25	0.020
10515702	Szt2	seizure threshold 2	-1.25	0.030
10591610	Dock6	dedicator of cytokinesis 6	-1.25	0.025
10373367	Coq10a	coenzyme Q10 homolog A (yeast)	-1.25	0.012
10521566	Tmem128	transmembrane protein 128	-1.25	0.005
10459766	Scarna17	small Cajal body-specific RNA 17	-1.25	0.008
10461642	Scarna17	small Cajal body-specific RNA 17	-1.25	0.008
10423742	Polr2k	polymerase (RNA) II (DNA directed) polypeptide K	-1.25	0.032
10453318	Abcg5	ATP-binding cassette, sub-family G (WHITE), member 5	-1.25	0.033
10360412	Olfr419	olfactory receptor 419	-1.25	0.027
10416503	Snora31	small nucleolar RNA, H/ACA box 31	-1.25	0.017
10552284	Pin4	protein (peptidyl-prolyl cis/trans isomerase) NIMA-interacting, 4 (parvulin)	-1.25	0.000
10409709	Mir7-1	microRNA 7-1	-1.26	0.046
10406838	Gm8780	predicted gene 8780	-1.26	0.019
10589909	Trim71	tripartite motif-containing 71	-1.26	0.030
10353729	Gm5415	predicted gene 5415	-1.26	0.046
10528970	Gm5299	predicted gene 5299	-1.26	0.019
10584466	Olfr923	olfactory receptor 923	-1.26	0.034
10488430	Gm10750	predicted gene 10750	-1.26	0.035
10443110	Syngap1	synaptic Ras GTPase activating protein 1 homolog (rat)	-1.26	0.013
10553475	Rps27a	ribosomal protein S27A	-1.26	0.004
10370833	Uqcr11	ubiquinol-cytochrome c reductase, complex III subunit XI	-1.26	0.040
10451145	Capn11	calpain 11	-1.26	0.031
10416700	Pcdh17	protocadherin 17	-1.26	0.013
10550459	Gm5155	predicted gene 5155	-1.27	0.018
10412054	Ndufaf2	NADH dehydrogenase (ubiquinone) 1 alpha subcomplex, assembly factor 2	-1.27	0.003
10586240	Dennd4a	DENN/MADD domain containing 4A	-1.27	0.036
10516943	Atpif1	ATPase inhibitory factor 1	-1.27	0.013
10354504	Gm5976	glyceraldehyde-3-phosphate dehydrogenase pseudogene	-1.27	0.010
10346109	Dnahc7b	dynein, axonemal, heavy chain 7B	-1.27	0.022
10353731	Gm5415	predicted gene 5415	-1.27	0.028
10601755	Rpl36a	ribosomal protein L36A	-1.28	0.028
10394671	Gm16497	predicted gene 16497	-1.28	0.034
10449979	Morc2b	microrchidia 2B	-1.28	0.001
10360648	Psen2	presenilin 2	-1.28	0.006
10366519	Cnot2	CCR4-NOT transcription complex, subunit 2	-1.28	0.022
10415957	Gm4573	predicted gene 4573	-1.28	0.008
10415045	Mrpl52	mitochondrial ribosomal protein L52	-1.28	0.005
10347351	Ctdsp1	CTD (carboxy-terminal domain, RNA polymerase II, polypeptide A) small phosp	-1.28	0.028
10421972	Rpl36a	ribosomal protein L36A	-1.28	0.008
10428707	Has2	hyaluronan synthase 2	-1.28	0.008
10508721	Snora44	small nucleolar RNA, H/ACA box 44	-1.29	0.029
10513536	Gm2173	predicted gene 2173	-1.29	0.021
10359849	Uck2	uridine-cytidine kinase 2	-1.29	0.019
10578153	Gm6100	predicted gene 6100	-1.29	0.004
10398332	Mir673	microRNA 673	-1.29	0.018
10534654	Znhit1	zinc finger, HIT domain containing 1	-1.29	0.001
10377418	Tmem107	transmembrane protein 107	-1.29	0.008
10443120	Ggnbp1	gametogenetin binding protein 1	-1.30	0.002
10379524	**Ccl11**	**chemokine (C-C motif) ligand 11**	**-1.30**	**0.004**
10591614	Dock6	dedicator of cytokinesis 6	-1.30	0.015
10399677	Cox7a2l	cytochrome c oxidase subunit VIIa polypeptide 2-like	-1.30	0.048
10426889	Sec61b	Sec61 beta subunit	-1.30	0.002
10455948	Chsy3	chondroitin sulfate synthase 3	-1.30	0.023
10392464	Fam20a	family with sequence similarity 20, member A	-1.31	0.044
10597490	Rps27	ribosomal protein S27	-1.31	0.025
10445145	Olfr118	olfactory receptor 118	-1.31	0.048

10512487	Rmrp	RNA component of mitochondrial RNAase P	-1.32	0.012
10397083	Rbm25	RNA binding motif protein 25	-1.32	0.004
10495107	Adora3	adenosine A3 receptor	-1.32	0.008
10584758	Fam103a1	family with sequence similarity 103, member A1	-1.33	0.002
10468881	Zfp826	zinc finger protein 826	-1.33	0.011
10439409	BC031361	cDNA sequence BC031361	-1.33	0.023
10436552	Rbm11	RNA binding motif protein 11	-1.33	0.001
10554569	Fam103a1	family with sequence similarity 103, member A1	-1.33	0.001
10514300	Ifna12	interferon alpha 12	-1.33	0.018
10542317	Cdkn1b	cyclin-dependent kinase inhibitor 1B	-1.34	0.038
10496735	Rpl36a	ribosomal protein L36A	-1.34	0.011
10606902	Tmsb15b1-Tms	Tmsb15b1-Tmsb15b2 readthrough transcript	-1.34	0.000
10504831	Sec61b	Sec61 beta subunit	-1.34	0.003
10544638	Tra2a	transformer 2 alpha homolog (Drosophila)	-1.34	0.010
10397081	Rbm25	RNA binding motif protein 25	-1.35	0.000
10445008	Lsm5	LSM5 homolog, U6 small nuclear RNA associated (S. cerevisiae)	-1.35	0.001
10407120	Rps3a	ribosomal protein S3A	-1.36	0.016
10502816	Gipc2	GIPC PDZ domain containing family, member 2	-1.36	0.027
10505837	Mir491	microRNA 491	-1.37	0.004
10401309	Cox16	COX16 cytochrome c oxidase assembly homolog (S. cerevisiae)	-1.37	0.004
10567072	Psma1	proteasome (prosome, macropain) subunit, alpha type 1	-1.38	0.001
10446713	Snord53	small nucleolar RNA, C/D box 53	-1.38	0.027
10591616	Dock6	dedicator of cytokinesis 6	-1.39	0.004
10499748	Rps27	ribosomal protein S27	-1.39	0.021
10362440	Trdn	triadin	-1.39	0.002
10484791	Olfr1222	olfactory receptor 1222	-1.39	0.012
10353034	Snord87	small nucleolar RNA, C/D box 87	-1.40	0.019
10546337	Gm7755	predicted gene 7755	-1.41	0.048
10520388	Rbm33	RNA binding motif protein 33	-1.41	0.012
10373610	Olfr767	olfactory receptor 767	-1.42	0.042
10454828	Pnet-ps	prenatal ethanol induced mRNA, pseudogene	-1.43	0.029
10544971	Lsm5	LSM5 homolog, U6 small nuclear RNA associated (S. cerevisiae)	-1.46	0.002
10532164	Atp5k	ATP synthase, H+ transporting, mitochondrial F1F0 complex, subunit e	-1.48	0.001
10524060	Gm10417	predicted gene 10417	-1.48	0.047
10566254	Hbb-b1	hemoglobin, beta adult major chain	-1.48	0.037
10566258	Hbb-b1	hemoglobin, beta adult major chain	-1.49	0.029
10411454	Sec61b	Sec61 beta subunit	-1.51	0.004
10400581	Fkbp3	FK506 binding protein 3	-1.52	0.000
10516906	Snora73b	small nucleolar RNA, H/ACA box 73b	-1.52	0.033
10398416	Mir487b	microRNA 487b	-1.53	0.041
10438813	Mir690	microRNA 690	-1.54	0.048
10516908	Snora73a	small nucleolar RNA, H/ACA box 73a	-1.57	0.019
10500268	Mrps21	mitochondrial ribosomal protein S21	-1.78	0.002
10455015	Vaultrc5	vault RNA component 5	-1.89	0.027
10544523	Rny1	RNA, Y1 small cytoplasmic, Ro-associated	-2.74	0.026

8.4 Affymetrix chip analysis – RT2 and RT2/hTNC mice (III)

Table 8: Gene expression between RT2 and RT2/hTNC mice from angiogenic islet pools

Affymetrix chip analysis of angiogenic islet pools of 8 weeks old RT2 and RT2/hTNC mice. Fold-changes were compared between angiogenic RT2/hTNC and angiogenic RT2 islet pools. Data were filtered for fold-changes of minimally ±1.2-fold or more with a significance value of $p \leq 0.05$. List contains 68 gene candidates. Data are sorted according descending fold-changes.

Annex Table 8 - RT2/hTNC versus RT2 (angiogenic)

Probe Set ID	Gene Symbol	Gene Description	Fold-change	p-value
10376885	Snord49b	small nucleolar RNA, C/D box 49B	1.57	0.045
10351043	Snord47	small nucleolar RNA, C/D box 47	1.56	0.049
10442327	Cldn6	claudin 6	1.43	0.012
10398075	Serpina3n	serine (or cysteine) peptidase inhibitor, clade A, member 3N	1.43	0.018
10403018	IghmAC38.205.	Ig mu chain V region AC38 205.12	1.43	0.009
10448182	Mir703	microRNA 703	1.37	0.025
10536667	Ptprz1	protein tyrosine phosphatase, receptor type Z, polypeptide 1	1.36	0.019
10413314	Pde12	phosphodiesterase 12	1.33	0.042
10362896	Cd24a	CD24a antigen	1.33	0.029
10531724	Plac8	placenta-specific 8	1.31	0.016
10606369	Itm2a	integral membrane protein 2A	1.29	0.043
10391561	Pyy	peptide YY	1.27	0.014
10460968	Rasgrp2	RAS, guanyl releasing protein 2	1.27	0.007
10365974	Dcn	decorin	1.27	0.029
10429564	Ly6a	lymphocyte antigen 6 complex, locus A	1.27	0.050
10593015	Cd3g	CD3 antigen, gamma polypeptide	1.27	0.039
10450242	C4b	complement component 4B (Childo blood group)	1.26	0.024
10488678	Dusp15	dual specificity phosphatase-like 15	1.25	0.028
10458419	Slc25a2	solute carrier family 25 (mitochondrial carrier, ornithine transporter) member 2	1.25	0.019
10445894	Erh	enhancer of rudimentary homolog (Drosophila)	1.25	0.041
10580183	Ier2	immediate early response 2	1.24	0.015
10396074	Mgat2	mannoside acetylglucosaminyltransferase 2	1.24	0.008
10447383	Epcam	epithelial cell adhesion molecule	1.24	0.027
10427199	Pfdn5	prefoldin 5	1.24	0.047
10407211	Ppap2a	phosphatidic acid phosphatase type 2A	1.24	0.015
10603266	Nudt10	nudix (nucleoside diphosphate linked moiety X)-type motif 10	1.24	0.033
10606868	Bex1	brain expressed gene 1	1.23	0.022
10555260	Olfr521	olfactory receptor 521	1.23	0.041
10461629	Ms4a4d	membrane-spanning 4-domains, subfamily A, member 4D	1.23	0.036
10392410	Gm10838	predicted gene 10838	1.23	0.027
10544573	Rarres2	retinoic acid receptor responder (tazarotene induced) 2	1.22	0.004
10506736	Magoh	mago-nashi homolog, proliferation-associated (Drosophila)	1.22	0.027
10603151	Gpm6b	glycoprotein m6b	1.22	0.008
10583034	Dcun1d5	DCN1, defective in cullin neddylation 1, domain containing 5 (S. cerevisiae)	1.22	0.007
10401278	Erh	enhancer of rudimentary homolog (Drosophila)	1.22	0.047
10398338	Mir665	microRNA 665	1.21	0.045
10483353	Scn7a	sodium channel, voltage-gated, type VII, alpha	1.21	0.004
10569017	Ifitm3	interferon induced transmembrane protein 3	1.21	0.030
10542965	Sgce	sarcoglycan, epsilon	1.21	0.012
10552406	Nkg7	natural killer cell group 7 sequence	1.21	0.029
10403079	LOC435333 //	similar to monoclonal antibody heavy chain // similar to monoclonal antibody h	1.21	0.002
10410124	Ctsl	cathepsin L	1.21	0.019
10403706	Psma2	proteasome (prosome, macropain) subunit, alpha type 2	1.21	0.025
10461148	Snhg1	small nucleolar RNA host gene (non-protein coding) 1	1.21	0.003
10430846	Ndufa6	NADH dehydrogenase (ubiquinone) 1 alpha subcomplex, 6 (B14)	1.21	0.035
10532956	Cabp1	calcium binding protein 1	1.20	0.029
10578145	Erh	enhancer of rudimentary homolog (Drosophila)	1.20	0.049
10523275	Gm6450	ribosomal protein L9 pseudogene	1.20	0.041
10501922	Snhg8	small nucleolar RNA host gene 8	1.20	0.026
10429573	Ly6c2	lymphocyte antigen 6 complex, locus C2	1.20	0.039
10405918	Rsl1	regulator of sex limited protein 1	-1.20	0.012
10584248	Gm7257	predicted gene 7257	-1.20	0.037
10576160	Acsf3	acyl-CoA synthetase family member 3	-1.20	0.022
10489522	Wfdc16	WAP four-disulfide core domain 16	-1.21	0.044
10591123	Fat3	FAT tumor suppressor homolog 3 (Drosophila)	-1.21	0.046
10510125	Mcrs1	microspherule protein 1	-1.21	0.003
10419122	Gm8020	predicted gene 8020	-1.23	0.027
10511835	Fhl5	four and a half LIM domains 5	-1.24	0.014
10539310	Pcgf1	polycomb group ring finger 1	-1.24	0.008
10548829	Gucy2c	guanylate cyclase 2c	-1.24	0.019
10350864	Sec16b	SEC16 homolog B (S. cerevisiae)	-1.24	0.003
10362147	Taar1	trace amine-associated receptor 1	-1.25	0.021
10421517	Cysltr2	cysteinyl leukotriene receptor 2	-1.25	0.000
10541515	Dppa3	developmental pluripotency-associated 3	-1.33	0.045
10601503	Dach2	dachshund 2 (Drosophila)	-1.35	0.041
10526724	Smok3c	sperm motility kinase 3C	-1.37	0.041
10598085	ATP6	ATP synthase F0 subunit 6	-1.50	0.007
10538882	Gm5571	predicted gene 5571	-1.67	0.021

8.5 Affymetrix chip analysis – Rip-hTNC and wildtype mice

Table 9: Gene expression between non-tumorigenic islets from Rip-hTNC and wildtype mice

Affymetrix chip analysis of islet pools from 12 weeks old Rip-hTNC and wildtype mice. Fold-changes were compared between Rip-hTNC and wildtype islet pools. Data were filtered for fold-changes of minimally ±1.2-fold or more with a significance value of $p \leq 0.100$. List contains 582 gene candidates. Data were screened by searching for the keywords “extracellular matrix”, “angiogenesis”, “cell cycle”, “immune”, “inflammation” and “regulation of transcription” in the GO biological process or GO cellular component terms and are highlighted in bold. Gene products mentioned in the text are highlighted in grey. p-values ≤ 0.05 are highlighted in grey. Data are sorted according descending fold-changes.

Annex Table 9 - Rip-hTNC versus wildtype

Probe Set ID	Gene Symbol	Gene Description	Fold-change	p-value
10545175	Igk // Igk	immunoglobulin kappa chain complex // immunoglobulin kappa chain complex	2.39	0.062
10487588	**Il1a**	**interleukin 1 alpha**	**2.00**	**0.006**
10402608	1700001K19Rik	RIKEN cDNA 1700001K19 gene	1.99	0.023
10598203	**Ccl28**	**chemokine (C-C motif) ligand 28**	**1.93**	**0.042**
10355403	**Fn1**	**fibronectin 1**	**1.85**	**0.094**
10362428	Trdn	triadin	1.81	0.094
10531415	**Cxcl10**	**chemokine (C-X-C motif) ligand 10**	**1.74**	**0.059**
10531100	Sult1d1	sulfotransferase family 1D, member 1	1.73	0.006
10444824	H2-Q6	histocompatibility 2, Q region locus 6	1.73	0.053
10503334	Gem	GTP binding protein (gene overexpressed in skeletal muscle)	1.72	0.023
10456005	**Cd74**	**CD74 antigen (invariant polypeptide of major histocompatibility complex,**	**1.70**	**0.021**
10508663	Laptm5	lysosomal-associated protein transmembrane 5	1.69	0.099
10364950	**Gadd45b**	**growth arrest and DNA-damage-inducible 45 beta**	**1.68**	**0.024**
10362424	Trdn	triadin	1.66	0.016
10383289	Baiap2	brain-specific angiogenesis inhibitor 1-associated protein 2	1.61	0.004
10517165	Cd52	CD52 antigen	1.61	0.091
10438738	**Bcl6**	**B-cell leukemia/lymphoma 6**	**1.60**	**0.020**
10366881	**Ddit3**	**DNA-damage inducible transcript 3**	**1.59**	**0.023**
10523156	**Cxcl2**	**chemokine (C-X-C motif) ligand 2**	**1.59**	**0.033**
10428302	**Klf10**	**Kruppel-like factor 10**	**1.59**	**0.026**
10427035	**Nr4a1**	**nuclear receptor subfamily 4, group A, member 1**	**1.58**	**0.045**
10596568	**Rbm15b**	**RNA binding motif protein 15B**	**1.58**	**0.040**
10464905	**Npas4**	**neuronal PAS domain protein 4**	**1.57**	**0.027**
10494643	Hmgcs2	3-hydroxy-3-methylglutaryl-Coenzyme A synthase 2	1.56	0.026
10377439	**Per1**	**period homolog 1 (Drosophila)**	**1.56**	**0.063**
10455514	Kcnn2	potassium intermediate/small conductance calcium-activated channel, subfami	1.55	0.006
10404606	**Ly86**	**lymphocyte antigen 86**	**1.53**	**0.039**
10444291	**H2-Ab1**	**histocompatibility 2, class II antigen A, beta 1**	**1.52**	**0.026**
10460157	Cpt1a	carnitine palmitoyltransferase 1a, liver	1.52	0.027
10512470	Cd72	CD72 antigen	1.51	0.013
10409486	Pdlim7	PDZ and LIM domain 7	1.51	0.022
10424400	**Myc**	**myelocytomatosis oncogene**	**1.51**	**0.046**
10360406	**Ifi205**	**interferon activated gene 205**	**1.51**	**0.044**
10362426	Trdn	triadin	1.49	0.018
10566583	Gm8995	predicted gene 8995	1.49	0.051
10445412	Nfkbie	nuclear factor of kappa light polypeptide gene enhancer in B-cells inhibitor, eps	1.48	0.059
10399691	**Id2**	**inhibitor of DNA binding 2**	**1.47**	**0.053**
10376060	**Irf1**	**interferon regulatory factor 1**	**1.47**	**0.084**
10444229	**H2-DMa**	**histocompatibility 2, class II, locus DMa**	**1.46**	**0.026**
10582997	Casp4	caspase 4, apoptosis-related cysteine peptidase	1.46	0.020
10477935	Gm1332	predicted gene 1332	1.46	0.007
10450069	Gm7035	predicted gene 7035	1.46	0.063
10450154	**H2-Aa**	**histocompatibility 2, class II antigen A, alpha**	**1.46**	**0.076**
10360391	Ifi203	interferon activated gene 203	1.45	0.014
10580202	Dand5	DAN domain family, member 5	1.45	0.008
10593756	Chrna3	cholinergic receptor, nicotinic, alpha polypeptide 3	1.45	0.003
10449000	Msln	mesothelin	1.45	0.099
10487392	**Kcnip3**	**Kv channel interacting protein 3, calsenilin**	**1.45**	**0.043**
10444814	H2-gs10	MHC class I like protein GS10	1.44	0.017
10350516	Ptgs2	prostaglandin-endoperoxide synthase 2	1.44	0.040
10454077	**Taf4b**	**TAF4B RNA polymerase II, TATA box binding protein (TBP)-associated fa**	**1.44**	**0.010**
10416340	Gfra2	glial cell line derived neurotrophic factor family receptor alpha 2	1.43	0.001
10417371	ENSMUSG000(	predicted gene, ENSMUSG00000068790	1.43	0.049
10362440	Trdn	triadin	1.43	0.002
10416175	Nefl	neurofilament, light polypeptide	1.43	0.019
10360377	AI607873	expressed sequence AI607873	1.41	0.065
10401607	**Pgf**	**placental growth factor**	**1.41**	**0.011**
10399973	**Hdac9**	**histone deacetylase 9**	**1.41**	**0.018**
10474972	Chac1	ChaC, cation transport regulator-like 1 (E. coli)	1.40	0.047
10540472	**Bhlhe40**	**basic helix-loop-helix family, member e40**	**1.40**	**0.014**
10503107	6330407A03Rik	RIKEN cDNA 6330407A03 gene	1.40	0.066
10453797	AK220484	cDNA sequence AK220484	1.40	0.070
10490818	Stmn2	stathmin-like 2	1.40	0.009
10517169	Sh3bgrl3	SH3 domain binding glutamic acid-rich protein-like 3	1.40	0.027
10504838	**Nr4a3**	**nuclear receptor subfamily 4, group A, member 3**	**1.39**	**0.045**
10493555	Kcnn3	potassium intermediate/small conductance calcium-activated channel, subfami	1.39	0.017
10509577	Pla2g2d	phospholipase A2, group IID	1.39	0.024
10357488	**Cd55**	**CD55 antigen**	**1.39**	**0.094**
10463945	Dusp5	dual specificity phosphatase 5	1.39	0.078
10525880	Fam101a	family with sequence similarity 101, member A	1.39	0.005
10578207	Lonrf1	LON peptidase N-terminal domain and ring finger 1	1.38	0.042
10363541	Ass1	argininosuccinate synthetase 1	1.38	0.004
10493995	S100a10	S100 calcium binding protein A10 (calpactin)	1.38	0.071
10560575	**Relb**	**avian reticuloendotheliosis viral (v-rel) oncogene related B**	**1.38**	**0.047**
10427461	Ptger4	prostaglandin E receptor 4 (subtype EP4)	1.38	0.008
10415074	Rem2	rad and gem related GTP binding protein 2	1.38	0.015
10361771	**Plagl1**	**pleiomorphic adenoma gene-like 1**	**1.38**	**0.055**
10430302	Csf2rb2	colony stimulating factor 2 receptor, beta 2, low-affinity (granulocyte-macropha	1.38	0.054
10585851	Hcn4	hyperpolarization-activated, cyclic nucleotide-gated K+ 4	1.37	0.003

10356020	Dock10	dedicator of cytokinesis 10	1.37	0.085
10467979	Scd1	stearoyl-Coenzyme A desaturase 1	1.37	0.099
10571312	Dusp4	dual specificity phosphatase 4	1.37	0.002
10418921	Sncg	synuclein, gamma	1.37	0.000
10365492	Gm5174	predicted gene 5174	1.37	0.057
10593767	Chrnb4	cholinergic receptor, nicotinic, beta polypeptide 4	1.37	0.002
10569017	Ifitm3	interferon induced transmembrane protein 3	1.36	0.043
10379511	**Ccl2**	**chemokine (C-C motif) ligand 2**	**1.36**	**0.055**
10435704	Cd80	CD80 antigen	1.36	0.022
10563858	Gabrg3	gamma-aminobutyric acid (GABA) A receptor, subunit gamma 3	1.36	0.001
10471154	Ass1	argininosuccinate synthetase 1	1.36	0.008
10428809	Klhl38	kelch-like 38 (Drosophila)	1.36	0.044
10381082	**Rara**	**retinoic acid receptor, alpha**	**1.36**	**0.001**
10580282	**Junb**	**Jun-B oncogene**	**1.35**	**0.035**
10413314	E430028B21Ril	RIKEN cDNA E430028B21 gene	1.35	0.004
10401238	**Zfp36l1**	**zinc finger protein 36, C3H type-like 1**	**1.35**	**0.059**
10566993	Galntl4	UDP-N-acetyl-alpha-D-galactosamine:polypeptide N-acetylgalactosaminyltrans	1.35	0.067
10426284	Acr	acrosin prepropeptide	1.35	0.092
10441003	**Runx1**	**runt related transcription factor 1**	**1.35**	**0.008**
10579347	Ifi30	interferon gamma inducible protein 30	1.35	0.023
10389207	**Ccl5**	**chemokine (C-C motif) ligand 5**	**1.35**	**0.059**
10569370	Th	tyrosine hydroxylase	1.35	0.068
10512291	**Dctn3**	**dynactin 3**	**1.35**	**0.030**
10511665	Necab1	N-terminal EF-hand calcium binding protein 1	1.35	0.027
10443527	Pim1	proviral integration site 1	1.35	0.062
10501586	**S1pr1**	**sphingosine-1-phosphate receptor 1**	**1.35**	**0.097**
10347948	Sp100	nuclear antigen Sp100	1.34	0.074
10444821	**H2-Q8**	**histocompatibility 2, Q region locus 8**	**1.34**	**0.080**
10384458	Plek	pleckstrin	1.34	0.080
10557855	Trim72	tripartite motif-containing 72	1.34	0.080
10461614	Ms4a6c	membrane-spanning 4-domains, subfamily A, member 6C	1.34	0.074
10593233	Htr3a	5-hydroxytryptamine (serotonin) receptor 3A	1.34	0.098
10367582	Vip	vasoactive intestinal polypeptide	1.34	0.096
10474064	Trp53i11	transformation related protein 53 inducible protein 11	1.33	0.077
10388958	Evi2a	ecotropic viral integration site 2a	1.33	0.095
10574098	Nlrc5	NLR family, CARD domain containing 5	1.33	0.018
10420483	Phf11	PHD finger protein 11	1.33	0.014
10522388	Slc10a4	solute carrier family 10 (sodium/bile acid cotransporter family), member 4	1.33	0.008
10453057	Cyp1b1	cytochrome P450, family 1, subfamily b, polypeptide 1	1.33	0.080
10370721	**Sbno2**	**strawberry notch homolog 2 (Drosophila)**	**1.32**	**0.052**
10556244	Ipo7	importin 7	1.32	0.071
10378240	P2rx1	purinergic receptor P2X, ligand-gated ion channel, 1	1.32	0.095
10517513	**C1qc**	**complement component 1, q subcomponent, C chain**	**1.32**	**0.043**
10375574	Olfr1373	olfactory receptor 1373	1.32	0.056
10604175	Fam70a	family with sequence similarity 70, member A	1.32	0.004
10392410	Gm10838	predicted gene 10838	1.32	0.056
10442834	**Rpusd1**	**RNA pseudouridylate synthase domain containing 1**	**1.32**	**0.025**
10350977	4930523C07Ril	RIKEN cDNA 4930523C07 gene	1.32	0.060
10357516	**C4bp**	**complement component 4 binding protein**	**1.31**	**0.040**
10599562	1100001E04Ril	RIKEN cDNA 1100001E04 gene	1.31	0.049
10363224	Fabp7	fatty acid binding protein 7, brain	1.31	0.024
10442840	Mslnl	mesothelin-like	1.31	0.029
10561204	Itpkc	inositol 1,4,5-trisphosphate 3-kinase C	1.31	0.021
10460631	**Rela**	**v-rel reticuloendotheliosis viral oncogene homolog A (avian)**	**1.31**	**0.072**
10515399	**Plk3**	**polo-like kinase 3 (Drosophila)**	**1.31**	**0.063**
10607562	Cnksr2	connector enhancer of kinase suppressor of Ras 2	1.31	0.010
10601980	Mum1l1	melanoma associated antigen (mutated) 1-like 1	1.31	0.031
10576784	Cd209a	CD209a antigen	1.31	0.031
10445347	Clic5	chloride intracellular channel 5	1.31	0.049
10453272	**Zfp36l2**	**zinc finger protein 36, C3H type-like 2**	**1.30**	**0.084**
10530029	Lgi2	leucine-rich repeat LGI family, member 2	1.30	0.094
10516266	**Zc3h12a**	**zinc finger CCCH type containing 12A**	**1.30**	**0.012**
10401900	Sel1l	sel-1 suppressor of lin-12-like (C. elegans)	1.30	0.035
10572635	Sfn	stratifin	1.30	0.087
10574027	Mt1	metallothionein 1	1.30	0.035
10391577	**Hdac5**	**histone deacetylase 5**	**1.29**	**0.012**
10562709	Cd33	CD33 antigen	1.29	0.027
10362422	Trdn	triadin	1.29	0.019
10513666	**Akna**	**AT-hook transcription factor**	**1.29**	**0.049**
10603551	Cybb	cytochrome b-245, beta polypeptide	1.29	0.077
10389047	Accn1	amiloride-sensitive cation channel 1, neuronal (degenerin)	1.29	0.023
10572456	**Jund**	**Jun proto-oncogene related gene d**	**1.29**	**0.096**
10480027	Zbtb2	zinc finger and BTB domain containing 2	1.29	0.091
10530130	Rell1	RELT-like 1	1.29	0.063
10602081	Vsig1	V-set and immunoglobulin domain containing 1	1.29	0.033
10404885	Gmpr	guanosine monophosphate reductase	1.29	0.003
10445879	**Kcnh8**	**potassium voltage-gated channel, subfamily H (eag-related), member 8**	**1.29**	**0.022**
10604713	Arhgef6	Rac/Cdc42 guanine nucleotide exchange factor (GEF) 6	1.29	0.033
10434773	Rtp1	receptor transporter protein 1	1.29	0.003
10368970	**Prdm1**	**PR domain containing 1, with ZNF domain**	**1.29**	**0.028**
10411235	Iqgap2	IQ motif containing GTPase activating protein 2	1.29	0.018

10557326	**Il4ra**	**interleukin 4 receptor, alpha**	**1.28**	**0.068**
10360173	Slamf7	SLAM family member 7	1.28	0.073
10511416	Tox	thymocyte selection-associated high mobility group box	1.28	0.023
10363070	Gp49a	glycoprotein 49 A	1.28	0.064
10570388	Fam70b	family with sequence similarity 70, member B	1.28	0.012
10393620	**Cbx4**	**chromobox homolog 4 (Drosophila Pc class)**	**1.28**	**0.064**
10574023	Mt2	metallothionein 2	1.28	0.036
10364093	Derl3	Der1-like domain family, member 3	1.28	0.076
10425321	Apobec3	apolipoprotein B mRNA editing enzyme, catalytic polypeptide 3	1.28	0.094
10533180	**Ddx54**	**DEAD (Asp-Glu-Ala-Asp) box polypeptide 54**	**1.28**	**0.066**
10532085	**Tgfbr3**	**transforming growth factor, beta receptor III**	**1.28**	**0.017**
10595400	Gm8228	predicted gene 8228	1.28	0.045
10571601	Pdlim3	PDZ and LIM domain 3	1.28	0.013
10455942	A730017C20Ri	RIKEN cDNA A730017C20 gene	1.28	0.033
10495794	Pde5a	phosphodiesterase 5A, cGMP-specific	1.28	0.043
10369615	Srgn	serglycin	1.27	0.055
10405179	**S1pr3**	**sphingosine-1-phosphate receptor 3**	**1.27**	**0.012**
10356262	Gm7609	predicted gene 7609	1.27	0.069
10569393	R74862	expressed sequence R74862	1.27	0.065
10476395	**Bmp2**	**bone morphogenetic protein 2**	**1.27**	**0.046**
10375360	**Ebf1**	**early B-cell factor 1**	**1.27**	**0.043**
10405587	Tgfbi	transforming growth factor, beta induced	1.27	0.072
10358525	Hmcn1	hemicentin 1	1.27	0.035
10562192	Fxyd5	FXYD domain-containing ion transport regulator 5	1.27	0.058
10529937	Kcnip4	Kv channel interacting protein 4	1.27	0.084
10544660	Osbpl3	oxysterol binding protein-like 3	1.27	0.025
10552339	Vmn2r60	vomeronasal 2, receptor 60	1.27	0.082
10408359	Nrsn1	neurensin 1	1.27	0.028
10382653	Myo15b	myosin XVB	1.27	0.081
10523260	Shroom3	shroom family member 3	1.26	0.016
10413461	Erc2	ELKS/RAB6-interacting/CAST family member 2	1.26	0.073
10548030	Cd9	CD9 antigen	1.26	0.078
10604763	Arpc1b	actin related protein 2/3 complex, subunit 1B	1.26	0.002
10350733	Rgs16	regulator of G-protein signaling 16	1.26	0.088
10522530	Kit	kit oncogene	1.26	0.039
10387890	**Cxcl16**	**chemokine (C-X-C motif) ligand 16**	**1.26**	**0.042**
10566580	Gm4759	GTPase, very large interferon inducible 1 pseudogene	1.26	0.082
10365482	**Timp3**	**tissue inhibitor of metalloproteinase 3**	**1.26**	**0.054**
10462005	Tmem2	transmembrane protein 2	1.26	0.059
10399360	**Rhob**	**ras homolog gene family, member B**	**1.26**	**0.015**
10561516	Nfkbib	nuclear factor of kappa light polypeptide gene enhancer in B-cells inhibitor, bet	1.26	0.070
10407481	Pfkp	phosphofructokinase, platelet	1.26	0.075
10404071	Trim38	tripartite motif-containing 38	1.26	0.058
10556297	Adm	adrenomedullin	1.26	0.070
10527667	4930434E21Ri	RIKEN cDNA 4930434E21 gene	1.26	0.027
10541532	**Foxj2**	**forkhead box J2**	**1.26**	**0.007**
10460196	1810055G02Ri	RIKEN cDNA 1810055G02 gene	1.26	0.086
10600419	**Plxna3**	**plexin A3**	**1.26**	**0.035**
10526277	**Mlxipl**	**MLX interacting protein-like**	**1.26**	**0.095**
10375137	Kcnmb1	potassium large conductance calcium-activated channel, subfamily M, beta me	1.26	0.000
10439936	**Nfkbiz**	**nuclear factor of kappa light polypeptide gene enhancer in B-cells inhibit**	**1.26**	**0.060**
10458314	**Tmem173**	**transmembrane protein 173**	**1.25**	**0.047**
10538247	Npy	neuropeptide Y	1.25	0.053
10417561	Fam107a	family with sequence similarity 107, member A	1.25	0.011
10509030	**Runx3**	**runt related transcription factor 3**	**1.25**	**0.041**
10574102	Nlrc5	NLR family, CARD domain containing 5	1.25	0.098
10570741	**Defb1**	**defensin beta 1**	**1.25**	**0.074**
10358027	**Elf3**	**E74-like factor 3**	**1.25**	**0.046**
10461152	Snhg1	small nucleolar RNA host gene (non-protein coding) 1	1.25	0.077
10433776	**Snai2**	**snail homolog 2 (Drosophila)**	**1.25**	**0.020**
10555174	Lrrc32	leucine rich repeat containing 32	1.25	0.060
10466938	5033414D02Ri	RIKEN cDNA 5033414D02 gene	1.25	0.037
10591630	Dock6	dedicator of cytokinesis 6	1.25	0.075
10600836	Msn	moesin	1.25	0.048
10564290	**Klf13**	**Kruppel-like factor 13**	**1.25**	**0.069**
10345445	**Arid5a**	**AT rich interactive domain 5A (MRF1-like)**	**1.25**	**0.094**
10529264	**Spon2**	**spondin 2, extracellular matrix protein**	**1.25**	**0.029**
10555510	Pde2a	phosphodiesterase 2A, cGMP-stimulated	1.25	0.011
10395534	LOC100047081	hypothetical protein LOC100047081	1.25	0.003
10379518	**Ccl7**	**chemokine (C-C motif) ligand 7**	**1.25**	**0.031**
10423791	4930447A16Ri	RIKEN cDNA 4930447A16 gene	1.25	0.083
10574149	Nlrc5	NLR family, CARD domain containing 5	1.25	0.067
10444780	**H2-D1**	**histocompatibility 2, D region locus 1**	**1.25**	**0.013**
10435565	Hcls1	hematopoietic cell specific Lyn substrate 1	1.25	0.072
10554938	Rab30	RAB30, member RAS oncogene family	1.25	0.037
10415885	**Sox7**	**SRY-box containing gene 7**	**1.25**	**0.024**
10548899	Rerg	RAS-like, estrogen-regulated, growth-inhibitor	1.25	0.036
10567580	Igsf6	immunoglobulin superfamily, member 6	1.24	0.013
10473809	**Sfpi1**	**SFFV proviral integration 1**	**1.24**	**0.088**
10397145	Acot2	acyl-CoA thioesterase 2	1.24	0.035
10477169	**Id1**	**inhibitor of DNA binding 1**	**1.24**	**0.085**

10416566	Epsti1	epithelial stromal interaction 1 (breast)	1.24	0.032
10432404	Tuba1a	tubulin, alpha 1A	1.24	0.009
10562223	Fxyd3	FXYD domain-containing ion transport regulator 3	1.24	0.011
10564713	Mfge8	milk fat globule-EGF factor 8 protein	1.24	0.074
10484708	Olfr1160	olfactory receptor 1160	1.24	0.013
10400357	**Baz1a**	**bromodomain adjacent to zinc finger domain 1A**	**1.24**	**0.005**
10468898	**Lax1**	**lymphocyte transmembrane adaptor 1**	**1.24**	**0.043**
10411949	Rgs7bp	regulator of G-protein signalling 7 binding protein	1.24	0.029
10512830	Anks6	ankyrin repeat and sterile alpha motif domain containing 6	1.24	0.013
10430596	Unc84b	unc-84 homolog B (C. elegans)	1.24	0.057
10523190	9130213B05Rik	RIKEN cDNA 9130213B05 gene	1.24	0.011
10370780	Pcsk4	proprotein convertase subtilisin/kexin type 4	1.23	0.022
10418842	3425401B19Rik	RIKEN cDNA 3425401B19 gene	1.23	0.003
10368947	Aim1	absent in melanoma 1	1.23	0.042
10418835	Slc18a3	solute carrier family 18 (vesicular monoamine), member 3	1.23	0.001
10383891	Cabp7	calcium binding protein 7	1.23	0.087
10430649	**Cbx7**	**chromobox homolog 7**	**1.23**	**0.040**
10472199	Upp2	uridine phosphorylase 2	1.23	0.002
10376950	**Pmp22**	**peripheral myelin protein 22**	**1.23**	**0.002**
10376868	Trpv2	transient receptor potential cation channel, subfamily V, member 2	1.23	0.002
10576046	**Foxf1a**	**forkhead box F1a**	**1.23**	**0.014**
10427026	Grasp	GRP1 (general receptor for phosphoinositides 1)-associated scaffold protein	1.23	0.008
10458663	Dpysl3	dihydropyrimidinase-like 3	1.23	0.036
10521759	Slit2	slit homolog 2 (Drosophila)	1.23	0.054
10588203	Ky	kyphoscoliosis peptidase	1.23	0.032
10594540	Plekho2	pleckstrin homology domain containing, family O member 2	1.23	0.025
10450075	**H2-K1**	**histocompatibility 2, K1, K region**	**1.23**	**0.051**
10377265	Pik3r5	phosphoinositide-3-kinase, regulatory subunit 5, p101	1.23	0.014
10527441	Arpc1b	actin related protein 2/3 complex, subunit 1B	1.23	0.006
10444830	**H2-Q7**	**histocompatibility 2, Q region locus 7**	**1.23**	**0.043**
10492997	**Etv3**	**ets variant gene 3**	**1.23**	**0.074**
10377652	Gps2	G protein pathway suppressor 2	1.22	0.009
10507163	Cyp4a10	cytochrome P450, family 4, subfamily a, polypeptide 10	1.22	0.089
10398075	Serpina3n	serine (or cysteine) peptidase inhibitor, clade A, member 3N	1.22	0.042
10533751	Pitpnm2	phosphatidylinositol transfer protein, membrane-associated 2	1.22	0.057
10344879	A830018L16Rik	RIKEN cDNA A830018L16 gene	1.22	0.070
10553301	Ldha	lactate dehydrogenase A	1.22	0.004
10468311	Sh3pxd2a	SH3 and PX domains 2A	1.22	0.060
10503659	Epha7	Eph receptor A7	1.22	0.081
10358057	Shisa4	shisa homolog 4 (Xenopus laevis)	1.22	0.077
10522696	Arl9	ADP-ribosylation factor-like 9	1.22	0.010
10377547	**Kdm6b**	**KDM1 lysine (K)-specific demethylase 6B**	**1.22**	**0.043**
10449018	Haghl	hydroxyacylglutathione hydrolase-like	1.22	0.077
10567316	Tmc7	transmembrane channel-like gene family 7	1.22	0.028
10492469	**Mlf1**	**myeloid leukemia factor 1**	**1.22**	**0.056**
10597279	Ccrl2	chemokine (C-C motif) receptor-like 2	1.22	0.034
10590417	Kbtbd5	kelch repeat and BTB (POZ) domain containing 5	1.22	0.069
10412913	Gm8584	predicted gene 8584	1.22	0.002
10600886	Gpr165	G protein-coupled receptor 165	1.22	0.019
10577217	Gm7669	predicted gene 7669	1.22	0.030
10419416	3632451O06Rik	RIKEN cDNA 3632451O06 gene	1.22	0.031
10584628	**Thy1**	**thymus cell antigen 1, theta**	**1.22**	**0.090**
10458764	LOC100046618	similar to ribosomal protein	1.22	0.087
10449266	Itfg3	integrin alpha FG-GAP repeat containing 3	1.22	0.032
10456254	Nedd4l	neural precursor cell expressed, developmentally down-regulated gene 4-like	1.22	0.042
10353004	**Cks2**	**CDC28 protein kinase regulatory subunit 2**	**1.22**	**0.088**
10465278	Cdc42ep2	CDC42 effector protein (Rho GTPase binding) 2	1.22	0.052
10560685	**Bcl3**	**B-cell leukemia/lymphoma 3**	**1.22**	**0.001**
10547540	Mical3	microtubule associated monoxygenase, calponin and LIM domain containing 3	1.22	0.001
10436043	Gm7275	predicted gene 7275	1.22	0.098
10408677	Lyrm4	LYR motif containing 4	1.22	0.009
10436636	Ncam2	neural cell adhesion molecule 2	1.22	0.025
10502791	Ifi44	interferon-induced protein 44	1.22	0.093
10412537	B930046C15Rik	RIKEN cDNA B930046C15 gene	1.21	0.033
10388902	Lgals9	lectin, galactose binding, soluble 9	1.21	0.007
10462390	Cd274	CD274 antigen	1.21	0.046
10589076	Slc25a20	solute carrier family 25 (mitochondrial carnitine/acylcarnitine translocase), mem	1.21	0.075
10607870	**Tlr7**	**toll-like receptor 7**	**1.21**	**0.064**
10589192	Tmem89	transmembrane protein 89	1.21	0.093
10347364	Vil1	villin 1	1.21	0.056
10353844	Neurl3	neuralized homolog 3 homolog (Drosophila)	1.21	0.075
10408647	1810022C23Rik	RIKEN cDNA 1810022C23 gene	1.21	0.080
10426656	Prph	peripherin	1.21	0.016
10471882	Olfml2a	olfactomedin-like 2A	1.21	0.072
10426643	Prkag1	protein kinase, AMP-activated, gamma 1 non-catalytic subunit	1.21	0.080
10550274	**Meis3**	**Meis homeobox 3**	**1.21**	**0.022**
10360070	Fcer1g	Fc receptor, IgE, high affinity I, gamma polypeptide	1.21	0.041
10442968	Rgs11	regulator of G-protein signaling 11	1.21	0.065
10566132	**Rhog**	**ras homolog gene family, member G**	**1.21**	**0.068**
10373407	Esyt1	extended synaptotagmin-like protein 1	1.21	0.023
10356172	5033414K04Rik	RIKEN cDNA 5033414K04 gene	1.21	0.029

10437451	Fam100a	family with sequence similarity 100, member A	1.21	0.043
10587683	Bcl2a1a	B-cell leukemia/lymphoma 2 related protein A1a	1.21	0.098
10378681	Inpp5k	inositol polyphosphate 5-phosphatase K	1.21	0.028
10382797	Fam100b	family with sequence similarity 100, member B	1.21	0.016
10574104	Nlrc5	NLR family, CARD domain containing 5	1.21	0.026
10352576	**Esrrg**	**estrogen-related receptor gamma**	**1.21**	**0.027**
10348194	Efhd1	EF hand domain containing 1	1.21	0.020
10385768	Olfr1373	olfactory receptor 1373	1.21	0.078
10519346	1700109H08Rik	RIKEN cDNA 1700109H08 gene	1.20	0.081
10574135	Nlrc5	NLR family, CARD domain containing 5	1.20	0.039
10413710	Nt5dc2	5'-nucleotidase domain containing 2	1.20	0.075
10522208	Uchl1	ubiquitin carboxy-terminal hydrolase L1	1.20	0.033
10537819	Olfr438	olfactory receptor 438	1.20	0.083
10567355	Gprc5b	G protein-coupled receptor, family C, group 5, member B	1.20	0.061
10449284	**Dusp1**	**dual specificity phosphatase 1**	**1.20**	**0.062**
10592870	**Foxr1**	**forkhead box R1**	**1.20**	**0.015**
10551966	Hspb6	heat shock protein, alpha-crystallin-related, B6	1.20	0.092
10400926	Rtn1	reticulon 1	1.20	0.030
10573578	BC056474	cDNA sequence BC056474	1.20	0.041
10532180	Cplx1	complexin 1	1.20	0.009
10508454	Bsdc1	BSD domain containing 1	1.20	0.030
10373143	Mbd6	methyl-CpG binding domain protein 6	1.20	0.086
10564618	Fam174b	family with sequence similarity 174, member B	1.20	0.059
10417446	D830030K20Ri	RIKEN cDNA D830030K20 gene	1.20	0.019
10417452	D830030K20Ri	RIKEN cDNA D830030K20 gene	1.20	0.019
10600210	Slc6a8	solute carrier family 6 (neurotransmitter transporter, creatine), member 8	1.20	0.064
10385774	Olfr1371	olfactory receptor 1371	1.20	0.087
10451784	**Kcnh8**	**potassium voltage-gated channel, subfamily H (eag-related), member 8**	**1.20**	**0.030**
10405820	1810034E14Rik	RIKEN cDNA 1810034E14 gene	1.20	0.082
10534960	Gje1	gap junction membrane channel protein epsilon 1	1.20	0.063
10468893	Csf2ra	colony stimulating factor 2 receptor, alpha, low-affinity (granulocyte-macrophag	1.20	0.097
10451838	Slc5a7	solute carrier family 5 (choline transporter), member 7	1.20	0.090
10569707	Myadm	myeloid-associated differentiation marker	1.20	0.040
10485405	**Cd44**	**CD44 antigen**	**1.20**	**0.065**
10568174	Spn	sialophorin	1.20	0.061
10393058	H3f3b	H3 histone, family 3B	1.20	0.095
10534927	Pilra	paired immunoglobin-like type 2 receptor alpha	1.20	0.015
10500896	H3f3b	H3 histone, family 3B	1.20	0.075
10472923	Ak3l1	adenylate kinase 3-like 1	1.20	0.050
10509163	**Id3**	**inhibitor of DNA binding 3**	**1.20**	**0.045**
10586110	Cln6	ceroid-lipofuscinosis, neuronal 6	1.20	0.023
10379901	Bcas3	breast carcinoma amplified sequence 3	1.20	0.035
10368675	Marcks	myristoylated alanine rich protein kinase C substrate	1.20	0.099
10590389	Nktr	natural killer tumor recognition sequence	1.20	0.095
10401595	Rps6kl1	ribosomal protein S6 kinase-like 1	1.20	0.020
10366864	F420014N23Rik	RIKEN cDNA F420014N23 gene	1.20	0.073
10433114	Itga5	integrin alpha 5 (fibronectin receptor alpha)	1.20	0.080
10556828	Anks4b	ankyrin repeat and sterile alpha motif domain containing 4B	1.20	0.098
10360382	**Ifi204**	**interferon activated gene 204**	**1.20**	**0.068**
10463061	Gm5827	predicted gene 5827	1.20	0.045
10518812	**Camta1**	**calmodulin binding transcription activator 1**	**1.20**	**0.023**
10550067	**Zfp446**	**zinc finger protein 446**	**1.20**	**0.047**
10409118	Wnk2	WNK lysine deficient protein kinase 2	1.20	0.035
10479087	Stx16	syntaxin 16	-1.20	0.012
10346914	Fastkd2	FAST kinase domains 2	-1.20	0.071
10548194	Fkbp4	FK506 binding protein 4	-1.20	0.028
10354258	Uxs1	UDP-glucuronate decarboxylase 1	-1.20	0.051
10442458	Mlst8	MTOR associated protein, LST8 homolog (S. cerevisiae)	-1.20	0.015
10355037	Wdr12	WD repeat domain 12	-1.20	0.098
10360848	Mosc2	MOCO sulphurase C-terminal domain containing 2	-1.20	0.014
10489239	9430008C03Rik	RIKEN cDNA 9430008C03 gene	-1.20	0.053
10465804	Polr2g	polymerase (RNA) II (DNA directed) polypeptide G	-1.20	0.001
10457942	Syt4	synaptotagmin IV	-1.20	0.017
10399224	Kif3c	kinesin family member 3C	-1.20	0.010
10567173	Pik3c2a	phosphatidylinositol 3-kinase, C2 domain containing, alpha polypeptide	-1.20	0.081
10511843	1810074P20Rik	RIKEN cDNA 1810074P20 gene	-1.20	0.019
10567043	Rras2	related RAS viral (r-ras) oncogene homolog 2	-1.20	0.030
10594289	Glce	glucuronyl C5-epimerase	-1.20	0.009
10527940	Pftk1	PFTAIRE protein kinase 1	-1.20	0.022
10512391	Vcp	valosin containing protein	-1.20	0.006
10460102	1700034H14Rik	RIKEN cDNA 1700034H14 gene	-1.20	0.083
10498095	Cog6	component of oligomeric golgi complex 6	-1.20	0.006
10353871	Lman2l	lectin, mannose-binding 2-like	-1.20	0.029
10596207	Uba5	ubiquitin-like modifier activating enzyme 5	-1.20	0.015
10409786	1700013B16Rik	RIKEN cDNA 1700013B16 gene	-1.20	0.020
10376420	Gm12258	predicted gene 12258	-1.20	0.077
10350697	Nmnat2	nicotinamide nucleotide adenylyltransferase 2	-1.20	0.088
10562117	Ffar2	free fatty acid receptor 2	-1.20	0.010
10376803	Fam83g	family with sequence similarity 83, member G	-1.20	0.013

10514956	Scp2	sterol carrier protein 2, liver	-1.20	0.046
10423512	Fam173b	family with sequence similarity 173, member B	-1.20	0.007
10530652	Scfd2	Sec1 family domain containing 2	-1.20	0.001
10464445	Gm5521	predicted gene 5521	-1.21	0.087
10603533	Ssxb3	synovial sarcoma, X member B, breakpoint 3	-1.21	0.004
10498485	Slc33a1	solute carrier family 33 (acetyl-CoA transporter), member 1	-1.21	0.004
10601503	Dach2	dachshund 2 (Drosophila)	-1.21	0.089
10368511	Trmt11	tRNA methyltransferase 11 homolog (S. cerevisiae)	-1.21	0.061
10523206	Uso1	USO1 homolog, vesicle docking protein (yeast)	-1.21	0.007
10355464	Pecr	peroxisomal trans-2-enoyl-CoA reductase	-1.21	0.050
10360415	Grem2	gremlin 2 homolog, cysteine knot superfamily (Xenopus laevis)	-1.21	0.071
10503303	1110037F02Rik	RIKEN cDNA 1110037F02 gene	-1.21	0.028
10350473	B3galt2	UDP-Gal:betaGlcNAc beta 1,3-galactosyltransferase, polypeptide 2	-1.21	0.004
10601335	2610029G23Rik	RIKEN cDNA 2610029G23 gene	-1.21	0.032
10434675	Dnajb11	DnaJ (Hsp40) homolog, subfamily B, member 11	-1.21	0.036
10449989	Zfp422	zinc finger protein 422	-1.21	0.011
10441091	6530402D11Rik	RIKEN cDNA 6530402D11 gene	-1.21	0.034
10580870	Zfp319	zinc finger protein 319	-1.21	0.011
10582020	Gcsh	glycine cleavage system protein H (aminomethyl carrier)	-1.21	0.047
10384474	Pno1	partner of NOB1 homolog (S. cerevisiae)	-1.21	0.063
10462630	Pank1	pantothenate kinase 1	-1.21	0.010
10604226	C1galt1c1	C1GALT1-specific chaperone 1	-1.21	0.049
10410695	Rhobtb3	Rho-related BTB domain containing 3	-1.21	0.007
10554704	Mesdc2	mesoderm development candidate 2	-1.21	0.020
10423629	Pop1	processing of precursor 1, ribonuclease P/MRP family, (S. cerevisiae)	-1.21	0.058
10579969	Zfp330	zinc finger protein 330	-1.21	0.054
10390299	Pnpo	pyridoxine 5'-phosphate oxidase	-1.21	0.041
10436392	Cpox	coproporphyrinogen oxidase	-1.21	0.044
10518674	Rbp7	retinol binding protein 7, cellular	-1.21	0.008
10345368	D1Ertd448e	DNA segment, Chr 1, ERATO Doi 448, expressed	-1.21	0.002
10527920	Cyp51	cytochrome P450, family 51	-1.21	0.070
10603698	Gm1549	predicted gene 1549	-1.21	0.097
10545760	Paip2b	poly(A) binding protein interacting protein 2B	-1.22	0.007
10401968	Galc	galactosylceramidase	-1.22	0.037
10578916	Sc4mol	sterol-C4-methyl oxidase-like	-1.22	0.030
10472757	Cybrd1	cytochrome b reductase 1	-1.22	0.035
10488090	Tasp1	taspase, threonine aspartase 1	-1.22	0.018
10574899	Nutf2	nuclear transport factor 2	-1.22	0.026
10502105	**Egf**	**epidermal growth factor**	**-1.22**	**0.040**
10503010	Fpgt	fucose-1-phosphate guanylyltransferase	-1.22	0.060
10453436	Mcfd2	multiple coagulation factor deficiency 2	-1.22	0.021
10367481	Olfr776	olfactory receptor 776	-1.22	0.047
10607156	Dcx	doublecortin	-1.22	0.049
10395739	Srp54b	signal recognition particle 54b	-1.22	0.004
10500412	Gpr89	G protein-coupled receptor 89	-1.22	0.032
10599951	1110012L19Rik	RIKEN cDNA 1110012L19 gene	-1.22	0.046
10405488	Tmed9	transmembrane emp24 protein transport domain containing 9	-1.22	0.002
10540911	Tsen2	tRNA splicing endonuclease 2 homolog (S. cerevisiae)	-1.22	0.079
10408741	Txndc5	thioredoxin domain containing 5	-1.22	0.010
10548367	Clec1a	C-type lectin domain family 1, member a	-1.22	0.052
10367497	Olfr787	olfactory receptor 787	-1.22	0.044
10606835	Bex2	brain expressed X-linked 2	-1.22	0.071
10585395	Siva1	SIVA1, apoptosis-inducing factor	-1.22	0.046
10605522	Gm7173	predicted gene 7173	-1.23	0.045
10429666	Pycrl	pyrroline-5-carboxylate reductase-like	-1.23	0.078
10415262	Dcaf11	DDB1 and CUL4 associated factor 11	-1.23	0.001
10350337	A130050O07Rik	RIKEN cDNA A130050O07 gene	-1.23	0.031
10456904	Pstpip2	proline-serine-threonine phosphatase-interacting protein 2	-1.23	0.072
10352829	A130010J15Rik	RIKEN cDNA A130010J15 gene	-1.23	0.048
10386359	Guk1	guanylate kinase 1	-1.23	0.004
10549041	Slco1a5	solute carrier organic anion transporter family, member 1a5	-1.23	0.023
10473190	Dnajc10	DnaJ (Hsp40) homolog, subfamily C, member 10	-1.23	0.059
10526049	Mrps17	mitochondrial ribosomal protein S17	-1.23	0.049
10581538	Nqo1	NAD(P)H dehydrogenase, quinone 1	-1.23	0.031
10554863	Sytl2	synaptotagmin-like 2	-1.23	0.026
10479463	Slc17a9	solute carrier family 17, member 9	-1.23	0.082
10444439	Atf6b	activating transcription factor 6 beta	-1.23	0.027
10526514	Cldn15	claudin 15	-1.23	0.066
10496324	Slc39a8	solute carrier family 39 (metal ion transporter), member 8	-1.23	0.030
10563114	Snord32a	small nucleolar RNA, C/D box 32A	-1.24	0.039
10387797	Bcl6b	B-cell CLL/lymphoma 6, member B	-1.24	0.086
10494369	Sf3b4	splicing factor 3b, subunit 4	-1.24	0.082
10467162	Pank1	pantothenate kinase 1	-1.24	0.017
10369806	1700040L02Rik	RIKEN cDNA 1700040L02 gene	-1.24	0.046
10521979	Gm6632	predicted gene 6632	-1.24	0.000
10389581	Ypel2	yippee-like 2 (Drosophila)	-1.24	0.079
10597871	Higd1a	HIG1 domain family, member 1A	-1.24	0.067
10459405	Nars	asparaginyl-tRNA synthetase	-1.24	0.009
10426891	Mettl7a1	methyltransferase like 7A1	-1.25	0.038
10496605	Ccbl2	cysteine conjugate-beta lyase 2	-1.25	0.019
10412900	Nkiras1	NFKB inhibitor interacting Ras-like protein 1	-1.25	0.006

10571728	Rwdd4a	RWD domain containing 4A	-1.25	0.002
10390505	Snora21	small nucleolar RNA, H/ACA box 21	-1.25	0.041
10360076	Ndufs2	NADH dehydrogenase (ubiquinone) Fe-S protein 2	-1.25	0.000
10513061	Ctnnal1	catenin (cadherin associated protein), alpha-like 1	-1.25	0.008
10384968	Bod1	biorientation of chromosomes in cell division 1	-1.25	0.041
10423030	Prlr	prolactin receptor	-1.25	0.012
10495549	Dbt	dihydrolipoamide branched chain transacylase E2	-1.25	0.083
10532241	Slc26a1	solute carrier family 26 (sulfate transporter), member 1	-1.25	0.088
10545255	Rpia	ribose 5-phosphate isomerase A	-1.25	0.007
10555041	Alg8	asparagine-linked glycosylation 8 homolog (yeast, alpha-1,3-glucosyltransferas	-1.25	0.094
10459747	Mapk4	mitogen-activated protein kinase 4	-1.25	0.009
10509267	Wnt4	wingless-related MMTV integration site 4	-1.25	0.059
10363498	Ppa1	pyrophosphatase (inorganic) 1	-1.25	0.007
10430748	Rangap1	RAN GTPase activating protein 1	-1.26	0.064
10439409	BC031361	cDNA sequence BC031361	-1.26	0.029
10440566	Rnf160	ring finger protein 160	-1.26	0.090
10595466	Pgm3	phosphoglucomutase 3	-1.26	0.006
10590267	Snora62	small nucleolar RNA, H/ACA box 62	-1.26	0.082
10397553	Gm16368	eukaryotic translation initiation factor 1A pseudogene	-1.26	0.006
10601701	Tmem35	transmembrane protein 35	-1.26	0.006
10589413	Nme6	non-metastatic cells 6, protein expressed in (nucleoside-diphosphate kinase)	-1.26	0.021
10376929	Fam18b	family with sequence similarity 18, member B	-1.26	0.001
10359826	Uqcr	ubiquinol-cytochrome c reductase (6.4kD) subunit	-1.26	0.003
10397984	Ppp4r4	protein phosphatase 4, regulatory subunit 4	-1.26	0.010
10520080	Rint1	RAD50 interactor 1	-1.27	0.088
10538253	Mpp6	membrane protein, palmitoylated 6 (MAGUK p55 subfamily member 6)	-1.27	0.016
10586907	Mns1	meiosis-specific nuclear structural protein 1	-1.27	0.029
10605431	Rab39b	RAB39B, member RAS oncogene family	-1.27	0.047
10517147	Dhdds	dehydrodolichyl diphosphate synthase	-1.28	0.008
10580233	Gcdh	glutaryl-Coenzyme A dehydrogenase	-1.28	0.000
10476702	Sec23b	SEC23B (S. cerevisiae)	-1.28	0.009
10500345	Terc	telomerase RNA component	-1.28	0.076
10588357	Acad11	acyl-Coenzyme A dehydrogenase family, member 11	-1.28	0.000
10395628	Scfd1	Sec1 family domain containing 1	-1.28	0.008
10482762	Idi1	isopentenyl-diphosphate delta isomerase	-1.29	0.077
10549025	Slco1a6	solute carrier organic anion transporter family, member 1a6	-1.29	0.083
10595570	Slc25a40	solute carrier family 25, member 40	-1.30	0.020
10406287	Ttc37	tetratricopeptide repeat domain 37	-1.30	0.010
10508721	Snora44	small nucleolar RNA, H/ACA box 44	-1.30	0.080
10542477	Pik3c2g	phosphatidylinositol 3-kinase, C2 domain containing, gamma polypeptide	-1.30	0.095
10574415	1700047G07Ril	RIKEN cDNA 1700047G07 gene	-1.31	0.064
10473250	Mrpl18	mitochondrial ribosomal protein L18	-1.31	0.002
10403413	Idi1	isopentenyl-diphosphate delta isomerase	-1.31	0.050
10379866	Car4	carbonic anhydrase 4	-1.31	0.061
10575993	6430548M08Ri	RIKEN cDNA 6430548M08 gene	-1.32	0.045
10422608	Oxct1	3-oxoacid CoA transferase 1	-1.32	0.003
10457205	Crem	cAMP responsive element modulator	-1.33	0.010
10423049	Prlr	prolactin receptor	-1.33	0.012
10576216	Rpl13	ribosomal protein L13	-1.34	0.097
10360145	B930036N10Ri	RIKEN cDNA B930036N10 gene	-1.34	0.071
10448803	Hn1l	hematological and neurological expressed 1-like	-1.34	0.003
10577641	1810011O10Ril	RIKEN cDNA 1810011O10 gene	-1.35	0.056
10602198	Pak3	p21 protein (Cdc42/Rac)-activated kinase 3	-1.35	0.004
10563110	Snord34	small nucleolar RNA, C/D box 34	-1.36	0.083
10353034	Snord87	small nucleolar RNA, C/D box 87	-1.38	0.084
10603116	Asb11	ankyrin repeat and SOCS box-containing 11	-1.38	0.067
10565813	Gm5774	predicted gene 5774	-1.39	0.013
10380063	Rnu3b1	U3B small nuclear RNA 1	-1.39	0.010
10380061	Rnu3b1	U3B small nuclear RNA 1	-1.39	0.010
10380065	Rnu3b1	U3B small nuclear RNA 1	-1.39	0.010
10380059	Rnu3b1	U3B small nuclear RNA 1	-1.39	0.010
10606389	Gm379	predicted gene 379	-1.39	0.003
10409616	Spock1	sparc/osteonectin, cwcv and kazal-like domains proteoglycan 1	-1.40	0.008
10591169	Muc16	mucin 16	-1.41	0.042
10570432	Snora3	small nucleolar RNA, H/ACA box 3	-1.43	0.004
10556206	Snora3	small nucleolar RNA, H/ACA box 3	-1.45	0.005
10527963	Gm10484	predicted gene 10484	-1.47	0.088
10565811	Gm5775	predicted gene 5775	-1.49	0.003
10353036	Gm10567	predicted gene 10567	-1.49	0.049
10360443	Fh1	fumarate hydratase 1	-1.49	0.004
10549594	Ttyh1	tweety homolog 1 (Drosophila)	-1.51	0.027
10450363	Snord52	small nucleolar RNA, C/D box 52	-1.53	0.003
10563099	Snord35b	small nucleolar RNA, C/D box 35B	-1.53	0.014
10441813	Tcp1	t-complex protein 1	-1.56	0.045
10441680	Pde10a	phosphodiesterase 10A	-1.56	0.035
10545192	Rprl1	ribonuclease P RNA-like 1	-1.57	0.028
10558919	Snora52	small nucleolar RNA, H/ACA box 52	-1.58	0.060
10604076	Snora69	small nucleolar RNA, H/ACA box 69	-1.58	0.100
10377429	Snord118	small nucleolar RNA, C/D box 118	-1.59	0.071
10399428	Snord118	small nucleolar RNA, C/D box 118	-1.59	0.071
10556463	Arntl	aryl hydrocarbon receptor nuclear translocator-like	-1.62	0.100

10491058	Rprl2	ribonuclease P RNA-like 2	-1.63	0.033
10412394	Nnt	nicotinamide nucleotide transhydrogenase	-1.64	0.002
10571815	Gpm6a	glycoprotein m6a	-1.71	0.015
10439500	Upk1b	uroplakin 1B	-1.72	0.054
10563108	Snord35a	small nucleolar RNA, C/D box 35A	-1.76	0.062
10547073	Snora7a	small nucleolar RNA, H/ACA box 7A	-1.81	0.076
10512487	Rmrp	RNA component of mitochondrial RNAase P	-1.82	0.026
10454807	Snora74a	small nucleolar RNA, H/ACA box 74A	-1.92	0.031
10455015	Vaultrc5	vault RNA component 5	-2.02	0.082
10362674	Rnu3a	U3A small nuclear RNA	-2.07	0.016
10603736	Rnu2 // Rnu2	U2 small nuclear RNA // U2 small nuclear RNA // U2 small nuclear RNA // U2	-2.18	0.067
10499130	Rnu73b	U73B small nuclear RNA	-2.18	0.088
10578688	Rnu2 // Rnu2	U2 small nuclear RNA // U2 small nuclear RNA // U2 small nuclear RNA // U2	-2.25	0.069
10544523	Rny1	RNA, Y1 small cytoplasmic, Ro-associated	-2.28	0.045
10381472	Rnu2 // Rnu2	U2 small nuclear RNA // U2 small nuclear RNA // U2 small nuclear RNA // U2	-2.30	0.063
10391488	Rnu2 // Rnu2	U2 small nuclear RNA // U2 small nuclear RNA // U2 small nuclear RNA // U2	-2.30	0.063
10381470	Rnu2 // Rnu2	U2 small nuclear RNA // U2 small nuclear RNA // U2 small nuclear RNA // U2	-2.30	0.063
10381460	Rnu2 // Rnu2	U2 small nuclear RNA // U2 small nuclear RNA // U2 small nuclear RNA // U2	-2.30	0.063
10381458	Rnu2 // Rnu2	U2 small nuclear RNA // U2 small nuclear RNA // U2 small nuclear RNA // U2	-2.35	0.063

8.6 Manuscript 1: Tenascin-C promotes tumor angiogenesis and metastasis through repression of Dickkopf-1

Tenascin-C Promotes Tumor Angiogenesis and Metastasis through Repression of Dickkopf-1

Falk Saupe[1a], Isabelle Gasser[1a], Yundan Jia[1a,2], Anja Heinke[1b], Martial Kammerer[1b], Thomas Hussenet[1], Marija Marko[1], Olivier Lefebvre[1], Michael van der Heyden[1], Monika Hegi[3], Ruslan Hlushchuk[4], Jessica Kant[1], Wentao Huang[2], Anne-Catherine Feutz[2], Patricia Simon-Assmann[1], Michèle Kedinger[1], Valentin Djonov[4], Gerhard Christofori[5] and Gertraud Orend[1,2]*

a: equal contribution as first author

b: equal contribution as second author

* corresponding author, Phone: 33 (0)3 88 27 53 55, Fax:33 (0)3 88 26 35 38, E-mail: gertraud.orend@inserm.u-strasbg.fr

[1] Inserm, U682, Strasbourg, F-67200 France, University of Strasbourg, CHRU Strasbourg, Department of Molecular Biology, Strasbourg, 67200 France.

[2] Institute of Biochemistry and Genetics, Department of Biomedicine, University of Basel, Switzerland, team G. Orend

[3] Centre Hospitalier Universitaire Vaudois (CHUV), University Lausanne, Switzerland

[4] Department of Medicine, Gross Anatomy and Vascular Biology, University of Fribourg, Fribourg, Switzerland

[5] Institute of Biochemistry and Genetics, Department of Biomedicine, University of Basel, Switzerland, team G. Christofori

Characters (with spaces): 43`870

Abstract

The tumor microenvironment is instrumental in cancer progression. The extracellular matrix molecule tenascin-C (TNC) is a major component of the cancer specific matrix and high TNC expression is linked to bad prognosis in several cancers. To delineate TNC's functions in cancer, we established transgenic tumor mouse lines with varying levels of TNC expression and compared sporadic neuroendocrine tumor formation in abundance or absence of TNC. We show that TNC promotes tumor angiogenesis, carcinoma progression and lung micrometastasis formation. TNC represses the Dickkopf-1 (DKK1) promoter and induces Wnt target genes in TNC transgenic tumors and in cultured cells. While overexpression of DKK1 does not affect proliferation of tumor cells, it compromises the formation of vascularised tumors. Thus TNC-induced repression of DKK1 in tumor cells exerts a paracrine effect on the tumor microenvironment. Our results implicate canonical Wnt signalling as underlying mechanism for TNC-mediated promotion of tumor angiogenesis and subsequent metastasis. The transgenic cancer models will be useful to evaluate the efficacy of therapeutic approaches targeting TNC and downstream signalling pathways for repressing tumor angiogenesis and metastasis.

Key words: Angiogenesis, Dickkopf-1, metastasis, tenascin-C, Wnt signalling

Running title: Tumor progression by tenascin-C through DKK1 repression

Introduction

Manifestation of cancer requires many steps in which the microenvironment plays an essential role (Bissell and Labarge, 2005). Cells with oncogenic mutations do not readily cause cancer, a phenomenon known as tumor dormancy (Aguirre-Ghiso, 2007; Folkman and Kalluri, 2004). Angiogenesis presents an important step in awakening quiescent tumors and in promoting their development into malignant cancers (Almog 2010). Many factors are driving angiogenesis but the early events in tumor angiogenesis are poorly understood. Tumor cells secrete soluble factors that attract endothelial cells (EC) and EC progenitors. Blood and lymphatic EC invade the tumor tissue and establish a neovasculature within the tumor which provides the tumor with a connection to the blood circulation and the lymphatic vessel system. These routes may be used by disseminating cancer cells to seed metastasis in distant organs (Bergers and Benjamin, 2003; Kerbel, 2008). Thus in addition to the cancer cells other cell types and the extracellular matrix (ECM) constitute a major fraction of cancer tissue and contribute to tumor angiogenesis and metastasis.

An important component of the tumor specific ECM is tenascin-C (TNC). TNC is prominently expressed in the tumor microenvironment and plays a promoting role in malignant tumor progression (Midwood and Orend, 2009). TNC is causally linked to lung metastasis in experimental murine breast cancer (Calvo et al., 2008; Tavazoie et al., 2008) and melanoma (Fukunaga-Kalabis et al., 2010) models. Moreover, TNC is amongst a few genes with predictive value in glioma malignancy (Colman et al., 2010) and in human breast cancer metastasis to the lung (Minn et al., 2005). High levels of TNC are linked to tamoxifen resistance in breast cancer (Helleman et al., 2008). Although TNC is now well linked to cancer progression, and first mechanistic insights have been obtained (Midwood and Orend, 2009; Orend, 2005; Orend and Chiquet-Ehrismann, 2006; Tavazoie et al., 2008), it is still unknown how TNC promotes tumor angiogenesis and metastasis.

Since no *in vivo* model with TNC overexpression existed that would allow to address the role of TNC in tumor progression, here we generated mouse lines with different expression levels of TNC (overexpression, wildtype, knock out) in the neuroendocrine Rip1Tag2 (RT2) tumorigenesis model (Hanahan, 1985). In RT2 mice, oncogenic simian virus 40 T-antigen (SV40Tag) is expressed under the control of the rat insulin II promoter in the insulin-producing β-cells of the islets of Langerhans. SV40Tag sequesters and represses the function of the two tumor suppressor gene products p53 and pRb, thus initiating transformation and hyperplasia of β-cells, which in turn triggers angiogenesis and insulinoma formation in a reproducible and sequential manner (Hanahan, 1985). This model recapitulates multistage tumorigenesis as observed in a large fraction of human cancers (Nevins, 2001; Pipas and Levine, 2001).

Here, we demonstrate that TNC promotes tumor angiogenesis and tumor progression to metastasizing carcinoma. We provide a mechanistic basis for TNC's function by showing that TNC induces canonical Wnt signalling and the expression of specific Wnt target genes through repression of the soluble inhibitor Dickkopf-1 (DKK1). The described mechanism potentially applies to malignancy in human gliomas where high TNC expression correlates with low DKK1 and high Wnt target gene expression in a subset of glioblastoma (GBM) grade IV tumors. Thus, TNC and DKK1 could be attractive therapeutic targets for blocking tumor angiogenesis, tumor cell dissemination and metastasis.

Results

Tenascin-C promotes proliferation and carcinoma formation in a stochastic neuroendocrine tumor model

To determine the role of TNC in tumor onset and progression, we utilized the murine RT2 insulinoma model to generate double-transgenic mice with overexpression of human TNC. For the generation of RipTNC single-transgenic mice, the cDNA of human TNC was

cloned downstream of the rat insulin II promoter (**Suppl. Fig. 1**). Transgenic RipTNC mice ectopically expressed the human TNC protein in β-cells of the pancreas (**Fig. 1A**), were healthy and fertile and did not exhibit obvious alterations in tissue morphology. Pancreatic islets normally displayed glucagon-positive α-cells surrounding β-cells. RipTNC males also exhibited normal blood glucose levels after starvation (not shown). Thus, ectopic expression of TNC did not appear to interfere with the function of the endocrine pancreas in RipTNC mice.

RT2/TNC double-transgenic mice were generated by breeding. Tumors of double-transgenic mice expressed human TNC (**Fig. 1A**). To determine a potential effect of TNC on tumor onset, we analysed whether islet size, which correlates with the tumorigenic state (Hanahan, 1985), was different between RT2/TNC and RT2 mice. We measured islet diameter on tissue sections and observed that at 10 weeks the ratio of angiogenic and tumorigenic islets (> 0.5 mm) over that of normal and hyperplastic islets (< 0.5 mm) was higher in RT2/TNC (0.8) than in RT2 control mice (0.4) and was close to statistical significance ($p = 0.06$) (**Suppl. Table 1**). At 12 weeks there was no difference in tumor number (**Fig. 1B**) or tumor volume (**Fig. 1C**) detectable between genotypes.

Next, we addressed whether ectopically expressed TNC had an effect on apoptosis and proliferation. Staining for cleaved caspase-3, a marker of apoptotic cells, did not reveal differences between tumors from 12 week old RT2/TNC and RT2 mice (not shown). Upon immunofluorescent staining for the proliferation marker phospho-histone-H3 (P-H3) followed by quantification, we noticed that tumors of RT2/TNC mice exhibited about 1.7-fold more proliferating cells than those from RT2 mice (**Fig. 1D**).

To investigate whether TNC potentially influenced tumor invasion, we determined the percentage of carcinomas amongst tumors of RT2 and RT2/TNC mice using invasion of β-tumor cells into the exocrine pancreas, the lack of a continuous basement membrane and the presence of atypical nuclei as parameters for carcinomas. We observed that the

frequency of carcinomas and the ratio of carcinoma versus adenoma was higher in tumors of RT2/TNC mice (1.8) than in RT2 controls (0.8) (**Fig. 1E, Suppl. Table 2**).
In summary, in the spontaneous insulinoma model, ectopically expressed TNC promoted tumor cell proliferation and invasion.

Tenascin-C promotes tumor angiogenesis

We addressed the role of TNC during tumor angiogenesis by quantification of CD31-positive cells in tumor sections of both genotypes (**Fig. 2A**). The number of CD31-positive endothelial cells (EC) turned out to be 1.9-fold (10 weeks) and 2.2-fold (12 weeks) higher in tumors of RT2/TNC mice than in tumors of RT2 controls (**Fig. 2B, C**).

To determine a potential effect of TNC on vessel anatomy we investigated Mercox corrosion casts of the vasculature by scanning electron microscopy and observed that vessels of RT2/TNC tumors were very different to that of RT2 control tumors; vessels appeared larger, more dilated and disorganized (**Fig. 2D**).

A potential angiogenesis-promoting effect of TNC was addressed in the chick chorio-allantoic membrane (CAM) assay. Compared to control treatment purified TNC increased the number of vessels to a similar extent as PDGF-BB, a known angiogenic growth factor (**Fig. 2E**).
Together these data demonstrate that ectopically expressed TNC promoted angiogenesis in spontaneously arising tumors generating vessels with an abnormal morphology.

Tenascin-C increases lung micrometastasis

Since knock down of TNC reduced the ability of breast cancer cells (Calvo et al., 2008; Tavazoie et al., 2008) and melanoma cells (Fukunaga-Kalabis et al., 2010) to form lung metastasis in immune-compromised xenograft models we investigated whether expression levels of TNC had an effect on metastasis in RT2 tumor mice. In a C57Bl6 background, RT2 mice usually do not exhibit macrometastasis (Hanahan, 1985; our

result). Therefore, we determined potentially arising micrometastases in various organs (heart, liver, lung) of 12 to 14 week old tumor-bearing mice by qRT-PCR for insulin. In contrast to the background levels of insulin mRNA in lungs of control RipTNC and wildtype mice and in hearts of RT2/TNC mice (not shown), a strong insulin-specific signal was observed in livers and lungs of RT2 and RT2/TNC mice. Yet, while insulin expression of micrometastatic β-tumor cells was indistinguishable between liver tissues of RT2 and RT2/TNC mice (not shown), insulin levels in lungs of RT2/TNC double-transgenic mice were 6.5-fold higher in comparison to lungs of RT2 single-transgenic mice (**Fig. 3A**). This result suggests that ectopically expressed TNC enhanced lung but not liver metastasis.

In RT2/TNC-/- mice we investigated whether the absence of TNC had an impact on metastasis. Analysis of insulin expression by qRT-PCR revealed 10-fold lower insulin levels in the lungs of RT2/TNC-/- mice than in RT2 mice carrying one intact TNC allele (RT2/TNC+/-, **Fig. 3B**). Overall, insulin expression levels were lower (close to background) in lungs of tumor mice with no transgenic TNC expression. Moreover, less RT2/TNC-/- (4/13) mice exhibited significant insulin expression and thus less micrometastasis than RT2/TNC+/- littermates (8/13).

To determine whether the insulin-positive signals were indeed derived from tumor cells that had colonized the lung, we stained sections of lungs for insulin and could detect a considerable number of insulinoma cells in clusters of 50 and more cells within the lung parenchyma of RT2/TNC mice by immunofluorescence and histology (**Fig. 3C**).

Nuclear localization of β-catenin in RT2/TNC tumors

In search for a mechanism that could explain tumor progression by TNC, we investigated a potential link of TNC to Wnt signalling in RT2/TNC tumors, since Wnt signalling was activated by a TNC substratum in cultured GBM cells (Ruiz et al., 2004). Determining expression of β-catenin revealed a profound difference between tumors of the two

genotypes; in contrast to exclusively membraneous β-catenin in RT2 control tumors, in RT2/TNC tumors β-catenin was also found in the nucleus of cells inside the tumor and at the invading tumor front (**Fig. 4A, B**). In contrast, no nuclear β-catenin was found in RT2 tumors (**Fig. 4A**). Confocal microscopic analysis confirmed that the β-catenin signal was indeed nuclear (**Fig. 2C**, inlet). Together, these results demonstrate that in a tumor context with forced expression of TNC, β-catenin was stabilized and translocated into the nucleus.

Tenascin-C impact on Wnt signalling and DKK1 expression in RT2/TNC tumors

In RT2/TNC tumors we determined expression of Wnt target genes by qRT-PCR on RNA extracted from isolated tumors. We observed that expression of cyclin D1 (2.5-fold), cyclin D2 (1.6-fold), CD44 (1.8-fold) and Slug (1.8-fold) was significantly increased in small still mostly differentiated tumors of RT2/TNC mice over that in RT2 controls (**Fig. 5A, Suppl. Table 3**). This was in contrast to other Wnt target genes (c-myc, Id2 and Lgr5) which were not elevated (not shown). These results suggest induction of a subset of Wnt target genes in a TNC-dependent manner in nascent carcinomas potentially driving progression of adenomas into carcinomas.

To elucidate whether TNC potentially activated Wnt signalling through DKK1 repression in RT2/TNC tumors*,* as had been demonstrated in cultured GBM cells (Ruiz et al., 2004), we determined DKK1 levels in RT2 tumors by qRT-PCR. In RT2/TNC mice, 7-times more tumors (50%) lacked DKK1 expression as compared to RT2 mice (7.1%) (**Fig. 5B**). In tumors with detectable DKK1 expression, the levels were 3.2-fold reduced in RT2/TNC mice in comparison to RT2 controls (**Fig. 5C, Suppl. Table 3**). Moreover, in RT2 tumors with only one TNC allele DKK1 levels were significantly lower (2-fold) than in RT2/TNC-/- tumors completely lacking TNC (**Fig. 5D**), which suggests that expression of TNC and DKK1 are inversely linked.

Impact of tenascin-C on DKK1 expression and Wnt signalling in cultured tumor cells

We investigated DKK1 mRNA levels in various cultured cancer cells that were grown on fibronectin (FN) and on FN/TNC, a valid condition to investigate TNC functions as previously described (Chiquet-Ehrismann, 1990; Huang et al., 2001). We observed that in T98G cells, DKK1 levels exhibited 20-fold repression after 5h and 24h of culture in the presence of TNC. DKK1 levels remained more than 5-times lower over a period of 12 days representing 80 - 95% repression (**Fig. 6A**). Although DKK1 protein levels still remained high after 5h, they were reduced after 1, 2 and 6 days on the TNC containing substratum (**Fig. 6B**).

We determined whether DKK1 repression is a general response of tumor cells on a TNC substratum. Therefore we compared expression of DKK1 in T98G cells with that in KRIB osteosarcoma, MCF7 and MDA-MB435 breast carcinoma and Caco-2 colon cancer cells. We observed that in all tested tumor cells DKK1 expression was lowered ranging from 23.2 - fold (KRIB) to 2.8 - fold (MCF7) 24h after plating on FN/TNC (**Fig. 6C**).

To address whether a TNC substratum had an effect on DKK1 promoter activity we determined DKK1 promoter-driven luciferase expression. Therefore we cloned a 3.0 kbp DKK1 promoter sequence upstream of the transcriptional start site in front of the luciferase gene. This reporter construct was used to measure luciferase activity upon transfection into T98G cells in the presence or absence of TNC. On a FN substratum luciferase expression was high which was in contrast to growth on FN/TNC where luciferase expression driven by the DKK1 promoter was significantly and more than 2.5-fold reduced in comparison to FN (**Fig. 6E**). This suggests that cell adhesion to TNC blocked transcription of DKK1.

We investigated expression of Wnt target genes on a TNC substratum by qRT-PCR. Whereas expression of some Wnt target genes (c-myc, cyclin D1, cyclin D2, CD44, Lgr5)

was not elevated (not shown), Id2 and FN levels were increased on the TNC substratum in T98G cells up to 3.4- and 2.6-fold at 7 and 12 days of culture, respectively (**Fig. 6D**). Slug was also induced in the presence of TNC in a delayed response up to 2.1-fold and 2.4-fold after 7 and 12 days, respectively. To investigate induction of Wnt signalling by TNC in more detail we determined expression of Wnt target genes in other cell lines. Whereas in MDA-MB435 cells no induction by TNC was noted, in KRIB cells on a TNC substratum an increased expression of the Wnt target genes Sox4 (van der Flier et al., 2007) (2.1-fold) at 24h and of Slug (2.4-fold) and FN (2.2-fold) at 6 days was observed (**Suppl. Table 4**). This was in contrast to CD44, Id2, c-myc, Lgr5 and cyclin D1 that were not elevated in KRIB cells (not shown).

To address whether low DKK1 levels were responsible for derepression and activation of Wnt signalling by TNC we engineered T98G cells stably overexpressing DKK1 (**Fig. 6F**). Upon plating of T98G:DKK1 cells on FN/TNC for 24h we determined Wnt target gene expression and observed that Id2 dropped to levels as on FN (**Fig. 6G**) which was in contrast to parental cells with an elevated expression of Id2 on FN/TNC. This result suggests that expression of Id2 is regulated by a TNC substratum through DKK1.

Together our data had revealed that in RT2 tumors TNC and DKK1 are inversely expressed and that in cultured tumor cells a TNC substratum represses DKK1 transcription through promoter inhibition in an early and sustained manner which results in the induction of Wnt target genes.

Role of DKK1 in proliferation, migration, angiogenesis and tumorigenesis

A potential functional link between TNC, DKK1 repression and tumorigenesis was further addressed in a xenograft model with DKK1 overexpressing tumor cells (T98G, KRIB) that we had generated (**Fig. 6F, 7A**). First we determined whether high DKK1 expression had an impact on proliferation and noticed that proliferation was indistinguishable between parental and DKK1 overexpressing KRIB (**Fig. 7B**) and T98G cells (data not shown). In a wound closure migration assay we investigated whether ectopically expressed DKK1 had

an impact on cell migration. KRIB cells migrated to close the scratched area in 13h, while KRIB:DKK1 cells were significantly retarded to do so (**Fig. 7C**).

Parental and DKK1 overexpressing cells were subcutaneously grafted into nude mice. Whereas T98G cells failed to induce tumors, KRIB cells induced tumors with 100% penetrance independent of the DKK1 expression levels. But KRIB tumors overexpressing DKK1 were highly necrotic (not shown) and remained significantly smaller (15.1 mm^3) than tumors originating from parental KRIB cells (591.3 mm^3) (**Fig. 7D**). By staining for KI67 we noticed that DKK1 overexpressing tumor cells were nevertheless proliferative (not shown). Macroscopical inspection revealed that KRIB:DKK1 tumors were pale white which was in contrast to KRIB tumors that were reddish and exhibited multiple blood vessels at the tumor surface (**Fig. 7E**). This almost complete absence of vessels in the DKK1 overexpressing tumors was confirmed by largely reduced CD31 staining (**Fig 7F, G**).

Correlated expression of TNC, DKK1 and Wnt target genes in a subgroup of GBM tumors

Finally, we investigated DKK1 expression in human primary GBM with documented high expression of TNC and Id2 (Ruiz et al., 2004). Protein expression levels were determined by immunohistochemistry in human GBM (WHO IV) on a tissue microarray (Murat et al., 2008, visualized in **Fig. 8**). We observed that in 70% (28/40) of GBM with no or low DKK1 immuno-positivity a robust expression of TNC coincided with elevated levels of Id2 and/or cyclin D1 in the majority of cases (**Fig. 8**). Unlike with other Wnt-pathway antagonists (Lambiv et al. *in press*) the DKK1 promoter is not methylated in primary GBM (Gotze et al., 2010). Hence, repression of DKK1 and induction of Wnt signalling by TNC might be specifically relevant in the subset of GBM that exhibit high expression of TNC, Id2 and cyclin D1 and low DKK1 expression. We also correlated the expression of DKK1 mRNA to survival of patients with GBM IV that had been treated with combined chemoradiotherapy comprising temozolomide (Murat et al., 2008; Stupp et al., 2009). Interestingly, increased expression of DKK1 mRNA was associated with better outcome

as indicated by a Hazard ratio below 1.0 (0.73, with 95% confidence interval 0.548-0.981, n = 42; p = 0.037; Cox model corrected for MGMT methylation and age).

Discussion

TNC plays an instrumental role in events causing cancer progression and metastasis (Midwood and Orend, 2009; Orend and Chiquet-Ehrismann, 2006) but the underlying mechanisms are poorly understood. Here, we have phenocopied TNC actions in human cancer by ectopically expressing TNC in insulinoma-prone RT2 mice and observed that increased TNC expression promotes carcinoma progression by promoting proliferation, invasion, angiogenesis and lung micrometastasis formation. Our results prove for the first time in an immune-competent stochastic tumor model that TNC drives tumorigenesis resulting in enhanced lung metastasis.

Our data suggest that enhanced tumor progression by TNC occurs through the repression of DKK1, a soluble inhibitor of canonical Wnt signalling (Glinka et al., 1998), and subsequent activation of Wnt signalling. The Wnt/β-catenin signalling pathway has been documented to promote tumor angiogenesis (Dejana 2010), cancer progression (Giles et al., 2003) and metastasis (Nguyen et al., 2009). By using RT2 mice with different TNC expression levels (wildtype, knock out, overexpression) we showed that DKK1 expression inversely correlates with the TNC copy number suggesting that TNC has an impact on DKK1 expression in spontaneously arising tumors. We had previously shown that a TNC substratum repressed DKK1 in GBM cells, stabilized β-catenin and induced Wnt target genes (Ruiz et al., 2004). Now we extended this observation by showing that DKK1 was robustly and consistently repressed by TNC in several tumor cell lines derived from breast, brain, colon and bone cancer tissue. Repression of DKK1 by TNC was already detectable after 4h and DKK1 remained repressed until the last time point of analysis (12 days) which correlated with low DKK1 protein levels. Signalling pathways involving p53 (Wang et al., 2000), c-jun (Grotewold and Ruther, 2002), vitamin D3 (Pendas-Franco et al., 2008) and NANOG (Zhu et al., 2009) have been

shown to induce DKK1 gene transcription. Conversely, promoter methylation (Aguilera et al., 2006), histone acetylation, polycomb family members (Hussain et al., 2009), and endothelin-1 signalling (Clines et al., 2007) downregulate DKK1 expression. Here, we have shown that cell adhesion to TNC represses DKK1 transcription. It is intriguing to speculate that endothelin signalling could be involved in TNC-induced DKK1 repression since TNC induced the endothelin receptor type A (Lange et al., 2007).

In agreement with an effect of DKK1 on Wnt signalling, we observed activation of Wnt signalling in small yet mostly differentiated tumors of RT2/TNC mice as evidenced by nuclear localization of β-catenin and increased expression of the Wnt target genes cyclin D1, cyclin D2, CD44 and Slug. Elevated expression of these genes in still differentiated tumors could have been instrumental in driving their evolution into carcinomas which is supported by an enhanced carcinoma formation seen in RT2/TNC mice.

In tumor cells cultured on a TNC substratum we also observed induction of Wnt targets, Id2 (T98G) and Sox4 (KRIB) and, FN and Slug in both cell lines. We conclude that tumor cells repress DKK1 and induce autocrine Wnt signalling resulting in cell type-specific transcriptional responses that are presumably affected by the Wnt ligand/receptor status and intrinsic signalling components. Functionally, we showed that DKK1 overexpression diminished tumor cell migration *in vitro*. Our results are consistent with a model where DKK1 repression in tumor cells could result in an autocrine activation of Wnt signalling thus promoting tumor cell migration and carcinoma formation. Nevertheless, in tumors reduced levels of secreted DKK1 may also lead to activation of Wnt signalling in stromal cells in a paracrine fashion and thus promote tumor angiogenesis and metastasis (**Fig. 9**).

Angiogenesis represents an important step on the road to metastasis. Here, we have demonstrated that tumors of RT2/TNC mice display an increased number of EC which is a hallmark of enhanced angiogenesis. In RT2/TNC tumors, blood vessels appeared

chaotic and were presumably not functional in supplying blood but may still have contributed to metastasis as was documented for non functional blood vessels in another study (Rolny et al., 2011). TNC has been shown to act as chemoattractant for EC, to play a role in the generation of tumor derived endothelial cells (Pezzolo et al., 2011), and to promote EC tube formation *in vitro* (Martina et al., 2010; Orend and Chiquet-Ehrismann, 2006). Now, using the CAM assay, we showed that TNC also induced EC sprouting. Despite a documented role of VEGFA-associated signalling in TNC-stimulated tumor angiogenesis (Tanaka et al., 2004) and induction of several pro-angiogenic factors (Ruiz et al., 2004), by qRT-PCR we have not found evidence for an increased expression of any of these molecules and pathways in RT2/TNC tumors (data not shown). In contrast, our results suggest an important role of DKK1 and Wnt signalling in TNC-driven angiogenesis. To address whether DKK1 levels had an impact on tumorigenesis/angiogenesis *in vivo*, we had utilized KRIB osteosarcoma cells overexpressing DKK1 and indeed observed that these cells failed to induce vascularised tumors.

The role of DKK1 in tumor progression has remained controversial with apparently contradictory observations published. In colon cancer (Gonzalez-Sancho et al., 2005), melanoma (Kuphal et al., 2006) and advanced prostate cancer (Hall et al., 2006), DKK1 is downregulated in comparison to the corresponding healthy tissues. Whereas DKK1 is low in breast cancer cells with an osteoblastic metastasis potential, it is highly expressed in breast cancer cells with an osteolytic metastasis potential and, DKK1 promotes osteolytic metastasis in myeloma (Pinzone et al., 2009). Finally, overexpression of DKK1 in canine Ace-1 prostate cancer cells promoted their metastatic potential upon intracardiac injection (Thudi et al., 2010). The role of DKK1 in tumor angiogenesis is also not clear. Whereas DKK1 appears to mobilize EC progenitor cells (Aicher et al., 2008; Smadja et al. 2011) and slightly enhanced tumor angiogenesis of already established xenografted human HBCx-12 breast cancer cells upon peri-tumoral injection of recombinant DKK1 (Smadja et al. 2011) here we observed that DKK1 overexpressed by

osteosarcoma cells blocked tumor growth, presumably by inhibiting tumor angiogenesis. Possible explanations for the different effects of DKK1 may be found in the different experimental systems and settings used and the influence of non-canonical Wnt signalling pathways involving JNK (Thudi et al., 2010).

In summary, for the first time we had demonstrated that the TNC levels determine the extent of angiogenesis and metastasis in an immune competent sporadic tumorigenesis model. These results provide formal proof of a decisive role of TNC in cancer progression. We also provide a mechanistic basis for the described TNC actions by showing that TNC induces canonical Wnt signalling through transcriptional repression of DKK1 thus triggering expression of selective Wnt targets. The described mechanism may also apply to malignancy in human gliomas and could be relevant for therapy since a high expression of DKK1 was linked to a better chemo- and radiotherapy response rate in GBM patients. Based on these observations, TNC presents an attractive target for blocking tumor angiogenesis and tumor cell dissemination. Drugs targeting TNC in cancer are already in clinical trials (Brack et al., 2006; Pedretti et al., 2009; Reardon et al., 2008). Our tumor mice with transgenic human TNC in a TNC negative background could serve as an excellent preclinical model for evaluating the efficacy of drugs targeting human TNC.

Experimental Procedures *(additional information in Suppl. information)*

Generation of transgenic RipTNC mice

The human TNC cDNA sequence (accession number X78656.1, (Aukhil et al., 1993) was cloned into the Rip1 vector by using the intermediate pcDNA3.1/Hygro(-) vector (**Suppl. Fig. 1**). The construct was partially sequenced and transferred into fertilized oocytes. Three transgenic mouse lines with stable expression and transmission of the transgene in a C57Bl6 background were established. Transgenic mice were identified by PCR. All experimental procedures involving mice were done according to the guidelines of the Swiss Federal Veterinary Office and of Inserm.

Generation of tumor mice with different TNC expression levels

RT2/TNC and RT2/TNC-/- mice were generated by breeding RT2 transgenic mice (Hanahan, 1985) with RipTNC (this study) and TNC-/- mice (Forsberg et al., 1996), respectively. RT2/TNC and control mice were fed with 5% glucose starting at 10 weeks of age. Tumors in RT2/TNC-/- and RT2/TNC+/- mice were investigated in a mixed C57Bl6/129/Sv background at 15-17 weeks of age.

Generation of rabbit anti-TNC antibodies and tissue analysis

Rabbit antisera recognizing human and murine TNC were derived upon injection of recombinant human TNC protein (Lange et al., 2007). Pancreata were dissected and tumors were collected. Tumor diameter was measured with a caliper and used to determine the tumor volume with the formula $V = 4/3\ \pi\ (d/2)^3$. Pancreata or xenograft tumors were embedded in the Tissue Tek O.C.T. compound or were fixed in 4% paraformaldehyde (PFA) followed by freezing in Tissue Tek O.C.T. or embedding into paraffin. Tissue sections were stained with primary and Cy3-, Cy5-, FITC- or Dylight 488-labeled secondary antibodies. CD31-or PH3-positive signals were quantified per constant field by using the Image J software. Tumor material from patients had been acquired upon written consent according to conventional ethics standards, was frozen or

embedded into paraffin before tissue analysis. Relative expression of the indicated gene products was determined in 68 GBM (WHO IV) on a tissue micro array (Murat et al., 2008) using immunohistochemistry. The immunostainings were scored semi-quantitatively (score 0–3) and categorized as described previously (Sivasankaran et al., 2009). Briefly, tumors were ordered by similarity of protein expression profiles using the SPIN software (data are centered, divided by the mean) (Tsafrir et al., 2005).

DKK1 promoter luciferase assay

A 3kb human DKK1 promoter sequence was cloned into the multiple cloning site of pGL3-basic Luciferase reporter vector (Promega). T98G cells were transiently transfected with TK-Renilla and pGL3-DKK1 Promoter construct or empty pGL3-basic vector. Transfections were performed with JetPEI^{TM} (Polyplus transfection). Cells were cultured in 1% DMEM and transfected with the reporter gene constructs 40 hours before using the Dual-Luciferase Reporter Assay System (Promega). Transfection with the renilla luciferase vector was used for normalization. Luciferase activity is presented as the ratio of pGL3-DKK1/pGL3-basic.

Cell culture

The indicated cell lines (ATCC) were plated onto FN or FN/TNC coated dishes for up to 12 days in DMEM supplemented with 10% FCS (MCF7 and MDA MB435) or 1% FCS (T98G, KRIB, Caco2 and HT29; see details in Huang et al. (2001)). RNA was isolated with the NucleoSpin RNA extraction kit (Macherey-Nagel, France) according to the manufacturer's instructions. Expression of candidate genes was determined by qRT-PCR using expression of ß2-microglobulin for normalization. Primer sequences are available in **Supplemental Table 6**. Cells were lysed in Laemmli buffer and immunoblotting was performed with antibodies recognizing Anti-DKK1 (Sigma-Aldrich, AV48015), 1:400, Anti-DKK1, N-terminal (Sigma-Aldrich, D3195), 1:1500, Anti-6xHis tag (Abcam, ab18184), 1:5000, Anti-α-tubulin (CP06, Oncogene, Boston, MA, USA).

Generation of DKK1 overexpressing cells

A BamHI and an EcoRI site were added in the pCDNA 3.1 mDDK1 V5 His plasmid before the ATG or the stop codon of the mouse Dickkopf cDNA respectively, using the GeneEditor™ *in vitro* Site-Directed Mutagenesis System, with the primers 5'-P-GGTGGAATTGCCCTTGGATCCACATGATGGTTGTGT-3' and 5'-P-ACCATCACCATTGAGAA TTCACCCGCTGATCAGCC-3'. After BamHI-EcoRI digestion, the mDKK1 V5 His fragment was gel purified (NucleoSpin® Extract II, Machery-Nagel, France) and cloned in the BamHI-EcoRI site of the pQCXIP retroviral vector (Clontech, Ozyme, France) generating the pQCXIP-mDKK1 V5 His vector. Retroviral particles were produced with the pQCXIP-cherry and pQCXIP-mDKK1 V5 His vectors, that were then used to transduce the cell lines according to standard protocols. Transduced cells were selected using Puromycin.

Tumor xenograft experiment

KRIB osteosarcoma cells (ATCC) with parental and ectopic DKK1 expression (4 million cells/100μl) were injected in the left upper back of nude mice (Charles River, 5 mice per condition). Mice were sacrificed after 3.5 weeks before measurement of the tumor size with a caliper. Tumor tissue was embedded in OCT, frozen on dry ice, and conserved at -80° C.

Expression analysis of candidate genes in the RT2 tumor model

Tissue from 12 – 17 week old mice was isolated, immediately snap frozen and RNA was extracted using the RNA kit according to the manufacturer's protocol (NucleoSpin Extract II, Machery-Nagel, France). RNA was reverse transcribed and qRT-PCR was performed using SYBR green or Taqman reaction mixtures. Primer sequences are available (see **Suppl. Table 5**). Data were normalized to the average of three reference genes RPL9, TBP and GAPDH. Relative expression between RT2 and RT2/TNC samples was calculated based on the mean ΔΔCt-values.

Analysis of the vessel morphology

For preparation of vascular casts, a Mercox solution containing accelerator was perfused before the pancreas was excised and further processed. Tissue samples were sputtered with gold and examined in a scanning electron microscope. For TEM the samples were fixed in a 2% PFA/2.5% glutaraldehyde solution before further processing in a 1% OsO_4 solution, dehydration in ethanol and embedding in epoxy resin. Upon staining with lead citrate and uranyl acetate, tissue sections were analysed.

CAM assay

Egg white (5 ml) was removed from chicken eggs at day 3 after fertilization before incubation at 37°C in a humidified chamber. At day 8 Whatman paper (0.5 cm in diameter, Whatman) soaked with 20 µl PDGF-BB (200 ng/ml, Sigma), purified human TNC (2 µg/ml) in PBS/0.01% Tween-20 and PBST control was placed onto the CAM in a region devoid of blood vessels. At day 11 the CAMs were removed from the embryo and analysed for blood vessel density by light microscopy. The number of vessels in 20 squares of 1 mm x 1 mm were used to quantify vessel density around and on top (not shown) of each sample. Results derived from 3 independent experiments.

Statistical analysis

Statistical analysis was done on original data using GraphPad Prism version 5.00. For significance of an association (contingency) Fisher's exact test or chi-square test was applied (tumor staging, gene expression, metastasis incidence, GBM analysis). Statistical differences of events were analysed by unpaired t-test (Gaussian distribution) or nonparametric Mann-Whitney test (no Gaussian distribution). Gaussian data sets with different variances were analysed by unpaired t-test with Welch's correction. p-values < 0.05 were considered as statistically significant.

Acknowledgement

We thank A. Klein, C. Arnold, C. Alcon, K. Strittmatter, H. Antoniadis, P. Lorentz, M.-F. Hamou and S. Kraemer for excellent technical assistance, J. Mutterer for capturing the confocal pictures, B. Scolari and R. Buergy for preparation of tissue samples for electron microscopy and E. Domany for the SPIN software. We are grateful to R. Chiquet-Ehrismann and the transgene facility of the Friedrich Miescher Institute for Biomedical Research for assistance with the generation of the transgenic mice. We also like to thank R. Fässler for providing the TNC knock out mice. I.G. was supported by a grant from Inserm/Region Alsace. O.L. and P.S.A. were supported by Ligue contre le Cancer. G.O. was supported by Krebsliga Beider Basel, Association for International Cancer Research, Swiss National Science Foundation, Oncosuisse, Novartis Foundation for Biological and Medical Sciences, the Hospital Hautepierre, Association pour la Recherche contre le Cancer and a grant from the Institut National du Cancer.

Author contribution

F.S., I.G., Y.J., A.H., M.K., T.H., M.M., O.L., M.H., R.H. J.K., W.H. and A.C.F. had performed experiments and contributed results. G.O., V.J. and G.C. supervised experiments. G.O., F.S., I.G. and Y.J. designed the study and G.O. wrote the manuscript with support from G.C., T.H.,M.K., F.S. and P.S.A.

Conflict of interest

The authors declare no conflict of interests.

References

Aguilera, O., Fraga, M.F., Ballestar, E., Paz, M.F., Herranz, M., Espada, J., Garcia, J.M., Munoz, A., Esteller, M. and Gonzalez-Sancho, J.M. (2006) Epigenetic inactivation of the Wnt antagonist DICKKOPF-1 (DKK-1) gene in human colorectal cancer. *Oncogene*, **25**, 4116-4121.

Aguirre-Ghiso, J.A. (2007) Models, mechanisms and clinical evidence for cancer dormancy. *Nat Rev Cancer*, **7**, 834-846.

Aicher, A., Kollet, O., Heeschen, C., Liebner, S., Urbich, C., Ihling, C., Orlandi, A., Lapidot, T., Zeiher, A.M. and Dimmeler, S. (2008) The Wnt antagonist Dickkopf-1 mobilizes vasculogenic progenitor cells via activation of the bone marrow endosteal stem cell niche. *Circ Res*, **103**, 796-803.

Almog, N. (2010) Molecular mechanisms underlying tumor dormancy. *Cancer Lett*, **294**, 139-146.

Aukhil, I., Joshi, P., Yan, Y. and Erickson, H.P. (1993) Cell- and heparin-binding domains of the hexabrachion arm identified by tenascin expression proteins. *J Biol Chem*, **268**, 2542-2553.

Bergers, G. and Benjamin, L.E. (2003) Tumorigenesis and the angiogenic switch. *Nat Rev Cancer*, **3**, 401-410.

Bissell, M.J. and Labarge, M.A. (2005) Context, tissue plasticity, and cancer: are tumor stem cells also regulated by the microenvironment? *Cancer Cell*, **7**, 17-23.

Brack, S.S., Silacci, M., Birchler, M. and Neri, D. (2006) Tumor-targeting properties of novel antibodies specific to the large isoform of tenascin-C. *Clin Cancer Res*, **12**, 3200-3208.

Calvo, A., Catena, R., Noble, M.S., Carbott, D., Gil-Bazo, I., Gonzalez-Moreno, O., Huh, J.I., Sharp, R., Qiu, T.H., Anver, M.R., Merlino, G., Dickson, R.B., Johnson, M.D. and Green, J.E. (2008) Identification of VEGF-regulated genes associated with increased lung metastatic potential: functional involvement of tenascin-C in tumor growth and lung metastasis. *Oncogene*.

Chiquet-Ehrismann, R. (1990) What distinguishes tenascin from fibronectin? *Faseb J*, **4**, 2598-2604.

Clines, G.A., Mohammad, K.S., Bao, Y., Stephens, O.W., Suva, L.J., Shaughnessy, J.D., Jr., Fox, J.W., Chirgwin, J.M. and Guise, T.A. (2007) Dickkopf homolog 1 mediates endothelin-1-stimulated new bone formation. *Mol Endocrinol*, **21**, 486-498.

Colman, H., Zhang, L., Sulman, E.P., McDonald, J.M., Shooshtari, N.L., Rivera, A., Popoff, S., Nutt, C.L., Louis, D.N., Cairncross, J.G., Gilbert, M.R., Phillips, H.S., Mehta, M.P., Chakravarti, A., Pelloski, C.E., Bhat, K., Feuerstein, B.G., Jenkins, R.B. and Aldape, K. A multigene predictor of outcome in glioblastoma. (2010) *Neuro Oncol*, **12**, 49-57.

Dejana, E. (2010) The role of wnt signaling in physiological and pathological angiogenesis. *Circ Res*, **107**, 943-952.

Folkman, J. and Kalluri, R. (2004) Cancer without disease. *Nature*, **427**, 787.

Forsberg, E., Hirsch, E., Frohlich, L., Meyer, M., Ekblom, P., Aszodi, A., Werner, S. and Fassler, R. (1996) Skin wounds and severed nerves heal normally in mice lacking tenascin-C. *Proc Natl Acad Sci U S A*, **93**, 6594-6599.

Fukunaga-Kalabis, M., Martinez, G., Nguyen, T.K., Kim, D., Santiago-Walker, A., Roesch, A. and Herlyn, M. Tenascin-C promotes melanoma progression by maintaining the ABCB5-positive side population. (2010) *Oncogene*, **29**, 6115-6124.

Giles, R.H., van Es, J.H. and Clevers, H. (2003) Caught up in a Wnt storm: Wnt signaling in cancer. *Biochim Biophys Acta*, **1653**, 1-24.

Glinka, A., Wu, W., Delius, H., Monaghan, A.P., Blumenstock, C. and Niehrs, C. (1998) Dickkopf-1 is a member of a new family of secreted proteins and functions in head induction. *Nature*, **391**, 357-362.

Gonzalez-Sancho, J.M., Aguilera, O., Garcia, J.M., Pendas-Franco, N., Pena, C., Cal, S., Garcia de Herreros, A., Bonilla, F. and Munoz, A. (2005) The Wnt antagonist DICKKOPF-1 gene is a downstream target of beta-catenin/TCF and is downregulated in human colon cancer. *Oncogene*, **24**, 1098-1103.

Gotze, S., Wolter, M., Reifenberger, G., Muller, O. and Sievers, S. (2010) Frequent promoter hypermethylation of Wnt pathway inhibitor genes in malignant astrocytic gliomas. *Int J Cancer*, **126**, 2584-2593.

Grotewold, L. and Ruther, U. (2002) The Wnt antagonist Dickkopf-1 is regulated by Bmp signaling and c-Jun and modulates programmed cell death. *Embo J*, **21**, 966-975.

Hall, C.L., Kang, S., MacDougald, O.A. and Keller, E.T. (2006) Role of Wnts in prostate cancer bone metastases. *J Cell Biochem*, **97**, 661-672.

Hanahan, D. (1985) Heritable formation of pancreatic beta-cell tumours in transgenic mice expressing recombinant insulin/simian virus 40 oncogenes. *Nature*, **315**, 115-122.

Helleman, J., Jansen, M.P., Ruigrok-Ritstier, K., van Staveren, I.L., Look, M.P., Meijer-van Gelder, M.E., Sieuwerts, A.M., Klijn, J.G., Sleijfer, S., Foekens, J.A. and Berns, E.M. (2008) Association of an extracellular matrix gene cluster with breast cancer prognosis and endocrine therapy response. *Clin Cancer Res*, **14**, 5555-5564.

Huang, W., Chiquet-Ehrismann, R., Moyano, J.V., Garcia-Pardo, A. and Orend, G. (2001) Interference of tenascin-C with syndecan-4 binding to fibronectin blocks cell adhesion and stimulates tumor cell proliferation. *Cancer Res*, **61**, 8586-8594.

Hussain, M., Rao, M., Humphries, A.E., Hong, J.A., Liu, F., Yang, M., Caragacianu, D. and Schrump, D.S. (2009) Tobacco smoke induces polycomb-mediated repression of Dickkopf-1 in lung cancer cells. *Cancer Res*, **69**, 3570-3578.

Kerbel, R.S. (2008) Tumor angiogenesis. *N Engl J Med*, **358**, 2039-2049.

Kuphal, S., Lodermeyer, S., Bataille, F., Schuierer, M., Hoang, B.H. and Bosserhoff, A.K. (2006) Expression of Dickkopf genes is strongly reduced in malignant melanoma. *Oncogene*, **25**, 5027-5036.

Lambiv, W.L., Vassallo, I., Delorenzi, M., Shay, T., Diserens, A-C., Misra, A., Feuerstein, B.G., Murat, A., Migliavacca, E., Hamou, M-F., Sciuscio, D., Burger, R., Domany, E., Stupp, R., Hegi, M.E. The Wnt inhibitory factor 1 (WIF-1) is targeted in

glioblastoma and has tumor suppressing function potentially mediated by induction of senescence. Neuro Oncol. *in press.*

Lange, K., Kammerer, M., Hegi, M.E., Grotegut, S., Dittmann, A., Huang, W., Fluri, E., Yip, G.W., Gotte, M., Ruiz, C. and Orend, G. (2007) Endothelin receptor type B counteracts tenascin-C-induced endothelin receptor type A-dependent focal adhesion and actin stress fiber disorganization. *Cancer Res*, **67**, 6163-6173.

Martina, E., Degen, M., Ruegg, C., Merlo, A., Lino, M.M., Chiquet-Ehrismann, R. and Brellier, F. (2010) Tenascin-W is a specific marker of glioma-associated blood vessels and stimulates angiogenesis in vitro. *Faseb J*, **24**, 778-787.

Midwood, K.S. and Orend, G. (2009) The role of tenascin-C in tissue injury and tumorigenesis. *J Cell Commun Signal*. 3, 287 - 310.

Minn, A.J., Gupta, G.P., Siegel, P.M., Bos, P.D., Shu, W., Giri, D.D., Viale, A., Olshen, A.B., Gerald, W.L. and Massague, J. (2005) Genes that mediate breast cancer metastasis to lung. *Nature*, **436**, 518-524.

Murat, A., Migliavacca, E., Gorlia, T., Lambiv, W.L., Shay, T., Hamou, M.F., de Tribolet, N., Regli, L., Wick, W., Kouwenhoven, M.C., Hainfellner, J.A., Heppner, F.L., Dietrich, P.Y., Zimmer, Y., Cairncross, J.G., Janzer, R.C., Domany, E., Delorenzi, M., Stupp, R. and Hegi, M.E. (2008) Stem cell-related "self-renewal" signature and high epidermal growth factor receptor expression associated with resistance to concomitant chemoradiotherapy in glioblastoma. *J Clin Oncol*, **26**, 3015-3024.

Nevins, J.R. (2001) The Rb/E2F pathway and cancer. *Hum Mol Genet*, **10**, 699-703.

Nguyen, D.X., Chiang, A.C., Zhang, X.H., Kim, J.Y., Kris, M.G., Ladanyi, M., Gerald, W.L. and Massague, J. (2009) WNT/TCF signaling through LEF1 and HOXB9 mediates lung adenocarcinoma metastasis. *Cell*, **138**, 51-62.

Orend, G. (2005) Potential oncogenic action of tenascin-C in tumorigenesis. *Int J Biochem Cell Biol*, **37**, 1066-1083.

Orend, G. and Chiquet-Ehrismann, R. (2006) Tenascin-C induced signaling in cancer. *Cancer Lett*, **244**, 143-163.

Pedretti, M., Soltermann, A., Arni, S., Weder, W., Neri, D. and Hillinger, S. (2009) Comparative immunohistochemistry of L19 and F16 in non-small cell lung cancer and mesothelioma: two human antibodies investigated in clinical trials in patients with cancer. *Lung Cancer*, **64**, 28-33.

Pendas-Franco, N., Aguilera, O., Pereira, F., Gonzalez-Sancho, J.M. and Munoz, A. (2008) Vitamin D and Wnt/beta-catenin pathway in colon cancer: role and regulation of DICKKOPF genes. *Anticancer Res*, **28**, 2613-2623.

Pezzolo, A., Parodi, F., Marimpietri, D., Raffaghello, L., Cocco, C., Pistorio, A., Mosconi, M., Gambini, C., Cilli, M., Deaglio, S., Malavasi, F. and Pistoia, V. (2011) Oct-4(+)/Tenascin C(+) neuroblastoma cells serve as progenitors of tumor-derived endothelial cells. *Cell Res*. Mar 15, Epub ahead of print.

Pinzone, J.J., Hall, B.M., Thudi, N.K., Vonau, M., Qiang, Y.W., Rosol, T.J. and Shaughnessy, J.D., Jr. (2009) The role of Dickkopf-1 in bone development, homeostasis, and disease. *Blood*, **113**, 517-525.

Pipas, J.M. and Levine, A.J. (2001) Role of T antigen interactions with p53 in tumorigenesis. *Semin Cancer Biol*, **11**, 23-30.

Reardon, D.A., Zalutsky, M.R., Akabani, G., Coleman, R.E., Friedman, A.H., Herndon, J.E., 2nd, McLendon, R.E., Pegram, C.N., Quinn, J.A., Rich, J.N., Vredenburgh, J.J., Desjardins, A., Guruangan, S., Boulton, S., Raynor, R.H., Dowell, J.M., Wong, T.Z., Zhao, X.G., Friedman, H.S. and Bigner, D.D. (2008) A pilot study: 131I-antitenascin monoclonal antibody 81c6 to deliver a 44-Gy resection cavity boost. *Neuro Oncol*, **10**, 182-189.

Rolny, C., Mazzone, M., Tugues, S., Laoui, D., Johansson, I., Coulon, C., Squadrito, M.L., Segura, I., Li, X., Knevels, E., Costa, S., Vinckier, S., Dresselaer, T., Akerud, P., De Mol, M., Salomaki, H., Phillipson, M., Wyns, S., Larsson, E., Buysschaert, I., Botling, J., Himmelreich, U., Van Ginderachter, J.A., De Palma, M., Dewerchin, M., Claesson-Welsh, L. and Carmeliet, P. (2011) HRG inhibits tumor growth and metastasis by inducing macrophage polarization and vessel normalization through downregulation of PlGF. *Cancer Cell*, **19**, 31-44.

Ruiz, C., Huang, W., Hegi, M.E., Lange, K., Hamou, M.F., Fluri, E., Oakeley, E.J., Chiquet-Ehrismann, R. and Orend, G. (2004) Growth promoting signaling by tenascin-C [corrected]. *Cancer Res*, **64**, 7377-7385.

Sivasankaran, B., Degen, M., Ghaffari, A., Hegi, M.E., Hamou, M.F., Ionescu, M.C., Zweifel, C., Tolnay, M., Wasner, M., Mergenthaler, S., Miserez, A.R., Kiss, R., Lino, M.M., Merlo, A., Chiquet-Ehrismann, R. and Boulay, J.L. (2009) Tenascin-C is a novel RBPJkappa-induced target gene for Notch signaling in gliomas. *Cancer Res*, **69**, 458-465.

Smadja, D.M., d'Audigier, C., Weiswald, L.B., Badoual, C., Dangles-Marie, V., Mauge, L., Evrard, S., Laurendeau, I., Lallemand, F., Germain, S., Grelac, F., Dizier, B., Vidaud, M., Bieche, I. and Gaussem, P. (2011) The Wnt antagonist Dickkopf-1 increases endothelial progenitor cell angiogenic potential. *Arterioscler Thromb Vasc Biol*, **30**, 2544-2552.

Stupp, R., Hegi, M.E., Mason, W.P., van den Bent, M.J., Taphoorn, M.J., Janzer, R.C., Ludwin, S.K., Allgeier, A., Fisher, B., Belanger, K., Hau, P., Brandes, A.A., Gijtenbeek, J., Marosi, C., Vecht, C.J., Mokhtari, K., Wesseling, P., Villa, S., Eisenhauer, E., Gorlia, T., Weller, M., Lacombe, D., Cairncross, J.G. and Mirimanoff, R.O. (2009) Effects of radiotherapy with concomitant and adjuvant temozolomide versus radiotherapy alone on survival in glioblastoma in a randomised phase III study: 5-year analysis of the EORTC-NCIC trial. *Lancet Oncol*, **10**, 459-466.

Tanaka, K., Hiraiwa, N., Hashimoto, H., Yamazaki, Y. and Kusakabe, M. (2004) Tenascin-C regulates angiogenesis in tumor through the regulation of vascular endothelial growth factor expression. *Int J Cancer*, **108**, 31-40.

Tavazoie, S.F., Alarcon, C., Oskarsson, T., Padua, D., Wang, Q., Bos, P.D., Gerald, W.L. and Massague, J. (2008) Endogenous human microRNAs that suppress breast cancer metastasis. *Nature*, **451**, 147-152.

Thudi, N.K., Martin, C.K., Murahari, S., Shu, S.T., Lanigan, L.G., Werbeck, J.L., Keller, E.T., McCauley, L.K., Pinzone, J.J. and Rosol, T.J. (2010) Dickkopf-1 (DKK-1)

stimulated prostate cancer growth and metastasis and inhibited bone formation in osteoblastic bone metastases. *Prostate*, **71**, 615-625.

Tsafriri, D, Tsafrir, I., Ein-Dor, L., Zuk, O., Notterman, D.A. and Domany, E. (2005) Sorting points into neighborhoods (SPIN): data analysis and visualization by ordering distance matrices. *Bioinformatics*, **21**, 2301-2308.

Van der Flier, L.G., Sabates-Bellver, J., Oving, I., Haegebarth, A., De Palo, M., Anti, M., Van Gijn, M.E., Suijkerbuijk, S., Van de Wetering, M., Marra, G. and Clevers, H. (2007) The Intestinal Wnt/TCF Signature. *Gastroenterology*, **132**, 628-632.

Wang, J., Shou, J. and Chen, X. (2000) Dickkopf-1, an inhibitor of the Wnt signaling pathway, is induced by p53. *Oncogene*, **19**, 1843-1848.

Zhu, Y., Sun, Z., Han, Q., Liao, L., Wang, J., Bian, C., Li, J., Yan, X., Liu, Y., Shao, C. and Zhao, R.C. (2009) Human mesenchymal stem cells inhibit cancer cell proliferation by secreting DKK-1. *Leukemia*, **23**, 925-933.

Figure legends

Fig. 1 TNC promotes tumor proliferation and invasion

Expression of transgenic TNC in pancreatic islets (encircled) of a RipTNC pancreas and in RT2/TNC tumors (**A**) was determined by immunohistological staining of tissue sections with a human TNC specific antibody. (**B, C**) All macroscopical visible tumors from 12 week old mice and the tumor volume was determined with the formula $V=4/3\ \pi\ (d/2)^3$, (d=diameter in mm). RT2 (N = 33 mice, n = 156 tumors), RT2/TNC (N = 26; n = 117), not significant. (**D**) Proliferating cells in islets of 12 week old RT2 and RT2/TNC mice were identified with a phospho histone H3 (P-H3) specific antibody and quantified as event per mm^2 using the Image J program. RT2 (N = 13, n = 199 sections), RT2/TNC (N = 13, n = 176). $p < 0.0001$, Mann Whitney test. (**E**) The number of adenomas (Ad) and carcinomas (Ca) per mouse was determined in microscopic tumor sections of RT2 and RT2/TNC mice. RT2 (N = 22, n = 120 tumors), RT2/TNC (N = 24, n = 157). SEM, $p = 0.001$, unpaired t-test. Scale bar, 100 μm (upper panels), 500 μm (lower panels).

Fig. 2 Overexpressed TNC promotes tumor angiogenesis

(**A**) Staining and quantification of CD31 in tumors of 10 (**B**) and 12 (**C**) week old RT2 and RT2/TNC mice. Relative expression was determined as event per mm^2. Number of samples; (**B**) 10 weeks, RT2 (N = 5 mice, n = 13 tumors), RT2/TNC (N = 7, n = 19); 1.92-fold, SEM, $p = 0.0006$, unpaired t-test; (**C**) 12 weeks, RT2 (N = 6, n = 34, 203 data points) and RT2/TNC (N = 4, n = 17, 106 data points), 2.27-fold, SEM, $p < 0.0001$, Mann Whitney test. Scale bar 100 μm. (**D**) Reproduction of the vasculature in tumors of 12 week old RT2 and RT2/TNC mice in corrosion casts upon Mercox perfusion. (**E**) Blood vessel quantification in the CAM assay. Number of samples, PBS-Tween (PBST) = 12, PDGF = 10 and TNC = 9, 1.85 – fold (TNC over PBST), SD, $p = 0.001$, unpaired t-test.

Fig. 3 TNC enhances lung micrometastasis

(**A, B**) Relative expression of insulin in lung tissue of RT2, RT2/TNC, RT2/TNC-/- and RT2/TNC+/- tumor mice was determined by qRT-PCR. (**C**) Immunofluorescent anti-

insulin and H & E staining of lung tissue from a RT2/TNC mouse. Number of samples; (**A**) 14 weeks, RT2 (N = 26), RT2/TNC (N = 24), 6.5 – fold, p = 0.0229, unpaired t-test, (**B**) 16 – 17 weeks, RT2/TNC-/- (N = 13), RT2/TNC+/- (N = 13), 10.2 –fold, p = 0.0283 Mann Whitney test. Scale bar 50 μm.

Fig. 4 Nuclear localization of β-catenin in RT2/TNC tumors

Expression analysis of β-catenin was done by immunohistochemistry and immunofluorescence in tumors of 14 week old RT2 (N = 5) and RT2/TNC (N = 8) mice. Pictures display tumor cells with nuclear β-catenin inside the tumor (**A**), at the invading front (**B**) and at the tumor rim (**C,** inlet: confocal picture). White asterisks (**B, C**), cells with nuclear β-catenin. Scale bars, 100 μm (**B** inlet), 200 μm (**B – C**), 10 μm (**C**, inlet). Boxes represent areas of higher magnification.

Fig. 5 TNC impact on Wnt signalling and DKK1 expression in RT2 tumors

(**A**) Wnt target gene and (**B-D**) DKK1 expression was determined by qRT-PCR on RNA from tumors of 14-17 week old mice. (**B**) The number of tumors per genotype that lacked any DKK1 RNA is displayed as % of all analysed tumors, p = 0.0031, Fisher`s exact test. (**C**) DKK1 levels in RT2/TNC and control tumors of 14 week old mice with detectable expression, p = 0.0021, unpaired t-test with Welsh`s correction. (**D**) DKK1 expression in RT2/TNC-/- and RT2/TNC+/- tumors. p = 0.0230, Mann-Whitney test. Number of samples, RT2 (N = 11 mice, n = 28 tumors) and RT2/TNC mice (N = 3, n = 14). See details in **Suppl. Table 3**.

Fig. 6 Impact of TNC on DKK1 expression and Wnt signalling in cultured tumor cells

Different tumor cells were plated on a FN or FN/TNC substratum for the indicated time points, before extraction of RNA and subsequent qRT-PCR (**A**, **C**, **D**), or protein lysis and immunoblotting for DKK1 (T98G cells) (**B, F**). Gene expression levels in the presence of TNC are displayed in comparison to the absence of TNC (T98G). Note that a TNC

substratum strongly reduced DKK1 expression in multiple tumor cell lines after 24 hours (KRIB, MDA-MB435 (MDA), MCF7, Caco2 and T98G) (**C**) and over a period of 5 hours up to 12 days (T98G) (**A**). This correlated with induction of Wnt target genes in T98G (**D**) and KRIB cells (**Suppl. Table 4**). Unpaired t-test $*$ $p < 0.05$, $**$ $p < 0.01$, $***$ $p < 0.001$. (**E**) DKK1 promoter inhibition by TNC. T98G cells were transfected with a DKK1-promoter/luciferase (or empty pGL3 control) plasmid together with TK-Renilla before plating on FN or FN/TNC (triplicates) and subsequent determination of luciferase activity which is presented upon normalization to Renilla. $p < 0.01$. Paired t-test. (**F**) Ectopically expressed murine DKK1 is detected by immunoblotting for murine DKK1 and the His-tag. In contrast to indistinguishable levels of endogenous DKK1 a high expression of ectopic murine DKK1 is noted in T98G:DKK1 cells. (**G**) Id2 expression in parental and T98G:DKK1 cells on FN and FN/TNC was determined by qRT-PCR. SD, $p< 0.05$, unpaired t-test.

Fig. 7 Consequences of DKK1 overexpression in KRIB cells in vitro and in vivo

(**A – C**), Consequences of DKK1 overexpression in cultured KRIB cells. (**A**) Western blot of KRIB cells overexpressing DKK1. (**B**) Proliferation of KRIB:DKK1 and parental cells was determined after the indicated time points by using the MTS assay. (**C**) Cell migration of KRIB:DKK1 and parental cells was determined in a wound healing assay. The scratched area covered by cells at day 13 (t = 3) is represented in comparison to that at day 0 (t = 0) (%). Experiment was done in triplicates, SD, $p< 0.0001$, student`s t-test. (**D – G**) Consequences of DKK1 overexpression in KRIB cells upon xenografting in nude mice. (**D**) Determination of tumor volume, 39 – fold, $p = 0.0079$, Mann Whitney test. (**E**) Macroscopical appearance of tumors. (**F**) Quantification of the CD31 signal (area in mm^2 / tumor) in parental and KRIB:DKK1 tumors. 7.5 – fold, SEM, $p = 0.0079$, Mann Whitney test. (**G**) Immunostaining of representative slides from KRIB:DKK1 and parental KRIB derived tumors for the indicated molecules. d, days. Scale bar represents 100 μm.

Fig. 8 Correlated expression of TNC, DKK1 and Wnt target genes in a subgroup of GBM tumors

Relative expression of the indicated gene products was determined in 68 GBM (WHO IV) on a tissue microarray (Murat et al., 2008) using immunohistochemistry. Low DKK1 expression was significantly correlated with high cyclin D1 expression (Fisher`s exact test $p < 0.05$).

Fig. 9 Proposed model of TNC effect on Wnt signalling and subsequent tumor invasion, tumor angiogenesis and metastasis formation

(**A**) Adhesion of tumor cells to a TNC substratum blocks expression of the soluble Wnt inhibitor DKK1 by promoter inhibition which subsequently leads to stabilization and nuclear translocation of β-catenin and induction of Wnt target genes with an appropriate Wnt receptor/ligand setting. (**B**) Repression of DKK1 by TNC in tumor cells does not only have an autocrine effect on tumor cells such as promoting their invasion, but also may de-repress and promote Wnt signalling in stromal cells in a paracrine manner thus promoting tumor angiogenesis. This possibility is supported by DKK1 overexpressing tumor cells forming poorly vascularised tumors.

Fig. 1

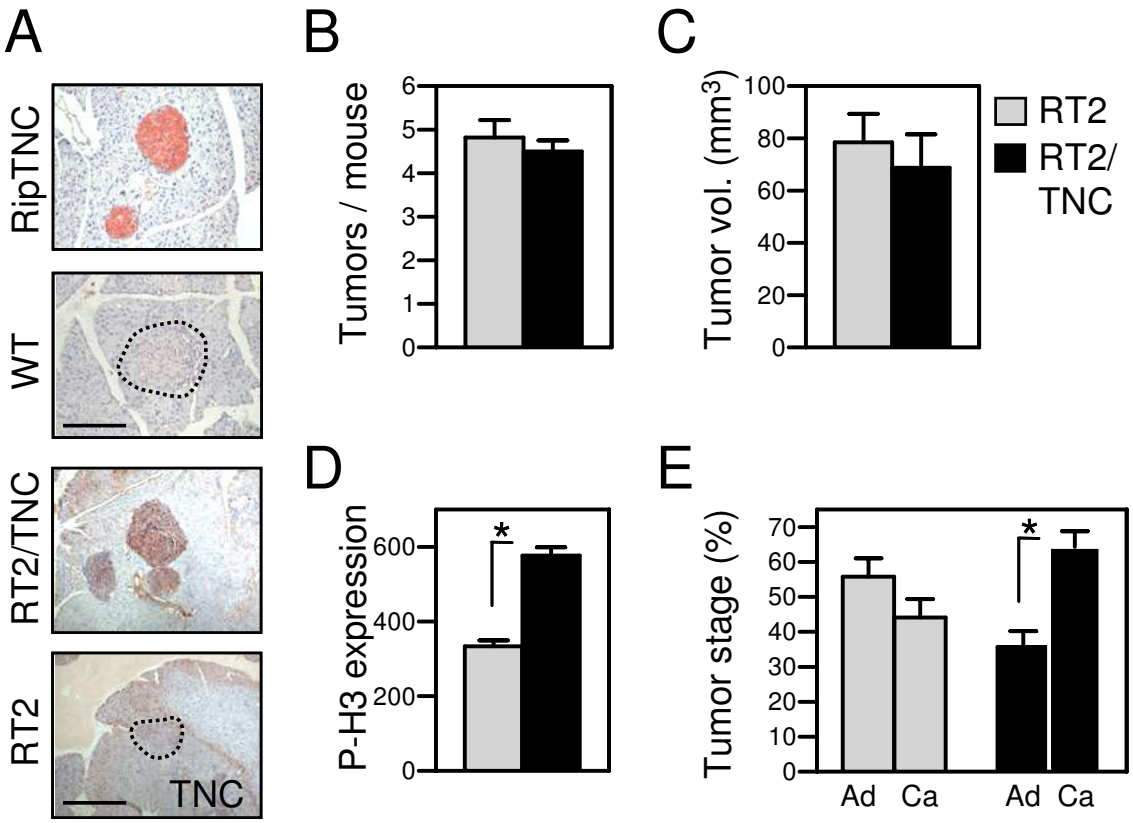
A
RipTNC
WT
RT2/TNC
RT2
TNC
B
Tumors / mouse
0
1
2
3
4
5
6
C
Tumor vol. (mm3)
0
20
40
60
80
100
RT2
RT2/
TNC
D
P-H3 expression
0
200
400
600
*
E
Tumor stage (%)
0
10
20
30
40
50
60
70
*
Ad
Ca
Ad
Ca

Fig. 2

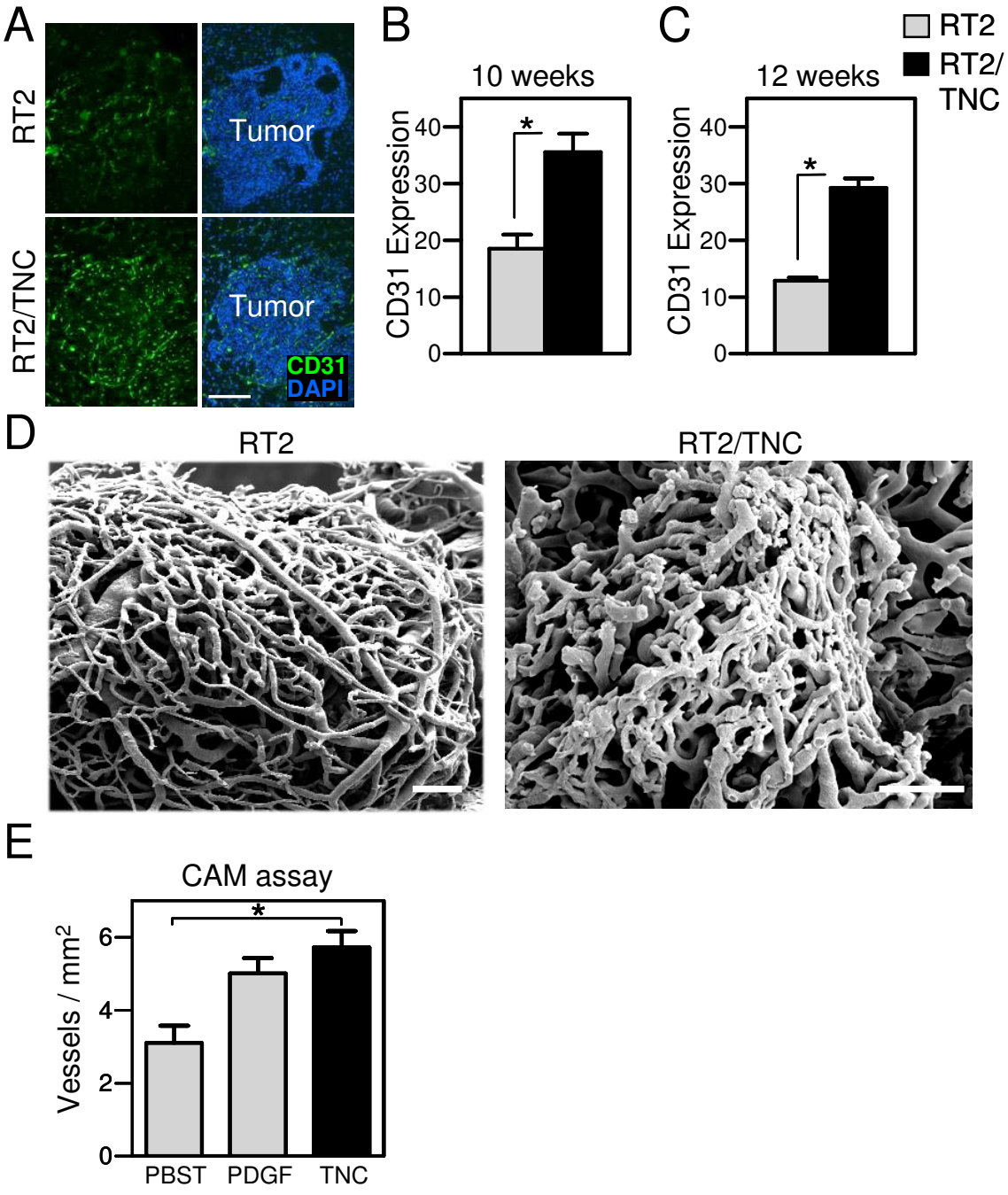
A
RT2
RT2/TNC
Tumor
Tumor
CD31
DAPI
B
10 weeks
CD31 Expression
40
30
20
10
0
*
C
12 weeks
CD31 Expression
40
30
20
10
0
*
RT2
RT2/
TNC
D
RT2
RT2/TNC
E
CAM assay
Vessels / mm2
6
4
2
0
*
PBST
PDGF
TNC

Fig. 3

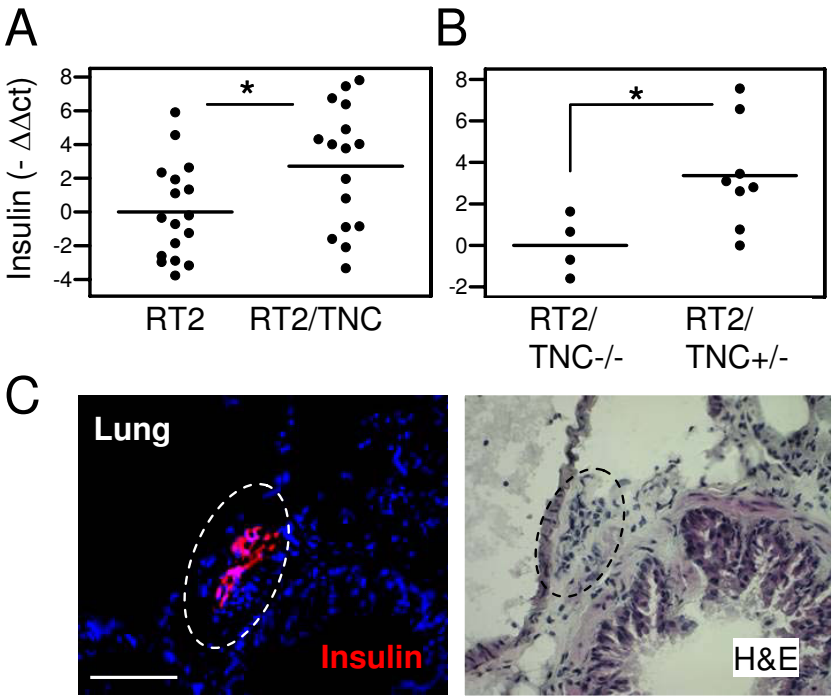
A
B
C
Insulin (- ΔΔct)
8
6
4
2
0
-2
-4
*
RT2
RT2/TNC
RT2/
TNC-/-
RT2/
TNC+/-
Lung
Insulin
H&E

Fig. 4

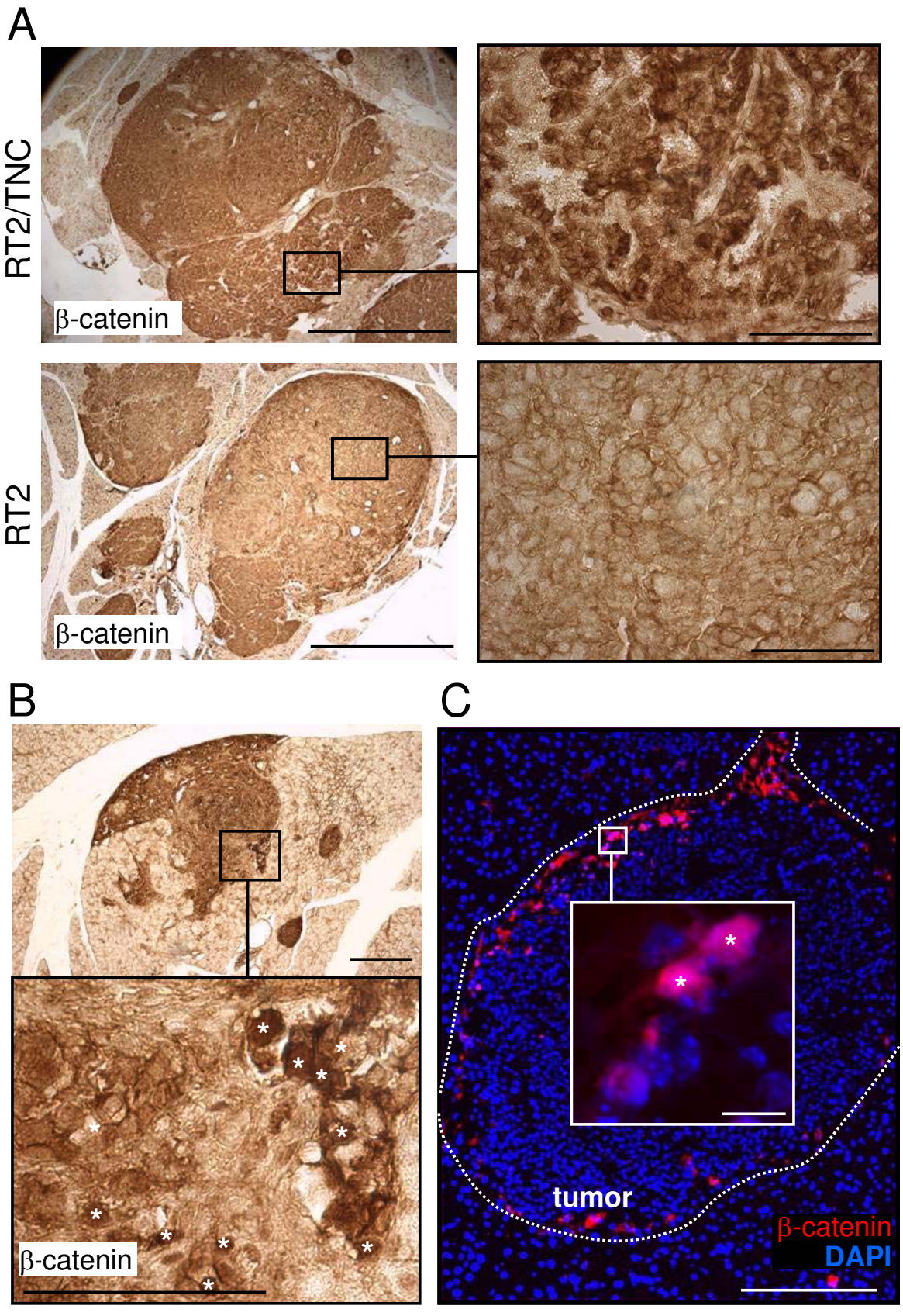
A
RT2/TNC
β-catenin
RT2
β-catenin
B
β-catenin
C
tumor
β-catenin
DAPI

Fig. 5

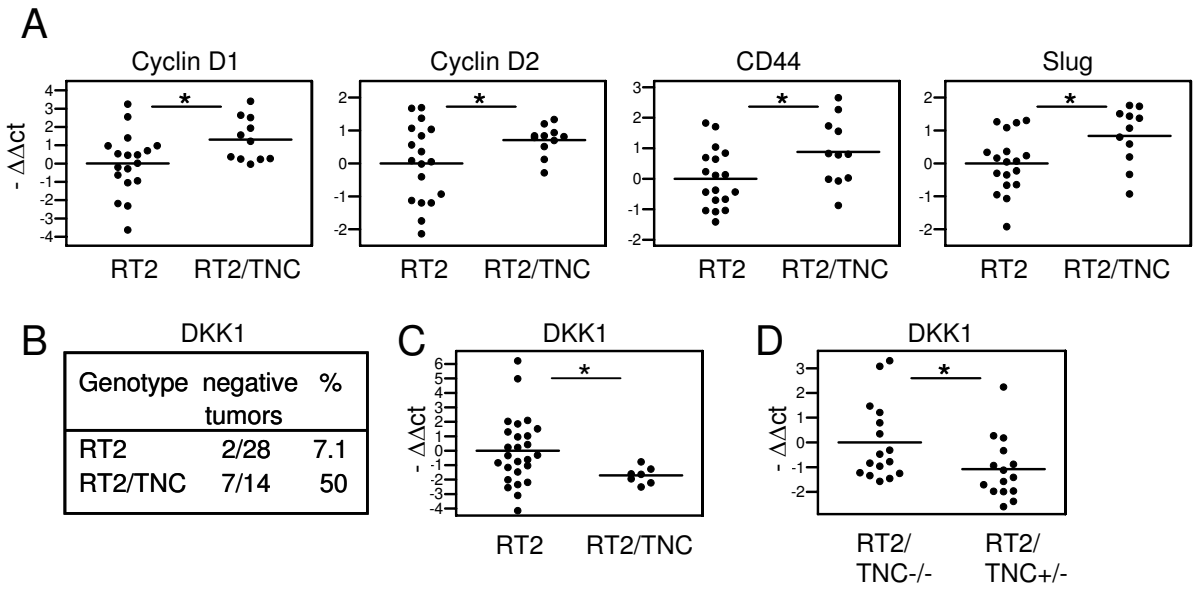

B

DKK1

Genotype	negative tumors	%
RT2	2/28	7.1
RT2/TNC	7/14	50

Fig. 6

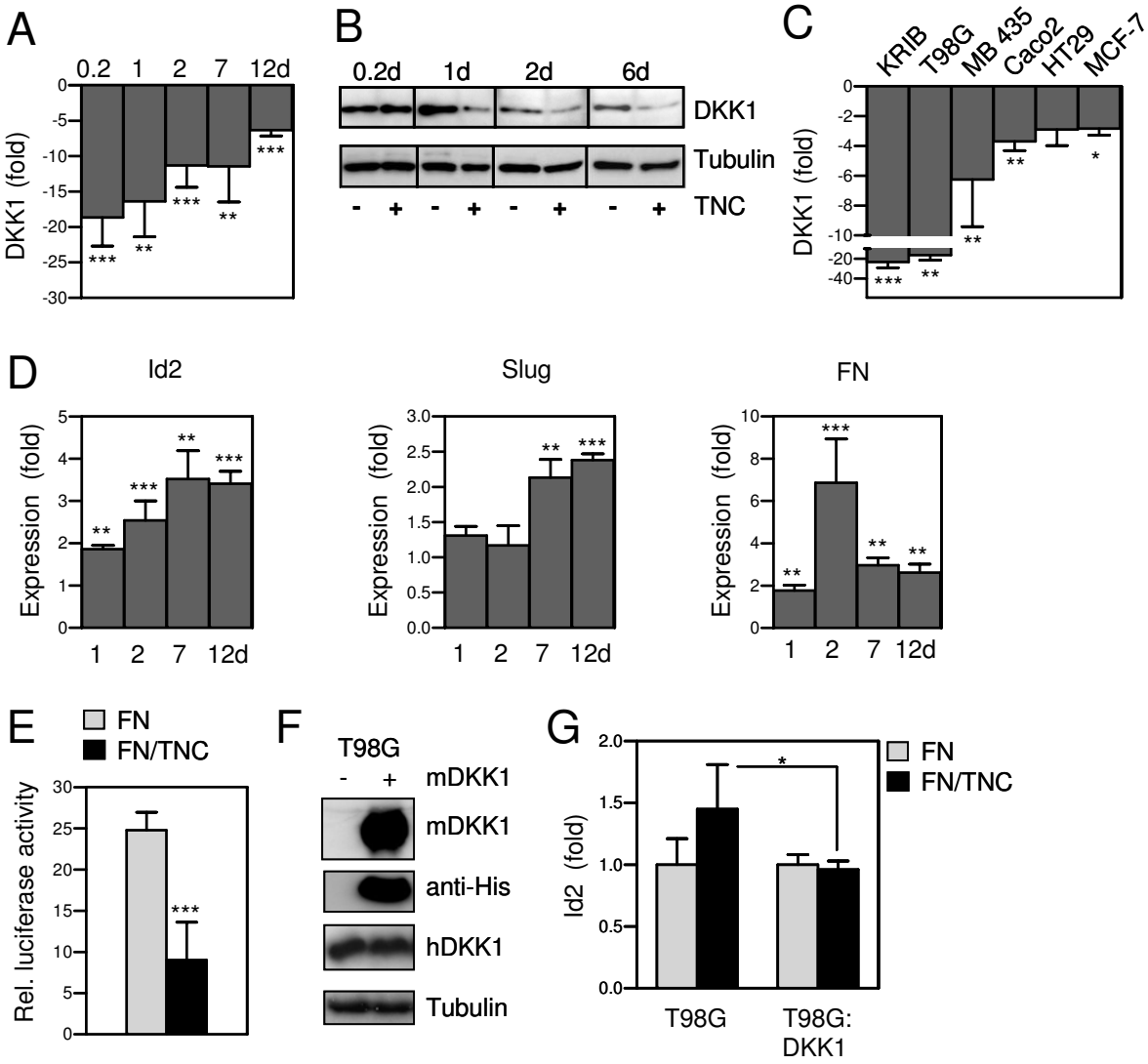
A
0.2 1 2 7 12d
DKK1 (fold)
B
0.2d 1d 2d 6d
DKK1
Tubulin
- + - + - + - +
TNC
C
KRIB T98G MB 435 Caco2 HT29 MCF-7
DKK1 (fold)
D
Id2
Slug
FN
Expression (fold)
1 2 7 12d
E
FN
FN/TNC
Rel. luciferase activity
F
T98G
- + mDKK1
mDKK1
anti-His
hDKK1
Tubulin
G
FN
FN/TNC
Id2 (fold)
T98G
T98G: DKK1

Fig. 7

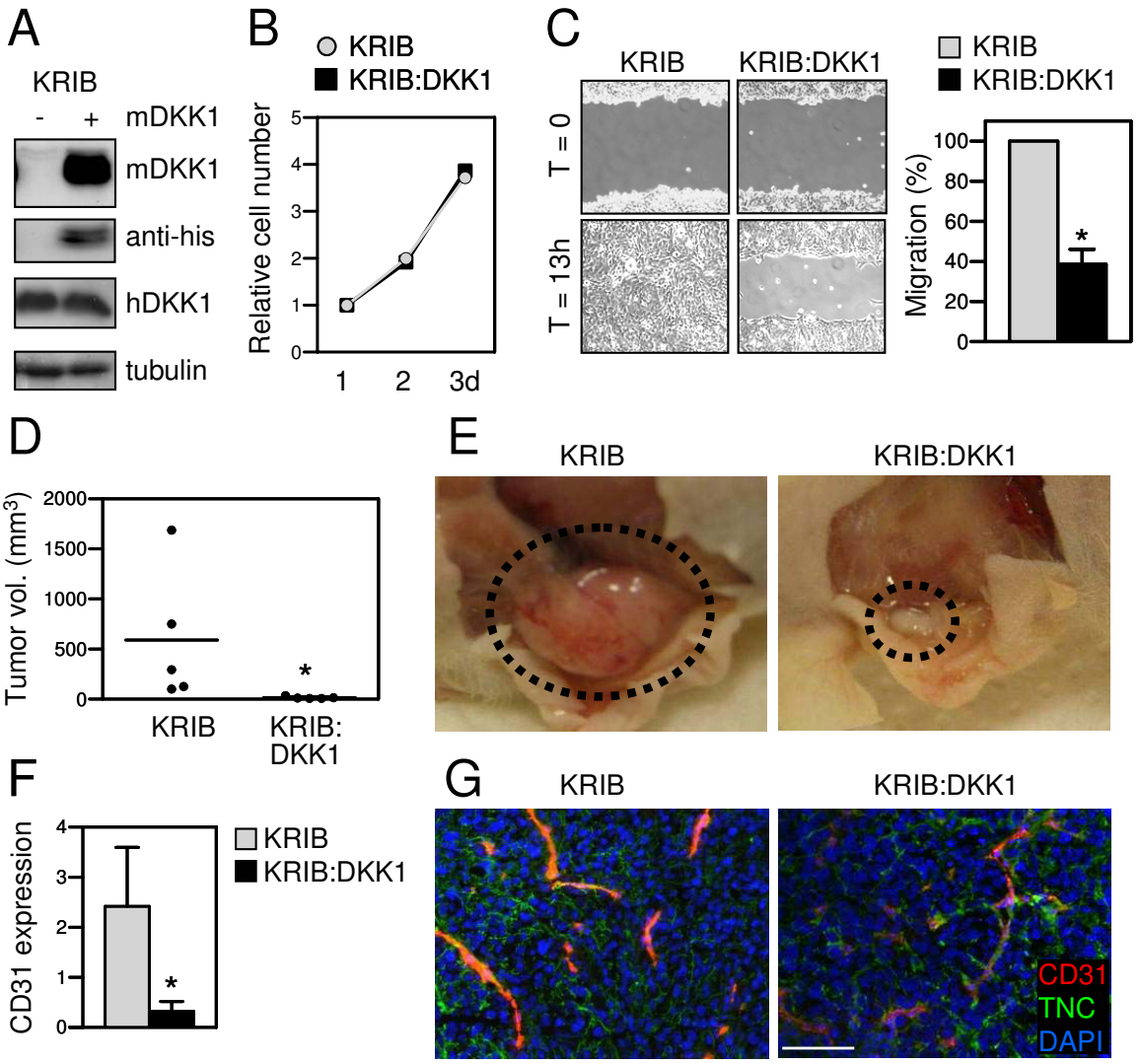
A
KRIB
- + mDKK1
mDKK1
anti-his
hDKK1
tubulin
B
KRIB
KRIB:DKK1
Relative cell number
1 2 3d
C
KRIB
KRIB:DKK1
T = 0
T = 13h
KRIB
KRIB:DKK1
Migration (%)
D
Tumor vol. (mm3)
KRIB
KRIB: DKK1
E
KRIB
KRIB:DKK1
F
CD31 expression
KRIB
KRIB:DKK1
G
KRIB
KRIB:DKK1
CD31
TNC
DAPI

Fig. 8

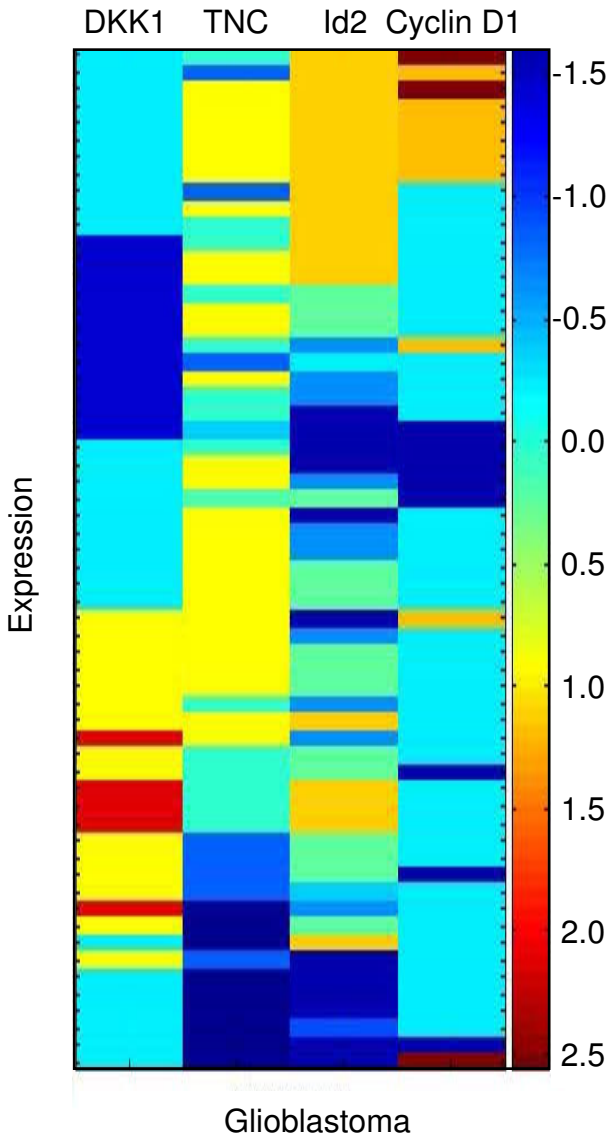
DKK1
TNC
Id2
Cyclin D1
Expression
Glioblastoma
-1.5
-1.0
-0.5
0.0
0.5
1.0
1.5
2.0
2.5

Fig. 9

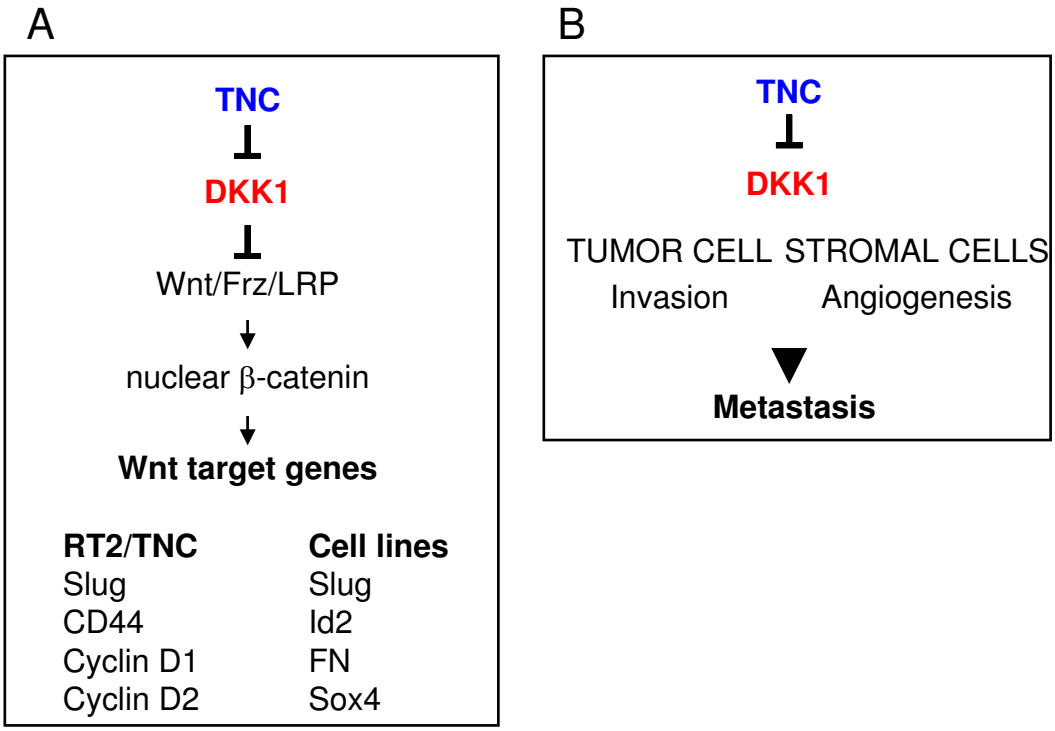
A
TNC
DKK1
Wnt/Frz/LRP
nuclear β-catenin
Wnt target genes
RT2/TNC
Slug
CD44
Cyclin D1
Cyclin D2
Cell lines
Slug
Id2
FN
Sox4
B
TNC
DKK1
TUMOR CELL
Invasion
STROMAL CELLS
Angiogenesis
Metastasis

Supplemental Fig. 1

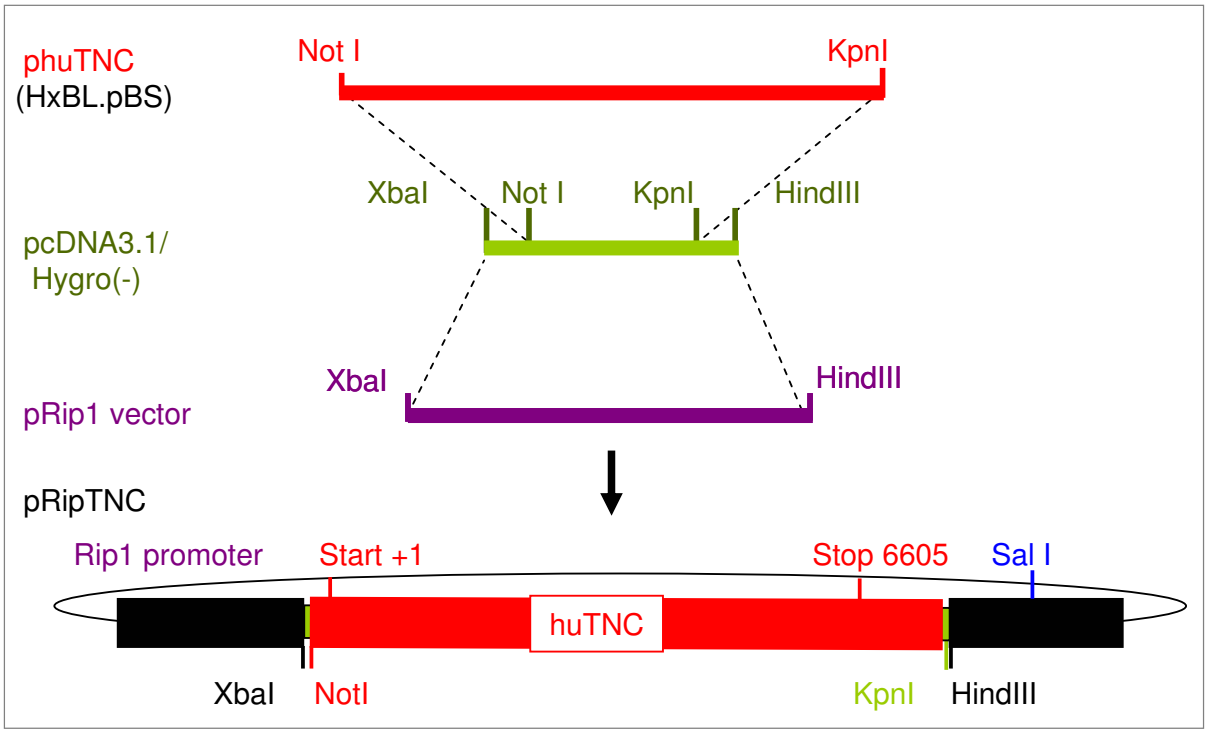

Supplemental Material and Methods

Construction of the TNC expression plasmid, generation of transgenic RipTNC mice and genotyping

The 7.5 kbp sequence of human TNC (accession number X78565.1) harboring a polyadenylation signal was removed from the HxBL.pBS plasmid (Aukhil et al., 1993; Gherzi et al., 1995) by restriction enzyme cleavage with NotI and KpnI and transferred into the intermediate pcDNA3.1/Hygro(-) vector (InVitrogen, Carlsbad, CA, USA). The resulting plasmid was cleaved with XbaI and HindIII before ligation behind the rat insulin II promoter into the corresponding cleavage sites of the 4.5 kb Rip1 vector containing an intron sequence (Hanahan, 1985). Successful cloning was confirmed by restriction enzyme cleavage and, by partial sequencing of 1000 bp around the start and the stop codon, respectively. Expression and secretion of the transgene product was determined upon 48h transient transfection of the expression plasmid into the established RT2 β-tumor cell line βT2 by immunofluorescence for human TNC with the B28.13 antibody (Wagner et al., 2003) in the absence of detergent for detection of secreted TNC. Secretion of human TNC was also determined by sandwich ELISA on conditioned medium from βT2 cells 48h after transfection using the B28.13 antibody for capturing and the TNC1.2. antibody (see below) for detection of bound human TNC (not shown). The RipTNC expression vector was used for injection into the pronucleus of fertilized oocytes upon linearization with SalI according to standard procedures (Labosky et al., 1994), giving rise to transgenic mice with stable transmission and expression of the transgene. Transgenic mice were identified by PCR with primers revP1 hTNC: 5`-GAA AGA CAC CTG CCA ACA GC-3` and RipES/VD: 5`-TAA TGG GAC AAA CAG CAA AG-3). For generation of double-transgenic RT2/TNC mice, single-transgenic RipTNC mice were crossed with RT2 mice (Hanahan, 1985).

Generation of RT2/TNCKO tumor model

RT2/TNCKO mice were generated by breeding of established transgenic Rip1Tag2 (Hanahan, 1985), TNCKO (Forsberg et al., 1996), respectively that had been crossed

into a C57Bl6 background. The respective genotype was determined by PCR with the following primers; RT2: Tag1 5`-GGACAAACCACAACTAGAATGCAG-3`, Tag2 5`-CAGAGCAGAATTGTGGAGTGG-3`; TNCKO: TNCup 5`-CTGCCAGGCATCTTTCTAGC-3`, TNCdown 5`-TTCTGCAGGTTGGAGGCAAC-3`, TNCNeoPA 5`-CTGCTCTTTACTGAAGGCTC-3`. Tumors in RT2/TNCKO and RT2/TNC+/- mice were investigated in a mixed C57Bl6 background containing 50-75% of 129/Sv. In this background tumorigenesis was delayed and mice were sacrificed at 15-17 weeks of age.

Generation of rabbit anti-TNC antibodies

Recombinantly expressed his-tagged human TNC was purified as described (Lange et al., 2007) and was used for injection into 2 rabbits, which gave rise to antisera TNC1.2 and TNC2.2 recognizing human and murine TNC by western blotting, IF and IHC.

Histological analysis and confocal microscopy

Pancreata from transgenic and control mice were isolated and fixed in 4% paraformaldehyde (PFA) overnight, fixed for 2h in 4% PFA and 20% sucrose overnight, and embedded in paraffin or Tissue Tek O.C.T. (Sakura Finetek Europe B.V., Zoeterwoude, Netherlands). Freshly isolated tissue was embedded in Tissue Tek O.C.T., frozen on dry ice or was snap frozen in liquid nitrogen. Histological analysis was done on H&E-stained paraffin sections. Immunostaining was done on paraffin sections (5 µm) or on cryosections (7 and 30 µm) as described (Compagni et al., 2000). The following antibodies were used: rabbit against TNC (TNC1.2, 1:200), phospho-histone-H3 (1:200, Upstate), cleaved caspase 3 (Cell Signalling), β-catenin (1:200, BD Transduction Laboratories), E-cadherin (1:200, BD Transduction Laboratories), KI67 (1:200, Thermo Scientific (RM-9106)), rat antibodies against murine TNC (MTn12, 1:100, (Aufderheide and Ekblom, 1988), CD31 (1:50, BD Pharmingen), the guineapig antibody against insulin (1:200, DakoCytomation) and mouse antibody B28.13 (1:50, Wagner et al., 2003). Nuclei were stained with 4`,6-diamino-2-phenylindole (DAPI).

The tumor diameter in 10 and 12 week old mice was measured on pictures of DAPI-stained tissue. Intra-tumoral microvessel density was analysed by quantifying CD31-positive signals per constant field using the Image J software (National Institute of Mental Health, Bethesda, MD). Students t-test was performed by using the Graph Pad Prism 4 Demo software. Histologic staging and grading of tumors was done on H&E sections. All sections were analysed with either an Axioskop2 plus light microscope using Axiovision 3.1 Software (Zeiss) or a Nikon Diaphot 300 immunofluorescence microscope (Nikon) using the Openlab 3.1.7. software (Improvision). Pancreatic islets were classified according to their size in diameter: normal islets (less than 0.2 mm), hyperplastic/dysplastic islets (0.2 – 0.5 mm), angiogenic islets (more than 0.5 up to 1.0 mm) and tumorigenic islets (more than 1.0 mm). Pancreatic islets were categorized according to size and morphology as normal/hyperplastic, including normal as well as enlarged islets; as angiogenic/tumorigenic (more than 0.5 mm), as adenoma (more than 1 mm), with well differentiated tumor cells, encapsulation, no invasive tumor edges; carcinoma grade 1, well differentiated and homogenous appearance of tumor cells, tumor capsule partially absent, one invasive tumor edge; carcinoma grade 2, partially dedifferentiated and heterogenous appearance of tumor cells, tumor capsule largely absent, more than one invasive tumor edge, carcinoma grade 3 or anaplastic tumor, complete loss of tumor cell differentiation, very heterogenous tumor appearance. For proliferation analysis tissue sections were stained with DAPI, insulin, and anti-PH3 antibody. Phospho-histone-H3 positive nuclei were counted in defined fields upon costaining with DAPI and insulin.

Immunohistochemical investigations of a panel of primary GBM was performed on a tissue micro array (Murat et al., 2008) according to standard procedures for paraffin sections using a heat induced epitope retrieval technique in citrate buffer (pH 6.0; pressure cooker, 3–5 min) and overnight incubation with the primary antibody. The following antibodies were used, anti-TNC (monoclonal, B28.13; dilution 1:2500; anti-DKK1 (IMGENEX ;1:500), Cyclin D1 (NeoMarker 1:500), and Id2 (Santa-Cruz; 1:10’000). The immunostainings were scored semiquantitatively. The tumors were

ordered by similarity of the expression profiles (scores 0–3) using the SPIN software (Tsafrir et al., 2005).

Expression analysis of candidate genes by qRT-PCR

Tissue from tumors, liver and lung of 12 – 17 week old mice was isolated and immediately snap frozen in liquid nitrogen. Total RNA was extracted using NucleoSpin RNA II kit (Macherey-Nagel, Düren, Germany) according to the manufacturer's protocol. Tissue from liver (1 µg), tumor or lung (2 µg) was treated with DNase I (Invitrogen) and reverse transcribed using MultiScribe reverse transcriptase (Applied Biosystems, Fostercity, CA, USA). cDNA was diluted with water to 100 µl (liver, lung) or 200 µl (tumors). QRT-PCR was performed on a 7500 Real Time PCR System (Applied Biosystems) using SYBR green (Applied Biosystems, Warrington, UK) or Taqman reaction mixtures (Applied Biosystems, Fostercity, CA, USA). Primers were found in the database (http://medgen.ugent.be/rtprimerdb/), designed using appropriate tools (Primer3 or Roche software, Roche) or Applied Biosystems (Taqman assay) and are listed in **Suppl. Tables 5** and **6**. Samples were analysed in 10 µl using 1 –5 µl (tumors) or 2.5 µl (liver, lung) cDNA. Data were normalized to a reference (sum of RPL9, TBP and GAPDH (tumors), TBP (liver, lung) and β2MG (cells). Relative expression between RT2 and RT2/TNC and, FN and FN/TNC samples was calculated based on the mean ΔΔct-value.

Scanning electron microscopy and transmission electron microscopy

For preparation of vascular casts, the systemic vasculature was perfused with a freshly prepared Mercox solution (Vilene Company, Japan) containing 0.1 ml of accelerator per 5 ml of resin. One hour after perfusion, the pancreas was excised and tissue was removed in 7.5% potassium hydroxide for up to 3 weeks. After washing, the casts were dehydrated in ethanol and dried in a vacuum desiccator. The samples were then sputtered with gold to a thickness of 10 nm and examined in a Philips XL-30 SFEG scanning electron microscope (SEM). Sections (80 - 90 nm) were prepared and mounted

on copper grids coated with Formvar (polyvinyl formal; Fluka, Buchs, Switzerland). They were stained with lead citrate and uranyl acetate prior to viewing in a Philips EM-400 electron microscope.

References to Supplemental Material

Aufderheide, E. and Ekblom, P. (1988) Tenascin during gut development: appearance in the mesenchyme, shift in molecular forms, and dependence on epithelial-mesenchymal interactions. *J Cell Biol*, **107**, 2341-2349.

Aukhil, I., Joshi, P., Yan, Y. and Erickson, H.P. (1993) Cell- and heparin-binding domains of the hexabrachion arm identified by tenascin expression proteins. *J Biol Chem*, **268**, 2542-2553.

Compagni, A., Wilgenbus, P., Impagnatiello, M.A., Cotten, M. and Christofori, G. (2000) Fibroblast growth factors are required for efficient tumor angiogenesis. *Cancer Res*, **60**, 7163-7169.

Forsberg, E., Hirsch, E., Frohlich, L., Meyer, M., Ekblom, P., Aszodi, A., Werner, S. and Fassler, R. (1996) Skin wounds and severed nerves heal normally in mice lacking tenascin-C. *Proc Natl Acad Sci U S A*, **93**, 6594-6599.

Gherzi, R., Carnemolla, B., Siri, A., Ponassi, M., Balza, E. and Zardi, L. (1995) Human tenascin gene. Structure of the 5'-region, identification, and characterization of the transcription regulatory sequences. *J Biol Chem*, **270**, 3429-3434.

Hanahan, D. (1985) Heritable formation of pancreatic beta-cell tumours in transgenic mice expressing recombinant insulin/simian virus 40 oncogenes. *Nature*, **315**, 115-122.

Labosky, P.A., Barlow, D.P. and Hogan, B.L. (1994) Embryonic germ cell lines and their derivation from mouse primordial germ cells. *Ciba Found Symp*, **182**, 157-168; discussion 168-178.

Murat, A., Migliavacca, E., Gorlia, T., Lambiv, W.L., Shay, T., Hamou, M.F., de Tribolet, N., Regli, L., Wick, W., Kouwenhoven, M.C., Hainfellner, J.A., Heppner, F.L., Dietrich, P.Y., Zimmer, Y., Cairncross, J.G., Janzer, R.C., Domany, E., Delorenzi, M., Stupp, R. and Hegi, M.E. (2008) Stem cell-related "self-renewal" signature and high epidermal growth factor receptor expression associated with resistance to concomitant chemoradiotherapy in glioblastoma. *J Clin Oncol*, **26**, 3015-3024.

Tsafrir, D., Tsafrir, I., Ein-Dor, L., Zuk, O., Notterman, D.A. and Domany, E. (2005) Sorting points into neighborhoods (SPIN): data analysis and visualization by ordering distance matrices. *Bioinformatics*, **21**, 2301-2308.

Wagner, S., Hofstetter, W., Chiquet, M., Mainil-Varlet, P., Stauffer, E., Ganz, R. and Siebenrock, K.A. (2003) Early osteoarthritic changes of human femoral head cartilage subsequent to femoro-acetabular impingement. *Osteoarthritis Cartilage*, **11**, 508-518.

Supplemental Figures

Suppl. Fig. 1 TNC expression vector

Cloning of the sequence encoding human TNC harboring a polyadenylation signal was removed from the HxBL.pBS plasmid by restriction enzyme cleavage with NotI and KpnI and was transferred into the Rip1 vector by using the indicated restriction enzymes and the pcDNA3.1 vector as intermediate. The inserted human cDNA sequence comprises 45 nucleotides upstream of the start site and 639 nucleotides downstream of the stop signal.

Suppl. Table 1 TNC-dependent pancreatic islet size in RT2 tumors

Genotype	N (%)	H (%)	A (%)	T (%)	N, H (%)	A,T (%)	AT/NH
RT2	12.3	58.9	24.7	4.1	71.2	28.8	0.4
RT2/TNC	15.2	40.5	35.4	8.9	55.7	44.3	0.8

Analysis of pancreatic islets of RT2 (n = 5) and RT2/TNC (n = 7) mice at 10 weeks of age. Islet diameter on tissue sections (average 12 tumors per mouse, total 73 RT2 and 79 RT2/TNC) was used for classification. Normal (N) (< 0.2 mm), hyperplastic (H) (0.2 - 0.5 mm), angiogenic (A) (> 0.5 - 1 mm) and tumorigenic (T) (> 1.0 mm). AT/NH, $p = 0.06$, Fisher`s exact test.

Suppl. Table 2 Carcinoma progression by TNC

Genotype	Adenoma (%)	Carcinoma (%) Grade 1	Grade 2	Grade 3	Grade 1 - 3	Ca/Ad
RT2	55.8	32.7	10.5	0.9	44.2	0.8
RT2/TNC	35.7	39.9	21.3	3.2	64.3	1.8

Analysis of numbers of adenomas and carcinomas grade 1 – 3 in 12 week old mice. The distribution of adenomas and compiled carcinomas grade 1 – 3 between genotypes was significantly different, $p < 0.05$, Fisher`s exact test.

Suppl. Table 3 Analysis of Candidate Gene expression in RT2 Tumors

Candidate gene	Tumor	ΔΔCt RT2/TNC versus RT2	p value	Relative expression
CD44	All	-0.46	0.22	1.38
	Small	-0.54	0.19	1.45
	Small + Diff	**-0.88**	**0.03**	**1.84**
	Big	0.71	0.11	-1.64
	Big + Diff	0.71	0.11	-1.64
	Diff	-0.54	0.15	1.46
Cyclin D1	All	-0.77	0.13	1.70
	Small	-1.02	0.11	2.02
	Small + Diff	**-1.30**	**0.03**	**2.46**
	Big	0.13	0.86	-1.10
	Big + Diff	0.51	0.50	-1.43
	Diff	-0.91	0.07	1.88
Cyclin D2	All	-0.38	0.29	1.30
	Small	-0.50	0.14	1.42
	Small + Diff	**-0.71**	**0.03**	**1.64**
	Big	0.43	0.37	-1.35
	Big + Diff	0.67	0.21	-1.59
	Diff	-0.41	0.21	1.33
DKK1	All	**1.71**	**<0.01**	**-3.23**
	Small	**1.61**	**0.02**	**-3.03**
	Small Diff	**1.36**	**0.02**	**-2.56**
	Big	1.88	n.a.	-3.70
	Big Diff	0.74	n.a.	-1.67
	Diff Only	**1.22**	**0.01**	**-2.33**
	Diff	n.a.	n.a.	n.a.
Slug	All	-0.25	0.43	1.19
	Small	**-0.72**	**0.04**	**1.64**
	Small + Diff	**-0.84**	**0.02**	**1.79**
	Big	1.29	0.05	-2.44
	Big + Diff	1.00	0.19	-2.00
	Diff	-0.44	0.18	1.36

Relative gene expression of candidate genes (alphabetical order) in RT2/TNC tumors versus RT2 tumors is based on ΔΔCt values that were determined by SYBR Green qRT-PCR on RNA isolated from 14 week old RT2 (N = 11 mice, n = 28 tumors) and RT2/TNC mice (N = 3, n = 14). Gene expression was normalized to the median value of three genes, TBP, GAPDH and RPL-9 and was used to determine ΔΔCt. Data are presented for all tumors (All), small tumors (Small, 1 – 3 mm in diameter, RT2 (n = 20), RT2/TNC (n = 11), big tumors (Big > 3 mm, RT2 (n = 8), RT2/TNC (n = 3), differentiated tumors (Diff., high expression of insulin and E-cadherin), RT2 (n = 23), RT2/TNC (n = 14), small and differentiated tumors (Small diff.), RT2 (n = 18), RT2/TNC (n = 11) and big and

differentiated tumors (Big diff.), RT2 (n = 5), RT2/TNC (n = 3). Statistical differences were calculated for the ΔΔCt values using adequate Student's t-test. Bold numbers represent statistically significant data: p values, cyclin D1 (p = 0.0336, t-test), cyclin D2 (p = 0.0321, t-test with Welsh correction), CD44 (p = 0.031, t-test), Slug (p .0195, t-test). n.a., not applicable due to too small sample number with detectable expression. DKK1, Dickkopf 1, Id2, inhibitor of differentiation 2.

Suppl. Table 4 TNC-dependent Gene Expression of Wnt Target Genes in Cultured Tumor Cells

Cell line	Time (days)	Id2	Slug	FN	Sox4
T98G	1	**1.9**	1.3	**1.8**	1.5
	2	**2.5**	1.2	**6.9**	0.9
	7	**3.5**	**2.1**	**3.0**	**2.0**
KRIB	1	0.9	0.8	1.0	**2.1**
	6	0.9	**2.4**	**2.2**	1.1
MDA MB435	1	0.6	0.7	0.3	1.0
	6	0.6	0.7	0.4	1.3

Gene expression was determined by qRT-PCR on RNA isolated from the indicated cell lines upon plating on FN or FN/TNC and is expressed as ratio FN/TNC versus FN (fold). Experiments were done in triplicates per time point. Bold, p value < 0.05.

Suppl. Table 5 Primer List for qRT-PCR on tumor and lung tissue

Gene	Forward primer	Reverse primer
CD44	GTCTGCATCGCGGTCAATAG	GGTCTCTGATGGTTCCTTGTTC
CyclinD1	CGCACTTTCTTTCCAGAGTCA	AAGGGCTTCAATCTGTTCCTG
CyclinD2	CACCGACAACTCTGTGAAGC	TCCACTTCAGCTTACCCAACA
DKK1	Taqman mDKK1 Mm00438422_m1	
DKK1	CCGGGAACTACTGCAAAAAT	CCAAGGTTTTCAATGATGCTT
E-Cadherin	CAGCCTTCTTTTCGGAAGACT	GGTAGACAGCTCCCTATGACTG
Insulin	TGGCTTCTTCTACACACCCAAG	ACAATGCCACGCTTCTGCC
Insulin	Taqman mIns1 Mm01259683_g1	
Slug	GAAAAGCACATTGCATCTTTTCT	TGTTCCTTTGGTTGAAATGGT
TNC mouse	GCGCAGACACACACCCTAGC	TTTCCAGGTCGGGAAAAGCA
TNC human	CCTTGCTGTAGAGGTCGTCA	CCAACCTCAGACACGGCTA
RPL9	ACCCTGGCCCGACGG	TACCCTTCCTCTTCCCTATGCC
TBP	CCCCACAACTCTTCCATTCT	GCAGGAGTGATAGGGGTCAT
GAPDH	Taqman Mm99999915_g1	

Suppl. Table 6 Primer List for qRT-PCR on cultured cells

Gene	Forward primer	Reverse primer
DKK-1	GACCATTGACAACTACCAGCCG	TACTCATCAGTGCCGCACTCCT
Id2	TCAGCCTGCATCACCAGAGA	CTGCAAGGACAGGATGCTGATA
Slug	ATGAGGAATCTGGCTGCTGT	CAGGAGAAAATGCCTTTGGA
Fibronectin	CCCATCAGCAGGAACACCTT	GGCTCACTGCAAAGACTTTGA A
Sox4	CAGCAAGAGAAACTGTGTGTGA	AAGAGCGTGCAAGAACTAGAGA
β2-Microglobulin	GTGGGATCGAGACATGTAAGCA	AATGCGGCATCTTCAAACCT

9 Acknowledgements

The present thesis is the result of a work performed within the mixed unit of Inserm and the University of Strasbourg “Inserm-UdS U682 – de l’homéostasie tissulaire au cancer et à l’inflammation” in the group of Gertraud Orend “Microenvironmental impact on angiogenesis and tumor invasion”.

I would like to thank Dr. Catherine Monnot, Prof. Dr. Christel Herold-Mende and Prof. Dr. Jan De Mey for the evaluation of the present work.

In particular, I would like to express my gratitude to Dr. Gertraud Orend for being my mentor during this thesis. I thank you for having given me the opportunity to perform my PhD as a part of your research group, for sharing your enormous knowledge about extracellular matrix and cancer and for the financial support given during the last four years. Without your remarkable constant motivation I would not have achieved what you hold in your hands now.

I thank Dr. Klaus-Peter Janssen and Dr. Patricia Simon-Assmann for evaluating my work as members of the half-term committee and for following the progress of my work until the end of this thesis.

I also thank Dr. Jean-François Launay and the director of the research unit Dr. Michèle Kedinger for helping me to better understand the French scientific system. I thank Dr. Thomas Hussenet and Dr. Benoît Langlois for the fruitful teamwork during the last months. I thank Anja Heinke, Thomas and Benoît for the constructive review of this thesis.

I wish to express my gratitude to everyone at the institute who helped me during my PhD training.

I thank the Swiss National Cancer Program Oncosuisse for the financial support given during the first years of this thesis. Notably, I thank the French Fondation des Treilles for appreciating my work by granting me their Young researcher award in 2011.

Zuletzt möchte ich meiner Familie, meinen Eltern Gislinde und Rolf, meiner Schwester Silvia, meinem Neffen Theo sowie meinen Großeltern Dorothea und Fritz, Inge und Gerhard, Ingrid und Heinz für Ihr großes Interesse an meinem wissenschaftlichen Leben und Ihrer unablässigen geistigen Unterstützung in aller Hinsicht danken.

Strasbourg, September 2011

10 References

Adams, J. M., and Cory, S. (2007). The Bcl-2 apoptotic switch in cancer development and therapy. Oncogene *26*, 1324-1337.

Adams, R. H., and Eichmann, A. (2010). Axon guidance molecules in vascular patterning. Cold Spring Harb Perspect Biol *2*, a001875.

Aguirre-Ghiso, J. A. (2007). Models, mechanisms and clinical evidence for cancer dormancy. Nat Rev Cancer *7*, 834-846.

Aicher, A., Kollet, O., Heeschen, C., Liebner, S.*, et al.* (2008). The Wnt antagonist Dickkopf-1 mobilizes vasculogenic progenitor cells via activation of the bone marrow endosteal stem cell niche. Circ Res *103*, 796-803.

Almog, N. (2010). Molecular mechanisms underlying tumor dormancy. Cancer Lett *294*, 139-146.

Alpert, S., Hanahan, D., and Teitelman, G. (1988). Hybrid insulin genes reveal a developmental lineage for pancreatic endocrine cells and imply a relationship with neurons. Cell *53*, 295-308.

Alves, T. R., da Fonseca, A. C., Nunes, S. S., da Silva, A. O.*, et al.* (2011). Tenascin-C in the extracellular matrix promotes the selection of highly proliferative and tubulogenesis-defective endothelial cells. Exp Cell Res.

Anand, P., Kunnumakkara, A. B., Sundaram, C., Harikumar, K. B.*, et al.* (2008). Cancer is a preventable disease that requires major lifestyle changes. Pharm Res *25*, 2097-2116.

Asparuhova, M. B., Ferralli, J., Chiquet, M., and Chiquet-Ehrismann, R. (2011). The transcriptional regulator megakaryoblastic leukemia-1 mediates serum response factor-independent activation of tenascin-C transcription by mechanical stress. Faseb J.

Aufderheide, E., and Ekblom, P. (1988). Tenascin during gut development: appearance in the mesenchyme, shift in molecular forms, and dependence on epithelial-mesenchymal interactions. J Cell Biol *107*, 2341-2349.

Aukhil, I., Joshi, P., Yan, Y., and Erickson, H. P. (1993). Cell- and heparin-binding domains of the hexabrachion arm identified by tenascin expression proteins. J Biol Chem *268*, 2542-2553.

Ballard, V. L., Sharma, A., Duignan, I., Holm, J. M.*, et al.* (2006). Vascular tenascin-C regulates cardiac endothelial phenotype and neovascularization. Faseb J *online Feb. 6*.

Baluk, P., Hashizume, H., and McDonald, D. M. (2005). Cellular abnormalities of blood vessels as targets in cancer. Current opinion in genetics & development *15*, 102-111.

Barkan, D., Green, J. E., and Chambers, A. F. (2010). Extracellular matrix: a gatekeeper in the transition from dormancy to metastatic growth. Eur J Cancer *46*, 1181-1188.

Bergers, G., and Benjamin, L. E. (2003). Tumorigenesis and the angiogenic switch. Nat Rev Cancer *3*, 401-410.

Bergers, G., and Hanahan, D. (2008). Modes of resistance to anti-angiogenic therapy. Nat Rev Cancer *8*, 592-603.

Borsi, L., Allemanni, G., Gaggero, B., and Zardi, L. (1996). Extracellular pH controls pre-mRNA alternative splicing of tenascin-C in normal, but not in malignantly transformed, cells. Int J Cancer *66*, 632-635.

Bourdon, M. A., Wikstrand, C. J., Furthmayr, H., Matthews, T. J.*, et al.* (1983). Human glioma-mesenchymal extracellular matrix antigen defined by monoclonal antibody. Cancer Res *43*, 2796-2805.

Brellier, F., Tucker, R. P., and Chiquet-Ehrismann, R. (2009). Tenascins and their implications in diseases and tissue mechanics. Scand J Med Sci Sports *19*, 511-519.

Breslin, M. B., Zhu, M., Notkins, A. L., and Lan, M. S. (2002). Neuroendocrine differentiation factor, IA-1, is a transcriptional repressor and contains a specific DNA-binding domain: identification of consensus IA-1 binding sequence. Nucleic Acids Res *30*, 1038-1045.

Bridges, E., Oon, C. E., and Harris, A. (2011). Notch regulation of tumor angiogenesis. Future Oncol *7*, 569-588.

Calvo, A., Catena, R., Noble, M. S., Carbott, D.*, et al.* (2008). Identification of VEGF-regulated genes associated with increased lung metastatic potential: functional involvement of tenascin-C in tumor growth and lung metastasis. Oncogene *27*, 5373-5384.

Carmeliet, P., and Jain, R. K. (2011a). Molecular mechanisms and clinical applications of angiogenesis. Nature *473*, 298-307.

Carmeliet, P., and Jain, R. K. (2011b). Principles and mechanisms of vessel normalization for cancer and other angiogenic diseases. Nat Rev Drug Discov *10*, 417-427.

Carmeliet, P., Moons, L., Luttun, A., Vincenti, V.*, et al.* (2001). Synergism between vascular endothelial growth factor and placental growth factor contributes to angiogenesis and plasma extravasation in pathological conditions. Nat Med *7*, 575-583.

Chiquet-Ehrismann, R. (2004). Tenascins. Int J Biochem Cell Biol *36*, 986-990.

Chiquet-Ehrismann, R., and Chiquet, M. (2003). Tenascins: regulation and putative functions during pathological stress. J Pathol *200*, 488-499.

Chiquet-Ehrismann, R., Mackie, E. J., Pearson, C. A., and Sakakura, T. (1986). Tenascin: an extracellular matrix protein involved in tissue interactions during fetal development and oncogenesis. Cell *47*, 131-139.

Chiquet-Ehrismann, R., Tannheimer, M., Koch, M., Brunner, A.*, et al.* (1994). Tenascin-C expression by fibroblasts is elevated in stressed collagen gels. J Cell Biol *127*, 2093-2101.

Chiquet-Ehrismann, R., and Tucker, R. P. (2011). Tenascins and the importance of adhesion modulation. Cold Spring Harb Perspect Biol *3*.

Chiquet, M., and Fambrough, D. M. (1984). Chick myotendinous antigen. II. A novel extracellular glycoprotein complex consisting of large disulfide-linked subunits. J Cell Biol *98*, 1937-1946.

Chun, M. G., and Hanahan, D. (2010). Genetic deletion of the desmosomal component desmoplakin promotes tumor microinvasion in a mouse model of pancreatic neuroendocrine carcinogenesis. PLoS Genet *6*.

Comoglio, P. M., and Trusolino, L. (2005). Cancer: the matrix is now in control. Nat Med *11*, 1156-1159.

Crocker, D. J., Murad, T. M., and Geer, J. C. (1970). Role of the pericyte in wound healing. An ultrastructural study. Exp Mol Pathol *13*, 51-65.

Darland, D. C., and D'Amore, P. A. (1999). Blood vessel maturation: vascular development comes of age. J Clin Invest *103*, 157-158.

De Langhe, S. P., Sala, F. G., Del Moral, P. M., Fairbanks, T. J.*, et al.* (2005). Dickkopf-1 (DKK1) reveals that fibronectin is a major target of Wnt signaling in branching morphogenesis of the mouse embryonic lung. Developmental biology *277*, 316-331.

De Wever, O., Nguyen, Q. D., Van Hoorde, L., Bracke, M.*, et al.* (2004). Tenascin-C and SF/HGF produced by myofibroblasts in vitro provide convergent pro-invasive signals to human colon cancer cells through RhoA and Rac. Faseb J *18*, 1016-1018.

Degen, M., Brellier, F., Kain, R., Ruiz, C.*, et al.* (2007). Tenascin-W is a novel marker for activated tumor stroma in low-grade human breast cancer and influences cell behavior. Cancer Res *67*, 9169-9179.

Degen, M., Brellier, F., Schenk, S., Driscoll, R.*, et al.* (2008). Tenascin-W, a new marker of cancer stroma, is elevated in sera of colon and breast cancer patients. Int J Cancer *122*, 2454-2461.

Dome, B., Hendrix, M. J., Paku, S., Tovari, J.*, et al.* (2007). Alternative vascularization mechanisms in cancer: Pathology and therapeutic implications. Am J Pathol *170*, 1-15.

Dor, Y., Porat, R., and Keshet, E. (2001). Vascular endothelial growth factor and vascular adjustments to perturbations in oxygen homeostasis. Am J Physiol Cell Physiol *280*, C1367-1374.

Drumea-Mirancea, M., Wessels, J. T., Muller, C. A., Essl, M.*, et al.* (2006). Characterization of a conduit system containing laminin-5 in the human thymus: a potential transport system for small molecules. J Cell Sci *119*, 1396-1405.

Du, Y. C., Lewis, B. C., Hanahan, D., and Varmus, H. (2007). Assessing tumor progression factors by somatic gene transfer into a mouse model: Bcl-xL promotes islet tumor cell invasion. PLoS Biol *5*, e276.

Ebos, J. M., Lee, C. R., Cruz-Munoz, W., Bjarnason, G. A.*, et al.* (2009). Accelerated metastasis after short-term treatment with a potent inhibitor of tumor angiogenesis. Cancer Cell *15*, 232-239.

Egeblad, M., Nakasone, E. S., and Werb, Z. (2010). Tumors as organs: complex tissues that interface with the entire organism. Dev Cell *18*, 884-901.

Erickson, H. P., and Bourdon, M. A. (1989). Tenascin: an extracellular matrix protein prominent in specialized embryonic tissues and tumors. Annu Rev Cell Biol *5*, 71-92.

Fearon, E. R., and Vogelstein, B. (1990). A genetic model for colorectal tumorigenesis. Cell *61*, 759-767.

Folberg, R., Hendrix, M. J., and Maniotis, A. J. (2000). Vasculogenic mimicry and tumor angiogenesis. Am J Pathol *156*, 361-381.

Folkman, J., Watson, K., Ingber, D., and Hanahan, D. (1989). Induction of angiogenesis during the transition from hyperplasia to neoplasia. Nature *339*, 58-61.

Forsberg, E., Hirsch, E., Frohlich, L., Meyer, M.*, et al.* (1996). Skin wounds and severed nerves heal normally in mice lacking tenascin-C. Proc Natl Acad Sci U S A *93*, 6594-6599.

Franco, C. A., Liebner, S., and Gerhardt, H. (2009). Vascular morphogenesis: a Wnt for every vessel? Current opinion in genetics & development *19*, 476-483.

Fukunaga-Kalabis, M., Martinez, G., Nguyen, T. K., Kim, D.*, et al.* (2010). Tenascin-C promotes melanoma progression by maintaining the ABCB5-positive side population. Oncogene *29*, 6115-6124.

Fuxe, J., Tabruyn, S., Colton, K., Zaid, H., *et al.* (2011). Pericyte requirement for anti-leak action of angiopoietin-1 and vascular remodeling in sustained inflammation. Am J Pathol *178*, 2897-2909.

Gaggioli, C., Hooper, S., Hidalgo-Carcedo, C., Grosse, R.*, et al.* (2007). Fibroblast-led collective invasion of carcinoma cells with differing roles for RhoGTPases in leading and following cells. Nat Cell Biol *9*, 1392-1400.

Garber, M. E., Troyanskaya, O. G., Schluens, K., Petersen, S.*, et al.* (2001). Diversity of gene expression in adenocarcinoma of the lung. Proc Natl Acad Sci U S A *98*, 13784-13789.

Garcion, E., Faissner, A., and ffrench-Constant, C. (2001). Knockout mice reveal a contribution of the extracellular matrix molecule tenascin-C to neural precursor proliferation and migration. Development *128*, 2485-2496.

Gaur, P., Bielenberg, D. R., Samuel, S., Bose, D., *et al.* (2009). Role of class 3 semaphorins and their receptors in tumor growth and angiogenesis. Clin Cancer Res *15*, 6763-6770.

Gherzi, R., Ponassi, M., Gaggero, B., and Zardi, L. (1995). The first untranslated exon of the human tenascin-C gene plays a regulatory role in gene transcription. FEBS Lett *369*, 335-339.

Glaw, J. T., Skalak, T. C., and Peirce, S. M. (2010). Inhibition of canonical Wnt signaling increases microvascular hemorrhaging and venular remodeling in adult rats. Microcirculation *17*, 348-357.

Greaves, M. F. (2000). Cancer : the evolutionary legacy, (Oxford: Oxford University Press).

Grumet, M., Hoffman, S., Crossin, K. L., and Edelman, G. M. (1985). Cytotactin, an extracellular matrix protein of neural and non-neural tissues that mediates glia-neuron interaction. Proc Natl Acad Sci U S A *82*, 8075-8079.

Hanahan, D. (1985). Heritable formation of pancreatic beta-cell tumours in transgenic mice expressing recombinant insulin/simian virus 40 oncogenes. Nature *315*, 115-122.

Hanahan, D., Christofori, G., Naik, P., and Arbeit, J. (1996). Transgenic mouse models of tumour angiogenesis: the angiogenic switch, its molecular controls, and prospects for preclinical therapeutic models. Eur J Cancer *32A*, 2386-2393.

Hanahan, D., and Folkman, J. (1996). Patterns and emerging mechanisms of the angiogenic switch during tumorigenesis. Cell *86*, 353-364.

Hanahan, D., and Weinberg, R. A. (2000). The hallmarks of cancer. Cell *100*, 57-70.

Hanahan, D., and Weinberg, R. A. (2011). Hallmarks of cancer: the next generation. Cell *144*, 646-674.

Hay, E. D. (1981). Extracellular matrix. J Cell Biol *91*, 205s-223s.

Helleman, J., Jansen, M. P., Ruigrok-Ritstier, K., van Staveren, I. L.*, et al.* (2008). Association of an extracellular matrix gene cluster with breast cancer prognosis and endocrine therapy response. Clin Cancer Res *14*, 5555-5564.

Hendrix, M. J., Seftor, E. A., Hess, A. R., and Seftor, R. E. (2003). Vasculogenic mimicry and tumour-cell plasticity: lessons from melanoma. Nature reviews *3*, 411-421.

Herlyn, M., Graeven, U., Speicher, D., Sela, B. A.*, et al.* (1991). Characterization of tenascin secreted by human melanoma cells. Cancer Res *51*, 4853-4858.

Herold-Mende, C., Mueller, M. M., Bonsanto, M. M., Schmitt, H. P., *et al.* (2002). Clinical impact and functional aspects of tenascin-C expression during glioma progression. Int J Cancer *98*, 362-369.

Herzig, M., Savarese, F., Novatchkova, M., Semb, H., *et al.* (2007). Tumor progression induced by the loss of E-cadherin independent of beta-catenin/Tcf-mediated Wnt signaling. Oncogene *26*, 2290-2298.

Hlubek, F., Brabletz, T., Budczies, J., Pfeiffer, S., *et al.* (2007). Heterogeneous expression of Wnt/beta-catenin target genes within colorectal cancer. Int J Cancer *121*, 1941-1948.

Irizarry, R. A., Bolstad, B. M., Collin, F., Cope, L. M., *et al.* (2003). Summaries of Affymetrix GeneChip probe level data. Nucleic Acids Res *31*, e15.

Jones, P. L., Chapados, R., Baldwin, H. S., Raff, G. W., *et al.* (2002). Altered hemodynamics controls matrix metalloproteinase activity and tenascin-C expression in neonatal pig lung. Am J Physiol Lung Cell Mol Physiol *282*, L26-35.

Kaariainen, E., Nummela, P., Soikkeli, J., Yin, M., *et al.* (2006). Switch to an invasive growth phase in melanoma is associated with tenascin-C, fibronectin, and procollagen-I forming specific channel structures for invasion. J Pathol *210*, 181-191.

Kalluri, R., and Zeisberg, M. (2006). Fibroblasts in cancer. Nat Rev Cancer *6*, 392-401.

Kant, J. (2008). Analysis of tenascin-C induced angiogenesis. Master thesis, University of Basel, Institute of Biochemistry and Genetics, Department of Biomedicine, Basel.

Kerbel, R. S. (1991). Inhibition of tumor angiogenesis as a strategy to circumvent acquired resistance to anti-cancer therapeutic agents. Bioessays *13*, 31-36.

Klaus, A., and Birchmeier, W. (2008). Wnt signalling and its impact on development and cancer. Nat Rev Cancer *8*, 387-398.

Kruse, J., Keilhauer, G., Faissner, A., Timpl, R., *et al.* (1985). The J1 glycoprotein--a novel nervous system cell adhesion molecule of the L2/HNK-1 family. Nature *316*, 146-148.

Kurz, H., Burri, P. H., and Djonov, V. G. (2003). Angiogenesis and vascular remodeling by intussusception: from form to function. News Physiol Sci *18*, 65-70.

Kutcher, M. E., and Herman, I. M. (2009). The pericyte: cellular regulator of microvascular blood flow. Microvasc Res *77*, 235-246.

Lambertini, E., Franceschetti, T., Torreggiani, E., Penolazzi, L., *et al.* (2010). SLUG: a new target of lymphoid enhancer factor-1 in human osteoblasts. BMC Mol Biol *11*, 13.

Lange, K., Kammerer, M., Saupe, F., Hegi, M. E., *et al.* (2008). Combined lysophosphatidic acid/platelet-derived growth factor signaling triggers glioma cell migration in a tenascin-C microenvironment. Cancer Res *68*, 6942-6952.

Leins, A., Riva, P., Lindstedt, R., Davidoff, M. S., *et al.* (2003). Expression of tenascin-C in various human brain tumors and its relevance for survival in patients with astrocytoma. Cancer *98*, 2430-2439.

Lightner, V. A., Gumkowski, F., Bigner, D. D., and Erickson, H. P. (1989). Tenascin/hexabrachion in human skin: biochemical identification and localization by light and electron microscopy. J Cell Biol *108*, 2483-2493.

Linzer, D. I., and Levine, A. J. (1979). Characterization of a 54K dalton cellular SV40 tumor antigen present in SV40-transformed cells and uninfected embryonal carcinoma cells. Cell *17*, 43-52.

Loges, S., Mazzone, M., Hohensinner, P., and Carmeliet, P. (2009). Silencing or fueling metastasis with VEGF inhibitors: antiangiogenesis revisited. Cancer Cell *15*, 167-170.

Lopez, T., and Hanahan, D. (2002). Elevated levels of IGF-1 receptor convey invasive and metastatic capability in a mouse model of pancreatic islet tumorigenesis. Cancer Cell *1*, 339-353.

Ludlow, J. W. (1993). Interactions between SV40 large-tumor antigen and the growth suppressor proteins pRB and p53. Faseb J *7*, 866-871.

MacDonald, B. T., Tamai, K., and He, X. (2009). Wnt/beta-catenin signaling: components, mechanisms, and diseases. Dev Cell *17*, 9-26.

Maniotis, A. J., Folberg, R., Hess, A., Seftor, E. A., *et al.* (1999). Vascular channel formation by human melanoma cells in vivo and in vitro: vasculogenic mimicry. Am J Pathol *155*, 739-752.

Martina, E., Degen, M., Ruegg, C., Merlo, A., *et al.* (2010). Tenascin-W is a specific marker of glioma-associated blood vessels and stimulates angiogenesis in vitro. Faseb J *24*, 778-787.

Maxwell, P. H., Pugh, C. W., and Ratcliffe, P. J. (2001). Activation of the HIF pathway in cancer. Current opinion in genetics & development *11*, 293-299.

McDonald, D. M., and Choyke, P. L. (2003). Imaging of angiogenesis: from microscope to clinic. Nat Med *9*, 713-725.

Midwood, K. S., Hussenet, T., Langlois, B., and Orend, G. (2011). Advances in tenascin-C biology. Cell Mol Life Sci *Published online August 2011*.

Midwood, K. S., and Orend, G. (2009). The role of tenascin-C in tissue injury and tumorigenesis. J Cell Commun Signal *3*, 287-310.

Mikheev, A. M., Mikheeva, S. A., Liu, B., Cohen, P.*, et al.* (2004). A functional genomics approach for the identification of putative tumor suppressor genes: Dickkopf-1 as suppressor of HeLa cell transformation. Carcinogenesis *25*, 47-59.

Min, J. K., Park, H., Choi, H. J., Kim, Y.*, et al.* (2011). The WNT antagonist Dickkopf2 promotes angiogenesis in rodent and human endothelial cells. J Clin Invest *121*, 1882-1893.

Minn, A. J., Gupta, G. P., Siegel, P. M., Bos, P. D.*, et al.* (2005). Genes that mediate breast cancer metastasis to lung. Nature *436*, 518-524.

Mitrovic, N., and Schachner, M. (1995). Detection of tenascin-C in the nervous system of the tenascin-C mutant mouse. J Neurosci Res *42*, 710-717.

Murphree, A. L., and Benedict, W. F. (1984). Retinoblastoma: clues to human oncogenesis. Science *223*, 1028-1033.

Naik, P., Christofori, G., and Hanahan, D. (1994). Insulin-like growth factor II is focally up-regulated and functionally involved as a second signal for oncogene-induced tumorigenesis. Cold Spring Harb Symp Quant Biol *59*, 459-470.

Naik, P., Karrim, J., and Hanahan, D. (1996). The rise and fall of apoptosis during multistage tumorigenesis: down-modulation contributes to tumor progression from angiogenic progenitors. Genes Dev *10*, 2105-2116.

Natali, P. G., Nicotra, M. R., Bartolazzi, A., Mottolese, M.*, et al.* (1990). Expression and production of tenascin in benign and malignant lesions of melanocyte lineage. Int J Cancer *46*, 586-590.

Nevins, J. R. (2001). The Rb/E2F pathway and cancer. Hum Mol Genet *10*, 699-703.

Niehrs, C. (2006). Function and biological roles of the Dickkopf family of Wnt modulators. Oncogene *25*, 7469-7481.

Nozawa, H., Chiu, C., and Hanahan, D. (2006). Infiltrating neutrophils mediate the initial angiogenic switch in a mouse model of multistage carcinogenesis. Proc Natl Acad Sci U S A *103*, 12493-12498.

Orend, G., and Chiquet-Ehrismann, R. (2000). Adhesion modulation by antiadhesive molecules of the extracellular matrix. Exp Cell Res *261*, 104-110.

Orend, G., and Chiquet-Ehrismann, R. (2006). Tenascin-C induced signaling in cancer. Cancer Lett *244*, 143-163.

Oskarsson, T., Acharyya, S., Zhang, X. H., Vanharanta, S.*, et al.* (2011). Breast cancer cells produce tenascin C as a metastatic niche component to colonize the lungs. Nat Med *doi:10.1038/nm.2379*.

Paez-Ribes, M., Allen, E., Hudock, J., Takeda, T.*, et al.* (2009). Antiangiogenic therapy elicits malignant progression of tumors to increased local invasion and distant metastasis. Cancer Cell *15*, 220-231.

Paget, S. (1889). Distribution of secondary growths in cancer of the breast. The Lancet *133*, 571-573.

Pandur, P., Lasche, M., Eisenberg, L. M., and Kuhl, M. (2002). Wnt-11 activation of a non-canonical Wnt signalling pathway is required for cardiogenesis. Nature *418*, 636-641.

Parangi, S., Dietrich, W., Christofori, G., Lander, E. S.*, et al.* (1995). Tumor suppressor loci on mouse chromosomes 9 and 16 are lost at distinct stages of tumorigenesis in a transgenic model of islet cell carcinoma. Cancer Res *55*, 6071-6076.

Parangi, S., O'Reilly, M., Christofori, G., Holmgren, L.*, et al.* (1996). Antiangiogenic therapy of transgenic mice impairs de novo tumor growth. Proc Natl Acad Sci U S A *93*, 2002-2007.

Paulis, Y. W., Soetekouw, P. M., Verheul, H. M., Tjan-Heijnen, V. C.*, et al.* (2010). Signalling pathways in vasculogenic mimicry. Biochim Biophys Acta *1806*, 18-28.

Perl, A. K., Wilgenbus, P., Dahl, U., Semb, H.*, et al.* (1998). A causal role for E-cadherin in the transition from adenoma to carcinoma. Nature *392*, 190-193.

Pezzolo, A., Parodi, F., Marimpietri, D., Raffaghello, L.*, et al.* (2011). Oct-4(+)/Tenascin C(+) neuroblastoma cells serve as progenitors of tumor-derived endothelial cells. Cell Res.

Pipas, J. M., and Levine, A. J. (2001). Role of T antigen interactions with p53 in tumorigenesis. Semin Cancer Biol *11*, 23-30.

Polakis, P. (2000). Wnt signaling and cancer. Genes Dev *14*, 1837-1851.

Polyak, K., Haviv, I., and Campbell, I. G. (2009). Co-evolution of tumor cells and their microenvironment. Trends Genet *25*, 30-38.

Ponder, B. A. (2001). Cancer genetics. Nature *411*, 336-341.

Ponta, H., Sherman, L., and Herrlich, P. A. (2003). CD44: from adhesion molecules to signalling regulators. Nat Rev Mol Cell Biol *4*, 33-45.

Ranganathan, P., Weaver, K. L., and Capobianco, A. J. (2011). Notch signalling in solid tumours: a little bit of everything but not all the time. Nat Rev Cancer *11*, 338-351.

Rehman, A. O., and Wang, C. Y. (2006). Notch signaling in the regulation of tumor angiogenesis. Trends Cell Biol *16*, 293-300.

Ricci-Vitiani, L., Pallini, R., Biffoni, M., Todaro, M.*, et al.* (2010). Tumour vascularization via endothelial differentiation of glioblastoma stem-like cells. Nature *468*, 824-828.

Roth-Kleiner, M., Hirsch, E., and Schittny, J. C. (2004). Fetal lungs of tenascin-C-deficient mice grow well, but branch poorly in organ culture. Am J Respir Cell Mol Biol *30*, 360-366.

Rubinfeld, B., Souza, B., Albert, I., Muller, O.*, et al.* (1993). Association of the APC gene product with beta-catenin. Science *262*, 1731-1734.

Ruiz, C., Huang, W., Hegi, M. E., Lange, K.*, et al.* (2004). Growth promoting signaling by tenascin-C [corrected]. Cancer Res *64*, 7377-7385.

Saga, Y., Yagi, T., Ikawa, Y., Sakakura, T.*, et al.* (1992). Mice develop normally without tenascin. Genes Dev *6*, 1821-1831.

Sarasa-Renedo, A., Tunc-Civelek, V., and Chiquet, M. (2006). Role of RhoA/ROCK-dependent actin contractility in the induction of tenascin-C by cyclic tensile strain. Exp Cell Res *312*, 1361-1370.

Scharer, C. D., McCabe, C. D., Ali-Seyed, M., Berger, M. F.*, et al.* (2009). Genome-wide promoter analysis of the SOX4 transcriptional network in prostate cancer cells. Cancer Res *69*, 709-717.

Schenk, S., Chiquet-Ehrismann, R., and Battegay, E. J. (1999). The fibrinogen globe of tenascin-C promotes basic fibroblast growth factor-induced endothelial cell elongation. Mol Biol Cell *10*, 2933-2943.

Schomber, T., Kopfstein, L., Djonov, V., Albrecht, I.*, et al.* (2007). Placental growth factor-1 attenuates vascular endothelial growth factor-A-dependent tumor angiogenesis during beta cell carcinogenesis. Cancer Res *67*, 10840-10848.

Seftor, E. A., Meltzer, P. S., Kirschmann, D. A., Pe'er, J.*, et al.* (2002). Molecular determinants of human uveal melanoma invasion and metastasis. Clin Exp Metastasis *19*, 233-246.

Shields, J. D., Kourtis, I. C., Tomei, A. A., Roberts, J. M.*, et al.* (2010). Induction of lymphoidlike stroma and immune escape by tumors that express the chemokine CCL21. Science *328*, 749-752.

Shojaei, F., Singh, M., Thompson, J. D., and Ferrara, N. (2008). Role of Bv8 in neutrophil-dependent angiogenesis in a transgenic model of cancer progression. Proc Natl Acad Sci U S A *105*, 2640-2645.

Shtutman, M., Zhurinsky, J., Simcha, I., Albanese, C.*, et al.* (1999). The cyclin D1 gene is a target of the beta-catenin/LEF-1 pathway. Proc Natl Acad Sci U S A *96*, 5522-5527.

Simo, P., Simon-Assmann, P., Bouziges, F., Leberquier, C.*, et al.* (1991). Changes in the expression of laminin during intestinal development. Development *112*, 477-487.

Sivasankaran, B., Degen, M., Ghaffari, A., Hegi, M. E.*, et al.* (2009). Tenascin-C is a novel RBPJkappa-induced target gene for Notch signaling in gliomas. Cancer Res *69*, 458-465.

Smadja, D. M., d'Audigier, C., Weiswald, L. B., Badoual, C.*, et al.* (2010). The Wnt antagonist Dickkopf-1 increases endothelial progenitor cell angiogenic potential. Arterioscler Thromb Vasc Biol *30*, 2544-2552.

Sparks, A. B., Morin, P. J., Vogelstein, B., and Kinzler, K. W. (1998). Mutational analysis of the APC/beta-catenin/Tcf pathway in colorectal cancer. Cancer Res *58*, 1130-1134.

Sporn, M. B. (1997). The war on cancer: a review. Ann N Y Acad Sci *833*, 137-146.

Steeg, P. S. (2003). Metastasis suppressors alter the signal transduction of cancer cells. Nat Rev Cancer *3*, 55-63.

Su, L. K., Vogelstein, B., and Kinzler, K. W. (1993). Association of the APC tumor suppressor protein with catenins. Science *262*, 1734-1737.

Talts, J. F., Wirl, G., Dictor, M., Muller, W. J.*, et al.* (1999). Tenascin-C modulates tumor stroma and monocyte/macrophage recruitment but not tumor growth or metastasis in a mouse strain with spontaneous mammary cancer. J Cell Sci *112 (Pt 12)*, 1855-1864.

Tanaka, K., Hiraiwa, N., Hashimoto, H., Yamazaki, Y.*, et al.* (2004). Tenascin-C regulates angiogenesis in tumor through the regulation of vascular endothelial growth factor expression. Int J Cancer *108*, 31-40.

Tavazoie, S. F., Alarcon, C., Oskarsson, T., Padua, D.*, et al.* (2008). Endogenous human microRNAs that suppress breast cancer metastasis. Nature *451*, 147-152.

Thiery, J. P., and Chopin, D. (1999). Epithelial cell plasticity in development and tumor progression. Cancer Metastasis Rev *18*, 31-42.

Thudi, N. K., Martin, C. K., Murahari, S., Shu, S. T.*, et al.* (2010). Dickkopf-1 (DKK-1) stimulated prostate cancer growth and metastasis and inhibited bone formation in osteoblastic bone metastases. Prostate *71*, 615-625.

Tucker, R. P., and Chiquet-Ehrismann, R. (2009). The regulation of tenascin expression by tissue microenvironments. Biochim Biophys Acta *1793*, 888-892.

Udalova, I. A., Ruhmann, M., Thomson, S. J., and Midwood, K. S. (2011). Expression and immune function of tenascin-C. Crit Rev Immunol *31*, 115-145.

Vajkoczy, P., Farhadi, M., Gaumann, A., Heidenreich, R.*, et al.* (2002). Microtumor growth initiates angiogenic sprouting with simultaneous expression of VEGF, VEGF receptor-2, and angiopoietin-2. J Clin Invest *109*, 777-785.

Van Obberghen-Schilling, E., Tucker, R. P., Saupe, F., Gasser, I.*, et al.* (2011). Fibronectin and tenascin-C: accomplices in vascular morphogenesis during development and tumor growth. Int J Dev Biol *55*, 511-525.

Wagner, S., Hofstetter, W., Chiquet, M., Mainil-Varlet, P.*, et al.* (2003). Early osteoarthritic changes of human femoral head cartilage subsequent to femoro-acetabular impingement. Osteoarthritis Cartilage *11*, 508-518.

Wang, R., Chadalavada, K., Wilshire, J., Kowalik, U.*, et al.* (2010). Glioblastoma stem-like cells give rise to tumour endothelium. Nature.

WHO (2008). World Cancer Report 2008. International Agency for Research on Cancer.

Wielenga, V. J., Smits, R., Korinek, V., Smit, L.*, et al.* (1999). Expression of CD44 in Apc and Tcf mutant mice implies regulation by the WNT pathway. Am J Pathol *154*, 515-523.

Wild, D., Behe, M., Wicki, A., Storch, D.*, et al.* (2006). [Lys40(Ahx-DTPA-111In)NH2]exendin-4, a very promising ligand for glucagon-like peptide-1 (GLP-1) receptor targeting. J Nucl Med *47*, 2025-2033.

Wilting, J., Christ, B., Bokeloh, M., and Weich, H. A. (1993). In vivo effects of vascular endothelial growth factor on the chicken chorioallantoic membrane. Cell Tissue Res *274*, 163-172.

Wong, M. H., Rubinfeld, B., and Gordon, J. I. (1998). Effects of forced expression of an NH2-terminal truncated beta-Catenin on mouse intestinal epithelial homeostasis. J Cell Biol *141*, 765-777.

Xian, X., Hakansson, J., Stahlberg, A., Lindblom, P.*, et al.* (2006). Pericytes limit tumor cell metastasis. J Clin Invest *116*, 642-651.

Yilmaz, M., and Christofori, G. (2009). EMT, the cytoskeleton, and cancer cell invasion. Cancer Metastasis Rev *28*, 15-33.

Yue, W. Y., and Chen, Z. P. (2005). Does vasculogenic mimicry exist in astrocytoma? J Histochem Cytochem *53*, 997-1002.

Zindl, C. L., and Chaplin, D. D. (2010). Immunology. Tumor immune evasion. Science *328*, 697-698.